Noriko Hasebe
Masato Honda
Keisuke Fukushi
Seiya Nagao *Editors*

Field Work and Laboratory Experiments in Integrated Environmental Sciences

Springer

Field Work and Laboratory Experiments in Integrated Environmental Sciences

Noriko Hasebe · Masato Honda · Keisuke Fukushi · Seiya Nagao
Editors

Field Work and Laboratory Experiments in Integrated Environmental Sciences

Springer

Editors
Noriko Hasebe
Institute of Nature and Environmental Technology
Kanazawa University
Kanazawa, Ishikawa, Japan

Keisuke Fukushi
Institute of Nature and Environmental Technology
Kanazawa University
Kanazawa, Ishikawa, Japan

Masato Honda
Botanical Garden, Institute of Nature and Environmental Technology
Kanazawa University
Kanazawa, Ishikawa, Japan

Seiya Nagao
Low Level Radioactivity Laboratory
Institute of Nature and Environmental Technology
Kanazawa University
Nomi, Ishikawa, Japan

ISBN 978-981-99-6531-1 ISBN 978-981-99-6532-8 (eBook)
https://doi.org/10.1007/978-981-99-6532-8

Preface

The surface environment of the Earth is a complex system consisting of atmospheric, oceanic, and terrestrial regions as well as the biota therein, all interacting to various extents. The integration of research disciplines including earth sciences, biology, chemistry, physics, and social sciences is a core of environmental science. This book introduces the variety of research skills required for integrated environmental science, which are applicable to atmospheric, oceanic, terrestrial, and biota studies. It encourages students and early career scientists to take a broad view of the whole environmental system. Detailed practical information for the field or laboratory work in this book helps students and scientists to plan research strategies for their own scope and interests. In addition, this book is also useful for professionals to teach field and laboratory work in environmental science to students.

This book is based on the Environmental Summer School Programme organized by the Institute of Nature and Environmental Technology, Kanazawa University, Japan. This summer school is open to international students. We take them to branch laboratories in the northern tip of the Noto peninsula, which is famous for its rural landscape, rich sea resources, and traditional lifestyle in the so-called Satoyama and Satoumi area. There, students study the marine animal taxonomy, vegetation survey, ecological management, ocean physiochemistry, and environmental pollution and its effect on the organism. Taking advantage of the preserved natural environment, an atmospheric observatory is established in Noto, and students also visit the observatory to learn instrument management. Students also learn to use radioactivity to monitor the environment or to estimate the time of past environmental events. The use of geological resources and its impact on the environment is also included as one of the topics of the summer school.

This textbook was reviewed by Prof. Nobuo Suzuki, Prof. Ning Tang, Prof. Akihiko Yokoyama, Dr. Noboru Nunomura, Associate Prof. Atsushi Matsuki, Assistant Prof. Tetsuya Matsunaka and Assistant Prof. Sakiko Ishino from Kanazawa University, Prof. Akira Asakura from Kyoto University, Associate Prof. Midori Iida from Niigata University, Prof. Seiichi Uno from Kagoshima University, Prof. Emeritus Akifumi Ohtaka of Hirosaki University, Prof. Kazuhiro Katoh from the Open University of Japan, and Assistant Prof. Eunice Tan from National University of

Singapore. We are grateful to all the professionals who contributed to this textbook. We are also grateful to the Japan Science and Technology Agency for their financial support in organizing the summer school.

Kanazawa, Japan
March 2023

Noriko Hasebe
Masato Honda
Keisuke Fukushi
Seiya Nagao

Contents

Chapter 1
A Perspective on Integrated Environmental Studies

Seiya Nagao and Shinya Ochiai

1.1 Introduction

Studies on the links between the land, ocean, and atmosphere are important to marine and fisheries science, sedimentology, and palaeo-oceanography (e.g., Tada et al., 1999; Meybeck et al. 2006; Ramesh et al. 2015). Issues related to land–ocean interactions in coastal zones are key for a sustainable and resilient future, in terms of both human society and nature, along the coasts with human presence (Ramesh et al. 2015). Verburg et al. (2015) noted that understanding the drivers, state, trends, and impacts of different terrestrial systems on social and natural processes can help design sustainable transformations through stakeholder engagement and land governance. However, several concepts are related to the link between sustainable development and integrated environmental studies, which depend on the research field, scientific subject, and environmental issues (Makino et al. 2013; Fredston-Hermann et al. 2016; Rölfer et al. 2021, etc.). A definition of the land–ocean link and integrated environmental studies is needed in each research field to avoid confusion regarding its usage and how it is discussed with stakeholders with various jobs and differing ages.

Satoyama and Satoumi is the landscape in land and coastal marine environments, respectively, which has been shaped and maintained by human activities (Watanabe et al. 2012). The Japanese government and the United Nations submitted the SatoyamaInitiative which has been acknowledged by the international community as a useful tool to better understand and support human-influenced natural environments for the benefit of biodiversity and human well-being (Takeuchi 2010; Watanabe et al. 2012). It is important to understand the linkage between Satoyama and Satoumi, that is land and coastal sea, since environmental preservation can be performed by

S. Nagao (✉) · S. Ochiai
Low Level Radioactivity Laboratory, Institute of Nature and Environmental Technology, Kanazawa University, Nomi, Japan
e-mail: seiya-nagao@se.kanazawa-u.ac.jp

N. Hasebe et al. (eds.), *Field Work and Laboratory Experiments in Integrated Environmental Sciences*, https://doi.org/10.1007/978-981-99-6532-8_1

human activity with a good balance between livelihood, ecosystem, and biodiversity based on dynamics of natural and anthropogenic materials such as nutrients, organic matter, and toxic substances. The concept of Satoyama–Satoumi is suitable to consider environmental preservation and social development as human activities, not only for the land watershed environment but also for coastal marine area. This chapter describes concepts and future direction of integrated environmental studies on aquatic environments, Satoyama–Satoumi region, at Noto Peninsula based on research being conducted at the Institute of Nature and Environmental Technology, Kanazawa University (K-INET).

Educational activities are also key to resolving various environmental issues in collaboration with various stakeholders and considering their counter measurements. However, education for undergraduate and graduate students based on integrated environmental studies is limited, particularly in the field of research. This chapter also describes how to perform hands-on training and lectures related to advanced research activities, based on integrated environmental studies.

1.2 Concept of Integrated Environmental Studies of the K-INET

The Institute of Nature and Environmental Technology, Kanazawa University (K-INET) has been accepted as the Joint Usage/Research Centre of transboundary pollution and its impact on environmental changes since 2016. We focused on the transport of toxic substances from the atmosphere to the coastal marine environment via river systems. Figure 1.1 shows a schematic illustration of the linkage between atmosphere-land-coastal marine environments and considers the linkage area as a watershed system. K-INET also considered the impacts of toxic substances on coastal marine ecosystems and human health. A case study shows and explains the research viewpoints based on integrated environmental studies organized by the K-INET.

Figure 1.2 shows maps of a study area on the Noto Peninsula in Japan; where the atmosphere–land–coastal marine environments are integrated. The Noto Peninsula, particularly Satoyama–Satoumi area, was recognized as one of the Globally Important Agricultural Heritage Systems (GIAHS) to ensure food security in 2011 (Ishikawa Prefecture 2021). The K-INET has been maintaining the atmospheric research facilities there with highly sensitive natural environmental sensors to monitor transboundary pollution. The Wajima Air Monitoring Station has been conducting monitoring surveys of polycyclic aromatic hydrocarbon (PAH) concentration and composition in aerosol since 2004 (Hayakawa et al. 2018). The PAHs concentration exhibits seasonal variation, being higher in winter and lower in summer season (Fig. 1.3). During the COVID-19, a decline of the PAHs concentration was observed from February to April 2020, up to 52.6%, in comparison with that of the same period in the previous year (Zhang et al. 2020). The $PM_{2.5}$, organic carbon and inorganic carbon concentrations in aerosol also decreased by 33%, 65%, and 35%,

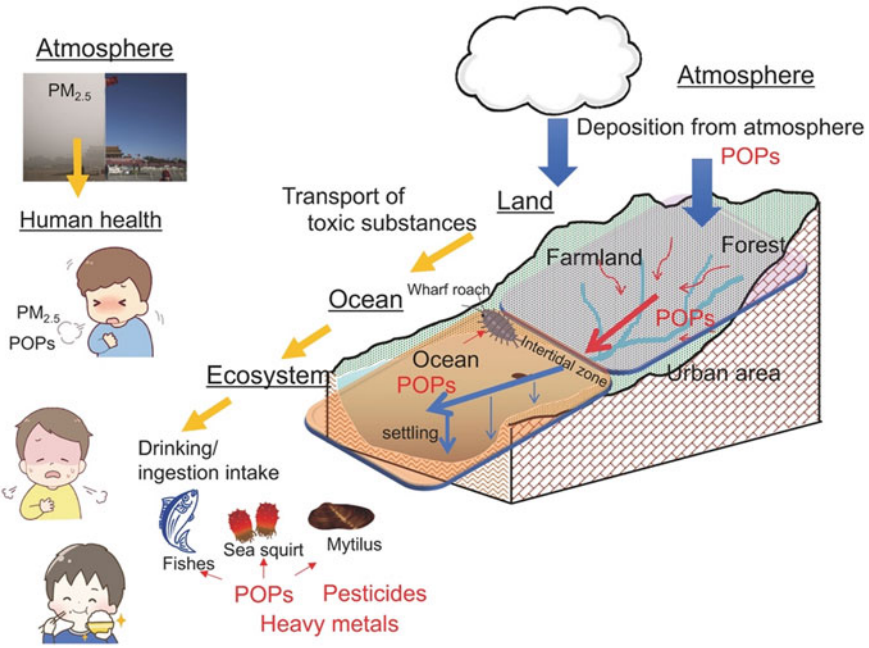

Fig. 1.1 Schematic showing the connections in integrated environmental research

respectively, compared with those of previous observations (Zhang et al. 2021). The data is available to assess the change in emission and transport of pollutants with the change in human activities quantitatively.

The Noto area was facing social issues, such as depopulation and an aging population of 40–50% in 2019 (Ishikawa Prefecture 2019). To ensure the sustainable development of rural areas, activities of primary industries such as fisheries and agriculture are necessary along with environmental protection and conservation. The Noto Peninsula also has the advantage of conducting integrated environmental studies as follows: (1) a small watershed of each river system with simple land use (forest in the upper and paddy fields in the middle-lower river), (2) rivers linked to semi-closed bays with aquaculture, and (3) research facilities located at the Noto Peninsula. Therefore, K-INET includes research areas in Suzu, Nanao, and Nakajima (Fig. 1.2). The Suzu and Nakajima fields focus on researching the links between the reservoir and its watershed using radionuclides (^{7}Be, ^{137}Cs, and ^{210}Pb) deposited in the atmosphere. Transport behavior was investigated using different radionuclide half-lives (53.2 d to 30.17 y) and residence times thereof from atmospheric deposition and sediment trap datasets. The Nakajima field also investigated the effects of deforestation on suspended solid transport in the watershed using sediment core samples (Ochiai et al. 2015a). Figure 1.4 shows changes in the sedimentation rate of a long sediment core collected from the Bishaguso-ike reservoir, as shown in Fig. 1.2. The sedimentation rate estimated from excess^{210}Pb ($^{210}Pb_{ex}$: total ^{210}Pb—^{210}Pb derived

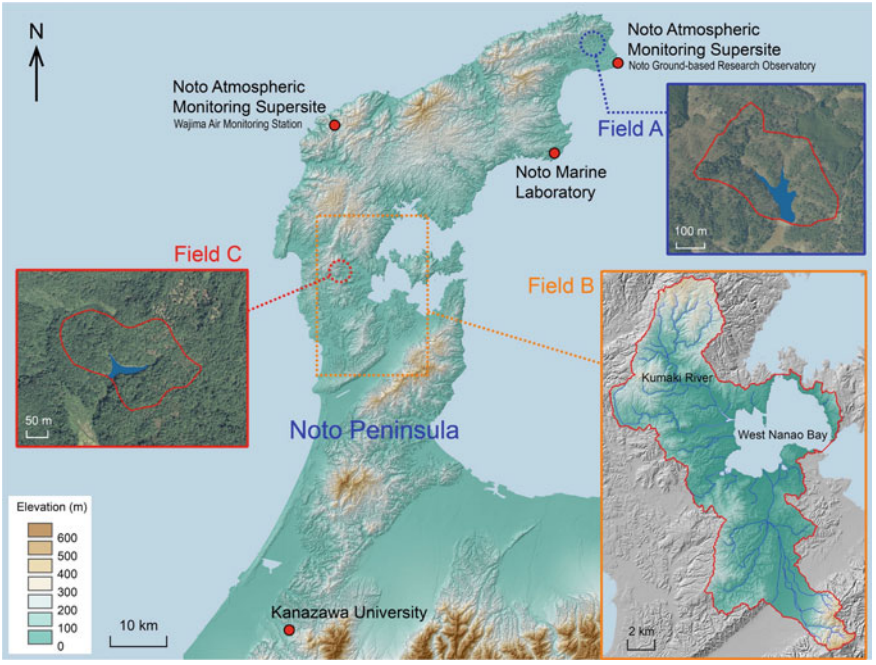

Fig. 1.2 The research field of integrated environmental studies on the Noto Peninsula in Japan. The map shows three research areas: **Field A** (Suzu site) an atmosphere–land–reservoir system, **Field B** (Nanao site) a land–coastal marine system, and **Field C** (Nakajima site) a land-reservoir system. Digital map data were based on the Fundamental Geospatial Data (Geospatial Information Authority of Japan), and National Land Numerical Information (Ministry of Land, Infrastructure, Transport and Tourism). The aerial photographs were obtained from the Geospatial Information Authority of Japan (year taken: 1975 and 2010)

from ^{226}Ra in soil and sediment) exhibited changes in the supply of suspended solids from the watershed due to forestation and plantation since the 1980s. Changes in river watershed environments lead to changes in the transport of suspended solids from river watersheds to lakes and coastal marine areas.

The Nanao field includes the Kumaki River and the semi-enclosed West Nanao Bay area, where oyster farming is a local occupation. The water quality in Nanao Bay, classified as an enclosed coastal area, has been monitored by the Ministry of the Environment in Japan (MOE, 2021a). At our institute, the transport behavior of dissolved and particulate substances from land to the ocean was investigated using radionuclides (^{7}Be, ^{137}Cs, and ^{210}Pb) derived from the atmosphere and carbon isotopes (δ^{13}C and Δ^{14}C) of organic matter in suspended solids in the Kumaki River (Nagao et al. 2020; Ochiai et al. 2020). Our studies note that rain events and snow melting in winter in river systems are driving forces for the transport of suspended solids in river systems. The lower reaches of paddy fields along the river are the main sources of riverine suspended solids in coastal marine areas under normal flow conditions.

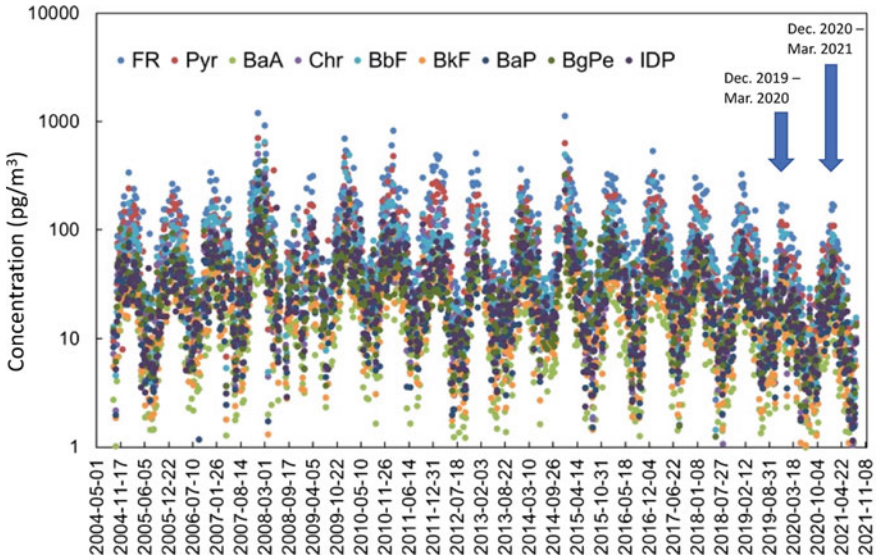

Fig. 1.3 The PAHs concentration and their composition in aerosol collected at the Wajima Air Monitoring Station of K-INET from 2004 to 2021. The data was sited from Zhang et al. (2020) and other additional data sources

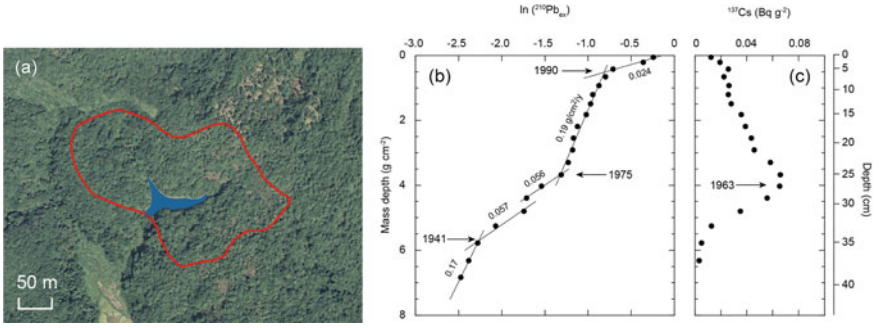

Fig. 1.4 The photograph of Bishaguso-ike reservoir watershed (left panel) and the sedimentation rate of a long core sample (right panel) collected from Bishaguso-ike reservoir on the Noto Peninsula in Japan. For detailed information, see Chap. 10 of this book. The aerial photograph was obtained from the Geospatial Information Authority of Japan (year taken: 1975)

The processes by which riverine suspended solids are deposited in coastal zones were studied using sediment core samples collected from several sites in West Nanao Bay. The dispersion of toxic substances is discussed based on the spatial distribution of surface sediments in terms of the sedimentation rate, grain size, total organic carbon (TOC) content, and the carbon and nitrogen isotope composition (e.g., Yamamoto 1968; Ochiai et al. 2022). Therefore, basic information on the transport of geomaterials is important for identifying the transport mechanisms from river

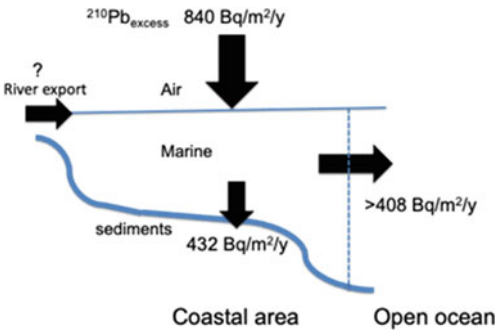

Fig. 1.5 The flux of $^{210}Pb_{excess}$ from the atmosphere to the marine surface, from seawater to the bottom sediment, and from the coastal area to the open ocean in Nanao Bay. The flux estimation was carried out by using the research result of atmospheric deposition (Yamamoto et al. 2006), the inventory of ex^{210}Pb and the sedimentation rate of the sediments (Ochiai et al. 2022). The difference between atmospheric deposition and sedimentation is considered as the export to the open ocean

watersheds through river systems to coastal marine areas. The inventory of $^{210}Pb_{ex}$ in soil surrounding the bay is 2.42 ± 0.48 Bq/cm^2 and corresponds to atmospheric deposition. The average value of inventory of the bottom sediments in West Nanao Bay is 1.39 ± 0.40 Bq/cm^2, except for the river mouth area (Ochiai et al. 2022). Figure 1.5 shows the deposition flux of $^{210}Pb_{ex}$ from the atmosphere to the ocean and land surface, and from seawater to bottom sediments. The atmospheric flux was obtained from Yamamoto et al. (2006). The flux of $^{210}Pb_{ex}$ from the seawater to the bottom sediment was estimated using the above sediment inventory at the steady state condition between the deposition flux of $^{210}Pb_{ex}$ and its radioactive decay in the sediment. The difference in $^{210}Pb_{ex}$ flux between the atmosphere–ocean and the ocean-bottom sediment was estimated to be over 408 Bq/m^2/y, and at least 49% of $^{210}Pb_{ex}$ from the atmosphere and the watershed was transferred to the open ocean, although Nanao Bay is classified as a semi-closed bay.

Submarine groundwater discharge (SGD) was also investigated using ^{222}Rn activity having a short half-life of 3.82 d in West Nanao Bay (Sugimoto et al. 2014). SGD is considered one of the transport routes of nutrients to coastal seas to support primary production and maintain coastal ecosystems. ^{222}Rn concentration in the bottom waters showed clear spatial variation, which was higher in shallower regions, but lower in deeper regions. From the mixing plot of salinity and ^{222}Rn concentration, a higher ^{222}Rn concentration was supplied by SGD. There is no clear relationship between ^{222}Rn and nutrient concentrations, but it may promote dissolved phosphate accumulation in hypoxic bottom waters.

From the linkage research of the atmosphere-land–ocean, we should consider the changes in climate and human activities, such as land-use type and agricultural activities due to an increase in the aging population (e.g., Lee et al. 2015; Ide et al. 2019; Manning et al. 2020). Changes in natural and social environments in watersheds are very sensitive to variations in coastal marine environments, such as changes in

ecosystems, biodiversity, and primary production. Therefore, it is necessary to assess the natural environment using integrated environmental studies.

The impact of toxic substances on ecosystems has been explored in monitoring-based research and laboratory experiments using polycyclic aromatic hydrocarbons (PAHs) with 2-rings to 6-rings. PAHs are formed by the incomplete combustion of organic matter and fossil fuels and/or are released from tanker accidents (Brekke and Solberg 2005; Manzetti 2013). Research that monitored water quality and pollutant accumulation in organisms has been conducted using *Ligia exotica* and *Mytilus coruscus* in coastal marine environments from Aomori Prefecture, north of Honshu Island and Nagasaki Prefecture, northern Kyushu Island, Japan (Honda et al. 2021). *L. exotica* lives on coastal reefs above the water level; therefore, it was used as an indicator for monitoring organisms in coastal land–ocean areas. *M. coruscus* was used as an indicator organism for the mussel watch, which monitors water quality and accumulation in organisms, through the NOAA mussel watch program (Apeti et al. 2018); the mussel watches in Japan (MOE 2021b) and Baltic Sea (HELCOM 2010), and the Asia–Pacific mussel watch program (Monirith et al. 2003). The transfer of PAHs from seawater to organisms was used as a parameter and concentration factor to assess the effects of current impacts and predict impacts on the response of source emissions.

Monitoring research on PAH concentrations and their composition in seawater has also been carried out in West Nanao Bay (Mundo et al. 2020 2021). Figure 1.6 shows the spatial distribution of PAHs, having 14 target PAHs with 2-rings and 6-rings, and their concentration in the surface seawaters of West Nanao Bay from May 2019 to September 2020. The average concentration of total PAHs was lower than 20.0 ng/l and represented very low–low acute environmental risk (Mundo et al. 2020). Higher PAHs concentration in August 2019 was observed as higher dissolved phase of PAHs in comparison with that of other sampling results. This is caused by the riverine discharge of PAHs after a heavy rain event caused by the cold front. Therefore, we should identify the linkage between land and coastal marine oceans at the present time and monitor the fate of toxic substances based on integrated environmental studies, including the social environment and human activities.

1.3 How to Assess and Use Integrated Environmental Studies in Sustainable Development

The transport behavior of geomaterials from watershed to river depends on watershed characteristics, such as soil and geological type, the slope of the riverbed and watershed, the wetness of the ground surface, and vegetation (Meybeck et al. 2006; Hilton et al. 2012; Song et al. 2016). Climatic conditions are also important factors that control transport. Heavy rain and rain events are the main driving forces for the transport of nutrients, organic matter, and suspended solids in river systems (e.g., Higueras et al. 2014; Selvaraj et al. 2015; Takata et al. 2020). To identify the export

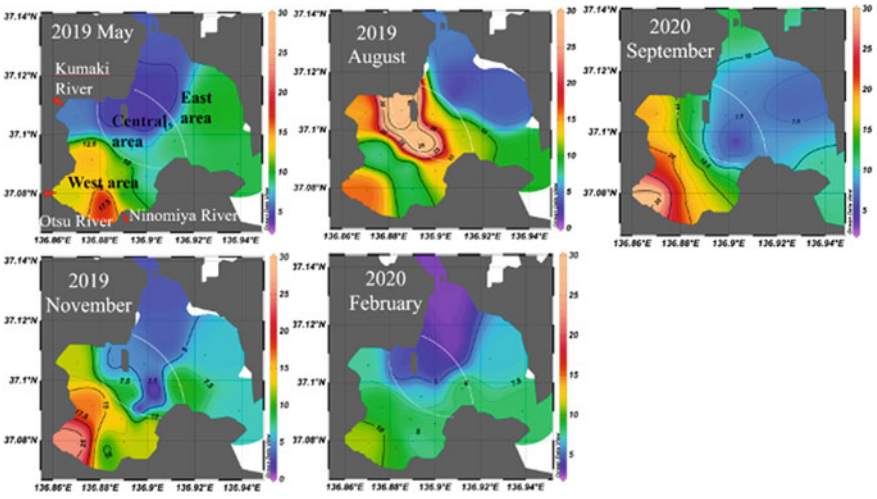

Fig. 1.6 The spatial distribution of PAHs concentration in surface seawaters from West Nanao Bay from May 2019 to September 2020. The figure is modified from Mundo et al. (2020)

of nutrients and organic matter, stable isotopes and radionuclides have been used as tracers in many river systems in various watershed environments (Bernardes et al. 2004, Nagao et al. 2005; Sarma et al. 2012; Froger et al. 2018). In the Noto area, Ochiai et al. (2015a) reported that the $\delta^{13}C$ and $\delta^{15}N$ of the sediments continued to decrease from the mid1980s to the present date owing to a decrease in the contribution of soil organic matter from the watershed. Research on radiocesium transport from land to the ocean can assess the transport behavior of dissolved and particulate phases of radiocesium from land to ocean (Nagao et al. 2013 2022; Ochiai et al. 2015b 2021, 2022) and can be used as a tracer of dissolved and particulate substances with similar geochemical properties. The combined use of stable isotopes and radionuclides is valuable for tracing geomaterials and identifying the source area in river–ocean watersheds.

Figure 1.7 shows a schematic illustration of the effects of watershed sizes on the assessment of linkage and transport between each boundary (atmosphere–land, land–ocean/–marine sediment, ocean organisms). The area of the watershed from land to the coastal marine environment is important for simulating the transport amount of dissolved and particulate substances, as shown in Fig. 1.7a (Meybeck et al. 2006; Wallin et al. 2015). Geomaterial behavior and dispersion in coastal marine areas is also related to watershed size and coastal currents. Climate change and land-use change are also important factors controlling the transport of particulate and dissolved substances from land to ocean (e.g., Ockenden et al. 2016; Levy et al. 2018; Farinosi et al. 2019). In the Noto Peninsula, where the research field and facilities of K-INET are located, Nakada (2021) showed the pulse input of water mass from rivers to West Nanao Bay after heavy rain events by the cold front. Understanding the environmental situation is important for assessing the transfer of toxic substances from seawater

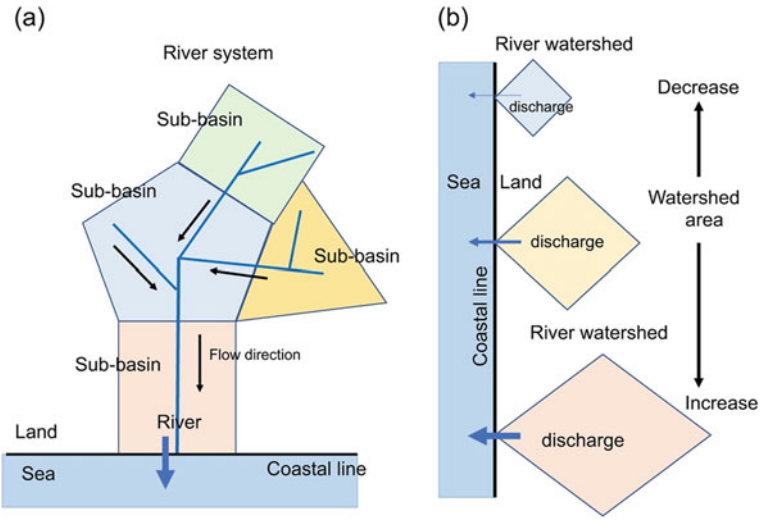

Fig. 1.7 Effects of watershed area on assessment of dynamics of toxic substances and their impacts on the ecosystem

to marine organisms. The combination of land water discharge and movement of water mass in the coastal marine area was used to identify the dispersion of toxic substances in the watershed from the upper river to the coastal marine zone.

There are other scale effects as well, such as a few sub-basins in a river system (Fig. 1.7b). The assessment of integrated environmental studies depends on the scale and watershed characteristics of each sub-basin (Lee et al. 2015). Grouping the upper, middle, and lower reaches is also an important scale in the assessment. When the entire watershed from the upper to lower reaches the lake or coastal marine environment, the approach method is different. Geographical features (slope of river watershed, land use type, land surface coverage, etc.) are also affected by the mass transport of dissolved and solid materials in land areas (Vercruysse et al. 2017). Therefore, the assessment must be determined based on research issues before performance.

1.4 Education of Integrated Environmental Studies

The foundation for integrated environmental education is communication and discussion among various stakeholders with a wide range of backgrounds to achieve sustainable development in rural areas. Scientific communicators are also important for linking scientists to government officers, scientists to citizens, officers to farmers, and fishermen, among others, based on scientific data and countermeasures. It is important to train young researchers in interdisciplinary approaches and communication

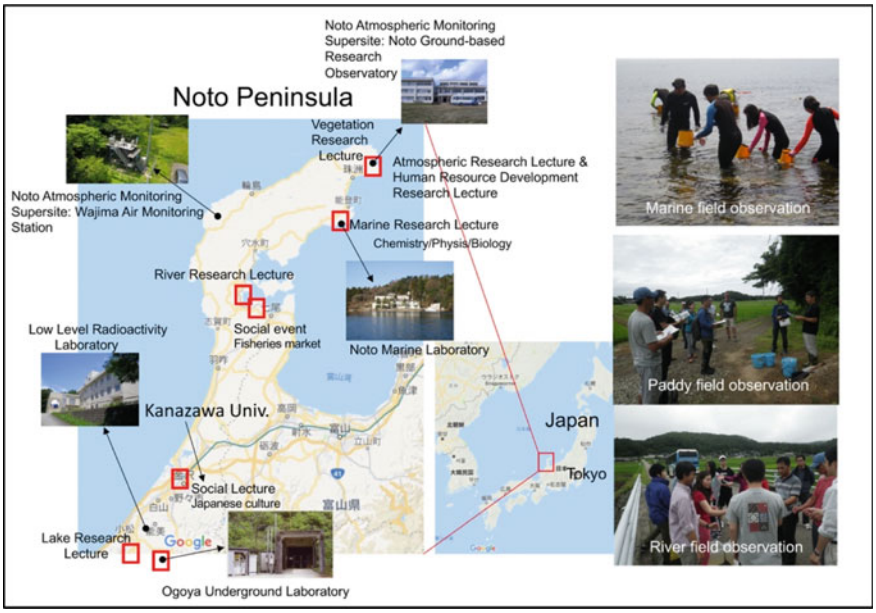

Fig. 1.8 Schematic illustration of the international summer school on the Noto Peninsula organized by the Institute of Nature and Environmental Technology, Kanazawa University (K-INET)

skills. The K-INET started an international summer school based on integrated environmental studies and field lectures on the Noto Peninsula in 2018 using our research facilities. Figure 1.8 shows the research facilities of the K-INET and lecture fields of the International Summer School for 6–10 days. The school is related to human resource development for undergraduate and graduate students from Kanazawa University and various other countries (China, Indonesia, Mongolia, and Taiwan). The program consists of lectures on atmospheric environmental research, terrestrial research, and marine research in physical, chemical, biological, and toxic research areas. The social scientific field is also taught to participants using the research contents of the Noto Satoyama Mister Program by Kanazawa University (Kanazawa University 2021) and enrich them with Japanese culture, especially local traditional knowledge. The Noto Peninsula is designated as the first Globally Important Agricultural Heritage Systems (GIAHS) "Noto's Satoyama and Satoumi" in Japan by the Food and Agriculture Organization of the United Nations (FAO) (Ishikawa Prefecture 2021). The international summer school has a specific advantage in terms of the geographical, social, and traditional features of the Noto Peninsula. This book consists of a textbook from an international summer school in addition to related basic information on field research.

Acknowledgements __The integrated environmental research was partly performed by the Joint Usage/Research Center Program entitled "International joint research center on transboundary

pollution and its environmental changes," from the Ministry of Education, Culture, Sports, Science and Technology (MEXT) in Japan.

References

Apeti D, Wirth E, Leight AK, Mason A, Pisarski E (2018) An assessment of contaminants of emerging concern in Chesapeake Bay, MD and Charleston Harbor SC. NOAA technical memorandum NOS NCCOS 240. Silver Spring, MD. 104 pp. https://doi.org/10.25923/p4nc-7m71.

Bernardes MC, Martinelli LA, Krusche AV, Gudeman J, Moreira M, Victoria RL, Ometto JPHB, Ballester MVR, Aufdenkampe AK, Richey JE, Hedges JI (2004) Riverine organic matter composition as a function of land use changes, southwest Amazon. Ecol Appl 14:263–279

Brekke C, Solberg AHS (2005) Oil spill detection by satellite remote sensing. Remote Sens Environ 95:1–13

Farinosi F, Arias ME, Lee E, Longo M, Pereira FF, Livino A, Moorcroft PR, Briscoe J (2019) Future climate and land use change impacts on river flows in the Tapajós Basin in the Brazilian Amazon. Earths Futur 7:993–1017

Fredston-Hermann A, Brown CJ, Albert S, Klein CJ, Mangubhai S, Nelson JL, Teneva L, Wenger A, Gaines SD, Halpern BS (2016) Where does river runoff matter for coastal marine conservation? Front Mar Sci 3:273

Froger C, Ayrault S, Evrard O, Monvoisin G, Bordier L, Lefèvre I, Quantin C (2018) Tracing the sources of suspended sediment and particle-bound trace metal elements in an urban catchment coupling elemental and isotopic geochemistry, and fallout radionuclides. Environ Sci Pollut Res Int 25:28667–28681

Hayakawa K, Tang N, Nagato EG, Toriba A, Sakai S, Kano F, Goto S, Endo O, Arashidani KI, Kakimoto H (2018) Long term trends in atmospheric concentrations of polycyclic aromatic hydrocarbons and nitropolycyclic aromatic hydrocarbons: a study of Japanese cities from 1997 to 2014. Environ Pollut 233:474–482

HELCOM (2010) Hazardous substances in the Baltic Sea-An integrated thematic assessment of hazardous substances in the Baltic Sea. Balt Sea Environ Proc 120B

Higueras M, Kerhervé P, Sanchez-Vidal A, Calafat A, Ludwig W, Verdoit-Jarraya M, Heussner S, Canals M (2014) Biogeochemical characterization of the riverine particulate organic matter transferred to the NW Mediterranean Sea. Biogeosciences 11:157–172

Hilton RG, Galy A, Hovius N, Kao SJ, Horng MJ, Chen H (2012) Climate and geomorphic controls on the erosion of terrestrial biomass from subtropical mountain forest. Global Biogeochem Cycles 26. https://doi.org/10.1029/2012GB004314

Honda M, Mukai K, Nagato E, Uno S, Oshima Y (2021) Correlation between polycyclic aromatic hydrocarbons in wharf roach (*Ligia* spp.) and environmental components of the intertidal and supralittoral zone along the Japanese Coast. Int J Environ Res Public Health 18:630

Ide J, Takeda I, Somura H, Mori Y, Sakuno Y, Yone Y, Takahashi E (2019) Impacts of hydrological changes on nutrient transport from diffuse sources in a rural river basin, western Japan. J Geophys Res Biogeosci 124:2565–2581

Ishikawa Prefecture (2019) Population estimates of age in Ishikawa prefecture. http://toukei.pref.ishikawa.jp/dl/3689/r01nennreigaiyou.pdf. Accessed 4 Nov 2021

Kanazawa University (2021) Noto Satoyama and Satoumi Meister training program. https://www.crc.kanazawa-u.ac.jp/meister/en/. Accessed 3 Nov 2021

Lee TY, Huang JC Jr, Lee JY, Jien SH, Zehetner F, Kao SJ (2015) Magnified sediment export of small mountainous rivers in Taiwan: Chain reactions from increased rainfall intensity under global warming. PLoS ONE 10:e0138283

Levy MC, Lopes AV, Cohn A, Larsen LG, Thompson SE (2018) Land use change increases streamflow across the arc of deforestation in Brazil. Geophy Res Lett 45:3520–3530

Makino A, Beger M, Klein CJ, Jupiter SD, Possingham HP (2013) Integrated planning for land-sea ecosystem connectivity to protect coral reefs. Biol Conserv 165:35–42

Manning DWP, Rosemond AD, Benstead JP, Bumpers PM, Kominoski JS (2020) Transport of N and P in U.S. streams and rivers differs with land use and between dissolved and particulate forms. Ecol Appl 30:e02130

Manzetti S (2013) Polycyclic aromatic hydrocarbons in the environment: environmental fate and transformation. Polycyclic Aromat Compd 33:311–330

Meybeck M, Dürr HH, Vörösmarty CJ (2006) Global coastal segmentation and its river catchment contributor: a new look at land-ocean linkage. Global Biogeochem Cycles 20(1) S 90:n/a-n/a

Ministry of the Environment (MOE) (2021a) Enclosed sea network. https://www.env.go.jp/water/heisa/heisa_net/waters/nanaowan.html. Accessed 3 Nov 2021

Ministry of the Environment (MOE) (2021b) Chemical substances and environment. http://www.env.go.jp/chemi/kurohon/index.html. Accessed 3 Nov 2021

Monirith I, Ueno D, Takahashi S, Nakata H, Sudaryanto A, Subramanian A, Karuppiah S, Ismail A, Muchtar M, Zheng J, Richardson BJ, Prudente M, Hue ND, Tana TS, Tkalin AV, Tanabe S (2003) Asia-Pacific mussel watch: monitoring contamination of persistent organochlorine compounds in coastal waters of Asia countries. Mar Pollut Bull 46:281–300

Mundo R, Matsunaka T, Iwai H, Ochiai S, Nagao S (2021) Geochemical control of PAHs by inflowing river water to West Nanao Bay, Japan, and its influences on ecological risk: Small-scale changes observed under near-background conditions at an enclosed bay. Int J Environ Res Public Health 18:310

Mundo R, Matsunaka T, Iwai H, Ogiso S, Suzuki N, Tang N, Hayakawa K, Nagao S (2020) Interannual survey on polycyclic aromatic hydrocarbons (PAHs) in seawater of North Nanao Bay, Ishikawa, Japan, from 2015 to 2018: sources, pathways and ecological risk assessment. Int J Environ Res Public Health 17:904

Nagao S, Kanamori M, Shimamura A, Morokado T, Putra DIP, Fujita T, Tomihara S, Ochiai S (2022) Temporal variation in radiocesium concentrations in waters of the Natsui and Same rivers, south Fukushima Prefecture, Japan during 2011 to 2020. Radiat Prot Dosimetry 198:947–956

Nagao S, Suzuki T, Ochiai S, Goto AS, Aramaki T, Hasegawa T (2020) Relationship between carbon isotope composition of river bottom sediments and land use effects on a watershed in a small river system: Kumaki River, Japan. Trans Jpn Geomorphol Union 41:295–311

Nagao S, Kanamori M, Ochiai S, Tomihara S, Fukushi K, Yamamoto M (2013) Export of ^{134}Cs and ^{137}Cs in the Fukushima river systems at heavy rains by Typhoon Roke in September 2011. Biogeosci 10:6215–6223

Nagao S, Usui T, Yamamoto M, Minagawa M, Iwatsuki T, Noda A (2005) Combined use of Δ^{14}C and δ^{13}C values to trace transportation and deposition processes of terrestrial particulate organic matter in coastal marine environments. Chem Geol 218:63–72

Nakada S (2021) Integration for high-frequent, high-density observation and high-resolution ocean simulation in aquafarms systems. Control Inf 65:27–32 (in Japanese)

Ishikawa Prefecture (2021) Noto's Satoyama Satoumi. http://www.pref.ishikawa.jp/satoyama/noto-giahs/sp/. Accessed 3 Nov 2021

Ochiai S, Fujita A, Tokunari T, Sakai H, Nagao S (2022) Distributions of ^{210}Pb, ^{137}Cs, and physical properties in bottom sediments of West Nanao Bay, Japan. Radiat Prot Dosimetry 198(13–15):1058–1065

Ochiai S, Nagao S, Yonebayashi K, Fukuyama T, Suzuki T, Yamamoto M, Kashiwaya K, Nakamura K (2015a) Effects of deforestation on the transport of particulate organic matter inferred from the geochemical properties of reservoir sediments in the Noto Peninsula, Japan. Geochem J 49:513–522

Ochiai S, Ueda S, Hasegawa H, Kakiuchi H, Akata N, Ohtsuka Y, Hisamatsu S (2015b) Effects of radiocesium inventory on ^{137}Cs concentrations in river waters of Fukushima, Japan, under baseflow conditions. J Environ Radioact 144:86–95

Ochiai S, Tokunari T, Suzuki T, Nagao S (2020) Transport processes of suspended and riverbed sediments inferred from atmospheric radionuclides in the Kumaki River, Japan. Trans Jpn Geomorphol Union 41:313–326

Ochiai S, Ueda S, Nagao S, Tsuji H, Tomihara S, Watanabe S, Suzuki K (2021) Spatial and temporal changes of ^{137}Cs concentrations in river waters and correlation with the radiocesium inventory in Fukushima and adjacent area. In: Nagao S (ed) Impacts of Fukushima nuclear accident on freshwater environments. Springer, Singapore, pp 51–64

Ockenden MC, Deasy CE, Benskin CMH, Beven KJ, Burke S, Collins AL, Evans R, Falloon PD, Forber KJ, Hiscock KM, Hollaway MJ, Kahana R, Macleod CJA, Reaney SM, Snell MA, Villamizar ML, Wearing C, Withers PJA, Zhou JG, Haygarth PM (2016) Changing climate and nutrient transfers: evidence from high temporal resolution concentration-flow dynamics in headwater catchments. Sci Total Environ 548–549:325–339

Ramesh R, Chen Z, Cummins V, Day J, D'Elia C, Dennison B, Forbes DL, Glaeser B, Glaser M, Glavovic B, Kremer H, Lange M, Larsen JN, Le Tissier M, Newton A, Pelling M, Purvaja R, Wolanski E (2015) Land-ocean interactions in the coastal zone: Past, present, and future. Anthropocene 12:85–98

Rölfer L, Liconti A, Prinz N, Klöcker CA (2021) Integrated research for integrated ocean management. Front Mar Sci 8:693373

Sarma VVSS, Arya J, Subbaiah ChV, Naidu SA, Gawade L, Praveen Kumar PP, Reddy NPC (2012) Stable isotopes of carbon and nitrogen in suspended matter and sediments from the Godavari estuary. J Oceanogr 68:307–319

Selvaraj K, Lee TY, Yang JYT, Canuel EA, Huang JC, Dai M, Liu JT, Kao SJ (2015) Stable isotopic and biomarker evidence of terrigenous organic matter export to the deep sea during tropical storms. Mar Geol 364:32–42

Song C, Wang G, Sun X, Chang R, Mao T (2016) Control factors and scale analysis of annual river water, sediments and carbon transport in China. Sci Rep 6:25963

Sugimoto R, Honda N, Suzuki T, Ochiai S, Taniguchi M, Nagao S (2014) Effects of submarine groundwater discharge on nutrient concentrations in the western part of Nanao Bay in summer. Boll Jpn Soc Fish Ocanogr 78:114–119 (in Japanese)

Tada R, Irino T, Koizumi I (1999) Land-ocean linkages over orbital and millennial timescales recorded in lake Quaternary sediments of the Japan Sea. Paleoceanography 14:236–247

Takata H, Inatomi N, Kudo N (2020) The contribution of ^{137}Cs export flux from the Tone River Japan to the marine environment. Sci Total Environ 701:134550

Takeuchi K (2010) Rebuilding the relationship between people and nature: the Satoyama Initiative. Ecol Res 25:891–897

Verburg PH, Crossman N, Ellis EC, Heinimann A, Hostert P, Mertz O, Nagendra H, Sikor T, Erb K-H, Golubiewski N, Grau R, Grove M, Konaté S, Meyfroidt P, Parker DC, Chowdhury RR, Shibata H, Thomson A, Zhen L (2015) Land system science and sustainable development of the earth system: a global land project perspective. Anthropocene 12:29–41

Vercruysse K, Grabowski RC, Rickson RJ (2017) Suspended sediment transport dynamics in rivers: multi-scale drivers of temporal variation. Earth Sci Rev 166:38–52

Wallin MB, Weyhenmeyer GA, Bastviken D, Chmiel HE, Peter S, Sobek S, Klemedtsson L (2015) Temporal control on concentration, character, and export of dissolved organic carbon in two hemiboreal headwater streams draining contrasting catchments. J Geophys Res Biogeosci 120:832–846

Watanabe T, Okuyama M, Fukamachi K (2012) A review of Japan's environmental policies for *Satoyama* and *Satoumi* landscape restoration. Glob Environ Res 12:125–135

Yamamoto M, Sakaguchi A, Sasaki K, Hirose K, Igarashi Y, Kim CK (2006) Seasonal and spatial variation of atmospheric ^{210}Pb and ^{7}Be deposition: Features of the Japan Sea side of Japan. J Environ Radioact 86:110–131–1131

Yamamoto Y (1968) The chemical composition of shallow-water deposits of Nanao Bay, Japan. J Oceanogr Soc Jpn 24:94–102

Zhang H, Zhang L, Yang L, Zhou Q, Zhang X, Xing W, Hayakawa K, Toriba A, Tang N (2021) Impact of the COVID-19 outbreak on the ling-range transport of common air pollutants in KUWAMS. Chem Pharm Bull (Tokyo) 69:237–245

Zhang L, Yang L, Zhou Q, Zhang X, Xing W, Zhang H, Toriba A, Hayakawa K, Tang N (2020) Impact of the COVID-19 outbreak on the ling-range transport of particulate PAHs in East Asia. Aerosol Air Qual Res 20:2035–2046

Chapter 2
$PM_{2.5}$ Pollution and Monitoring

Lulu Zhang and Ning Tang

2.1 Overview of $PM_{2.5}$

Air pollution, also known as atmospheric pollution, is defined by the International Organization for Standardization (ISO 2020) as the presence of certain substances in the atmosphere caused by human activities or natural processes at sufficient concentrations and for sufficient periods of time that harm human health and welfare or the environment. Exposure to air pollution can cause serious health consequences. According to the Health Effects Institute (HEI 2020), air pollution was the fourth leading risk factor for death globally in 2019, contributing to 6.67 million deaths worldwide. In addition, $PM_{2.5}$ is the air pollutant that contributes the most to mortality and life loss in all age groups.

2.1.1 Definition

$PM_{2.5}$ is defined as particulate matter with an aerodynamic equivalent diameter equal to or less than 2.5 μm in the air (USEPA 2021), which is finer than 1/20 the diameter of a human hair (Fig. 2.1). $PM_{2.5}$, a mixture of solid and liquid particles of organic and inorganic compounds, can be suspended in the air for a long time and pose a significant impact on air quality, visibility, and radiation budget. The monitoring of $PM_{2.5}$ will expand the understanding of its ambient level and dynamics, through

L. Zhang (✉)
Key Laboratory of Ecological Remediation of Lakes and Rivers and Algal Utilization of Hubei Province, Hubei University of Technology, Wuhan, China
e-mail: zhanglulu@hbut.edu.cn

L. Zhang · N. Tang
Institute of Nature and Environmental Technology, Kanazawa University, Kanazawa, Japan
e-mail: n_tang@staff.kanazawa-u.ac.jp

N. Hasebe et al. (eds.), *Field Work and Laboratory Experiments in Integrated Environmental Sciences*, https://doi.org/10.1007/978-981-99-6532-8_2

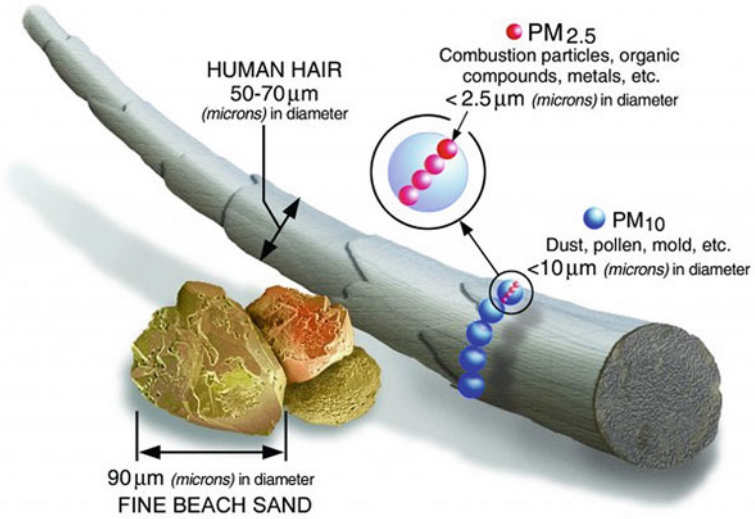

Fig. 2.1 Size comparisons for particulate matter (USEPA 2021)

which we can improve the assessment system of air quality and related health effects, and formulate policies to mitigate air pollution and climate change.

2.1.2 Sources

$PM_{2.5}$ can be directly emitted by a wide variety of man-made activities and natural processes. Man-made sources of $PM_{2.5}$ include industrial processes (such as power generation, metallurgy, petrochemical industries, building construction, textile dyeing and finishing, and cement manufacturing, etc.), agricultural activities (such as cultivation and burning agricultural residues, etc.), household activities (such as sweeping, heating, and cooking, etc.), and transportation (engine exhausts and wear-off from tire, road, and brake). Natural sources include soil dust, volcanic ash, sea salt, pollen, spores, and bacteria. In addition to primary emission sources, gaseous pollutants in the atmosphere can contribute to secondary particle formation through physical and chemical processes, extending the atmospheric lifetime and compositional diversity of $PM_{2.5}$. Moreover, short- and long-range transport of particles in the atmosphere is an important source of $PM_{2.5}$ in downwind areas and the regional atmosphere.

The source of $PM_{2.5}$ not only varies from place to place (urban, suburban, and remote areas), but also depending on the periods in concern (day and night, season, and monitoring duration). Therefore, the source analysis of $PM_{2.5}$ on different time and space scales is an essential part of air monitoring, which is crucial for $PM_{2.5}$ source tracing and pollution control.

2.1.3 Health Impacts

PM_{10} and total suspended particulate are two other particulate indicators of air quality, which are defined as particulate matter with an aerodynamic equivalent diameter equal to or less than 10 μm and 100 μm, respectively.

$PM_{2.5}$ comprises a portion of PM_{10} but differs from PM_{10} in source and composition. Compared with $PM_{2.5}$, the coarser particles in PM_{10} mainly come from mechanical processes (WHO 2021), such as construction, road, and natural dust, thus rich in inorganic components.

PM_{10} is known as inhalable particulate matter that can enter the respiratory system through the nose and mouth. Due to the smaller size, $PM_{2.5}$ can reach the end of the bronchioles after being inhaled and further penetrate through the respiratory system into the blood circulatory system, causing a variety of respiratory diseases and cardiovascular diseases. Moreover, the longer residence time and transport distance in the atmosphere allow $PM_{2.5}$ to produce environmental and health impacts on larger temporal and spatial scales.

In addition, the composition of $PM_{2.5}$ is complex (Liang et al., 2016), including sulfates, nitrates, ammonium salts, metal elements, elemental carbon, and organic carbon, many of which are toxic and harmful (such as polycyclic aromatic hydrocarbons, etc.). $PM_{2.5}$ can act as a carrier for these substances to enter the human body and pose health risks. Therefore, $PM_{2.5}$ is considered to be a more significant environmental risk factor for human health than coarser particles and has been shown to increase the risk of death from cerebrovascular disease, lung cancer, and chronic respiratory diseases globally (Ghosh et al., 2021).

The World Health Organization (WHO) has developed guideline values (Table 2.1) for particulate matter in an effort to reduce particle concentrations to levels with minimal health effects (WHO 2006) and updated the thresholds in 2021 to protect the health and welfare of more people around the world (WHO 2021). In these guidelines, interim targets are proposed as incremental steps in a progressive reduction of air pollution and are intended for use in areas where pollution is high (WHO 2006). Interim targets are air pollutant concentrations associated with a specific decrease in health risk. If these interim targets were to be achieved, one could expect significant reductions in risks for acute and chronic human health effects from air pollution. However, progress toward the guideline values remains the ultimate objective of air quality management and health risk reduction in all areas.

2.2 $PM_{2.5}$ Monitoring Methods

In order to objectively reflect air quality and protect human health, it is necessary to systematically monitor the concentration, variation trend, and time–space distribution of $PM_{2.5}$. This chapter will introduce the $PM_{2.5}$ monitoring methods commonly

Table 2.1 WHO air quality guidelines (AQG) and interim targets (IT) for $PM_{2.5}$ and PM10 (WHO 2006, 2021)

Document	WHO AQG (2021)					WHO AQG (2006)		
Pollutant	$PM_{2.5}$		PM_{10}		$PM_{2.5}$		PM_{10}	
Averaging time	Annual	24-h	Annual	24-h	Annual	24-h	Annual	24-h
IT-1 (μg/m^3)	35	75	70	150	35	75	70	150
IT-2 (μg/m^3)	25	50	5	100	25	50	50	100
IT-3 (μg/m^3)	15	37.5	30	75	15	37.5	30	75
IT-4 (μg/m^3)	10	25	20	50	–	–	–	–
AQG level (μg/m^3)	5	15	15	45	10	25	20	50

used around the world today (ACAP 2014; Bai et al. 2017; Quincey and Butterfield 2009; WHO 2005).

2.2.1 Manual Monitoring

Manual monitoring, i.e., the gravimetric method, is the most accurate approach to directly measure the mass of $PM_{2.5}$. Briefly, a sampler equipped with a filter of known weight is used to extract a certain volume of air at a constant flow rate, and $PM_{2.5}$ in the air sample is trapped on the filter after going through the impactor or cyclone (a separation device that effectively removes particles larger than 2.5 μm in size). Based on the weight difference of the filter before and after sampling and the actual volume of the air collected, the $PM_{2.5}$ concentration during the sampling period can be calculated.

The gravimetric method is believed to provide results with high accuracy and reliability due to its simple principle and is independent of the shape, size, and color of the particles. In addition, various chemical analyzes can be applied to the sampling filter following the gravimetric measurement of $PM_{2.5}$, which is an important aspect for scientific research and comprehensive evaluation of the $PM_{2.5}$ properties.

However, the gravimetric method has some limitations: (1) requires many manual operation steps (such as filter preparation, weighing, replacement, instrument calibration, etc.), which are labor-intensive, time-consuming, and costly; (2) artificial errors are inevitable in the monitoring, some of which are not traceable; (3) the monitoring results cannot be read in time and cannot reflect the $PM_{2.5}$ concentration in fine time intervals. These deficiencies limit the timely release and evaluation of

$PM_{2.5}$ pollution with a high temporal and spatial resolution by regulatory agencies and scientific research departments.

2.2.2 Automatic Monitoring

To meet the demands of improving time resolution and timeliness of $PM_{2.5}$ monitoring, automatic monitoring has been developed as the complementary method of manual monitoring, mainly including β-ray attenuation method and tapered element oscillating microbalance (TEOM) method.

The β-ray attenuation method indirectly measures the mass of $PM_{2.5}$ based on the attenuation ability of $PM_{2.5}$ to β-rays. In the automatic monitor, a ^{14}C source is employed to irradiate the blank filter and detect the intensity of the β-rays through the filter. The air is then pumped at a constant flow rate, and $PM_{2.5}$ is trapped on the filter after the air sample passes the impactor (or cyclone). The difference in the β-ray intensity between the blank filter and the filter loaded with $PM_{2.5}$ is detected to determine the β-ray attenuation, and the mass of $PM_{2.5}$ collected during the sampling period can be calculated accordingly.

The principle of the TEOM method is different from that of the β-ray attenuation method and more similar to the gravimetric method. The automatic monitor is equipped with a mass sensor inside, which contains a conical glass tube that oscillates with a fixed amount of energy through two tiny oscillating electrodes. A small filter is placed on the top of the conical glass tube to collect $PM_{2.5}$. During sampling, the accumulation of $PM_{2.5}$ alters the mass of the filter and hence the oscillation frequency of the conical glass tube. Based on these changes, the mass of $PM_{2.5}$ collected within the sampling period can be calculated.

For monitoring based on β-ray attenuation and TEOM methods, the sampling unit should be heated above the air dew point in order to prevent the influence of moisture condensation in the sampling. In addition, the entire measurement should be performed under constant temperature and humidity. The heating process can cause the loss of volatile and semi-volatile substances in $PM_{2.5}$, leading to an underestimation of the mass of $PM_{2.5}$. Nevertheless, the loss of volatile and semi-volatile substances can be corrected by installing a compensation device (such as a dynamic heating system and filter dynamics measurement system) to ensure the reliability of the results.

Compared with manual monitoring, automatic monitoring has the advantages of unattended operation, timely reading, and labor-saving. After strict comparison with the gravimetric results, β-ray attenuation and TEOM methods are able to provide accurate and reliable measurement results, which can meet the requirements of some scientific research and environmental regulation. In addition, despite the low maintenance cost of the β-ray attenuation method, the measurement has a relatively low time resolution (in hours). In contrast, the TEOM method can provide real-time data with high accuracy at the minute resolution but requires high equipment and maintenance costs.

Combining automatic monitoring with information technology and the Internet can build an automatic online monitoring system for $PM_{2.5}$. Based on the system, monitoring data can be timely transmitted to the data platform via the network to support the monitoring, evaluation, and early warning of $PM_{2.5}$ pollution by regulation departments. Moreover, the online platform enables the public to check the $PM_{2.5}$ concentration and air quality within a certain time and space range.

2.2.3 Portable Monitoring

In addition to the above three methods, the light scattering method is an emerging new method to monitor $PM_{2.5}$ (Koehler and Peters 2015) using a relatively low-cost sensor. The method employs a laser source to irradiate the collected $PM_{2.5}$ in the airflow, causing light scattering. The signal of scattered light, including the detection frequency and light intensity, is received by the photoelectric conversion element in a certain direction. The detection frequency and intensity of scattered light represent the number and size of particles, respectively. Through the laser scattering method, the number concentration of $PM_{2.5}$ can be directly counted to calculate the mass concentration of $PM_{2.5}$.

Since the laser scattering method measures the number of $PM_{2.5}$ rather than the mass, its results are essentially different from the previous methods and cannot be used as an equivalent method in environmental research and monitoring. Owing to the convenience and efficiency of the laser scattering method, it is commonly applied by portable monitors to perform safety detection on $PM_{2.5}$ in fixed environments, such as homes and workshops.

As summarized in Table 2.2, each of these monitoring methods has its own pros and cons. Therefore, it is necessary to select an appropriate method to measure $PM_{2.5}$ concentration based on multiple factors.

2.3 Application of $PM_{2.5}$ Monitoring

Our research team has been conducting large-scale monitoring and analysis of air pollutants in East Asia since 1997. The following two cases are taken from our recent research to illustrate the application of manual monitoring and automatic online monitoring of $PM_{2.5}$.

Table 2.2 Comparison of merits and demerits of commonly used $PM_{2.5}$ monitoring methods

Category	Manual monitoring	Automatic monitoring		Portable monitoring
Principle	Gravimetry	β-ray attenuation	Oscillating microbalance	Light scattering
Advantages	High accuracy, reliability, and stability of measurement; compatible with chemical analysis	Low maintenance cost	High time resolution	Convenient and instant to measure; easy to handle and carry; low working noise; low implementation cost
		Convenience, timeliness, accuracy, and reliability of measurement; supports online data sharing		
Disadvantages	Labor-intensive, time consuming, high filter cost, low time resolution	Relatively low time resolution	High equipment and maintenance costs	Low accuracy, reliability, and stability of measurement

2.3.1 *$PM_{2.5}$ Inside and Outside a Primary School Classroom in Beijing*

To assess the health risks of children exposed to $PM_{2.5}$ in the classroom, we measured $PM_{2.5}$ inside and outside a primary school classroom in Beijing, China based on manual monitoring methods, and examined its chemical composition (Zhang et al. 2019, 2020a).

$PM_{2.5}$ samples were collected using parallel low-volume (1.5 L/min) aerosol samplers (MP-ΣNII300, Sibata Scientific Technology LTD, Saitama, Japan) on Teflon filters (T60A20, Pallflex Products Corp., Pall Japan, Tokyo, Japan) and quartz fiber filters (2500QAT-UP, Pallflex Products, Putnam, CT, US), respectively. The Teflon filters were used for gravimetric analysis and inorganic analysis, and the quartz fiber filters were used for organic analysis. The $PM_{2.5}$ inside and outside the classroom was sampled simultaneously in the heating and non-heating periods following the same protocol. The sampler for outdoor $PM_{2.5}$ collection was placed on the balcony outside the classroom, 0.5 m from the wall. The sampler for indoor $PM_{2.5}$ collection was placed at the front of the classroom, 1 m above the floor. Chemical components include nine water-soluble ions, carbonaceous components (organic carbon and elemental carbon), eleven polycyclic aromatic hydrocarbons (PAHs), and ten nitro-PAHs (NPAHs) of each $PM_{2.5}$ sample were analyzed.

The average concentrations (± standard deviations) of $PM_{2.5}$ outside the classroom were 89.5 ± 36.7 $\mu g/m^3$ and 80.2 ± 23.4 $\mu g/m^3$ during the heating and non-heating periods (Fig. 2.2), respectively. Indoor $PM_{2.5}$ showed lower levels than outdoor values, which were 81.1 ± 35.8 $\mu g/m^3$ and 71.4 ± 34.0 $\mu g/m^3$ during the heating and non-heating periods (Fig. 2.2), respectively. Comparing with the Air Quality Guidelines released by WHO (2006), the average levels of both indoor and

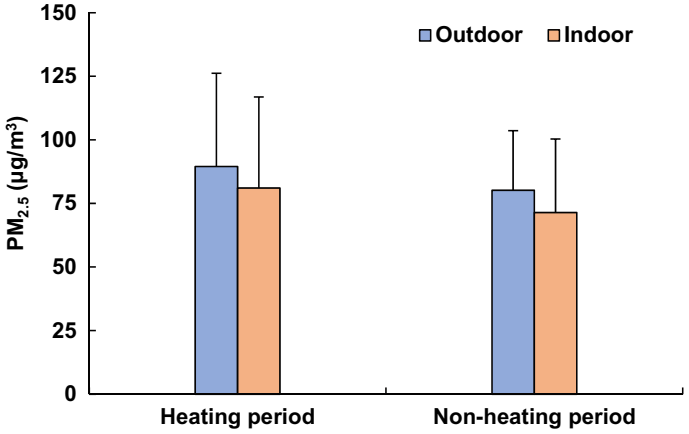

Fig. 2.2 Average concentrations of outdoor and indoor $PM_{2.5}$ during the heating and non-heating periods

outdoor $PM_{2.5}$ during the heating and non-heating periods were several times higher than the health-based guidance value (2.5 $\mu g/m^3$). In addition, a positive correlation was found between indoor and outdoor $PM_{2.5}$ ($r = 0.97$, $p < 0.01$). Since there were no obvious sources in the classroom, indoor $PM_{2.5}$ essentially depended on the input of outdoor $PM_{2.5}$ during both periods.

Based on the results of chemical analysis, ionic and carbonaceous components mainly constituted indoor and outdoor $PM_{2.5}$ during both periods. Consistent with the concentration of $PM_{2.5}$, most of its composition showed a strong indoor and outdoor correlation, confirming the essential impact of outdoor pollution sources on $PM_{2.5}$ inside the classroom. The source analysis of water-soluble ions, carbonaceous components, PAHs, and NPAHs showed that outdoor $PM_{2.5}$ was primarily affected by vehicle exhaust and coal combustion during the heating period and was characterized by secondary formation and traffic emission during the non-heating period.

The results of this research highlight that the children in the typical Chinese city were exposed to severe outdoor and indoor $PM_{2.5}$ pollution in primary school. These findings suggest that it is necessary to reduce the emission of outdoor pollution sources and the input of outdoor $PM_{2.5}$ indoors to alleviate the concentration of $PM_{2.5}$ in the classroom and its health risks to children.

2.3.2 Long-Term Monitoring of $PM_{2.5}$ at KUWAMS

Kanazawa University Wajima Air Monitoring Station (KUWAMS: 37.4°N, 136.9°E; 60 m above sea level) run by the Institute of Nature and Environmental Technology of Kanazawa University is located on the Noto Peninsula in western Japan (Fig. 2.3) and 2.1 km from the coastline of the Sea of Japan. This background observatory was

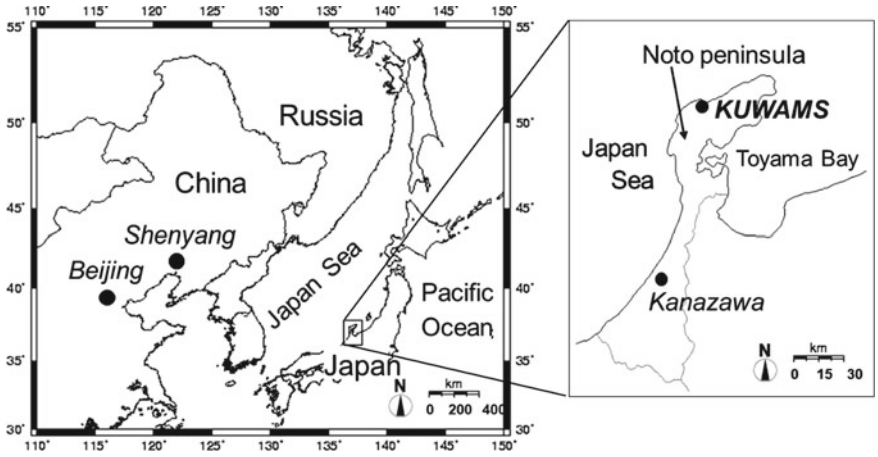

Fig. 2.3 Location of KUWAMS (Tang et al. 2014)

established to investigate the effects of air pollutants originating in the Asian continent on air quality and public health in Japan, as well as the physical and chemical changes of these pollutants during long-range transport (Tang et al. 2005, 2014, 2015; Yang et al. 2018, 2020; Zhang et al. 2020b, 2020c; Zhou et al. 2020). KUWAMS is equipped with completed automatic monitoring systems for air pollutants and air samplers for manual monitoring and chemical analysis, which provides an advanced air monitoring platform that allows researchers in Japan and abroad to collaborate on atmospheric observations and facilitate data sharing.

Our research team has been continuously monitoring $PM_{2.5}$ concentration at KUWAMS since 2016 by using particulate matter monitor PM-714 (Kimoto Electric Co. Ltd., Osaka, Japan) based on the β-ray attenuation method with a flow rate of 16.7 L/min (Zhang et al. 2020c). $PM_{2.5}$ is collected on a fluororesin tape filter and measured every hour, and the output hourly value is guaranteed high accuracy and stability. The concentration of $PM_{2.5}$ on different time scales can be calculated based on the Manual for Continuous Monitoring of Air Pollution of Japan. The automatic monitoring systems are maintained monthly and exhaustively examined by professionals every year.

Figure 2.4 presents the annual, seasonal, monthly, and diurnal variations in $PM_{2.5}$ concentration at KUWAMS from April 2016 to August 2019. The average annual concentration of $PM_{2.5}$ changed little between 2016 and 2019 (Fig. 2.4a), fluctuating around the annual standard for Japan (15 $\mu g/m^3$). However, the large standard deviation indicates the change in $PM_{2.5}$ concentration over a year.

From the seasonal perspective, $PM_{2.5}$ concentration was higher in spring, followed by summer, and lower in fall and winter (Fig. 2.4b). Further analysis of the monthly profile (Fig. 2.4c) suggests the influence of the East Asian monsoon on the variation of $PM_{2.5}$ at KUWAMS. Asian dust prevails from March to May each year, which is also in the East Asian winter monsoon period (November to May of the following

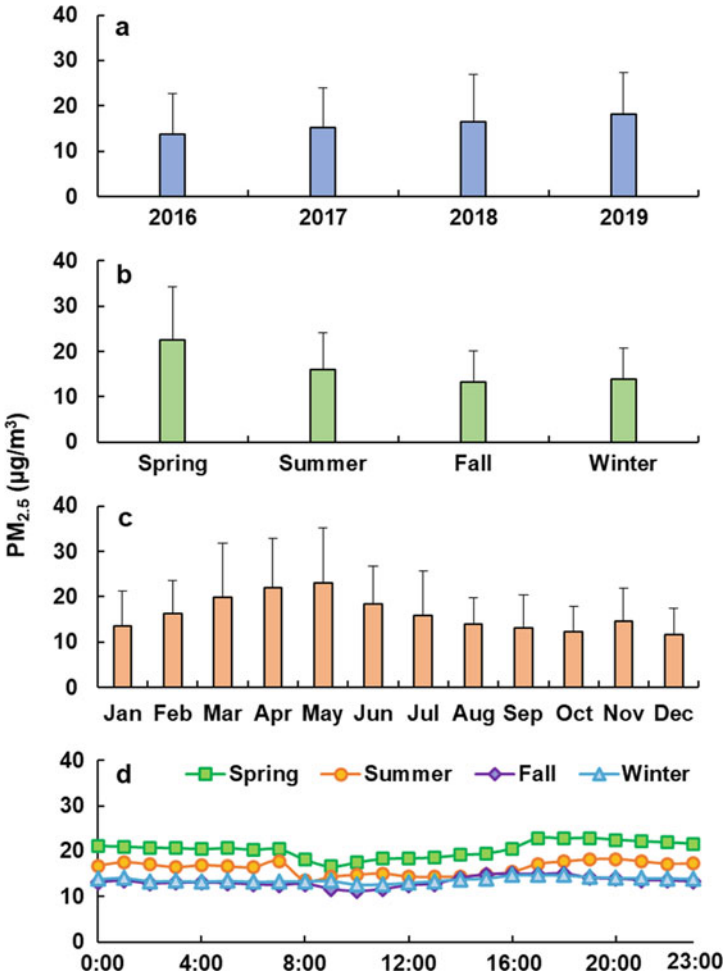

Fig. 2.4 **a** Annual, **b** seasonal, **c** monthly, and **d** diurnal variations in $PM_{2.5}$ concentration at KUWAMS from April 2016 to August 2019

year). Therefore, dust aerosols from the Asian continent were responsible for the increase in $PM_{2.5}$ concentration at KUWAM in spring. Since then, during the East Asian summer monsoon (June to October), the air masses arriving at KUWAMS mostly originated in the oceans to the south and west of Japan (Zhou et al. 2020), causing a decrease in $PM_{2.5}$ concentration. After switching to the next East Asian winter monsoon, the $PM_{2.5}$ concentration at KUWAMS increased again due to the transport of polluted aerosols from the Asian continent.

In addition, the local meteorological conditions and gaseous compositions suggested that the enhanced solar radiation and ozone concentration in spring, as well as the high temperature and radiation in summer created favorable conditions

for atmospheric chemical processes, which possibly promoted the generation of secondary $PM_{2.5}$ and increase the concentration of $PM_{2.5}$.

Diurnal variation in $PM_{2.5}$ concentration at KUWAMS was observed seasonally (Fig. 2.4d). The obvious diurnal variation of weather in spring and summer could cause $PM_{2.5}$ to accumulate at night and diffuse or decompose during the day. In comparison, the $PM_{2.5}$ concentration and weather conditions changed little from day to night in fall and winter. In addition to meteorological factors, emission sources have a greater influence on the variation of $PM_{2.5}$ (Tang et al. 2014, 2015), which needs to be discussed based on detailed analysis such as chemical composition and model calculation.

References

Asia Center for Air Pollution Research, Japan Environmental Sanitation Center (2014) Monitoring of $PM_{2.5}$ experience in Japan. https://www.acap.asia/en/publications-acap/. Accessed 16 Nov 2021

Bai ZP, Han JB, Azzi M (2017) Insights into measurements of ambient air $PM_{2.5}$ in China. Trends Environ Anal Chem 13:1–9. https://doi.org/10.1016/j.teac.2017.01.001

Ghosh R, Causey K, Burkart K, Wozniak S, Cohen A, Brauer M (2021) Ambient and household $PM_{2.5}$ pollution and adverse perinatal outcomes: A meta-regression and analysis of attributable global burden for 204 countries and territories. PLoS Med 18:e1003718. https://doi.org/10.1371/journal.pmed.1003718

International Organization for Standardization (2020) ISO 422.5:2020(E) air quality—General aspects—vocabulary. Switzerland

Koehler KA, Peters TM (2015) New methods for personal exposure monitoring for airborne particles. Curr Environ Health Rep 2:399–411. https://doi.org/10.1007/s40572-015-0070-z

Liang CS, Duan FK, He KB, Ma YL (2016) Review on recent progress in observations, source identifications and countermeasures of $PM_{2.5}$. Environ Int 86:150–170. https://doi.org/10.1016/j.envint.2015.10.016

Quincey P, Butterfield D (2009) Ambient air particulate matter PM_{10} and $PM_{2.5}$: developments in European measurement methods and legislation. Biomarkers 14(1):34–38. https://doi.org/10.1080/13547500902965484

Tang N, Hattori T, Taga R, Igarashi K, Yang XY, Tamura K, Kakimoto H, Mishukov VF, Toriba A, Kizu R, Hayakawa K (2005) Polycyclic aromatic hydrocarbons and nitropolycyclic aromatic hydrocarbons in urban air particulates and their relationship to emission sources in the Pan-Japan Sea countries. Atmos Environ 39:5817–5826. https://doi.org/10.1016/j.atmosenv.2005.06.018

Tang N, Sato K, Tokuda T, Tatematsu M, Hama H, Suematsu C, Kameda T, Toriba A, Hayakawa K (2014) Factors affecting atmospheric 1-, 2-nitropyrenes and 2-nitrofluoranthene in winter at Noto peninsula, a remote background site, Japan. Chemosphere 107:324–330. https://doi.org/10.1016/j.chemosphere.2013.12.077

Tang N, Hakamata M, Sato K, Okada Y, Yang XY, Tatematsu M, Toriba A, Kameda T, Hayakawa K (2015) Atmospheric behaviors of polycyclic aromatic hydrocarbons at a Japanese remote background site, Noto peninsula, from 2004 to 2014. Atmos Environ 120:144–151. https://doi.org/10.1016/j.atmosenv.2015.08.090

United States Environmental Protection Agency (2021) Particulate Matter (PM) basics. https://www.epa.gov/pm-pollution/particulate-matter-pm-basics. Accessed 16 Nov 2021

World Health Organization, Regional Office for Europe (2005) Review of methods for monitoring of $PM_{2.5}$ and PM_{10}: report on a WHO workshop, Berlin, Germany 11–12 October 2004.

Copenhagen: WHO Regional Office for Europe. https://apps.who.int/iris/handle/10665/107640. Accessed 16 Nov 2021

World Health Organization. Occupational and Environmental Health Team (2006) WHO Air quality guidelines for particulate matter, ozone, nitrogen dioxide and sulfur dioxide: global update 2005: summary of risk assessment. World Health Organization. https://apps.who.int/iris/handle/10665/69477. Accessed 16 Nov 2021

World Health Organization (2021) WHO global air quality guidelines: particulate matter ($PM_{2.5}$ and PM_{10}), ozone, nitrogen dioxide, sulfur dioxide and carbon monoxide. World Health Organization. https://apps.who.int/iris/handle/10665/345329. Accessed 16 Nov 2021

Yang L, Tang N, Matsuki A, Takami A, Hatakeyama S, Kaneyasu N, Nagato EG, Sato K, Yoshino A, Hayakawa K (2018) A comparison of particulate-bound polycyclic aromatic hydrocarbons long-range transported from the Asian continent to the Noto Peninsula and Fukue Island, Japan. Asian J Atmos Environ 12:369–376. https://doi.org/10.5572/ajae.2018.12.4.369

Yang L, Zhang LL, Zhang H, Zhou QY, Zhang X, Xing WL, Takami A, Sato K, Shimizu A, Yoshino A, Kaneyasu N, Matsuki A, Hayakawa K, Toriba A, Tang N (2020) Comparative analysis of $PM_{2.5}$-bound polycyclic aromatic hydrocarbons (PAHs), nitro-PAHs (NPAHs), and water-soluble inorganic ions (WSIIs) at two background sites in Japan. Int J Environ Res Public Health 17:8224. https://doi.org/10.3390/ijerph17218224

Zhang LL, Morisaki H, Wei, YJ, Li Z, Yang L, Zhou QY, Zhang X, Xing WL, Hu M, Shima M, Toriba A, Hayakawa K, Tang N (2019) Characteristics of air pollutants inside and outside a primary school classroom in Beijing and respiratory health impact on children. Environ Pollut 255(1): 113147. https://doi.org/10.1016/j.envpol.2019.113147

Zhang LL, Morisaki H, Wei, YJ, Li Z, Yang L, Zhou QY, Zhang X, Xing WL, Hu M, Shima M, Toriba A, Hayakawa K, Tang N (2020a) $PM_{2.5}$-bound polycyclic aromatic hydrocarbons and nitro-polycyclic aromatic hydrocarbons inside and outside a primary school classroom in Beijing: concentration, composition, and inhalation cancer risk. Sci Total Environ 705:135840. https://doi.org/10.1016/j.scitotenv.2019.135840

Zhang LL, Yang L, Zhou QY, Zhang X, Xing WL, Zhang H, Toriba A, Hayakawa K, Tang N (2020b) Impact of the COVID-19 outbreak on the long-range transport of particulate PAHs in East Asia. Aerosol Air Qual Res 20:2035–2046. https://doi.org/10.4209/aaqr.2020.07.0388

Zhang X, Zhang LL, Yang L, Zhou QY, Xing WL, Toriba A, Hayakawa K, Wei YJ, Tang N (2020c) Characteristics of polycyclic aromatic hydrocarbons (PAHs) and common air pollutants at Wajima, a remote background site in Japan. Int J Environ Res Public Health 17:957. https://doi.org/10.3390/ijerph17030957

Zhou QY, Zhang LL, Yang L, Zhang X, Xing WL, Hu M, Chen B, Han C, Toriba A, Hayakawa K, Tang N (2020) Long-term variability of inorganic ions in TSP at a remote background site in Japan (Wajima) from 2005 to 2015. Chemosphere 264:128427. https://doi.org/10.1016/j.chemosphere.2020.128427

Chapter 3
Importance of Particulate Matter in Cloud Formation

Yayoi Inomata and Atsushi Matsuki

3.1 Introduction

The earth reflects about a third of incoming solar radiation back to space. Such reflectivity or albedo of the earth is in large part governed by the bright clouds covering vast areas of the earth's surface at any time and place. The cloud is generally a mass of water droplets (and/or ice crystals). However, water vapor alone cannot initiate nucleation and growth of water droplets. Clouds can only exist with the help of pre-existing atmospheric particles that initially provide a surface for water condensation. A subset of particles that act as the seeds of droplets are called cloud condensation nuclei (CCN).

According to an Intergovernmental Panel on Climate Change (IPCC) report, increases in atmospheric particles (particulate matter or aerosols) cause a net reduction in the global atmospheric temperature, but with large uncertainty. A better understanding of the ability of atmospheric particles to form clouds (CCN activity) is crucial for the reduction of such uncertainty and precisely projecting the ongoing global warming, thereby, providing solid, scientific-based, policy-relevant future scenarios. Possible factors causing the large uncertainty can be related to the (1) chemical composition (i.e., water solubility), and (2) physical properties (i.e., number and size) of atmospheric particles.

Currently, the mass concentration of aerosols shown in terms of fine particles with an aerodynamic diameter of 2.5 μm or less ($PM_{2.5}$) is employed as an indicator of the air quality in many countries. For example, in Japan, the environmental criteria for $PM_{2.5}$ are 35 μg m^{-3} for 1-day average values and 15 μg m^{-3} for annual average values. However, it must be emphasized that $PM_{2.5}$ is only a measure of the total weight of the bulk of fine particles, and it does not tell us anything about what the particles are made of, and how many particles were there in different sizes. Such

Y. Inomata (✉) · A. Matsuki
Institute of Nature and Environmental Technology, Kanazawa University, Kanazawa, Japan
e-mail: yinomata@se.kanazawa-u.ac.jp

N. Hasebe et al. (eds.), *Field Work and Laboratory Experiments in Integrated Environmental Sciences*, https://doi.org/10.1007/978-981-99-6532-8_3

detailed chemical and physical properties of aerosols are exactly what determines the CCN activity of the particle population.

The reason why the aerosol–cloud interaction and its related climate impact remain the major source of uncertainty is partly due to the complexity of the mentioned factors that control the CCN activity. This is further complicated by the fact that aerosol chemical and physical properties vary significantly through time and space, depending on emission sources (both natural and anthropogenic), as well as modifications during transport in the atmosphere.

3.2 The Factors Controlling the CCN Activity of Atmospheric Particles

The amount of water vapor that can be stored in a given volume of air is a function of the temperature alone, and it is independent of the presence of other gases. It is called the saturation vapor pressure e_s expressed in hPa (or saturation vapor density in $\mu g\ m^{-3}$), which increases exponentially with temperature.

The relative humidity (RH, %) is expressed as the percentage of the ratio of ambient vapor pressure e over e_s. When e is equal to e_s, the air is saturated with water vapor and RH is at 100%, meaning that the water vapor is in equilibrium with the liquid water surface in contact. In such cases, the number of molecules that jumps in and out of the water surface at a given time remains constant (i.e., evaporation and condensation are balanced). But this is true only when the water surface is entirely flat.

Typical size of a cloud droplet is only 10 μm in diameter, and the initial droplet size is even smaller. This means that the droplet surface has a steep curvature. This makes water molecules in small droplets more prone to evaporation than from flat surfaces and requires even higher water vapor pressure (supersaturation, RH > 100%) to avoid evaporation. This is the so-called Kelvin curvature effect.

The Kelvin effect works more strongly on smaller droplets, so one may expect that newly born, minute droplets would instantly evaporate and not be able to survive to grow into clouds. What if, the small droplet was not composed of pure water but contained dissolved solutes? The Raoult's chemical law would tell us that the saturated water vapor pressure over a solution is always lower than the pressure of pure water and decreases proportionally to the mole fraction of a solute in the solution. Such depression of vapor pressure would act in opposition to the Kelvin effect and provide a higher chance for the droplets to survive in the atmosphere.

The salt particles made for example of NaCl or $(NH_4)_2SO_4$ deliquesce at higher relative humidity (RH > 80%) and their surface can be considered as highly concentrated solution. Such particles can dramatically reduce the water vapor pressure over the particle firstly by Raoult's effect, and secondary by the reduced Kelvin effect through its original size and further hygroscopic growth. This is exactly why a certain particle would act as CCN and is essential for the nucleation and growth of cloud

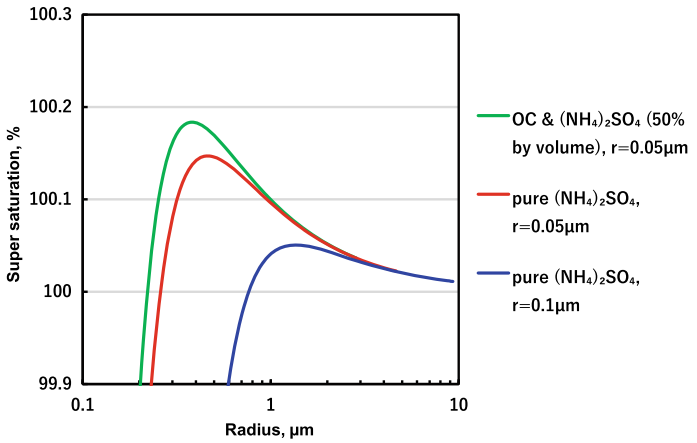

Fig. 3.1 Wet particle (droplet) radius as a function of water vapor supersaturation for pure $(NH_4)_2SO_4$ and its organic mixture (50% Organic Carbon by volume) with different dry starting radii (i.e., r = 0.05, 0.1 μm). The hygroscopicity parameter of OC was assumed as 0.2 (Petters and Kreidenweis 2007)

droplets under atmospherically relevant supersaturation conditions (RH < 101%). Figure 3.1. shows the level of supersaturations required for particles of different dry sizes (r = 0.05, 0.1 μm) and composition (i.e., hygroscopicity) to overcome the Kelvin effect and activate into water droplets. This curve (Köhler curve) is a balance between the competing Kelvin and Raoult's effects. It can be seen that the larger particle of the same composition (hygroscopicity) requires smaller supersaturation and is more prone to be activated as a cloud droplet. On the other hand, organic compounds, in general, are less hygroscopic, and their mixing with water-soluble inorganic species would require higher supersaturation for the particle to act as CCN.

Therefore, it is highly relevant to know the chemistry (water-soluble component), as well as the number concentration of particles in different sizes for precisely predicting the CCN concentration and hence the aerosol climate impact. We will now explore how such properties are being investigated.

3.3 Sampling Techniques of Atmospheric Particles

When it comes to collecting atmospheric particles, there are many issues related to sampling techniques, such as particle size separation, inlet aspects, sampling medium, sampler setup location, airflow measurement, and sampling frequency.

To implement efficient aerosol sampling, several points should be considered.

- Uncombined water should be removed from the sampled atmospheric particles.
- Atmospheric particles should be collected under minimal diffusion and without inertial losses in the sampling line.

- Atmospheric particles should be collected at a lower relative humidity (<40%) because the relative humidity strongly influences the size of atmospheric aerosols.
- Evaporation of volatile species in the collected atmospheric particles requires consideration.
- The aerosol instrument should be set in a box while maintaining the temperature between 15 °C and 30 °C.

In this section, common sampling methods, followed by analytical methods for chemical species, are briefly described.

3.3.1 Sampling Location and Inlet System

Air samples should be guided into the laboratory through a vertical stack with an inlet that is high enough above the ground level to minimize local influences. At sites without surrounding obstructive buildings, it is recommended to set the air sampler at the roof of the laboratory with a minimum height of 2–3 m. In the case of an air sampler set on the ground surface, the intake points of automatic instruments should occur 5 to 10 m above the ground without obstructions occurring around the sites. The distance from the air inlet to the atmospheric particle collection part (filter) should be smaller than 5 m.

The particle cut-off size of the atmospheric particle sampler is also important. The most widely employed cut-off sizes are PM_{10}, $PM_{2.5}$, and PM_1, which denote aerodynamic diameters of 10, 2.5, and 1 μm, respectively. Atmospheric particle size separation is generally conducted with an impactor or a cyclone.

3.3.2 Atmospheric Particle Collection System

Figure 3.2 shows a typical atmospheric particle collection system. The atmospheric particle collection system consists of a sampling inlet, size separation, denuder, filter, flow meter and/or mass flow controller, and pump. Furthermore, it is necessary to monitor the temperature and air pressure. In general, because the sampling system is installed outdoors, the apparatus is loaded in a protective box. It is desired that the temperature in the protection box remain at ±5 °C relative to the ambient air temperature to prevent evaporation of volatile species.

The ambient air inlet causes to loss of atmospheric particles due to collisions with the inlet wall. The fluctuation of the flow rate should be within ±4% of the set value over 24 h. To prevent the inflow of precipitation into the sampling line, a cover should be placed on top of the inlet system. The inlet and atmospheric particle separation systems are made from weather-resistant materials such as stainless steel, aluminum alloy, and anodized alumina.

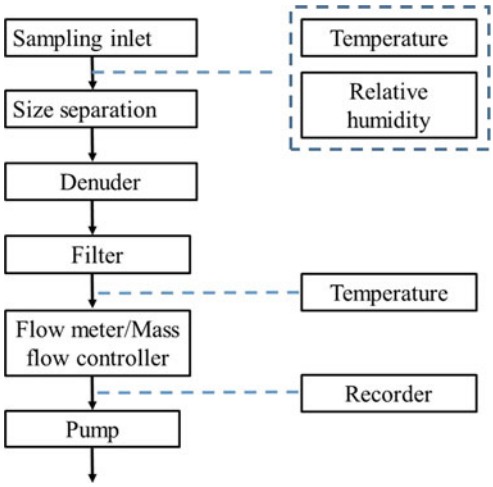

Fig. 3.2 Schematic diagram of the atmospheric particle-collecting sampler

There are several types of atmospheric particle size segregation, such as impaction, cyclone, and virtual impaction systems. These atmospheric particle separation systems should be cleaned with ultrapure water, ethanol, and acetone every 1–2 weeks. Sampling information, such as the air sampling volume, sampling start date and time, sampling end date and time, instantaneous flow, and integrated air volume, should be recorded.

During atmospheric particle sampling, several collected species experience adsorption and/or evaporation under the influence of reactive gases. To prevent the above artifacts during atmospheric particle sampling, a denuder is usually employed to remove reactive gases.

A diaphragm pump is recommended to ensure stable flow rates during sampling. Mass flow meters or mass flow controllers are recommended to measure the air volume. These devices measure the mass of air passing through a sensor, such as heat conductance measurements. The sensor should be periodically calibrated against known standards.

Mass flow meters should be adopted to avoid the effect of lower atmospheric pressures, especially at high-altitude sites located on mountains. A mass flow meter/mass flow controller should be installed between the filter holder and the pump. Gas volume meters containing flow rate meters (of the float type) are also acceptable. These meters should be calibrated under standard atmospheric pressure conditions. The air volume should be reported under the standard temperature and pressure conditions of 273.15 K and 1013.2 hPa, respectively.

3.3.3 Collection of Atmospheric Particles

To analyze the chemical species in atmospheric particles, filters should be selected by considering analytical methods, pretreatment methods, and the amount of chemical species. Furthermore, it is necessary to consider the following: (1) the collection efficiency of the filter against 0.3-μm particles should be higher than 99.9%, (2) low chemical reactivity, and (3) sufficient strength for filter analysis. In the case of measuring the mass concentrations of atmospheric particles, the chargeability of the filter should also be considered. In aerosol sampling and analysis, many kinds of filters, such as cellulose fibers, polytetrafluoroethylene (PTFE), glass fibers, quartz fibers, polystyrene fibers, membranes, and capillary pores, are employed. These filters are selected depending on the analytical technique and chemical composition. Table 3.1 summarizes the features of PTFE and glass fiber filters, which are generally implemented to collect atmospheric particles.

In addition to sampling filters, blanks such as blank filters, travel blank filters, and field blank filters should be prepared. A blank value should be determined as the median of analytical results of 3–5 blank filters. Blank filters are used to determine the content of the target species originally in the sampling filters without any operations. Travel blank filters should be transported to the sampling site together with the sampling filters and returned to the laboratory. The container with travel blank filters inside should remain open when the sample filter is placed in the sampler. The number of travel blank filters accounts for approximately 10% of that of the sampling filter. A travel blank is estimated to be the median value of three travel blank filter values for the target species. Field blanks are treated in the same procedure with sample

Table 3.1 Characteristics of PTFE and glass fiber filters. The table was adopted from MOEJ (2019) with modifications

Filter	PTEF	Glass fiber filers
Species	Inorganic elements Ion species Water soluble organic carbon PAH Mass concentrations	Ion species Carbon Water soluble organic carbon Levoglucosan PAH
Filter handling	When mass concentrations are measured, filters with support are easily treated	Filter strength is weak
Hygroscopic	Smaller	Larger
Measurement of mass weight concentration	Need to remove static electricity	Relative humidity can influence the measurements
Impurities	Relatively few	Inorganic elements, including the filter, and the adsorption of volatile organic species
Strength of filter	Large	Small

MOEJ: Ministry of Environment, Government of Japan

filters, i.e., transported to the sampling site and only placed in the sampling device without sampling. A field blank is prepared with at least three samples.

In most monitoring organizations, weekly or daily sampling is recommended. It is also considered that sampling should be conducted continuously throughout the year.

After sampling, samples need to be stored at a temperature lower than 4 °C. It is necessary to consider (i) minimizing the transportation time and (ii) cooling (refrigerating) the samples during transportation. Samples arriving at the laboratory should be stored in a refrigerator, and analysis should be performed as soon as possible.

3.3.4 Analysis of Mass Concentration of Aerosol Particles

There are various items analyzed using aerosol samples collected with filters. For example, in the case of the Ministry of Environment, Government of Japan (MOEJ) program, the mass concentration, major ion species, elementary carbon (EC), organic carbon (OC), and trace metals, in $PM_{2.5}$ are analyzed. Among these, the mass concentration of atmospheric particles is a fundamental parameter because the air quality is first considered based on the mass concentration. The aerosol particle mass concentration in air is commonly determined from the net aerosol particle mass on a filter within the recommended relative humidity (RH) range, divided by the volume of air sampled. The air volume is corrected to standard temperature and pressure conditions. Considering that the water content in the atmosphere depends on the ambient temperature and relative humidity, it is necessary to measure the mass concentration in atmospheric particles while maintaining constant temperature and constant RH conditions. Prior to determining the mass concentration, the filters were equilibrated at a constant temperature and relative humidity for 24–48 h. Constant temperature and RH values of 20 °C ± 1 °C and 20% ±5%, respectively, are recommended.

3.3.5 Analytical Methods of Water-Soluble Ion Species in Atmospheric Particles

In this section, we focus on the water-soluble ion species, which account for a major part of the aerosol mass and play an important role in the formation of clouds in the atmosphere.

Before chemical analysis, we usually determine the mass concentrations in the sampled filter, as described in the previous section. Then, analysis of the chemical species should be performed as soon as possible. In the case of water-soluble ion species analysis, the sampled filter is placed in a polypropylene vial (with caps), and ultrapure water is added to the vial. In addition, the preparation of a blank filter,

which suggests an unused filter, is necessary. First, the sampled and blank filters are extracted in ultrapure water by using a shaker or an ultrasonic bath for 20–30 min. After extraction, the solution is injected into the analytical system after removing insoluble particles with a membrane filter previously washed well with ultrapure water.

Ion chromatography (IC) is generally adopted in the analysis of water-soluble species. The dominant water-soluble species include sulfate (SO_4^{2-}), nitrate (NO_3^-), chloride (Cl^-), ammonium (NH_4^+), sodium (Na^+), potassium (K^+), magnesium (Mg^{2+}), and calcium (Ca^{2+}). It is recommended that duplicate analysis should be performed for every 10–20 samples to estimate the uncertainty.

3.3.6 Determination of Water-Soluble Species by IC

Anionic species (Cl^-, NO_3^-, and SO_4^{2-}) and cationic species (Na^+, NH_4^+, K^+, Mg^{2+}, and Ca^{2+}) in atmospheric particles are separated in an ion exchange column depending on their affinity toward the exchange material. It should be noted that other ion species, such as F^-, NO_2^-, and Br^-, are also detected if their concentrations in atmospheric particles are high. Anion separation is employed with a polymer coated with quaternary ammonium active sites. Anions pass through a strong acid cation exchange column wherein all cations are exchanged for H^+ ions beyond an electric suppressor. Anion species are detected as acids with a conductivity detector. Regarding cation species, cation exchange columns with active surfaces are usually employed. Cation species are also detected with a conductive detector.

A typical chromatogram for anion and cation analysis of a $PM_{2.5}$ sample is shown in Fig. 3.3.

3.3.7 Calculation of the Concentrations

The concentrations of the water-soluble ion species are calculated as follows:

$C_{Air} = (C_{Sol,sample} - C_{Sol,blank}) \times V_{upw}/V_{air}$.

C_{Air}: Concentration of the target species in the air (ng m^{-3});

$C_{Sol,sample}$: Net concentration of the target species from the sampled filter in solution (extracted in ultrapure water) (ng L^{-1});

$C_{Sol,blank}$: Concentration of the target species from the blank filter in solution (extracted in ultrapure water) (ng L^{-1});

V_{upw}: Volume of the extracted ultrapure water (L); and.

V_{air}: Volume of the sampled air corrected at 275.15 (K) and 1 atm (m^{-3}).

When a blank value is higher than the sample value, the data should be treated as non-detected data. If the sampled data include extremely high concentrations, the data should be regarded as unrecorded data.

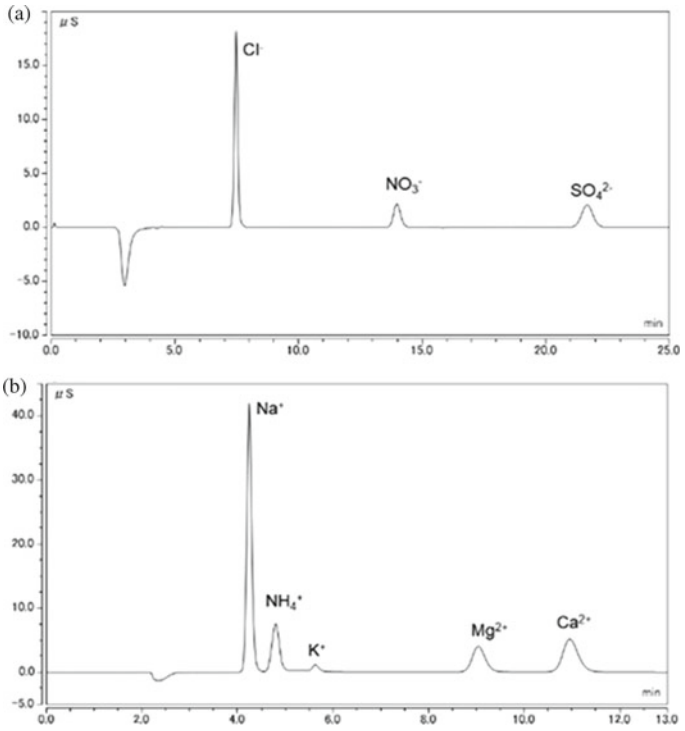

Fig. 3.3 The determination of water-soluble anions and cations in $PM_{2.5}$. **a** Anion and **b** Cation

3.4 Temporal and Spatial Variations of Chemical Compositions in $PM_{2.5}$ in Japan

3.4.1 Sampling of Atmospheric Particles for Chemical Analysis

High-volume (HV) air samplers are often adopted by the MOEJ to perform chemical analysis of $PM_{2.5}$ (Fig. 3.4). The advantage of HV air samplers is that we do not consider any sampling losses inside the sampling line because of open-face sampling. The filter is placed in a holder, and the collected particle size depends on the application. To collect $PM_{2.5}$, a high-volume impactor for $PM_{2.5}$ ($HVI_{2.5}$) was developed and simply attached to a conventional aerosol filter holder in the HV sampler (Kaneyasu 2010). Atmospheric particles collected with $HVI_{2.5}$ were divided into two size ranges: PM_{10} (aerodynamic diameter 2.5–10 μm) and $PM_{2.5}$ (aerodynamic diameter < 2.5 μm). The PM collection efficiency of the $HVI_{2.5}$ impactor was a 50% cut-off aerodynamic diameter of 2.5 μm at a flow rate of 740 L min^{-1}. The

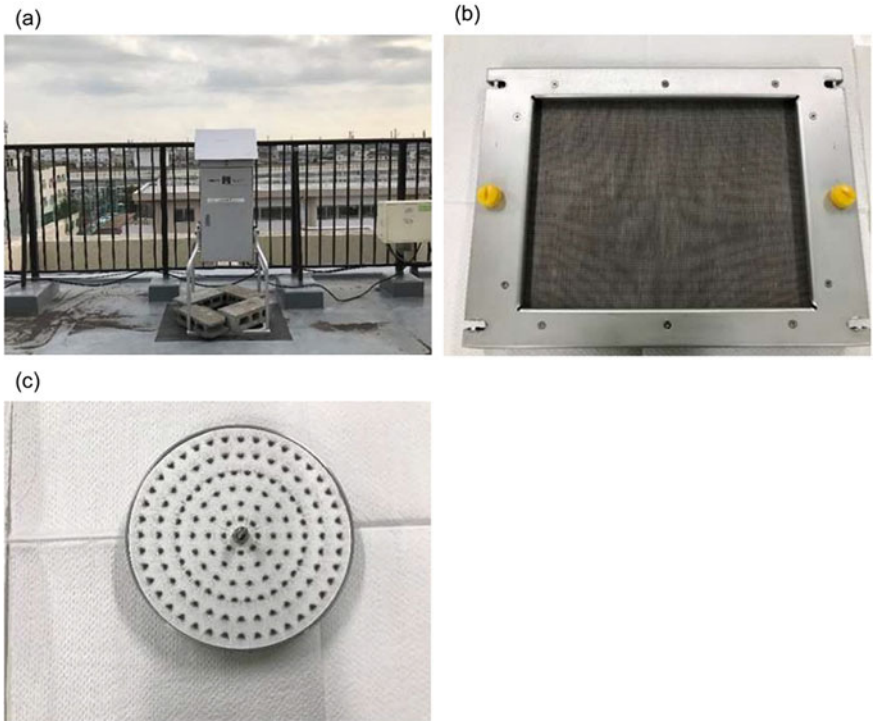

Fig. 3.4 High-volume air sampler with a $PM_{2.5}$ impactor. **a** $HVI_{2.5}$ sampler, **b** $PM_{2.5}$ samples, and **c** PM_{10} samples collected in urban sites in Japan

materials of filters are selected depending on the analytical technique and chemical composition, as listed in Table 3.1.

3.4.2 Chemical Composition of Particulate Matter in Japan

The aerosol properties including its CCN activity, are highly variable in time and space. It is important to measure chemical species as precursors of aerosols as well as CCN in as many locations of the world as possible. Also, the selection of the measurement site is important to ensure the regional representativeness. In addition, long-term perspective is important to be able to cover seasonal and yearly variations.

Figure 3.5 shows the $PM_{2.5}$ monitoring stations in 2016 in Japan, where the aerosol samplings were conducted for the MOEJ program. $PM_{2.5}$ was collected every day during the intensive observation periods (approximately, two weeks in each season; spring, summer, autumn, and winter) to investigate the $PM_{2.5}$ mass concentrations and its chemical composition in Japan, by the MOEJ.

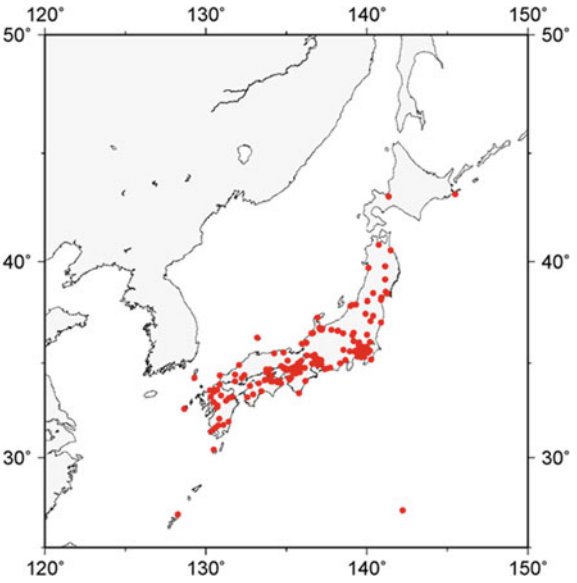

Fig. 3.5 The $PM_{2.5}$ monitoring stations (171 stations) used for $PM_{2.5}$ chemical analysis in 2016 in Japan

Figure 3.6 shows the annual average chemical composition and mass concentration of $PM_{2.5}$ in Japan from 2011 to 2016. In Japan, the environmental standard of the $PM_{2.5}$ mass concentration was set to a value lower than 15 $\mu g\ m^{-3}$ for annual average values and lower than 35 $\mu g\ m^{-3}$ for daily average values. The annual average $PM_{2.5}$ concentration tends to decrease gradually and is lower than the environmental standard in 2016 in Japan.

The major composition of chemical species in particulate matter consists of water-soluble ion species (WSION), trace metals, organic carbon (OC), elementary carbon (EC), and unknown species. The average concentrations of each chemical compound in $PM_{2.5}$ and their ratios against the $PM_{2.5}$ mass concentration from 2011 to 2016 are

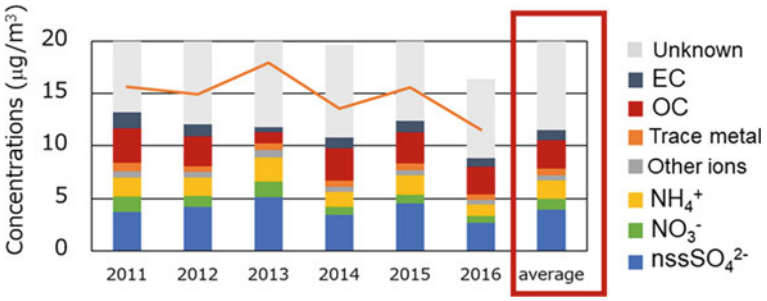

Fig. 3.6 Annual average chemical composition in $PM_{2.5}$ and mass weight concentrations (orange line) from 2011 to 2016 in Japan. The average concentrations in this period are also shown. The data were obtained from MOEJ reports

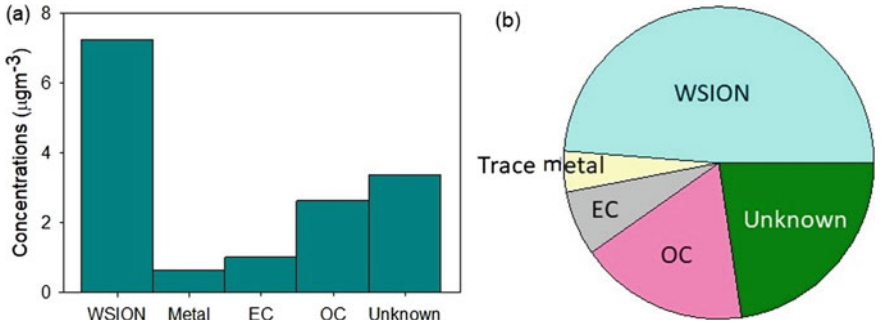

Fig. 3.7 The averaged concentrations of each species in $PM_{2.5}$ from 2011 to 2016 in Japan. **a** The averaged concentrations of each chemical composition and **b** contribution (%) of each chemical species in $PM_{2.5}$

also shown in Fig. 3.7. The average concentrations (and their ratios) in $PM_{2.5}$ from 2011–2016 were 7.3 μg m^{-3} (49%) for water-soluble ion species, 0.63 μg m^{-3} (4%) for trace metals, 1.0 μg m^{-3} (18%) for OC, 2.6 μg m^{-3} (7%) for EC, and 3.4 μg m^{-3} (23%) for unknown species.

Water-soluble ion species account for almost half (49%) of the mass concentration in $PM_{2.5}$. The dominant species are chloride ions (Cl^-), nitrate ions (NO_3^-), sulfate ions (SO_4^{2-}), sodium ions (Na^+), ammonium ions (NH_4^+), potassium ions (K^+), magnesium ions (Mg^{2+}), and calcium ions (Ca^{2+}). Among these ions, SO_4^{2-}, NO_3^-, and NH_4^+, are first emitted as gas phases (SO_2, NO, NO_2, and NH_3) into the atmosphere and then oxidized and/or condensed into the particulate phase. The production of these.

secondary inorganic aerosols is extremely complicated by numerous chemical reactions, such as reactions on pre-existing aerosol surfaces (heterogeneous reactions) and reactions within pre-existing gaseous phases (homogenous reactions). Furthermore, meteorological factors such as photochemical intensity, water (relative humidity), and temperature play an important role in the formation of aerosols. These secondary inorganic aerosols largely occur in the fine particulate fraction and are transported far away from the major emission sources and/or urban areas. Sea salt species such as Na^+, Cl^-, sea salt (ss) Ca^{2+}, and $ssMg^{2+}$ also occur in $PM_{2.5}$. Non-sea salt (nss) Ca^{2+} is considered an indicator of transport of Asian dust (KOSA). OC is emitted directly by emission sources as primary organic carbon or produced in the atmosphere as a result of gas-particle transformation. EC is a primary pollutant emitted by the incomplete combustion of fossil fuels. Trace metals, such as Sb, As, Cd, Pb, Ni, Se, Ag, Tl, and Zn, are considered toxic elements originating primarily from anthropogenic sources. The unknown category is defined as the difference between the particulate mass and the total concentration of the chemical components.

Although the chemical mass closure study presented here is also commonly used for studying the health effects of $PM_{2.5}$, the fraction of WSION is of particular interest in terms of CCN activity of aerosol particles. Furthermore, water–soluble fraction of

OC and some surface-active organic compounds that can change the surface tension of the solution is also relevant for the detailed study of aerosol–cloud interactions.

3.5 In-Situ Counting Techniques of Atmospheric Particles

Imagine a ray of light coming into the dark room through a slit of curtains. Often you would find countless shining dust swaying in the light. You are seeing the weak light being scattered by the dust particles at a given angle from the direction of the propagating light, which otherwise is not noticeable in the bright environment. In this case, the ray of light is acting as the sensing probe, and your eyes as the detector. This is in many ways similar to the principle employed in the real-time counting of tiny particles.

3.5.1 Mie Scattering Theory

The electromagnetic waves (i.e., solar radiation) propagating through the atmosphere undergo scattering by air molecules, aerosols, and cloud droplets (or ice crystals). There are different scattering processes involved, and the predominant process is determined as a function of the incoming wavelength of the magnetic wave λ and the radius r of the scattering particle. For example, the intensity of the solar radiation is at its maximum (wavelength, $\lambda \approx 0.5\ \mu m$) within the visible light range (0.4–0.8 μm). Coincidentally, this band of wavelength is very similar to the typical size range of the sub-micron particles that are often predominant in any aerosol population in terms of number concentration. At these overlapping ranges of wavelength and particle size (assuming spherical shape), the light scattering process can be well defined by the Mie theory.

Because of the proximity between the central wavelengths of the solar radiation and the typical size range of the aerosols, Mie theory is convenient for describing the light scattering phenomenon caused by the majority of atmospheric particles (and typical cloud droplets). The Mie scattering by a spherical particle is dependent on the light wavelength, particle size, as well as complex refractive index. The complex refractive index depends on the material (i.e., chemical composition described in the above sections) of the scattering particle, which is given as the ratio of the propagating speed of light in the material with respect to vacuum by also taking into account the light absorption.

3.5.2 Optical Particle Counters

As mentioned, a large part of the light scattering phenomenon involving atmospheric particles can be expressed by the Mie theory. This means that under the fixed wavelength (and by assuming spherical particle and constant particle complex refractive index), the intensity of the scattered light at given angles can be used to narrow down and derive the size (diameter, D_p) of the scattering particle. This is the working principle of the optical particle counters (OPC) used for real-time, in-situ counting of particles of different sizes.

The optical particle counter typically has a laser of a fixed wavelength (e.g., 655, 675, or 780 nm) focused on the beam of aerosols traveling within a laminar air flow. Then, the scattered light is guided and detected by the photodiode. The detected light is converted into the electric pulse signals. The intensity of the scattered light corresponds to the height of the electric pulse (thus particle size), and the pulse height analysis can be applied to obtain the overall particle number size distributions. Besides counting number concentration, such an optical detection principle is also used to derive the mass concentration of particles by assuming the atmospherically relevant particle density (kg/m^3). This principle is increasingly employed in palm-sized, low-cost $PM_{2.5}$ sensors.

3.5.3 Condensation Particle Counters

The scattering efficiency of the visible light is at its maximum in the submicron particle range, and asymptotically approach to a constant value in the super-micron range. This makes particles in $0.1 < D_p < 1$ μm size range the most efficient scatterers of visible light, and being most sensitive to OPCs. However, the scattering efficiency decreases sharply as the particle size drops into nanometer range (Fig. 3.8). Therefore, conventional OPCs all suffer from optically detectable size limits and typically work only for $D_p > 0.1$ μm.

As far as particle mass is concerned, the optical detection limit is not much of a problem, since no matter how many nanoparticles there are, they account for negligible mass as compared to a few larger particles. However, freshly born particles or large fractions of CCN exist in the $D_p < 0.1$ μm and they often overwhelm the larger particles by number. Therefore, it is important to be able to "count" those invisible, nanoparticles when CCN activity is concerned.

How can one make these nanoparticles visible by light? Recall that clouds can only exist with the help of pre-existing atmospheric particles that initially provide a surface for water condensation. The optical detection limit of nanoparticles can be overcome by taking advantage of this unique ability of aerosols to act as CCN. By carefully controlling the temperature and vapor pressure of the condensate (e.g., water) in the growth tube installed at the upstream section of the optical detection cell, the particles can be forcibly activated into droplets and subsequently grown

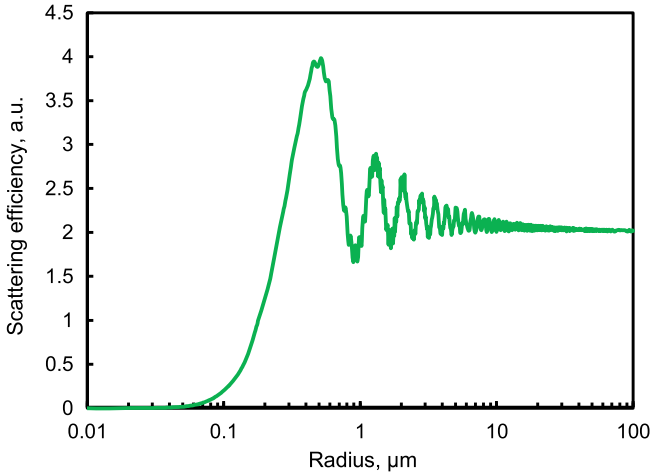

Fig. 3.8 Scattering efficiency of visible light (green, $\lambda = 0.5$ μm) by a spherical particle (water, refractive index = 1.33) as a function of radius (μm)

under the supersaturated condition (Fig. 3.9). This will typically lead to as much as 2–3 orders of magnitude increase in the particle diameter with respect to the original diameter of 10 nm. The resulting droplets generally exceed a few microns in size, and they can be easily detected at the following OPC section. This is the working principle of condensation particle counters (CPC) (Hering et al. 2005). It is also a good illustration of how initially invisible nanoparticles can suddenly start scattering significant amounts of light and explains exactly why the CCN activity of aerosols matters so much in regulating the radiation budget of the atmosphere.

Several types of working fluids are used as condensates of different CPCs, including water, butanol, and isopropyl alcohol. The degree of supersaturation determines the smallest size of the activated particle. The CPC in principle activates whatever particles are larger than the lowest activation diameter, so that it loses the information on the original particle size distribution of nanoparticles. This limitation is often overcome by coupling a CPC with the size segregating device called the Differential Mobility Analyzer (DMA) that can extract particles having the same size based on the corresponding electrical mobility (Knutson and Whitby 1975). By scanning the voltage applied to the DMA, only particles having the same electrical mobility (≈size) can enter the downstream CPC at a time, and number size distribution can be obtained.

In order to avoid miscounting the smallest of the nanoparticles (high-performance CPCs can even activate particles as small as few nm), the supersaturation condition within the growth tubes of typical CPCs is set to unrealistically high values (RH > 200%) as compared to atmospheric conditions. While CPCs in principle are built to activate as small particles as possible in order to obtain the quasi-total concentration of all particles, there is another type of condensation particle counter that regulates the growth tube under modest, atmospherically relevant supersaturation conditions

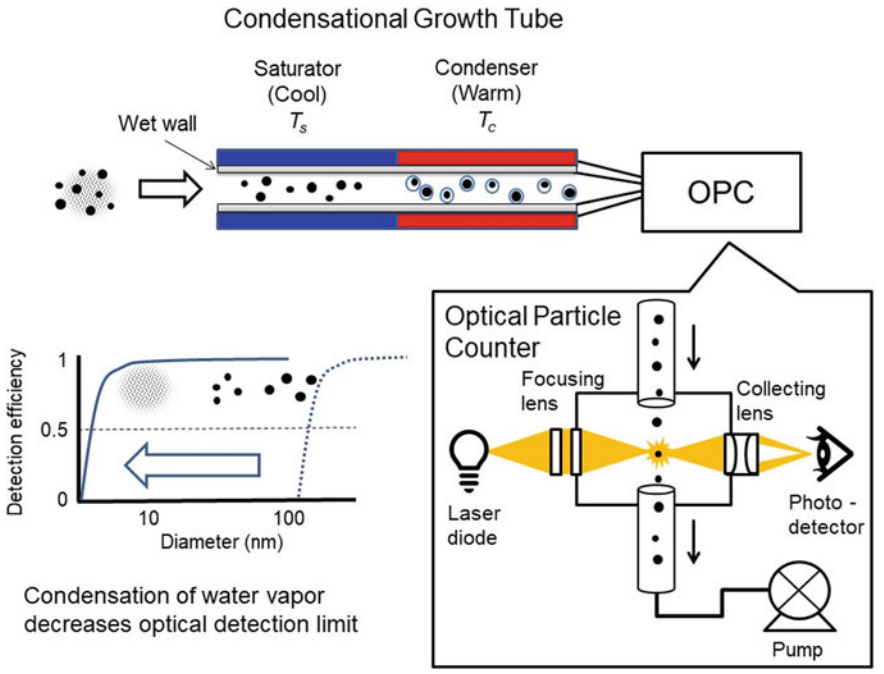

Fig. 3.9 Schematic diagram of the water-based condensation particle counter. It is comprised of a growth tube section upstream of the optical particle detection cell

(RH < 101%). This is called the CCN counter, designed to count the actual CCN number concentration at corresponding supersaturations (Roberts and Nenes 2005). Therefore, with the set of a CPC and CCN counter running side by side, one can determine the number of CCN at a given supersaturation with respect to the total number of aerosol particles. Combination of DMA would further add the information on the size distributions of aerosols (and CCN).

3.6 Spatial and Temporal Variation of CCN Concentrations

In order to reduce the uncertainty related to the aerosol climate impact, state-of-the-art knowledge gained from a broad range of research methods must be integrated, which includes in-situ observations (as highlighted in this section), indoor chamber experiments, satellite-borne remote sensing, and numerical simulations. For example, sophisticated chemical transport models need to be validated against the in-situ observation data whether the computer can simulate the present-day atmosphere correctly or not, before pushing the clock forward and predicting the future climate change.

As mentioned, the aerosol properties including its CCN activity, are highly variable in time and space, therefore, it is important to measure them in as many locations of the world as possible. Also, the selection of the measurement site is important to ensure the regional representativeness. It is not relevant if the CCN counter was installed, e.g., right next to an exhaust pipe of a car or a stack of coal-burning boilers. In addition, long-term perspective is important to be able to cover seasonal and yearly variations.

There has been an effort to integrate long-term CCN observations across different parts of the world. It was mostly a collection of regionally representative measurement stations situated far from cities and major industries (Fig. 3.10). Such an intercomparison study of an unprecedented scale revealed how variable CCN concentration can be across time and space in the world. In particular, our station in the Noto peninsula, Japan (although the location is considered representative of a remote background station far from major cities and industrial activity), showed a very high concentration reflecting the severity of the regional pollution in East Asia. It also highlighted the significant seasonal variation due to distinct monsoons in this region.

3.7 Future Implications

Will the air in East Asia ever be cleared away? Due to recent stringent emission control policies employed in China, the $PM_{2.5}$ in East Asia and its downwind regions are experiencing a sharp decrease in mass and change in composition. It may be a great news for the public health of the people living in these regions, but not necessarily in terms of climate change, because we can no longer count on the cooling effect of the aerosols and clouds. Again, $PM_{2.5}$ is only a measure of the aerosol mass and it does not directly translate to the number of aerosols and CCN. It is important to keep our eyes on how both the chemical and physical properties of aerosols in this region will evolve with the ongoing reduction of anthropogenic emissions, and how clouds would respond to such changes and eventually affect the regional climate change and water cycles.

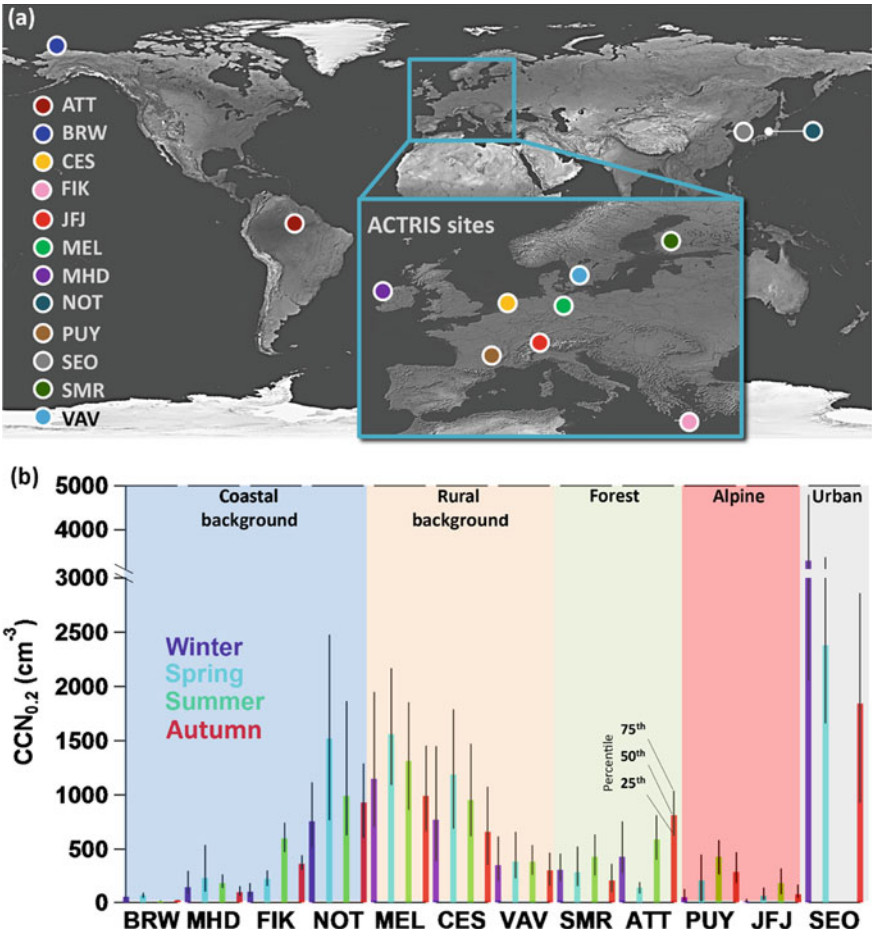

Fig. 3.10 **a** Map showing locations of the measurement stations. NOT represents Noto peninsula. Other station abbreviations can be found elsewhere (Schmale et al. 2018). **b** Median and interquartile ranges of the seasonal CCN number concentrations at a supersaturation of 0.2%. This figure is adopted from Schmale et al. (2018)

References

EANET (2013) Technical manual for air concentration monitoring in East Asia, EANET

Hering SV et al (2005) A laminar-flow, water-based condensation particle counter (WCPC). Aerosol Sci Technol 39(7):659–672. https://doi.org/10.1080/02786820500182123

Kaneyasu N (2010) Development of $PM_{2.5}$ impactor for the conventional high-volume air sampler. J Jpn Soc Atmos Environ 45:171–174 (in Japanese)

Knutson EO, Whitby KT (1975) Aerosol classification by electric mobility: apparatus, theory and applications. J Aerosol Sci 6:443–451

MOEJ (2019) Chemical analysis in particulate matter: chemical analysis manual for atmospheric particulate matter. Collecting methods of atmospheric particles for chemical analysis. (In Japanese)

Petters MD, Kreidenweis SM (2007) A single parameter representation of hygroscopic growth and cloud condensation nucleus activity. Atmos Chem Phys 7:1961–1971. https://doi.org/10.5194/acp-7-1961-2007

Roberts GC, Nenes A (2005) A continuous-flow streamwise thermal gradient CCN chamber for atmospheric measurements. Aerosol Sci Technol 39(3):206–221. https://doi.org/10.1080/027868290913988

Schmale J et al (2018) Long-term cloud condensation nuclei number concentration, particle number size distribution and chemical composition measurements at regionally representative observatories. Atmos Chem Phys 18:2853–2881. https://doi.org/10.5194/acp-18-2853-2018

WMO (2016) WMO/GAW aerosol measurement procedures, guidelines and recommendations, WMO report

Chapter 4
Biodiversity of Marine Animals: Introduction to Marine Animals with a Focus on Taxonomy

Noboru Nunomura, Nobuo Suzuki, Shouzo Ogiso, and Toshio Sekiguchi

4.1 Introduction

If we examine the underside of just one stone on the seashore or observe a drop of water from a plankton net under a microscope, we will find a surprising diversity of animal life belonging to many phyla. Life was born in the sea four billion years ago, and it evolved to comprise an amazing variety of groups, some of which, such as various phyla including Arthropoda, Mollusca, Nematoda, Nematomorpha, Annelida, Platyhelminths, and Chordata, have advanced onto land. The remaining groups remain in the sea or have already become extinct. Most specialists consider the animal kingdom to contain about 35 phyla, of which approximately 12 are exclusively found in marine environments. Most of these phyla are represented on the seashore of the Noto Peninsula and its neighboring sea. The body plans of animals that inhabit the marine environment differ from those that inhabit the terrestrial environment owing to different environmental factors. For instance, the respiratory system of marine animals is different from that of terrestrial animals. Marine animals absorb oxygen dissolved in the seawater through the epidermis, gills, or respiratory tree, whereas terrestrial animals take up oxygen from the air using respiratory organs, including the lungs, book lungs, and trachea. Moreover, there is a wide variety of sessile animals such as sponges, sea anemones, corals, moss animals, barnacles, and ascidians in the marine environment. They appear similar to algae and lack the body structure such as fin and feet to chase prey and escape from predators because seawater contains a large amount of food.

In this chapter, we introduce two important concepts associated with biodiversity and show the characteristics and members of each animal phyla. The current Chapter aims to help students to learn the diversity of marine animals. Primarily, we hope

N. Nunomura (✉) · N. Suzuki · S. Ogiso · T. Sekiguchi
Noto Marine Laboratory, Institute of Nature and Environmental Technology, Division of Marine Environmental Studies, Kanazawa University, Noto-Cho, Ishikawa 927-0553, Japan
e-mail: toukyaku@pure.ocn.ne.jp

N. Hasebe et al. (eds.), *Field Work and Laboratory Experiments in Integrated Environmental Sciences*, https://doi.org/10.1007/978-981-99-6532-8_4

that students use it as a textbook to study before the field activity on the seashore of the Noto Peninsula. Therefore, we mainly describe the various phyla of the marine invertebrates and represent a significant species inhabiting the inshore or offshore of the Noto Peninsula.

4.1.1 Taxonomic Rank

The Swedish naturalist Carolus Linnaeus (1707–1778) invented the binominal classification system to classify organisms. In order to increase inclusiveness, this system includes the following categories (taxonomic rank or taxonomic hierarchy): species, genus, family, order, class, division (plants) or phylum (animals), and kingdom (with domain recently added as a higher rank). Additionally, many supplementary classes are now used, such as suborder, infraorder, and superfamily.

The classification system is based on taxonomy and "taxon" is a taxonomic unit: a name given, a particular ranking. The word taxon (plural [pl]: taxa) is from the Greek "taxis," meaning arrangement, and "nomos," meaning law (Fig. 4.1). Taxonomy is a field of study involving grouping organisms based on many fields of biological science, including morphology, ecology, and genetics. It has shown rapid progression, and the classification systems have changed rapidly. This Chapter is primarily based on the study of Brusca et al. (2016) and partly on several other literatures. If students are willing to study the recent progress of taxonomy, we recommend the article by Laumer et al. (2019). Furthermore, we refer to the following articles to study deeper the chapter or different taxonomic theories: Barnes (1963), Russel-Hunter (1979), Hillis et al. (2012), Margulis and Schwartz (1997), and Zimmer and Emlen (2013).

4.1.2 Basic Body Plans of Animals

The body plan of multicellular animals is categorized into nonbilateral, radially symmetrical, and bilateral. The bilaterally symmetric body plan has an anterior end and a posterior end, i.e., a distinction exists between the head and tail, as well as a distinction between the dorsal and ventral. Taxonomically, the two groups are not formally ranked. A few groups have developed a secondary nonbilateral body plan, for example, snails and many groups of the phylum Echinodermata that have obtained secondary radial symmetry. Animals with a bilateral body plan are composed of three well-developed germ layers, the endoderm, mesoderm, and ectoderm, i.e., they are triploblastic, whereas nonbilaterian animals are diblastic or non-blastic. Generally speaking, the respective germ layers of Bilateria form the following organs: The endoderm forms mainly digestive organs including the stomach, the liver, the pancreas, and the bladder. The ectoderm forms the neuron and epidermis, including the lens of the eye. The mesoderm forms the body cavity, skeletal system, muscle, circulatory system, and so on.

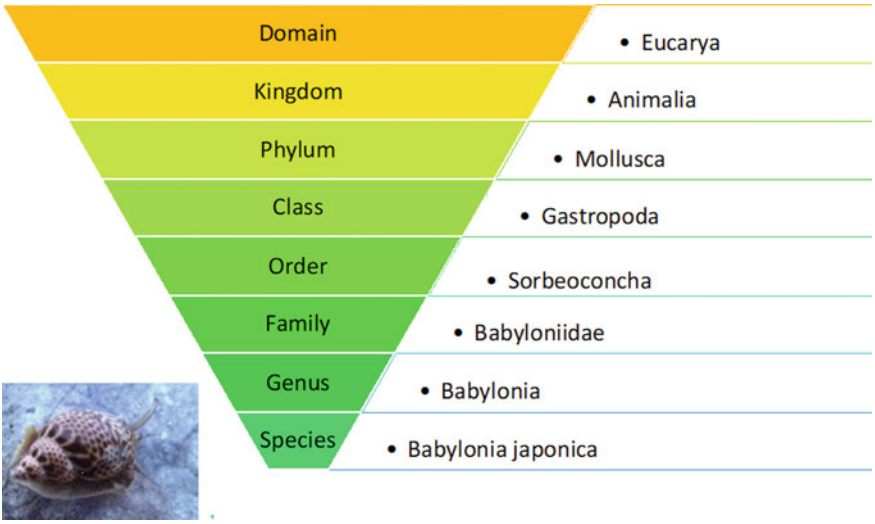

Fig. 4.1 Taxonomic rank (example of sea snail: *Babylonia japonica*)

For a long time, multicellular animals had been summed up into three groups: acoelomates, pseudocoelomates, and eucoelomates. Acoelomates are animals without a body cavity in non-blastic animals (such as Porifera), diblastic animals (such as Cnidaria), and primitive triblastic animals (such as Platyhelminthes). Pseudocoelomates have a pseudocoelom, i.e., a body cavity derived from the blastocoel and not from the mesoderm. Rotifera and some phyla, including a part of Nematoda, have been classified as pseudocoelomates. Eucoelomates have a deuterocoel and comprise phyla including Annelida, Mollusca, Arthropoda, Echinodermata, and Chordata.

4.1.3 Protostomes and Deuterostomes

Animals in which the blastopore (i.e., the first opening of the embryonic gut) develops into the mouth are called protostomes, whereas animals in which the blastopore develops into the anus are called deuterostomes. The differences between these two groups are shown in Table 4.1; however, they are both contained within the rank of infrakingdom.

Protostomes consist of the Lophotrochozoa, Ecdysozoa, and the phylum Chaetognatha. Lophotrochozoa comprises the following phyla: Platyhelminthes, Gnathostomulida, Micrognathozoa, Rotifera, Nemertea, Acanthocephala, Gastrotricha, Cycliophora, Entoprocta, Ectoprocta, Brachiopoda, Phoronida, Mollusca, and Annelida (including Echiura and Sipuncula). Dicyemida and Orthonectida are also considered to be included in this group. Ecdysozoa comprises the following phyla: Kinorhyncha,

Table 4.1 Differences between protostomes and deuterostomes

	Protostomes	Deuterostomes
The first opening of the embryonic gut	Mouth	Anus
Cleavage during cell division	Spiral cleavage	Radial cleavage
Development	Schizocoelous	Enterocoelic
Main digestive tube	Dorsal	Ventral
Representative phyla	Mollusca, Arthropoda, and Annelida	Echinodermata and Chordata

There are exceptions in many cases(1)

(1)The phyla Brachiopoda and Bryozoa belong protostomes, but their mouth does not originate from the first opening of the embryonic gut, and they exhibit a radial type cleavage during cell division. The phylum Chaetognatha has many features similar to other protostome phyla, except that the mouth and anus are formed secondarily after the closure of the blastopore

Priapulida, Loricifera, Nematoda, Nematomorpha, Tardigrada, and Arthropoda. Deuterostomes consist of the Echinodermata, Hemichordata, and Chordata. We do not discuss the phyla Placozoa, Orthonectida, Rhombozoa, Gnathostomulida, Cycliophora, Micrognathozoa, Phoronida, Nematomorpha, Kinorhyncha, Loricifera, Priapulida, Tardigrada, and Onychophora because they do not occur in the sea of Noto and its neighboring waters, they are very small, or they are deep-sea dwellers.

4.2 Classification of Animals

4.2.1 Phylum Porifera

Colorful sponges, belonging to the Porifera, can often be seen covering rocks or stones. Sponges lack digestive, circulatory, and nervous systems as well as other distinct organs. They only have a unique water-based circulatory system that maintains a constant flow of water through their bodies to obtain food and oxygen from the water (Fig. 4.2). Sponges have large and small pores; they obtain food and fresh seawater through small pores known as ostia (pl. of ostium) using flagellated choanocytes and discharge water through large pores known as oscula (pl. of osculum).

Hitherto, more than 5,000 species of sponges have been recorded. Taxonomically, sponges are classified into four classes: Calcarea (calcareous sponge), Hexactinellida (glass sponges), Demosponges, and Sclerospongiae. Demosponges include Halichondrida that are found on the rocky shore. Most of the members of the Sclerospongiae have been known only as fossils.

Fig. 4.2. Porifera, *Halichondria* sp. (*Photo* by Nunomura)

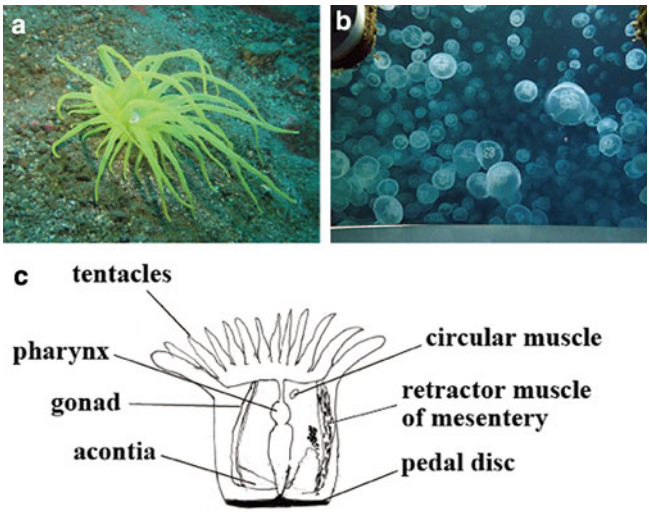

Fig. 4.3 Cnidaria. **a** *Dofleinia armata* (Photo by Ogiso), **b** *Aurelia aurita* (Photo by Ogiso), **c** Body of a sea anemone. The right half shows the part of the mesentery; the left half shows the part of the gonad (Original drawing by Nunomura)

4.2.2 Phylum Cnidaria

The phylum Cnidaria includes sea anemones (Fig. 4.3a), jellyfish (Fig. 4.3b), and corals. More than 11,000 Cnidaria species exist, and these are predominantly found in marine environments. They can be separated into three subphyla: Medusozoa (including Hydrozoa, Cubozoa, and Scyphozoa), Anthozoa, and the parasitic Myxozoa. The distinguishing feature of the Cnidaria is their cnidocytes, specialized cells that are used mainly to capture prey. Although Cnidaria were formerly placed in the phylum Coelenterate together with the Ctenophores, they were subsequently separated into two phyla.

The body of Cnidaria (Fig. 4.3c) has radial symmetry with a mouth located in the center of their body and surrounded by tentacles bearing cnidocytes. It contains

mesoglea, a nonliving jelly-like substance that is sandwiched between two layers of epithelium. Their alignment canals have a single opening, and their body cavities (a gastrovascular system) are used for digestion and respiration.

Generally, heterogony is observed in cnidarians. The majority of the Cnidaria exhibit alternation of two basic forms: swimming sexually reproductive medusae and sessile asexually reproductive polyps. Fertilized eggs hatch into planulae larvae, which are bilaterally symmetrical, ciliated, and free-swimming. The planulae larvae metamorphose into polyps followed by medusa. Many cnidarian species produce colonies that comprise medusa-like and/or polyp-like zooids.

Several free-swimming species of Cubozoa and Scyphozoa possess balance-sensing statocysts, and some groups have simple eyes. Some of the anthozoans form coral reefs, which form ecosystems that nurture a diversity of animal life in tropical and subtropical seas. Some corals are considered valuable as jewels and some parts of jellyfish are edible. Some of the most common species of the Cnidaria in the Noto Peninsula are *Carybdea brevipedalia*, *Aurelia aurita*, and *Anthopleura* spp.

4.2.3 Phylum Ctenophora

The phylum Ctenophora includes the comb jellies, which look like jellyfish due to their soft and gelatinous bodies. Most species of ctenophores have sticky colloblasts that adhere to prey, are composed of jelly-like mesoglea between two layers of epithelia, and lack eyes and apical organs. The mouth of a ctenophore is situated at its rear end, whereas the anus is at the anterior end. They discharge unwanted small particles from their anal pores, but many unwanted pieces are cast out using the mouth. The outer surface of the ctenophoran species usually bears eight rows of combs known as swimming plates, which are used for swimming. Many ctenophoran species found in shallow water are colorless and almost transparent; however, some deeper-living species are strongly pigmented and luminescent. Ctenophora comprises of approximately 100 species. In general, the Ctenophora, along with the Porifera and Cnidaria, are considered prebilateral, whereas the other phyla discussed in the following section are likely to be bilateral, except for some that have a secondary nonbilateral body plan.

4.2.4 Phylum Platyhelminthes

We can commonly find wide but dorsoventrally flat animals (Fig. 4.4a) creeping on the underside of stones or among the holdfast of algae on the seashore. They are members of the phylum Platyhelminthes.

The Platyhelminthes comprises more than 25,000 species, including flatworms (Turbellaria) and infamous parasites such as tapeworms (Cestoda), monogeneans, and flukes (Trematoda); however, some unidentified species may still exist.

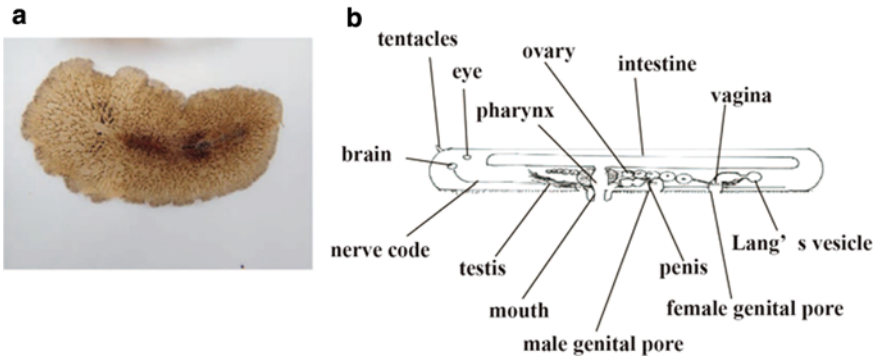

Fig. 4.4 Platyhelminthes. **a** *Planocera multitentaculata* (Photo by Ogiso), **b** Body of a Turbellaria (Original drawing by Nunomura)

Herein, we describe the characteristics of Platyhelminthes using Turbellaria as an example (Fig. 4.4b). In Turbellaria, many species are free-living, whereas some are parasitic. Because of the absence of circulatory and respiratory systems, these species obtain oxygen by direct permeation through the epidermis. Accordingly, relatively large-sized groups of Platyhelminthes have flat-shaped bodies to effectively absorb oxygen. Turbellarians can move using the many cilia found on their ventral surface, and they occasionally swim by winding cilia on the ventral surface. As a sensory system, some species have eye spots or tentacles on their anterior part, whereas species that inhabit the soft sea bottom have statocysts instead of eyes. Most Turbellarians, except for a few species, have a mouth but lack an anus. As far as Polycladida, the most conspicuous order of Turbellarians, is concerned, the mouth is usually located near the center of the ventral side of the body, and the intestine has a complex branching pattern. The excretory system is the most primitive, with protonephridium-bearing flame cells. Polyclad Turbellarians are carnivorous and primarily prey on bivalves. The majority of Turbellarians are hermaphrodites; they have big testes and ovaries that occupy most of their body space. Among Turbellarians, small-sized groups are found in the interstitial environment of sandy beaches.

Cestoda and Trematoda lack sensory organs because of the adaptation to parasites. Moreover, Cestoda lacks digestive organs.

The most common species are *Notoplana humilis* and *Planocera multitentaculata* in the Noto Peninsula (Fig. 4.4a).

4.2.5 Phylum Nemertea (Nemertini)

Many members of the phylum Nemertea or ribbon worm (Fig. 4.5a) inhabit the underside of stones or holdfast of algae on the seashore or on the sandy bottom. It comprises more than 1,000 species. Like the platyhelminths, the Nemertea lack a

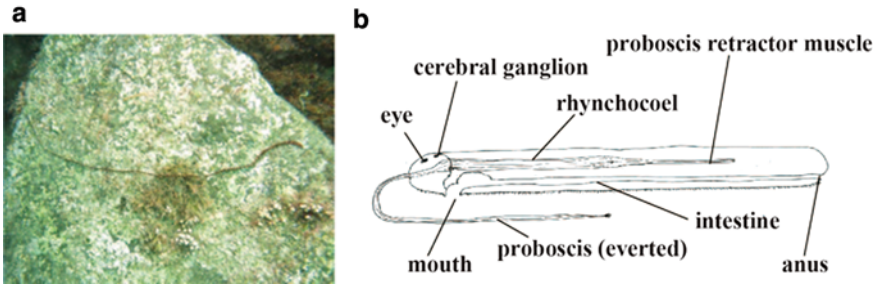

Fig. 4.5 Nemertea. *Notospermus geniculatus* (Photo by Ogiso), B. Body of Nemertea (Original drawing by Nunomura)

coelom and have pronephridium-type excretory organs. However, they have a thick and elongate body (Fig. 4.5b) because they possess a circulatory system, which transports oxygen and nutrients via vessels. Typical nemerteans are carnivores that hunt for prey using a unique eversible proboscis, which is stretched by a muscle lying in the large cavity of the rhynchocoel during the inactive state. The mouth opening of nemerteans is at the anterior margin, whereas the anus is at the rear end. Nemerteans move slowly, using their external cilia to glide on the surface. Although they have a long-unsegmented body, the muscle is alternatively thick and thin. Thus, larger species can move using muscular waves. *Notospermus geniculatus* and *Lineus fuscoviridis* may be relatively commonly seen in the Noto Peninsula.

4.2.6 Phylum Annelida

The phylum Annelida includes ragworms, earthworms, leeches, and various other groups. There are more than 17,000 valid species. Traditionally, annelids bearing many chaetae and parapodia (pl. of parapodium) were summarized as "Polychaeta." However, the classification of the Annelida has changed markedly over time, and the "Polychaeta" is now considered to be a paraphyletic group: the "Polychaeta" has been proved to include groups that are distantly related to each other. In addition, tube worms (Vestimentifera), peanut worms (Sipuncula), and spoon worms (Echiura) were previously considered to be separate phyla, but they have all recently been incorporated into the phylum Annelida. The typical marine annelids are Polychaeta-shaped, (Fig. 4.6a) which are long segmented worms found among the holdfast of algae or under stones on the seashore. Their bodies (Fig. 4.6b) consist of many annular segments, except for some unsegmented annelids belonging to Archiannelida, Echiura, and Sipuncula. The first segment bears eyes on other sensory organs, while the second segment bears a mouth opening. The anus opens on the last segment, i.e., the pygidium. Each segment bears a pair of fleshy protrusions, the parapodia, and many chaetae (chitinous bristle). The body of Annelida is composed of three germ layers, and they have a closed circularity system in the coelom in the mesoderm.

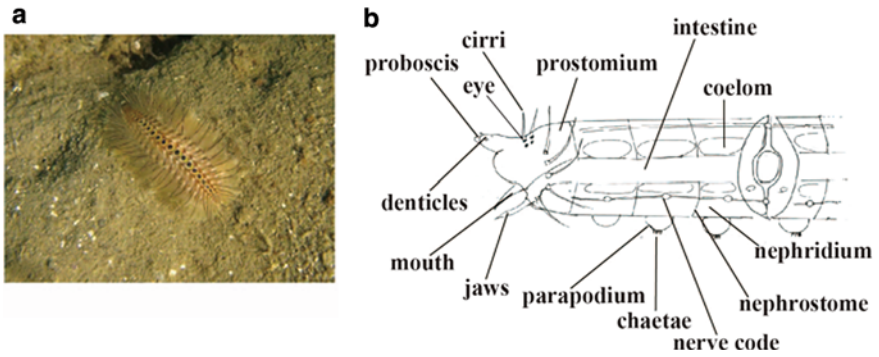

Fig. 4.6 Annelida. **a** *Chloeia flava* (Photo by Ogiso), **b** Body of Polychaetous Annelida (Original drawing by Nunomura)

Many species are sexually gonochoristic, whereas some species are hermaphroditic. During their development, they carry spiral cleavage postfertilization and larvae are typically trochophores; subsequently, they become only a few-segmented larvae, and finally they reach the adult stage. The body surface and parapodia of Annelida function as respiratory organs. The metanephridium has developed as an excretory organ. The nervous system is ladder-like and runs along the ventral side.

Several species are used as fishing bait and, rarely, some are used for food. The most common "polychaetous" annelids in the Noto Peninsula are *Nereis multignatha*, *Platynereis bicanaliculata*, *Perinereis cultrifera*, and *Chloeia flava* (Fig. 4.6b).

4.2.7 Phylum Mollusca

The phylum Mollusca, including Gastropoda, Bivalvia, Cephalopoda, Scaphopoda, Polyplacophora, and some other classes, is arguably one of the most popular marine animal groups. The body of many groups consists of the head, viscera, muscular foot, and mantle (Fig. 4.7). Essentially, they have a bilaterally symmetrical body. However, many snails have a secondary asymmetrical form due to coiling. The body of Mollusca has three germ layers, but their coelom is small due to their strongly developed muscles. Their main body cavity is an open circular system, i.e., haemocoel, except for in Cephalopoda. Their excretory system comprises large metanephridia (pl. of metanephridium), i.e., the kidneys. Some members of the group possess a buccal region with a grater-like radula. Many members also bear a hard calcareous shell. They do not have inner skeletons and lack segmentation, whereas most groups have mantle-containing shell glands that secrete the calcareous epidermis shell. Many species are gonochoristic, but others are hermaphroditic. They possess many types of sensory organs, e.g., eyes, osphradia (pl. of osphradium), and statocysts. During development, they show spiral cleavage after fertilization, and

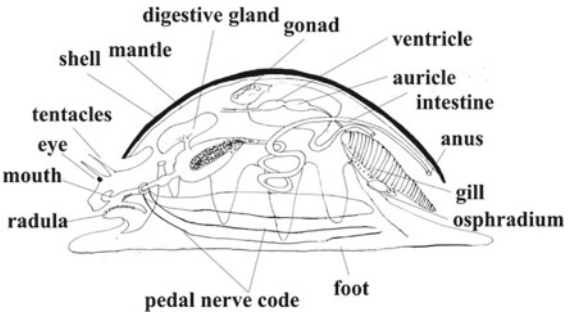

Fig. 4.7 Schematic pattern of a hypothetical ancestral form of Mollusca (Modified after Barnes 1963)

typical larvae become trochophores and then veligers (except for those of Polyplacophora). Many Mollusca groups move rather slowly, but some can swim fast using jet injection. Mollusca comprise the second largest phylum, containing 112,000 species. The other Mollusca groups, except for those mentioned below, are omitted from the discussion because they may not exist in the Noto Peninsula or its neighboring area, they are very small, or they are deep-sea dwellers.

4.2.7.1 Class Gastropoda

The Gastropoda comprises various groups such as the keyhole limpets, top shells, sundials, tower shells, horn shells, and conches; some groups have their original gills, some have secondary gills instead of their lost original ones, and others have lungs instead of gills. Many species of snails occur on the rocky shore. Gastropods have essentially a bilateral body, but many groups show coiling. However, in limpets and some other gastropods, coiling is lost. The Gastropoda have well-developed heads with tentacles and eyes. The buccal part has a grater-like radula.

The Gastropoda were formerly classified into three subclasses depending on the position of the gills and heart: Prosobranchia (gills situated in front of the heart), Opisthobranchia (gills behind the heart), and Pulmonata (possessing lungs but not gills). Recently a new classification system to divide the Gastropoda into five subclasses has been proposed. We will show the diversity of the Gastropoda according to the new classification system (Ponder and Lindberg 1997).

The subclass Patellogastropoda, comprising the true limpets having a flat shell, are found on rocks and wave-out blocks. Many species of the Patellogastropoda leave "scars" on the rock to which they return between tides. Only a few species from the families Patellidae and Acmaeidae occur in the Noto Peninsula.

The subclass Vetigastropoda (Fig. 4.8a) comprises many groups of representative sea snails, including abalones and some limpets such as keyhole limpets. Many species of Vetigastropoda have a single pair of cephalic tentacles as well as a distinct snout containing the mouth. The lateral sides of the body typically have sensory epipodial tentacles. Many species of the families Tegulidae and Turbinidae are commonly found in the Noto Peninsula.

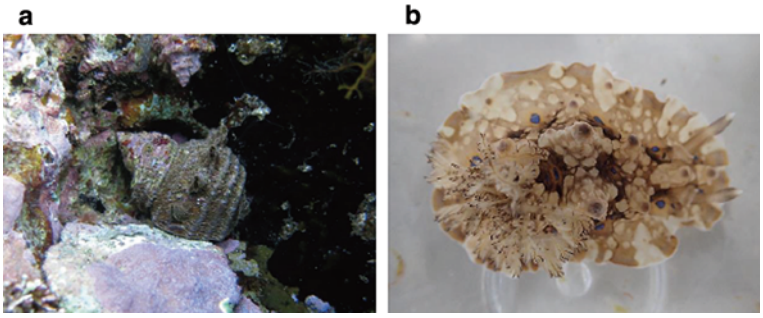

Fig. 4.8 Mollusca, Gastropoda. **a** *Turbo sazae* (Photo by Ogiso), **b** *Homoiodoris japonica* (*Photo* by Nunomura)

The subclass Neritaemorphi has wide shell entrances and slight torsion; therefore, they are similar to both limpets and typical snails. Internally, only the left ctenidium is present. The Neritidae is a relatively common family of snails found in the Noto Peninsula. This group includes some terrestrial and freshwater species.

The subclass Caenogastropoda includes many snails belonging to two groups: Architaenioglossa (river snails and terrestrial Cyclopohoridae) and Sorbeoconcha (many snails including creepers, turret shells, periwinkles, cowries, triton shells, whelk volutes, and rock shells). Many species are relatively abundant in the Noto Peninsula.

The subclass Heterobranchia comprises various groups including snails such as those belonging to Pyramidellidae. Their shell whorls change when they develop from a larva into an adult. The whorls of adult and larval shells are coiled in the opposite directions. Heterobranchia also contains the formally independent subclasses "Opisthobranchia" (Fig. 4.8b), including sea hares and sea slugs, and "Pulmonata," including terrestrial snails and slugs. Many species of the Opisthobranchs have secondary gills located after the heart. However, the concept of "Opisthobranchia" has become invalid. It includes many groups that are rich in variation. Not a few groups have well-developed shell; however, sea hares, some of which are rather large species, have a residual shell on the dorsal side of their body, and many sea slugs lost their shell perfectly. When *Aplysia* species of sea hares and related genera are attacked or disturbed, they can release ink from their ink glands, which creates a smoke-like toxic screen that is whitish, purple, or red in color. Not a few sea slugs have brilliant coloration and some are poisonous. Their coloration is regarded as a warning. Members of the order Pulmonata have lungs instead of gills. Sea Pulmonata, i.e., false limpets, occur on rocks and have lungs instead of gills.

4.2.7.2 Class Bivalvia

The Bivalvia, comprising clams, mussels, oysters, and many other shellfish groups, bears two connected valves that can be closed tightly using two calcareous valves

by a ligament and adductor muscle. Many bivalves are not often visible on the rocky shore, but they are abundant on the soft bottom, e.g., the sandy bottom or sandy-muddy bottom. A limited number of groups inhabit rocky surfaces, e.g., mussels can attach to a surface using a soft byssus. Some oysters inhabit the hard sea bottom; the valves of the oyster are highly calcified but rather irregular in shape. They are filter feeders and take food and oxygen using an incurrent and excurrent siphon. Many bivalves, the pelecypods, have a well-developed muscular foot. There are many classification systems of bivalves. Here, we will deal with four subclasses: Protobranchia, Pteriomorphia, Palaeoheterodonta, and Heterodonta. Subclass Pteriomorphia (Pteriomorpha) is a group comprising Ostreoida, Pectinoida, Pterioida, and Mytiloida. This group possesses a byssus in the adult stage or in younger periods. For example, *Mytilus galloprovincialis* and other species of Mytilidae attach to rock or wharf pilings using a thread-like byssus. Oysters attach to the hard bottom and only possess byssi in their younger stage. Oysters such as *Crassostrea nippona* are very important fishery products in the Noto Peninsula. Subclass Palaeoheterodonta occurs mainly in freshwater and brackish water; they have two shells of equal size and hinge teeth in a single row. Subclass Heterodonta bears two types of hinge teeth: cardinal teeth and lateral teeth. They also possess two adductor muscles. This subclass comprises many kinds of representative clams such as those from the families Veneridae and Mactridae. Many species are edible and important products for fisheries. Protobranchia dwells in the deep sea.

4.2.7.3 Class Cephalopoda

The Cephalopoda includes squids, cuttlefishes, octopuses, and nautiluses. The Cephalopoda body consists of an anterior head-foot and posterior visceral mass, and members have eight, ten, or more tentacles as well as a mouth with a strong beak. The ancestors of squids, cuttlefish, and octopus are nautilus-like or ammonite-like. Many existent cephalopods have reduced shells, i.e., cuttlefish have a thick shell, squids often have a thin shell, and octopuses lack a shell. The female *Argonauta* forms a shell for an egg case, which is secreted by two specially modified arms. Generally, Cephalopoda has strong locomotion ability and high intelligence. Cephalopods exchange gas by forcing seawater through their gills; they have a branchial heart at the basal part of the gills. They also have a visual cortex and camera-type eyes with high functionality, similar to those of vertebrates. Cephalopods, except for Nautiloidea, have an ink sac from which they can release ink when alarmed. The Noto Peninsula is famous for the fishery of squids such as *Todarodes pacificus.*

4.2.7.4 Class Scaphopoda

The Scaphopoda, i.e., the tusk shells or tooth shells, is relatively unfamiliar because they inhabit the subtidal zone or relatively deeper waters. Their foot extends from the

larger end of the shell and bears a thread-like captacula (pl. of captaculum), which may be used to burrow into the substrate.

4.2.7.5 Class Polyplacophora

The Polyplacophora, i.e., chitons, has a series of eight separate shell plates on their dorsal part surrounded by spicules, bristles, hairy tufts, or snake-like scales (Fig. 4.9). Their nervous system is ladder-like and similar to that of Annelida. Some species exhibit homing behavior. The most common chitons in the Noto Peninsula are *Ischnochiton comptus*, *Ischnochiton boninensis*, *Acanthopleura japonica*, *Acanthochitona achates*, and *Lepidozona coreanica* (Fig. 4.9).

4.2.8 Phylum Entoprocta

The members of Entoprocta or "Kamptozoa" are mostly sessile aquatic animals of up to 7 mm in size that form colonies. They occur on the stems of sea algae or on the surface of dead shells. Their body consists of a flower-like calyx bearing tentacles and a stem; thus, they resemble Hydrozoa. Their anus opens within the crown of tentacles.

4.2.9 Phylum Rotifera

The Rotifera are small and often occur as plankton. They possess a goblet-type body covered with a lorica and corona or "wheel organ" bearing ciliated field. Their most

Fig. 4.9 Mollusca, Polyplacophora, *Lepidozona coreanica* (*Photo* by Ogiso)

unique feature may be a large pharynx known as a "trophy" or "mastax." Many individuals of the Rotifera are usually female; males appear for a limited time only in a season. Hitherto, about 2,000 species have been reported. Many are used as natural bait for aquaculture.

4.2.10 Phylum Bryozoa (Ectoprocta) and Related Phyla

The Bryozoa or "moss animals" (Fig. 4.10a) can be found attached to rocks, stones, or the surface of other organisms on the intertidal rocky shore at ebb tide. Bryozoa mostly make colonies consisting of many small zooids (Fig. 4.10b). They have a crown of ciliated tentacles on their upper surface and a mouth in the center, followed by a U-shaped gut and an anus that opens outside of the crown. Members do not possess circulatory or excretory organs, but possess a network of "funiculus," which functions like a circulatory system. Besides normal autozooids, heterzooids exist: avicularia (pl. of avicularium), which resemble a birds' head, serve to protect the colonies, and a vibracula (pl. of vibraculum) with a flagellum-like modified operculum serves to clean the surface of the colony.

The Bryozoa has been treated as Tentaculata or Lophophorata together with the Phoronida and Brachiopoda because not only they have a lophophore, i.e., a crown of tentacles used for filter feeding, but also a body composed of three parts (prosoma, mesosoma, and metasoma).

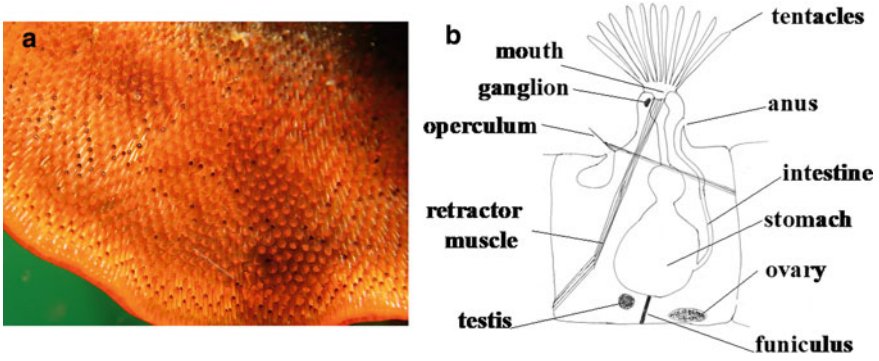

Fig. 4.10 Bryozoa. **a** *Watersipora suboboidea* (Photo by Ogiso), **b** Body of Bryozoa (Original drawing by Nunomura)

4.2.11 Phylum Chaetognatha

The Chaetognatha, also known as arrow worms, have a slender body, and moves like an arrow. To date, 120 species have been recorded. Although approximately 80% of Chaetognatha species are planktonic and approximately 20% are benthic, planktonic species have much larger populations. The latter species has muscles for locomotion and is found in the low tidal zone. Chaetognaths have translucent dart-shaped bodies covered by a cuticle. Their bodies are bilateral with one or two paired lateral fins and a caudal fin; therefore, by their outline, chaetognaths resemble fish. They have both ovaries and testes (testes and ovaries are found in the posterior half and anterior part, respectively), but they lack circulatory, respiratory, and excretory systems. Seminal receptacles are situated near the caudal end, and the female gonophores are located near the middle part of the lateral margin. From the mouth, a straight intestine travels to the anus, located in the posterior part of the body. Chaetognaths are carnivorous and capture their prey using a characteristic grasping spine.

4.2.12 Phylum Nematoda

The Nematoda or round worms are mostly small, free-living, thread-like animals; however, the parasitic species are large and harmful to plants and animals including humans. Large numbers of free-living species can, for example, be found in the interstitial environment of the sandy beach. Their bodies are unsegmented and bilaterally vermiform. Some groups have cephalic sense organs known as amphids, whereas others have caudal sense organs known as phasmids. Excretal organs of some species are unique one or two renette cells. Because they are thin, the Nematoda possess special circulatory organs and lack respiratory organs. To date more than 80,000 species have been recorded, but more may be still undescribed because they are almost all a similar shape and interpreting the taxonomy of the Nematoda is difficult. Most nematodes are gonochoristic and their cleavage is holoblastic. The phylum Nematomorpha, which includes mostly terrestrial members, is closely related to the Nematoda.

4.2.13 Phylum Arthropoda

The Arthropoda comprises more than 1,134,000 species. Their bodies are covered by cuticular exoskeletons; therefore, they must replace their exoskeletons by undergoing ecdysis. They shed the old exoskeleton after growing a new one that is not yet hardened. Arthropod bodies are segmented, and the nervous, muscular, circulatory, and excretory systems also have repeating components. Many species also have well-developed articulated legs. Therefore, most arthropods can move quickly; they are

"athletic," although large-sized species are relatively rare. This phylum is divided into four subphyla: Chelicerata, Myriapoda, Crustacea, and Hexapoda. The subphylum Chelicerata includes horseshoe crabs, spiders, mites, and scorpions; they are characterized by their chelicerae, i.e., appendages situated near the mouth, and four pairs of walking legs. The subphylum Myriapoda includes the millipedes, centipedes, and some other groups; they have many body segments and each segment bears one or two pairs of legs and/or a pair of antennae. The subphylum Crustacea includes shrimps, lobsters, crabs, barnacles, crayfish, and many groups; they are primarily aquatic and are characterized by their biramous appendages and two pairs of antennae. The subphylum Hexapoda comprises of the insects and insect-like animals, which possess six thoracic legs and a pair of antennae. Descriptions of the subphyla Myriapoda and Hexapoda are not included below because they are essentially terrestrial groups. In addition, a few subphyla, such as Artiopoda, include extinct animals, such as Trilobita. Here, they are also omitted.

4.2.13.1 Subphylum Chelicerata

The bodies of chelicerates are composed of two parts: the prosoma and opisthosoma. The first pair of appendages is chelicerae, the second pair is pedipalps, and the third to sixth pairs are walking legs; this group lacks antennae. All classes except Pycnogonida are omitted below because they are essentially terrestrial groups. The Class Pycnogonida is a group comprising of the sea spiders. Their bodies are composed of a head and trunk (segmented thorax) with conspicuously long legs and a reduced abdomen. A proboscis with four ocelli (pl. of ocellus) tubercles on a tubercle is observed in the cephalosoma. The first pair of legs are known as chelifores, the second pair of legs are known as palps (these serve as sensory organs and food-grasping appendages), and the third pair of legs are known as ovigers (these are used by males to carry eggs). Another group of the subphylum is the Arachnida, including the mites, spiders, and scorpions, which are not included here because of their terrestrial nature.

4.2.13.2 Subphylum Crustacea

The bodies of crustaceans are composed of a head (cephalon), thorax (pereon), abdomen (roughly pleon), and a tail (telson). The head comprises six segments that bear simple ocelli and/or compound eyes. Each segment, except the first, possesses a pair of appendages, i.e., the first antenna, second antenna, mandibles, first maxilla, and second maxilla. The mouth opens at the anterior part. Each appendage consists of the protopod and rami; each ramus is biramous, but one is often reduced to become uniramous. Some of the anterior thoracic appendages have become maxillipeds, i.e., appendages of the mouth part. Crustaceans comprise the following classes: Remipedia, Cephalocarida, Branchiopoda, Copepoda, Ostracoda, Thecostraca, Malacostraca, Branchiura, Mystacocarida, Tantulocarida, and Pentatomida. In this book, we

only focus on the group that is most conspicuous and larger than average in size. Several groups that do not inhabit the shore of the Noto Peninsula or are small in size are excluded.

Class Copepoda

If a water drop from a plankton net is examined with a microscope, a large number of copepods will usually be found. Many copepods are planktonic and are important natural food for fish. Some copepods are benthic and a few groups are also serious parasites of fish and other animals; the latter are often largely deformed in shape. Primarily, the body of copepods is composed of a head with five segments, six pereonal and five abdominal segments and a telson, and an abdomen composed of three segments without appendages and an anal segment. Demarcation of the segments has often partly disappeared in many groups.

Subclass Thecostraca

On the surface of the rocky shore or wharf piling, barnacles (Fig. 4.11a) may be found. Barnacles are representative of the Cirripedia, which are members of the Thecostraca. Adult barnacles (Fig. 4.11b) are sessile; they are attached to substrata through cement glands. Six pairs of recurved vines form their cirri (pl. of cirrus), each of which is divided into two branches. Their body is essentially composed of a five-segmented cephalon, seven-segmented thorax, three-segmented abdomen, and an anal segment, but they have four swimming larval stages. After hatching, they become a one-eyed nauplius, after which they progress into a cyprid stage, and finally become a sessile adult. Barnacles adapt to sessile life, even though the reproduction of this group involves copulation. To increase the chances of meeting both sexes, they are adapted as hermaphrodites with a long penis and dwarf males sometimes appear. Besides, the same species dwell close together. In parasitic groups, there is a tendency toward reduction of segmentation of the body. Around 1,000 barnacle species are currently known. Another subclass Mystacocarida is omitted below. In the Noto Peninsula, *Chthamalus challengeri*, *Megabalanus rosa*, *Balanus trigonus*, and *Capitulum mitella* (Fig. 4.11a) are commonly seen.

Class Malacostraca

The Malacostraca includes many shrimps, crabs, hermit crabs, mantis shrimps, woodlice, mysids, and many other groups. The Malacostraca body essentially originally consists of 19 or 20 segments: the cephalon is composed of 6 segments with mouthparts and 2 pairs of antennae, 1 of which is sometimes branched. They often have compound eyes with stalks. The thorax is essentially eight-segmented, but mostly the anterior one–three segments are fused to their head, and their legs are

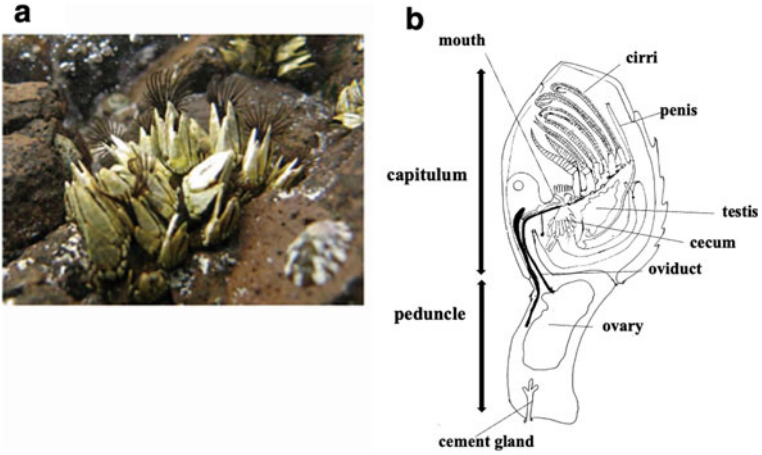

Fig. 4.11 Arthropoda, Thecostraca, Cirripedia. **a** *Capitulum mitella* (Photo by Ogiso), **b** Body of Cirripedia (Modified after McLaughlin 1980)

converted into maxillipeds as a part of mouthparts and often covered with a carapace along with a head. The abdomen (here, it means pleon) consists of six segments (seven in Phyllocarida) and a telson, but the last pleonal segment is fused to the telson.

This class comprises three subclasses: Phyllocarida, Hoplocarida, and Eumalacostraca.

The subclass Phyllocarida contains the order Leptostraca. The body is composed of a six-segmented head, eight thoracic and six to seven pleonal segments, and a narrow tail. Their carapace covers cephalon, thorax, and anterior part of abdominal somites. *Nebalia japonica* may be found in eutrophic and relatively dirty water in Japan.

The subclass Hoplocarida contains the order Stomatopoda, i.e., the mantis shrimp. Their bodies have a cylindrical abdomen as well as a flat well-developed tail with a wide uropod. The cephalon bears two pairs of antennae with well-developed eyes and a movable rostrum. The carapace covers the head and thoracic segments 1–4. Thoracic segments 1–5 are uniramous with subchelate legs. The unique appendage in the mantis shrimp is the second maxilliped. The first to fifth thoracic legs lack exopods. *Oratosquilla oratoria* is important edible species found in the middle region of Japan.

The subclass Eumalacostraca comprises three superorders: Peracarida, Eucarida, and Syncarida (omitted here). Their bodies have 19 segments in total: five cephalic, eight thoracic, and six abdominal segments. A carapace envelops the thoracic region. They bear movable stalked eyes; the antennae and other appendages are essentially biramous, but a few groups have uniramous versions. Many groups have natatory exopods on the thoracic limbs with a tail fan formed by the lamellar rami of the uropods on either side of the telson.

The superorder Peracarida comprises the orders Mysida, Amphipoda, Cumacea, Isopoda, Tanaidacea, and several little-known orders. Mature females have brood pouches formed by oostegites (extensions from the coxae); they lay their eggs in these brood pouches, and the young exits the pouch after it hatches. Consequently, females lay a relatively small number of eggs in the brood pouch. More than 25,000 species of the Peracarida are known, and there may be many species as yet undescribed or undiscovered. The abundance of peracarids in the sea is similar to that of insects in terrestrial environments. In addition to the abovementioned five orders, some orders, Lophogastrida, Mictacea, Spelaeogriphacea, and Thermosbaenacea, are not described below.

The order Mysida, the opossum shrimps, is relatively small shrimp-like crustaceans. Both of their antennae are bifid. The basal part of first antenna has masculine processus in males. The pereopods of mysids are biramous and without gills. The pleopods are reduced in males, and the endopods of uropods have statocysts. Young individuals are hatched already bearing all pereopods. Many benthic species make daily vertical migrations from the deeper parts to shallower waters.

The order Cumacea or the hooded shrimp/comma shrimp is generally abundant on the sea bottom. Their bodies have a large carapace and a relatively long and slender abdomen. Their second antenna consists of numerous segments in males, but the number of segments is notably reduced in females; the first three pairs of pereopods have become maxillipeds.

The order Amphipoda often occurs in large numbers on algae or under stones, and they usually swim sideways. Their bodies lack a carapace and are generally compressed "side-to-side." Amphipods are 1–340 mm in size and are mostly detritivores or scavengers. Almost 10,000 species have been described so far; these contained suborders Gammaridea, Caprellidea, Hyperiidea, and Ingolfiellidea. The Gammaridea seems to be the typical group, i.e., small, shrimp-like crustaceans, but their anterior legs face the anterior direction, whereas their posterior legs face the posterior direction. Many species are commonly seen in the rocky shore of the Noto Peninsula. The Caprelloidea, known as the skeleton shrimp, have a stick-like body. The first two pairs of pereopods are modified into gnathopods, which are used for feeding, defense, and locomotion. The third and fourth pair of pereopods are reduced with two pairs of gills. The fifth to seventh pair of pereopods is used for clasping objects.

The order Isopoda comprises 10,000 known species worldwide. Isopodan crustaceans lack a carapace and generally have a "top-to-bottom" (dorsoventrally) depressed body. Many species have seven pairs of walking legs (some are prehensile or reduced) followed by five pairs of plate-shaped pleopods. Pill bugs or sow bugs are well-known, and the wharf roach "*Ligia*" can often be observed running on the rocks of the shore; however, these are classed as terrestrial groups. Nevertheless, many diverse groups exist in marine environments, e.g., under the rocks of the intertidal zone: Sphaeromatidae such as *Gnorimosphaeroma ray*i, Cirolanidae such as *Cirolana harfordi,* and Anthuroidea such as *Paranthura japonica* are often found in the Noto Peninsula. Among seaweed colonies, Valvifera such as *Synidotea laevidorsalis* can also be found.

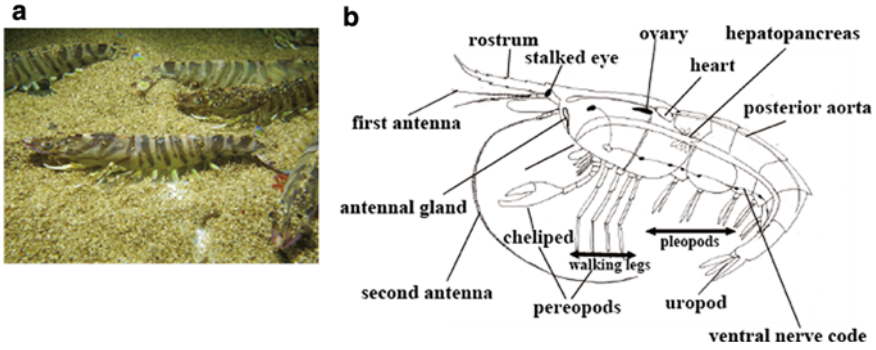

Fig. 4.12 Arthropoda, Decapoda. **a** *Marsupenaeus japonicus* (Photo by Ogiso), **b** Body of a shrimp (Original drawing by Nunomura)

The order Tanaidacea is somewhat similar to Isopoda in terms of external shape, but they have a cephalon fused to first and second thorax somites and covered with a carapace. The first pairs of legs are large gnathopods.

The superorder Eucarida includes two important orders: Decapoda (Fig. 4.12a) and Euphausiacea. The carapace of the Eucarida is fused and covers the head and thorax. Generally, their sensory and nervous systems, as well as their muscles, are well developed; therefore, they have strong locomotion ability. Their breeding patterns involve oviparity: females release eggs into the sea, and after they have hatched, they pass into the nauplius larvae stage.

The order Decapoda includes about 14,400 species such as true shrimps, ghost shrimps, porcelain crabs, hermit crabs, mole crabs, sand crabs, and regular crabs. Specifically, the Decapoda comprises two subclasses: Dendrobranchiata and Pleocyemata. Their carapace covers the cephalon and thorax perfectly, and the sensory, nervous, and muscular systems are highly developed leading to advanced locomotion ability. The exopods of their maxilla are wide, and they play a role in sending water toward the gill chamber. The first three pairs of pereopods have become maxillipeds. The fourth to eighth appendages are well-developed for walking, grasping, and other functions; thus, many groups may have ten walking legs, although one or more pairs may be reduced. Outwardly, the body is distinctly separated into a cephalothorax and abdomen. Thoracic legs are outwardly visible, and the exoskeleton is usually well calcified. Decapoda have well-developed gills and a branchial chamber. The cephalon is also well-developed with stalked compound eyes.

The suborder Dendrobranchiata (Fig. 4.12b) includes more than 400 species and comprises prawns such as *Marsupenaeus*. Adults bear finely branched and feathered gills, except for the genus *Lucifer*. The gonads open at the base of the fifth pair of walking legs in males; the male genitalia, known as the petasma, is located at the inner side of the first pair of pleopods. The gonads open at the base of the third pair of walking legs in females; the female genitalia known as the thelycum is located at the inner sides of the fourth and fifth walking legs. These are important for identification.

The suborder Pleocyemata includes nearly 14,000 species and comprises infraorders Caridea, Achelata, Anomala, Brachyura, and several others. Here, only the important and conspicuous groups are described. In this group, the fertilized eggs are protected by the female. They remain stuck to her swimming leg, and the zoea larvae hatch from this location.

The infraorder Caridea includes many types of shrimp. The second pleonal segment of this group is wide and overlaps the first and third segments. They have one pair of stalked eyes, which is sometimes covered by the carapace. Their gills are within a thin plate, and the muscle of the abdomen is well-developed to enable rapid locomotion. They have five pairs of walking legs; the first two pairs form chelipeds in many groups. Sometimes, one of the chelipeds is huge in males.

The infraorder Achelata is rather large in size and important for fisheries. Their body, walking legs, and second antennae all bear a hard well-developed exoskeleton. The second antennae are long with a few flagellar segments. The bodies of younger individuals are as broad as phyllosoma. The members of this group are exclusively warm-water dwellers.

The infraorder Anomala (Anomura) comprises various groups, including the porcelain crabs, hermit crabs, mole crabs, and sand crabs. Among these, the hermit crabs are possibly the most familiar group. Their abdomen and tail are not well-developed, and they are collapsed toward the ventral side of the cephalothorax or they insert themselves into the shells of dead sea snails; however, some species attack snails to obtain a suitable shell. However, hermit crabs can use many kinds of shells, including the shells of scaphopods, and even artificial materials. The first pairs of walking legs are cheliped and the fifth (sometimes also the fourth) pairs are short; therefore, they appear to have only three pairs of walking legs. Almost all species of hermit crabs have soft spirally curved abdomens, into which the whole body can retract; thus, their body can be protected from predators when using an empty shell. In some groups, the claw on one side is often much bigger than that on the other side. Porcelain crabs also belong to Anomura. Their exterior shape is similar to that of a regular crab. The carapace is rounded and the anterior rostrum is not well developed. The first walking legs are well-developed chelipeds, but the right and left sides are often asymmetrical, while the fifth leg is reduced and located within the gill chamber.

The infraorder Brachyura or the regular crabs (Fig. 4.13) include more than 6,500 species. They have a rigid, chitinous, cephalothorax that occupies most of their body, but their abdomen is thin and narrow, especially in males. They have a pair of stalked compound eyes and two pairs of short antennae in the anterior margin. They also possess a pair of mandibles, maxillulae, maxillae, and three pairs of maxillipeds; the third maxilliped covers the mouth parts on the ventral surface. The thorax has five pairs of pereopods; the first walking legs are chelipeds used to grasp prey or frighten enemies. In the genus *Uca*, the male has an extremely large cheliped, which is used during courtship. In many crabs, side-stepping locomotion is common; however, Mictyridae walks forward, Raninidae walks backward, and Inachidae can walk in any direction. Members of Portunidae have an oar-shaped last pair of legs that are used for swimming.

Fig. 4.13 Arthropoda, Decapoda, *Leptodius exaratus* (*Photo* by Nunomura)

The order Euphausiacea or krill resembles true shrimp or opossum shrimp. The cephalon and thorax are wholly covered by a carapace, and the abdomen is composed of six segments and a telson. The thorax is composed of eight segments, each with a pair of appendages, but they are not modified to maxillipeds. The second and third pairs are modified as chelipeds in some groups, and the posterior 1–2 pairs are reduced in some groups. Branched gills have developed at the base of the thoracic appendages, but they are not covered by the carapace. Euphausiacea have statocysts in their uropods. They are gonochoric and their spermatophores are sticky.

Class Ostracoda

The Ostracoda is small-sized with a body enclosed by two valves, which are closed by an adductor muscle and hinged dorsally. Body segmentation is much reduced, with only six to eight pairs of appendages. Ostracods are found on seaweeds and the sandy bottom of the shore.

4.2.14 Phylum Echinodermata

The Echinodermata, which belongs to Deuterostomia, comprises five major unique groups: the sea urchins (class Echionoidea), sea stars, (class Asteroidea), brittle stars (class Ophiuroidea), sea cucumbers (class Holothuria), and sea lilies (class Crinoidea). Although adult Echinodermata are recognizable by their (usually five-point) radial symmetry, the larvae show bilateral symmetry. They possess a unique water vascular system; this comprises a network of fluid-filled canals derived from the body cavity (Fig. 4.14). It functions not only in gas exchange and feeding but also in sensory perception and locomotion. Adult echinoderms are found on the sea bed, but the larvae are planktonic; thus, the morphology of adults and larvae clearly differs. The Echinodermata is relatively large in size and the phylum contains about 7,000 living species, none of which are freshwater or terrestrial species.

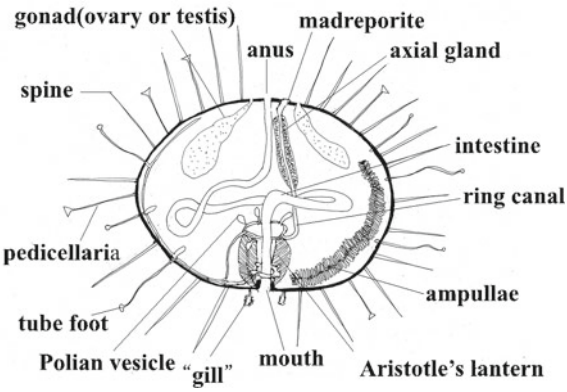

Fig. 4.14 Body of Echinonoidea from Echinodermata (Original drawing by Nunomura)

4.2.14.1 Class Echioidea

Typical echinoids are spherical and chestnut-burr-shaped, but elliptical and flat species also exist. They have a hard epidermis and three types of protuberances from the epidermis: spines, tube feet, and pedicellariae (pl. of pedicellaria) (Fig. 4.14). The length of spines varies according to species. For example, *Diadema* has long poisonous spines. The pedicellariae are used for protection and may also contain poison; for instance, the flower urchin, *Toxopneustes pileolus*, can administer a dangerous, painful, and medically significant poison when touched, which is rarely lethal. The tube feet of echinoids are soft, flexible, and their tips adhere to the substrata; they are organs used largely for locomotion as well as grasping food. Echinoids possess a typical water vascular system, the opening of which is a hydropore with a sieve-like madreporite near the central part of the upper side, i.e., close to the anus in a "typical" sea urchin (Fig. 4.14). The hydropore is connected to a thin duct (a stone canal) and extends to a ring canal, after which it branches off to short lateral canals, each one ending in an ampulla and tube foot (Fig. 4.14). The area of the surface with tube feet is known as the ambulacral zone, whereas the surface without tube feet is called the interambulacral zone. The part with ampulla can protrude through a pore (or a pair of pores), to the exterior of which is a tube foot. The water vascular system serves to distribute nutrients throughout the body; it is most obviously expressed in the tube feet, which can move by extension or contraction caused by the redistribution of fluid between the foot and the internal sac, which functions in gas exchange, feeding, sensory perception, and locomotion. The mouth of regular echinoids is located near the central part of the lower surface, and the pharynx is surrounded by a strong jaw termed Aristotle's lantern. The anus is located near the central area of the upper surface. The gonopore also opens near the anus at the upper part of a regular sea urchin. The most common species found in the Noto Peninsula are *Heliocidaris crassispina* and *Hemicentrotus pulcherrimus* (Fig. 4.15a).

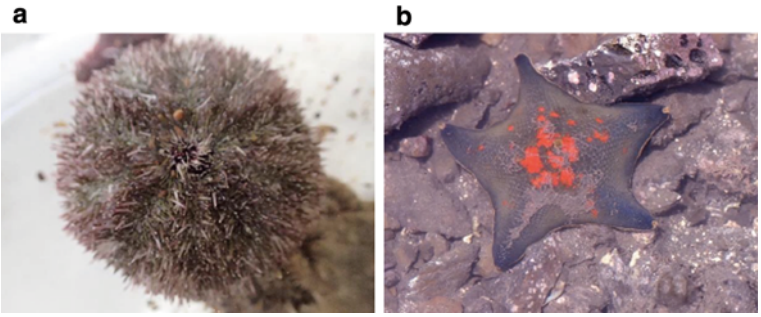

Fig. 4.15 Echinodermata. **a** Echioidea, *Hemicentrotus pulcherrimus* (Photo by Nunomura), **b** Asteroidea, *Patiria pectinifera* (Photo by Nunomura)

4.2.14.2 Class Asteroidea

The body of Asteroidea has five (or more) arms. Thus, they are star-shaped, and they bear ambulacral grooves on the ventral side of the arms, which possess many tube feet. Adults are recognizable by their radial symmetry. In the Asteroidea water vascular system, radial canals extend along the arms from a circular canal. Sea stars are carnivorous and attack bivalves and other prey: they expel their stomach from their mouth and use it to consume prey outside of their body. Larvae of asteroids are initially bipinnaria, similar to those of Auricularia of Holothuroidea; subsequently, they transform into brachiolaria and finally into adult forms. The most common species in the Noto Peninsula are *Patiria pectinifera* (Fig. 4.15b), *Aquilonastra bather*, and *Certonardoa semiregularis.*

4.2.14.3 Class Ophiuroidea

The body of Ophiuroidea, the brittle stars, consists of an obvious central disk and five or more whip-like or snake-tail-like arms with spines: these are sometimes branched and used to crawl along the sea bed. Some ophiuroids, such as basket stars, have complicatedly branched arms. Their mouth is rimmed with five jaws. Ophiuroids are abundant not only onshore but also on the deep-sea bottom where they may feed on the skeletons of fish and hard parts of animals; thus, they are of great advantage to clean the sea bottom. Ophiuroidea larvae, Ophiopluteus, are similar to those of Echionoidea. The most common species in Noto is perhaps *Ophioplocus japonicus* (Fig. 4.16a).

4.2.14.4 Class Holothuroidea

The Holothuroidea, the sea cumbers, has soft bodies that lack a single rigid big skeleton but have small ossicles embedded beneath the skin. Sea cucumbers

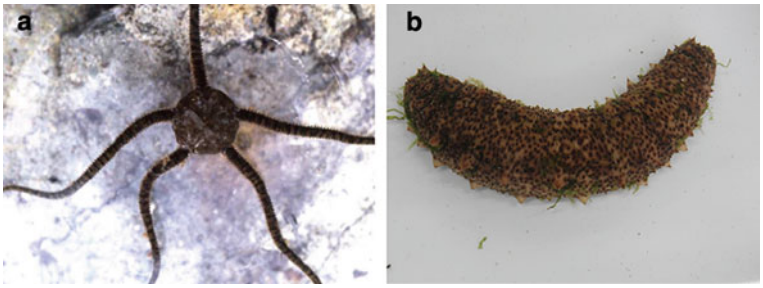

Fig. 4.16 Echinodermata. **a** Ophiuroidea, *Ophioplocus japonicus* (Photo by Nunomura), **b** Holothuroidea, *Apostichopus armata* (*Photo* by Sekiguchi)

are deposit or suspension feeders; their mouths are situated at the anterior end, surrounded by feeding tentacles, whereas the anus is found at the posterior end in the anal area. Characteristic respiratory trees are located in the posterior part of the body; they open in the rectum and gas exchange is completed using seawater taken in through the anus. Sometimes organisms such as pearlfish (Carapidae) or pea crabs (Pinnotheridae) inhabit the cloaca of sea cucumbers. Certain holothurians have characteristic defense methods, one of which is the Cuvierian organ: when they are attacked by enemies, they extrude sticky clusters of fine tubes from the base of the respiratory trees in the cloaca. After these tubules contact seawater, they lengthen, become adhesive, and effectively deter enemies. Another defense mechanism, used by some species when they are severely threatened, involves emitting the viscera; this can be regenerated in time. The larvae of holothurians, the auricularia, are somewhat similar to the bipinnaria of Asteroidea. The most common species in the Noto Peninsula are *Apostichopus armata* (Fig. 4.16b) and *Holothuria decorata.*

4.2.14.5 Class Crinoidea

Members of the Crinoidea have a flower-like body with many feather-like arms. They live on subtidal rocks in the sea. In adult crinoids, the mouth is situated on the upper surface. Primitive groups of Crinoidea in the deep sea are known to have a stem. However, more recently evolved feather stars have lost this stem, although juvenile feather stars do possess a short stem. The first larvae of crinoids are doliolaria, followed by cystidians, pentacrinoids, and finally the adult form.

4.2.15 Phylum Hemichordata

The Hemichordata, including the acorn worms, is rather rare vermiform animals. Their bodies consist of three parts: a proboscis (prosoma), collar (mesosoma), and trunk (metasome). The circulatory system is open with the heart situated on the

dorsal side. The mouth cavity is tubular and bears a narrow stomochord that extends up into the proboscis. A plexus of nerves lies in both the dorsal and ventral nerve cords. Some hemichordates have pelagic larvae known as tornaria, which resemble the bipinnaria or auricularia of Echinodermata. Some species produce an iodoform smell.

4.2.16 Phylum Chordata

The Chordata includes various groups, e.g., the ascidians, lanceolates, and vertebrates; they have a fluid-filled body cavity (coelom) and pharyngeal slits (gill slits) throughout life or during the early developmental stages. The pharynx is part of the throat situated immediately behind the mouth. Many terrestrial groups use their tails for balance and many other roles. The chordates have a notochord, a fairly stiff rod that extends along the anterior–posterior axis of the body; a dorsal neural tube runs along the notochord. The endostyle is a groove in the ventral wall of the pharynx that assists in filter-feeding but has disappeared in the adult of many groups; it is considered to be homologous to the thyroid gland in vertebrates. The Chordata comprises more than 66,000 species and the group is divided into three subdivisions: Cephalochordata, Tunicata (Urochordata), and Craniata (Vertebrata).

4.2.16.1 Subphylum Tunicata (Urochordata)

The subphylum Tunicata contains 3,000 species and comprises the classes Ascidiacea (sea squirts), Thaliacea (salps), and Appendicularia (larvaceans). Adult sea squirts (Fig. 4.17a) are solitary or colonial sessile animals after their larval phases, whereas members of Thaliacea and Appendicularia are planktonic or swim slowly. The larvae of Tunicata are tadpole-shaped and swim; they also have an otolith, a notochord, a dorsal nerve formed from a neural plate, an ocellus, and muscles; however, the larval stage is short. Sea squirts (Fig. 4.17b) have a rounded body, thick body wall tunic, and two siphons: the oral siphon (opening internally) and atrial siphon. Seawater containing small planktonic particles is ingested from the oral siphon and discharged from the atrial siphon (Fig. 4.17b). Though the seawater is passed through many pores of the branchial sac, food particles are first captured by a mucous net secreted from the endostyle in the branchial sac and then transported to the digestive tract, including the esophagus, stomach, and intestine (Fig. 4.17b). After digestion and absorption are completed in the digestive tract, undigested food is discharged from the anus (Fig. 4.17b). Solitary sea squirts reproduce both sexually and asexually. The classes Thaliacea and Appendicularia can be planktonic or may swim. In the Noto Peninsula, *Styela plicata*, (Fig. 4.17a) *Halocynthia roretzi*, and many colonial species are often observed.

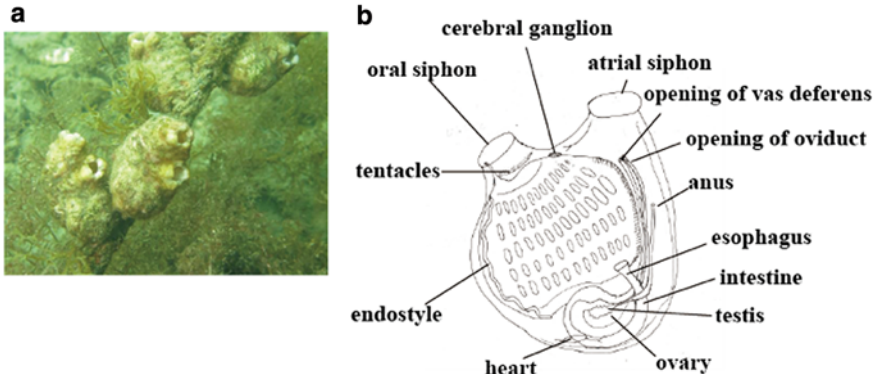

Fig. 4.17 Chordata, Tunicata. **a** *Styela plicata* (Photo by Ogiso), **b** Body of an ascidian (Modified after Brusca, Moore, Shuster, 2016)

4.2.16.2 Subphylum Cephalochordata

The Cephalochordata, the fish-shaped lancelets, has a dorsal nerve tube and notochord running from the head to the tail. The notochord is maintained throughout their life. Their head lacks a brain, although they possess specialized sense organs. The members of the Cephalochordata are essentially burrowing filter feeders that are found on the clean sandy bottom.

4.2.16.3 Subphylum Vertebrata

The Vertebrata, including fishes, amphibians, reptiles, birds, and mammals, is the most well-known subgroup of the chordates. The vertebrates possess a backbone that runs through the length of their body. A dorsal neural tube develops into the spinal cord, which is the main communication trunk of the nervous system, and a large brain is protected by a skull. The mouth is situated at or near the anterior part of the body, whereas the anus opens at the posterior part of the body. The posterior behind the anus is known as the tail. The internal organs of vertebrates are suspended in the abdominal cavity. In particular, the heart and circulatory system are well developed. Fish is one of the most major marine vertebrates and they can be grouped into two groups: Cyclostomata, including hagfish, lampreys, and Gnathostomata, i.e., jawed vertebrates, including Chondrichthyes, and Osteichthyes.

References

Barnes RD (1963) Invertebrate zoology. Saunders College Publishing Philadelphia, 893pp
Brusca RC, Moore W, Shuster SM (2016) Invertebrates. Third Edition Sinauer. 1104pp
Hillis et al., 2012Hillis DM, Sadava DE, Hill RW et al (2012) Principles of life. W. H. Freeman, 908pp
McLaughlin PA (1980) Comparative morphology of recent Crustacea xii, 1–177, figs. 1–53. Freeman, W. H. & Cy, San Francisco, U.S.A. and Oxford, UK
Margulis L, Schwartz KV (1997) Five Kingdoms: an illustrated guide to the phyla of life on earth. W.H. Freeman & Company, 520pp
Laumer CE, Fernández R, Lemer S et al (2019) Revisiting metazoan phylogeny with genomic sampling of all phyla. Proc R Soc B 286:1–10
Ponder WF, Lindberg DR (1997) Towards a phylogeny of gastropod molluscs: an analysis using morphological characters. Zool J Linn Soc 119:83–275
Russel-Hunter WD (1979) A life of invertebrates. Macmillan, New York, p 650
Zimmer C, Emlen DJ (2013) Evolution: making sense of life. Roberts & Company, 752pp

Chapter 5
Observation of Marine Invertebrates in the Noto Peninsula

Toshio Sekiguchi, Yoichiro Kitani, and Shouzo Ogiso

5.1 General Description of the Noto Peninsula and the Sea of Japan

The Noto Peninsula is a landform that protrudes from the mainland of Honshu, Japan, into the Sea of Japan. It is located to the east of Toyama Bay. The Sea of Japan is an enclosed sea to the open ocean and only connected by the Tsushima, Mamiya, Soya, and Tsugaru Straits. The Tsushima Warm Current flows northward through the Tsushima Strait, and the Liman Cold Current flows southward through the Mamiya Strait. Due to those warm and cold currents, both southern and northern marine animals can be observed on the coast of the Noto Peninsula. For example, the brown paper nautilus *Argonauta hians* and the spiny puffer *Diodon holocanthus*, which are usually found further southern region, have been observed in the waters of the Noto Peninsula. These animals travel from tropical and subtropical waters by drifting with the Tsushima Current during spring and summer, but fail to survive the cold sea temperatures during winter. On the other hand, *Rhizopsammia minuta mutsuensis* (Phylum Cnidaria, Class Anthozoa) is a northern species that has also been observed in the coastal waters of the Noto Peninsula (Yajima et al. 1979). Additionally, the beard worm, *Oligobrachia mashikoi* (Phylum Annelida, Family Siboglinidae), has been collected from Tsukumo Bay, the eastern side of the Noto Peninsula, nevertheless Siboglinidae mainly inhabits cold water in the deep sea (Sasayama et al. 2003). *O. mashikoi* possesses beard-like tentacles, which would allow gaseous exchange. The beard worm lacks a digestive system that includes the mouth, gut, and anus (Fig. 5.1) and, instead, possesses a trophosome, an organ containing specialized cells called bacteriocytes, which include chemosynthetic bacteria (Deguchi et al.

T. Sekiguchi (✉) · Y. Kitani · S. Ogiso
Noto Marine Laboratory, Institute of Nature and Environmental Technology, Division of Marine Environmental Studies, Kanazawa University, Noto-Cho, Ishikawa 927-0553, Japan
e-mail: t-sekiguchi@se.kanazawa-u.ac.jp

N. Hasebe et al. (eds.), *Field Work and Laboratory Experiments in Integrated Environmental Sciences*, https://doi.org/10.1007/978-981-99-6532-8_5

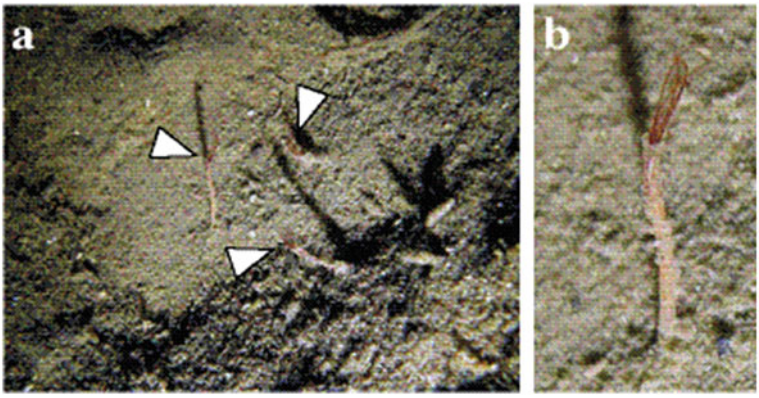

Fig. 5.1 *Oligobrachia mashikoi* (Photo by Ogiso). Three individuals are indicated with arrowheads (**a**). **b** is enlarged photo of **a**

2007). Thus, the beard worm obtains nutrients via the chemosynthetic bacteria in the bacteriocytes.

5.2 Features of the Intertidal Zone in the Sea of Japan

Field observation of marine animals is commonly conducted in the intertidal zone because we can safely observe this ecosystem which is formed by tidal change. The intertidal zone is affected by changes in tidal levels (Fig. 5.2), which are caused by the tide-generating force of gravity between the sun and moon. Because the Earth rotates once a day, most places on the Earth have two cycles consisting of low and high tides each day. Every full and new moon, when the moon, sun, and Earth are aligned once every two weeks, the tidal variation is significant because both the force of gravity exerted on the Earth by the moon and sun produce the tidal force. This tidal condition is designated as a spring tide. In contrast, the tidal range is the smallest during a neap tide, the period before and after the young or old moon. The intertidal zone is the area covered between high and low tide lines of the spring tide. The area that remains dry during the highest tidal level of the spring tide is designated as the supratidal zone. In contrast, the area flooded at the lowest tidal level of the spring tide is known as the subtidal zone. The width of the intertidal zone greatly differs between the coast of the Sea of Japan and that of the Pacific Ocean. The daily tidal range of the Sea of Japan coast is small compared to that of the Pacific Ocean (Fig. 5.3). Therefore, the area of the intertidal zone is smaller along the coast on the Sea of Japan compared to the coast along the Pacific Ocean. In addition, seasonal variations in the tidal range of the Sea of Japan are larger than the diurnal variations. The tide level is higher in summer than in the winter on the coast of the Sea of Japan.

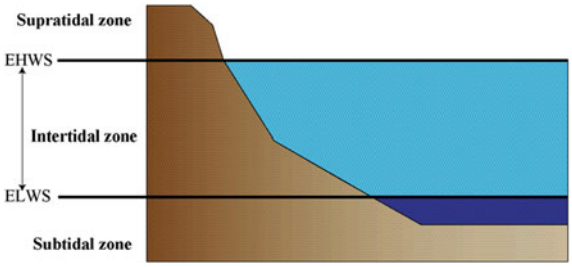

Fig. 5.2 Intertidal zone, depicting the extreme high water of spring tides (EHWS) and the extreme low water of spring tides (ELWS)

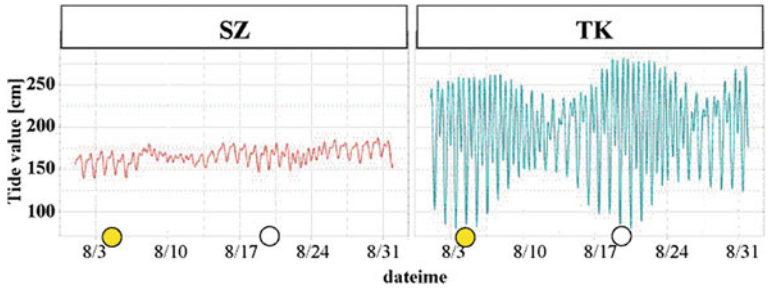

Fig. 5.3 Tidal change on the coasts of the Sea of Japan (Suzu: SZ) and the Pacific Ocean (Tokyo: TK) in August 2020. In August 2020, the full and the new moons were on the 4th and 19th, respectively. This graph is provided by Shinya Uryu at the Center for Design-Oriented AI Education and Research, Tokushima University and described by *R package jmastats* (https://gitlab.com/uribo/jmastats) using data obtained from the Japan Meteorological Agency

5.3 Plankton and Benthos

Aquatic animals can be classified according to their lifestyle, such as planktonic, neustonic, nektonic, and benthic (Lalli and Parsons 1997). Plankton and nekton are animals that live in water columns and exhibit different behaviors. Plankton float and cannot move against the currents (further details on Plankton in Sect. 5.6), while nekton includes all aquatic animals that can swim, such as fish. Neuston is the category of aquatic animals that live on the surface of the water, such as water striders. In marine environments, neuston include animals such as sea skaters and by-the-wind sailors. Benthos is the general term for animals that live on or under the seafloor, such as sea urchins, shellfish, polychaetes, and crustaceans. Many benthic animals, including adult sea urchins, crabs, shrimps, and shellfish, exist as plankton in their larval stages.

5.4 Collecting Benthic Animals from the Intertidal Zone

Benthos is classified into five groups: megabenthos, including all organisms larger than 4 mm, such as sea urchins, shellfish, crabs, and seaweed; macrobenthos, which include animals between 1 and 4 mm, such as polychaetes and small shellfish; and meiobenthos, which include animals between 0.031 and 1 mm, such as nematodes; nanobenthos, which categorizes animals 0.002–0.0031 mm in size, such as ciliates and flagellates; and, finally, picobenthos (less than 0.002 mm), which are primarily bacteria. The macrobenthos and megabenthos are the main targets for marine animal collections in educational activities.

Collection of marine animals is usually conducted during daytime in summer. As explained in Sect. 5.2, the daily tidal change is small (approximately 30 cm) in the seashore of the Noto Peninsula, even though the annual tidal level is the highest in summer in the Sea of Japan. The coastal area exposed during low tide is narrow. Students need to immerse themselves waist-deep in water to observe and collect the animals (Fig. 5.4).

5.4.1 Equipment Required for the Observation and Collection of Marine Animals

Here we describe the equipment that is essential for the observation of marine animals in the Sea of Japan. Although some items are necessary specifically for collection activities on the shores of the Sea of Japan, most items are useful for observation of marine animals in other locations.

- Clothing
  Students should don sportswear such as long-sleeved tops and legwear to prevent them from cutting their limbs on rocks or being stung by dangerous marine animals. In shallow water, waders are useful. Wearing a life jacket is strongly recommended for safety (in the event of an accident or when one goes into

Fig. 5.4 Observation of marine animals in the rocky shore. The university students wear sports clothes under life jackets

deeper water). When immersing in waist-deep water, wetsuits are also suitable. Because wetsuits are buoyant, lifejackets are not needed. Moreover, wetsuits protect students from rocks and dangerous animals. For safety, diving weights should not be worn.

- Cap/Hat
  Students should wear a cap/hat to protect their head from the sun and avoid heat stroke.
- Gloves
  Wearing gloves is important to protect hands from jagged rocks and dangerous animals.
- Marine boots
  Students should wear marine boots to protect their feet. If marine boots are not available, the student should wear shoes with similar functions, such as jogging shoes.
- Diving mask or boxed water glass
  These instruments are useful for underwater observation.
- Collecting equipment
  Students should use tweezers to collect animals. A butter knife is useful for peeling off animals that adhere to the rocks, such as limpets and chitons. Buckets are necessary to store animals during sampling.
- Fresh water
  To prevent dehydration, plenty of fresh water and/or electrolyte drinks should be carried all the time.
- First aid kit
  A first aid kit should always be at hand, in the event of injury or heat stroke. After emergency treatment, the injured student should be transported to the hospital if warranted.

5.4.2 How to Collect Benthic Animals in the Intertidal Zone

Marine animals are zonally distributed in a vertical direction from the subtidal zone to the supratidal zone. Family Littorinidae, periwinkle, such as *Nodilittorina radiata* and *Littorina brevicula*, have relatively small shells and inhabit the rocks of the supratidal zone close to the intertidal zone (Fig. 5.5a). The shell lengths of *N. radiata* and *L. brevicula* are approximately 11 and 15 mm, respectively. Limpets, such as *Cellana toreuma*, are attached to rocks on the shoreline (Fig. 5.5b, c). On the rocky shore, snails such as *Lunella coreensis*, *Monodonta confusa*, and *Omphalius rusticus* can be also observed. Crabs such as *Leptodius exaratus* (see Fig. 4.13 in Chap. 4) and hermit crabs, such as *Pagurus filholi*, inhabit the rocky bottom in shallow water. Many animals hide under the rocks, and students should turn over rocks to find them. Along the rocky shore in the intertidal zone, dominant echinoderms are brittle stars (*Ophioplocus japonicus*), sea urchins (*Heliocidaris crassispina* and *Hemicentrotus pulcherrimus* (see Fig. 4.15 in Chap. 4) and sea stars (*Patiria pectinifera*; Fig. 4.15 in

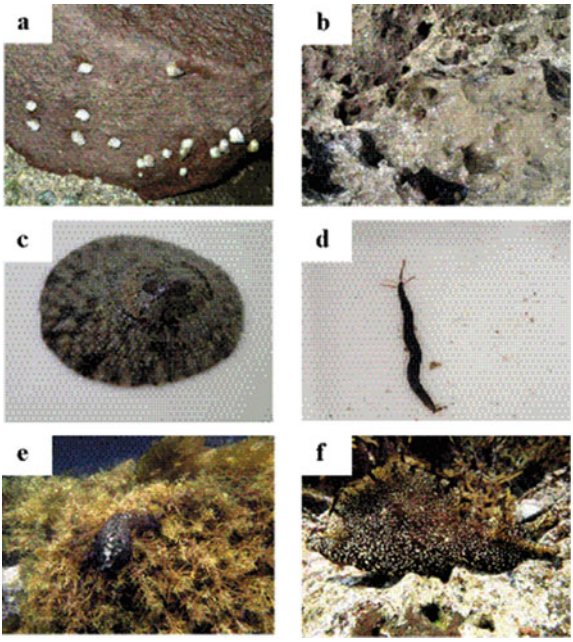

Fig. 5.5 Marine invertebrates observed in the Noto Peninsula (Photos by Sekiguchi and Ogiso). **a** *Nodilittorina radiata.* **b**, **c** *Cellana toreuma.* **d** *Acrocirrus validus.* **e**, **f** *Aplysia kurodai*

Chap. 4). Polychaeta, *Acrocirrus validus* can also be observed under rocks (Fig. 5.4d). Students can also observe *Acanthopleura japonica*, a polyplacophora mollusk (see Sect. 4.2.7.5), and several species of Platyhelminthes, such as *Planocera reticulata* (see Sect. 4.2.4). Aplysia is also common on the seaweed bed (Fig. 5.5e, f). Furthermore, a species of skeleton shrimp attached to seaweed, is a crustacean that eats suspended materials in seawater. Because of their small size, the animals must be observed under a microscope. Students can bring samples of seaweed back to the laboratory and wash them with filtered seawater to collect the skeleton shrimp.

5.4.3 Dangerous Animals

There are some dangerous animals in the intertidal zone. As shown in Fig. 5.6, some harmful animals exist on the coast of the Noto Peninsula. The redfin waspfish *Paracentropogon rubripinnis* lives on the sea floor and possesses poisonous spines on the dorsal fin (Fig. 5.6a). It does not move much but should not be caught by hand. Sea urchins, such as *Heliocidaris crassispina* and *Diadema clarki* (Fig. 5.6b), have long spines. The tips of the spines of *D. clarki* contain a poison. Being stung by one of these spines is quite painful, and the spines are difficult to remove; therefore, students should be warned not to touch or step on them. Some cnidarians have a strong venom contained in the nematocytes (stinging cells) of the tentacles. In the Noto Peninsula,

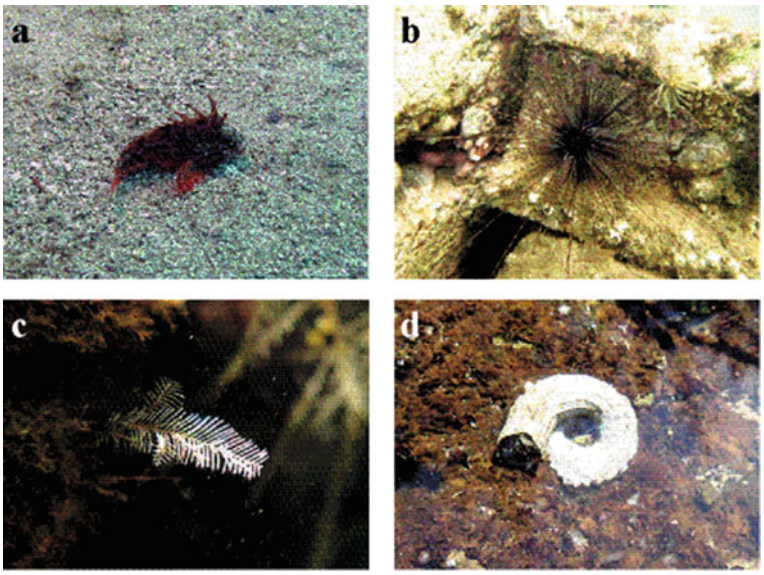

Fig. 5.6 Dangerous animals (photos by Ogiso). **a** *Paracentropogon rubripinnis*. **b** *Diadema clarki*. **c** *Aglaophenia whiteleggei*. **d** *Thylacodes adamsii*

Carybdea brevipedalia, *Chrysaora pacifica,* and *Aglaophenia whiteleggei* (Fig. 5.6c) are commonly observed but should not be touched.

C. brevipedalia and *C. pacifica* drift in the water column and cannot move quickly, while *A. whiteleggei* is sessile. Thus, they can be easily avoided if one keeps a safe distance. The nematocytes will not penetrate long sleeves, leggings, gloves, and marine shoes; therefore, students should be sure to wear these protective clothing when they are in the water. Another hazard is sharp edges of the shells of barnacles and scaly worms (*Thylacodes adamsii*, Fig. 5.6d), attached to rocks. Student should be careful not to cut their hands and body against these sharp edges.

5.5 Benthos Sampling Using a Dredge

Benthos are categorized as epifauna and infauna. Epifauna are animals that inhabit the sea floor, including sessile animals, such as anthozoans, tunicates, and asteroids. Infauna are animals that live beneath the sea floor and include bivalves, irregular sea urchins, and polychaetes. Epifauna and infauna inhabiting the subtidal zone are collected using a bottom sampler, also known as a dredge (Fig. 5.7a). To collect benthic animals, the dredge, which is towed by a boat, gathers the bottom sediment of the seafloor. The collected sediment is moved to a box, and the collected material is hauled up (Fig. 5.7b–d). Either in the boat or at the laboratory, the sediment is then sifted using a sieve to uncover the marine animals. Irregular sea urchins

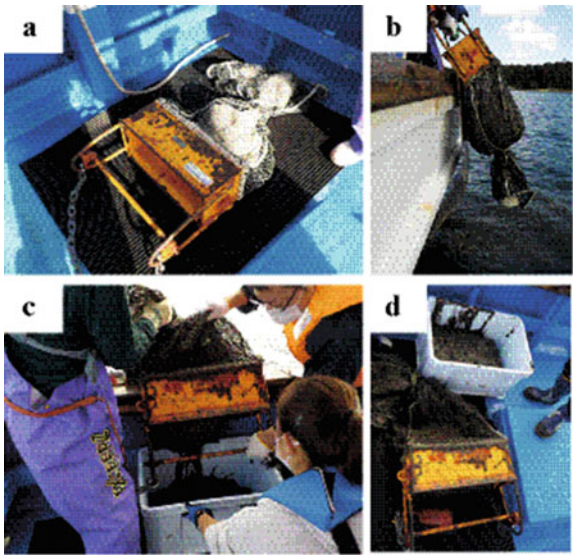

Fig. 5.7 Dredge sampling. **a** A dredge consists of a metal frame and bag-shaped net. **b** Sediment is collected in the dredge, which is towed along the sea floor by a boat. **c**, **d** Sediment is moved from the dredge to the sampling box

(Echinodermata), including *Peronella japonica* and *Schizaster lacunosus*, which bury themselves in the muddy bottom, are usually collected during dredge sampling. Polychaetes, bivalves, and crustaceans are also obtained using the sampling method. The species collected will vary depending on the condition of sediments on the sea floor. Thus, collecting sea floor sediment with a survey dredge will help clarify the relationship between fauna and sediment condition.

5.6 Plankton in Tsukumo Bay

5.6.1 What is Plankton?

Plankton is an ecological category of organisms that live in water and cannot move against the current. Plankton consists of both plants (phytoplankton) and animals (zooplankton), including anything from viruses (nanoplankton, submicrometer scale) to huge jellyfish (megaplankton, meter scale).

Plankton is a very important group in terms of its foundational place in the food chain of any hydrosphere, including seawater. Phytoplankton collectively accounts for the largest biomass on Earth (Brierley 2017). Phytoplankton are the primary producers in the marine food chain, converting sunlight energy and inorganic carbon to organic substances, such as sugar. Plankton serves as food for zooplankton as well as many fish species.

Diatoms, a major phytoplankton group, consist of organisms with a silica cell wall (Fig. 5.8). The source of bioavailable silica (mainly silicic acid) is from the

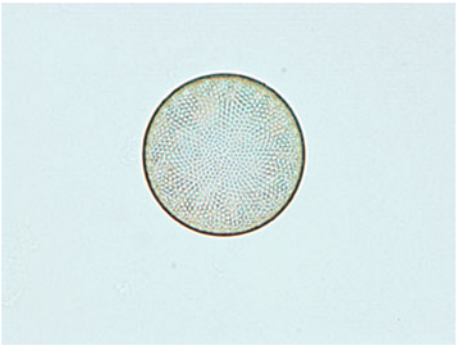

Fig. 5.8 Diatom collected at Tsukumo Bay

soil via the rivers, and, in our experience, diatom overgrowth is frequently observed after heavy rain in Tsukumo Bay. The diatom production is strongly related to the silicate content in water (Chap. 7). Here, we introduce the collection and observation methods of plankton, especially diatoms, in Tsukumo Bay.

5.6.2 Plankton Sampling

Planktonic organisms (also called "plankters") can be collected using a plankton net. This equipment consists of a towing line, bridles, conical nylon mesh, and a cod end (Fig. 5.9). The collected plankters are condensed in the cylinder of the cod end and the contents can be retrieved from the collecting port. The net mesh size, usually less than 100 μm, should be carefully selected depending on the target organisms. The volume of water that passes through the plankton net is important for quantifying the plankton amount in the test area. The flow meter can be used to calculate the water volume by water flow and the area of the net frame.

5.6.2.1 Operation of the Net

To collect the plankton, the net is towed slowly for several minutes from a boat (Fig. 5.10a). If the inclination angle can be adjusted, the towing depth can be estimated. Suitable types of nets can be chosen according to the target plankters, based on habitat depth, body size, and density of plankton. From the coast, it is also possible to throw and retrieve the net horizontally (Fig. 5.10b). In this case, the towing speed should be adjusted to keep the net near the water surface. Otherwise, the net may catch on the bottom of the sea and be lost. The plankton collection efficiency depends on the user's throwing skill. If one quantifies the plankton density by this method, the retrieval distance and opening size of the net must be noted. Where the sea bottom with a sharp decline, the net can be towed vertically (Fig. 5.10c). This method is

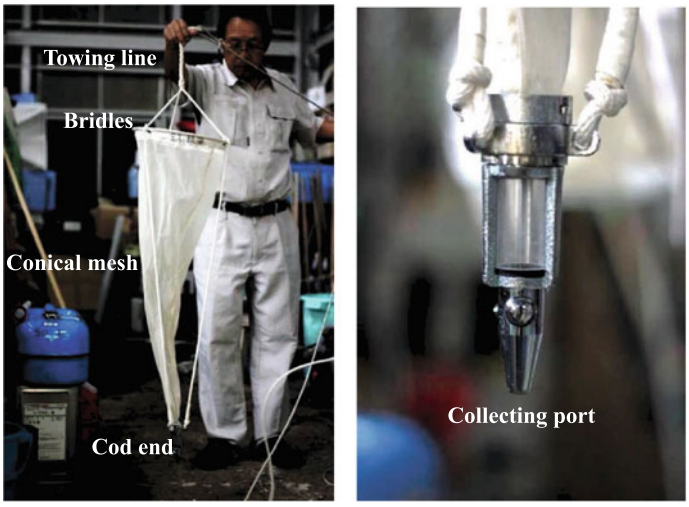

Fig. 5.9 Plankton net. Left; entire system of the net, right; cod end

simple and useful for collecting plankton from Tsukumo Bay. The details of this vertical towing method are described below.

Vertical towing

- Sink the net slowly.
- When the cod end is felt to reach the bottom, the net is slowly retrieved. Pulling the net up too fast may decrease the collection efficiency.
- When pulling up the net, pull it directly upwards until it breaks the water surface (otherwise, plankton will escape from the net).
- The inside of the net surface must be rinsed by pouring seawater onto the net surface from the outside. Do not put water directly into the net as you may introduce plankton that may then contaminate your sample.
- Observe the transparent cylinder of the cod end. When it appears cloudy, open the valve of the cod end to empty the contents into the sampling bottle for collection.
- Repeat the rinsing and collection at least twice.
- The sampling bottle should be kept on ice to avoid autolysis of the plankton. Aeration is required to keep the zooplankton alive. Otherwise, plankton can be fixed by adding 1/10 volume of formalin (39% formaldehyde solution).

5.6.2.2 Observation of Plankton

To observe the plankton, a stereoscopic microscope or optical transmission microscope is necessary (Fig. 5.11). If plankton counter slide is used (Fig. 5.12, Funakoshi), plankton can be easily observed.

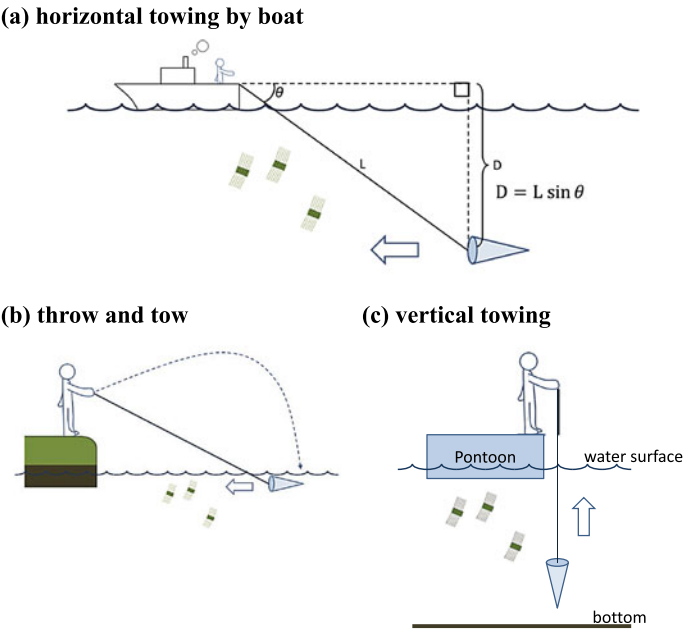

Fig. 5.10 Operation of the plankton net. **a** horizontal towing by boat, **b** throw and tow, **c** vertical towing

Fig. 5.11 Optical transmission microscope with coaxial video camera mounted

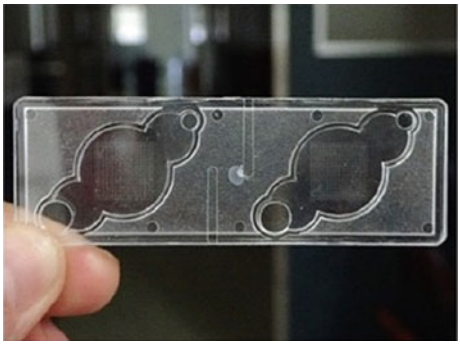

Fig. 5.12 Plankton counter slide. Grid gap; 0.5 mm

- A few drops of the plankton suspension is transferred to the chamber of the plankton counter slide. Do not pour a large amount of the plankton sample into the chamber.
- Mount the glass slide for observation under the microscope.
- You can observe the plankton and take a picture with a smartphone through the eyepiece.

Acknowledgements We are grateful to Dr. Eunice Jingmei Tan for the proofing of the manuscript and fruitful comments. We thank Dr. Shinya Uryu for providing the tidal change figure.

References

Brierley AS (2017). Plankton. Curr Biol CB. 27:R478–R483

Deguchi M, Kubota N, Matsuno A et al (2007) Actual distribution of bacteriocytes in the trophosome of a beard worm (*Oligobrachia mashikoi*, Siboglinidae, Annelida): clarification using whole-mount *in situ* hybridization. Acta Zool (stockholm) 88:129–135

Lalli CM, Parsons TR (1997) Chapter 1—Introduction. In: Biological oceanography: an introduction, 2nd edn. Butterworth-Heinemann, Oxford, pp P1–15

Sasayama Y, Matada M, Fukumori Y et al (2003) External morphology of the posterior end, the "opisthosoma", of the beard worm *Oligobrachia mashikoi* (Pogonophora). Zool Sci 20:1411–1416

Yajima T, Sinya T, Matada M (1979) Distribution and Habitat of *Rhizopsammia minuta mutsuensis* Yabe et Eguchi at the Shore Region in the Vicinity of Tsukumo Bay in the East Side of Noto Peninsula. In: Bulletin of the Japan Sea Research Institute, vol 11. Kanazawa University, pp 81–91

Chapter 6
Assessing the Influence of Polycyclic Aromatic Hydrocarbons on Aquatic Animals

Toshio Sekiguchi, Masato Honda, Nobuo Suzuki, Naohiro Mizoguchi, Takeshi Hano, Yuki Takai, Yuji Oshima, Umi Kawago, Kaito Hatano, Yoichiro Kitani, and Masato Kiyomoto

6.1 Introduction

Polycyclic aromatic hydrocarbons (PAHs) are ubiquitous environmental contaminants that comprise two or more benzene rings. Airborne PAHs are generated by the incomplete combustion of fossil fuels and organic matter. They are transported to the aquatic environment through dry and wet deposition and through industrial

T. Sekiguchi (✉) · N. Suzuki · U. Kawago · K. Hatano · Y. Kitani
Noto Marine Laboratory, Institute of Nature and Environmental Technology, Division of Marine Environmental Studies, Kanazawa University, Noto-Cho, Ishikawa 927-0553, Japan
e-mail: t-sekiguchi@se.kanazawa-u.ac.jp

M. Honda
Botanical Garden, Institute of Nature and Environmental Technology, Kanazawa University, Kakuma, Kanazawa 920-1192, Ishikawa, Japan

N. Mizoguchi
Chemicals Evaluation and Research Institute, Japan (CERI), 3-2-7 Miyanojin, Kurume-Shi, Fukuoka 839-0801, Japan

T. Hano
Environment Conservation Division, Fisheries Technology Institute, National Research and Development Agency, Japan Fisheries Research and Education Agency, 2-17-5 Maruishi, Hatsukaichi 739-0452, Hiroshima, Japan

Y. Takai · Y. Oshima
Laboratory of Marine Environmental Science, Department of Bioscience and Biotechnology, Faculty of Agriculture, Kyushu University, Fukuoka 819-0395, Japan

M. Kiyomoto
Tateyama Marine Laboratory, Institute of Marine and Coastal Research, Ochanomizu University, Tateyama 294-0301, Japan

N. Hasebe et al. (eds.), *Field Work and Laboratory Experiments in Integrated Environmental Sciences*, https://doi.org/10.1007/978-981-99-6532-8_6

runoff that contains PAHs. Oil spills are an important source of marine PAH contamination because petroleum contains considerable quantities of PAHs. Examples of these accidental oil spills are the Mauritius oil spill in 2020, the Deepwater Horizon incident in 2010, and the Nakhodka accident in 1997.

PAHs are known to be biologically toxic carcinogens, endocrine disruptors, and developmental mutagens. Sixteen PAHs are listed by the United States Environmental Protection Agency (US EPA) as causing considerable risk to human health. PAHs are also regarded as harmful to aquatic animals. Tumorigenesis and developmental defects such as disturbances in the dorsal–ventral axis and heart formation have been observed in experiments in which teleosts were exposed to PAHs. Aquatic invertebrates including the arthropods *Daphnia magna*, *Hyalella azteca*, and *Chironomus tentan*s and the annelid, *Stylaria lacustris*, have been used to assess the effects of PAHs (Suedel and Rodgers 1996).

Exposure to PAHs was shown to disturb the dorsal–ventral axis formation via the beta-catenin pathway in embryos of the sea urchin, *Lytechinus anemesis* (Pillai et al. 2003). These findings strongly suggest that PAHs have the potential to negatively impact the aquatic ecosystem. To predict the influence of PAHs on the aquatic organisms, bioassay assessments are essential. In this chapter, we will introduce three bioassay systems for evaluating the influence of PAHs on aquatic animals.

6.2 PAH Bioassay Using Aquatic Animals

In this section, we introduce the sea urchin and medaka as model animals to assess the influence of PAHs on the aquatic environment. We also demonstrate the cultured fish scale system as an assay for evaluating the effects of PAHs on bone metabolism of fish.

Sea urchins, which belong to the class Echinoidea (see Chap. 4), have historically been used to study developmental biology because of their external fertilization and transparent embryos. Sea urchins have also been utilized in ecotoxicological research. Medaka is a fish that is commonly used in genetics investigations and is widely used as a model organism in biological research and toxicological studies. The Organization for Economic Co-operation and Development (OECD) has proposed guidelines for testing chemicals using medaka. Fish scales contain osteoblasts and osteoclasts, which are similar to the cellular composition of bones and are regulated by calcemic hormones like bones. Therefore, fish scales can be used as a model for analyzing bone metabolism, and the fish scale culture system has been used to understand the influence of harmful chemicals on bone metabolism.

In the following section, we show how to analyze the influence of PAHs using these assay systems.

6.3 Influence of PAHs on Sea Urchin Fertilization

Sea urchins are distributed throughout the ocean and have been historically used in studies of fertilization and development. Adult sea urchins can be easily collected because many sea urchin species inhabit rocky and sandy seashores. Moreover, it is possible to obtain a large quantity of eggs and sperm from sea urchins, and fertilization events occur externally. Furthermore, embryos are transparent and their internal morphology can be observed using a light microscope. For these reasons, sea urchins have been regarded as a useful experimental model for ecotoxicological studies. Bioassay to assess toxic agents using sea urchin embryos or gametes have been conducted since the 1970s (Hagström and Lönning 1973; Kobayashi 1971). The US EPA has published embryotoxicity test protocols using sea urchin. Assessing the impact of PAHs on sea urchin fertilization and development has also been evaluated. For instance, phenanthrene was shown to induce the ectopic nuclear accumulation of ß-catenin in the embryo, which resulted in exogastrula formation; these changes were similar to those of lithium-exposed embryos (Pillai et al. 2003). In addition, benzo[*c*]anthracene was shown to suppress spicule formation of the pluteus larvae in *Hemicentrotus pulcherrimus* (Sekiguchi et al. 2018). In this section, students will study the normal sea urchin fertilization process and how to evaluate the influence of PAHs on fertilization.

6.3.1 Observation of Normal Fertilization in Sea Urchins

To evaluate the influence of marine pollutants, including PAHs, on sea urchin fertilization, students should first be able to recognize normal fertilization events.

6.3.1.1 Preparation for the Experiment

- Sea urchins
  Two sea urchin species, *Heliocidaris crassispina* and *Hemicentrotus pulcherrimus*, populate the rocky shores of Japan and are commonly used in research and education throughout the country (Fig. 6.1). They have a pentaradial body plan and a water vascular system, which are distinctive features of echinoderms. These sea urchins are classified as regular sea urchins because their mouth and anus are located at the bottom and top of the body, respectively (see Sect. 4.2.15). The breeding seasons of *H. crassispina* and *H. pulcherrimus* are summer (July–September) and winter (January–April), respectively.

Materials needed:

- Filtered seawater or artificial seawater
- Glass beaker and watch glass

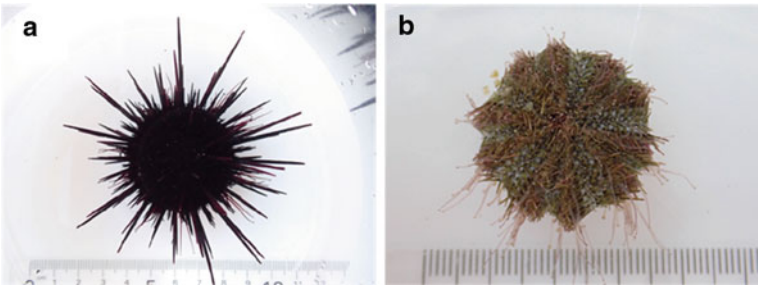

Fig. 6.1 Representative sea urchins found in Japan. *H. crassispina* (**a**). *H. pulcherrimus* (**b**)

- Scissors and tweezers
- Pipettes for the sperm and egg. Note: use separate pipettes for sperm and eggs
- 0.5 M KCl or 2 mM acetylcholine for artificial spawning
- Slides and cover glasses
- Indian ink solution.

6.3.1.2 Collect Eggs and Sperms from Adult Sea Urchins

Eggs and sperm are collected from adult sea urchins using the following procedures:

- Cut off the spines of *H. crassispina* using a pair of scissors (Fig. 6.2a, b) and then wash the specimen with seawater. If *H. pulcherrimus* is used in the experiment, then cutting off the spines is unnecessary.
- Turn the mouth (on the bottom side) upwards and cut the soft membrane surrounding the mouth (Fig. 6.2c).
- Remove the Aristotle's lantern, which are the teeth of the sea urchin (see Fig. 4.14 in Chap. 4 and Fig. 6.2d), then discard the body fluid.
- Pour 0.5 M KCl solution into the mouth.
- If eggs are released, transfer the sea urchin to a beaker filled with filtered seawater or artificial seawater. If sperm is released, transfer the sea urchins to a watch glass. Note: the eggs are a tan/orange color.
- Wash the eggs twice with filtered seawater. Note: When acetylcholine is injected into the vicinity of the mouth by syringe, gametes can be collected from live sea urchins.

6.3.1.3 Observe the Eggs and Jelly Layer

A jelly layer composed of fucose sulfate glycoconjugate surrounds the sea urchin egg and is involved in the attraction, activation, and acrosome reaction of the sperm (Suzuki 1990). Use the following procedures to observe the eggs and jelly layer:

- Transfer the eggs to a microscope slide.

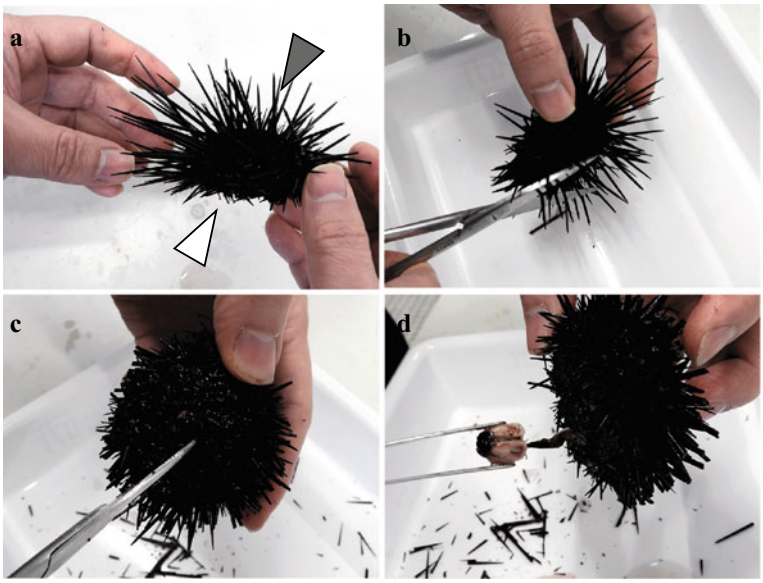

Fig. 6.2 Preparation of sea urchin. Side view of *H. crassispina*. Gray and white arrowheads indicate the anus side and oral side, respectively (**a**). Cut spines using a pair of scissors (**b**). Turn over the sea urchin and cut the soft membrane surrounding the mouth (**c**). Remove the Aristotle's lantern (**d**)

- Add one drop of Indian ink solution to the egg solution and mix gently.
- Place a cover glass on the slide.
- Observe the eggs under the microscope. The jelly layer should be visible as a white region surrounding the egg (Fig. 6.3).

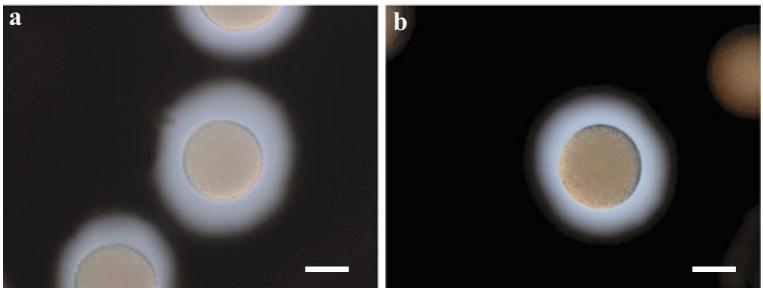

Fig. 6.3 Sea urchin egg jelly coat. Unfertilized egg of *H. crassispina* (**a**) and *H. pulcherrimus* (**b**). The egg jelly coat is made visible by Indian ink. The scale bar is 50 μm

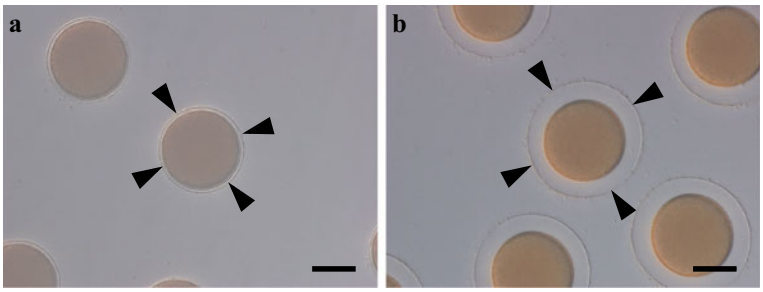

Fig. 6.4 Fertilization membranes of sea urchins. Fertilized egg of *H. crassispina* (**a**) and *H. pulcherrimus* (**b**). Fertilization envelopes are indicated by the arrowheads. The scale bar is 50 μm

6.3.1.4 Artificial Fertilization

Procedure for artificial fertilization:

- Place several eggs on a microscope slide.
- Use a needle to add the sperm solution to the eggs on the microscope slide.
- Observe the fertilization under a light microscope. The optimum fertilization temperatures for *H. crassispina* and *H. pulcherrimus* are 20–25 °C and 14–18 °C, respectively. The fertilization envelope can be observed; this envelope is a vitelline membrane formed by the release of cortical granules to prevent polyspermy (Fig. 6.4).

6.3.2 Sea Urchin Fertilization Bioassay to Evaluate PAH Toxicity

PAHs can inhibit sea urchin fertilization. In this experiment, sea urchin sperm is exposed to PAHs, after which the inhibition of fertilization activity is assessed.

6.3.2.1 Materials Needed

Students should prepare the following materials:

- 5 ml brown glass vials
- PAH test solutions (e.g., naphthalene, phenanthrene, benzo[*c*]phenanthrene, anthracene, benz[*a*]anthracene, and benzo[*a*]pyrene):

  In brown glass vials, prepare 1 ml of test solutions (2, 0.2, 0.02, and 0.002 μg/ml PAH) in seawater. First, PAH powder is dissolved in dimethyl sulfoxide (DMSO) in a brown glass vial, which is stored as a stock solution. The stock solution is further diluted with DMSO until the concentration reaches saturated solubility; then the seawater is added.

For example, 2 mg of PAH powder is dissolved in 1 ml of DMSO to produce a 2,000 μg/ml PAH stock solution. The stock solution is successively diluted with DMSO to obtain 200 and 20 μg/ml PAH solutions. These solutions are further diluted 1,000- or 10,000-fold with seawater. Finally, 1 ml of 2, 0.2, 0.02, and 0.002 μg/ml PAH solutions in seawater are obtained.

- DMSO dissolved in seawater
  This reagent is used as a solvent control. The DMSO concentration of the solvent control must be the same as that of the test solution. According to the OECD guideline, the DMSO concentration should be less than 0.01% (100 mg/l or 0.1 ml/l). For example, 10 μl of DMSO is diluted with 990 μl of seawater to prepare a 1% DMSO solution. Next, 10 μl of 1% DMSO is added to 990 μl of seawater to prepare a 0.01% DMSO solution. However, if the test chemical solutions have high concentrations, then 0.1% DMSO is allowed to be used as the solvent control and, indeed, has been used in various research studies.
- Diluted sperm
  Add dry sperm (10 μl) to 1 ml of seawater in a 1.5 ml tube and mix well, then add 50 μl of the diluted sperm to 25 ml of seawater.
- Eggs
  Count out approximately 50 eggs/ml and store 1 ml egg solution in a 5 ml brown glass vial.

6.3.2.2 Evaluate the Effect of PAHs on Sea Urchin Fertilization

The procedure to evaluate the effect of PAHs on sea urchin fertilization is as follows:

- Add 1 ml of diluted sperm to each PAH vial and leave for 10 min at the optimum temperature stated in Sect. 6.3.1.4.
- Add all of the PAH-exposed sperm sample to an egg sample.
- Leave for 10 min at the optimum temperature.
- Observe the eggs under a microscope.
- Count the fertilized eggs. Fertilized eggs can be confirmed by the presence of a fertilization envelope.
- Calculate the fertilization ratio using the following formula:
  Fertilization ratio = fertilized eggs/total eggs.
- Plot the data with the x-axis as the dilution ratio and the y-axis as the fertilization ratio.

6.4 Assess the Effect of PAHs on Medaka *Oryzias Latipes* Embryos

Medaka (*Oryzias latipes*) has been widely used as a model organism for vertebrates in developmental biology and genetics (Fig. 6.5a), and many mutant and inbred strains have been maintained. Medaka is easy to obtain and breed, has a short generation time of 3–4 months, transparent eggs, and is amenable to in vitro fertilization. Therefore, the embryos can be observed from the early stages of development. Furthermore, the whole genome was sequenced in 2007 (Kasahara et al. 2007). For these reasons, medaka is widely used as a model organism not only in many biochemical experiments but also in toxicity tests (e.g., OECD test method TG203).

The nanoinjection method is a technique whereby a chemical substance is directly administered into the oil droplet of a fish embryo using an ultrafine injection needle (i.e., microneedle, Fig. 6.5b) (Chen et al. 2017; Hano et al. 2009; Takai et al. 2020; Qiu et al. 2019). Nanoinjection is used to observe the effects of a chemical substance in the early stage of embryogenesis. It does not inhibit chemical uptake by the fetal membrane; thus, this method reproduces the transfer of the administered substance from an adult fish to the next generation (Nassef et al. 2010). This method is also advantageous because it can be used for toxicity assessments in fish, accurate quantities of chemicals can be administered, less distress is caused to the organism, and more sensitive tests are possible (Hano et al. 2007).

6.4.1 Test Organism

- Place an appropriate number of males and females (male: female = 1: 2) in an aquarium (e.g., 60 cm × 30 cm × 30 cm, standard breeding density: 1 fish/l) filled with water (e.g., groundwater, dechlorinated tap water, or conditioned water).
- Maintain the water temperature at 25 ± 1 °C, with a light cycle (light: dark) of 16:8 h.

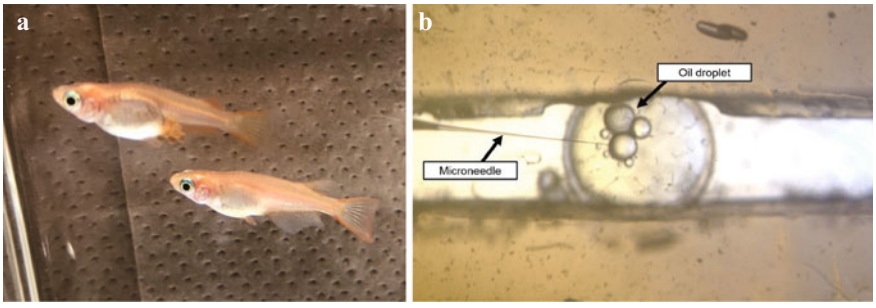

Fig. 6.5 Japanese medaka *Oryzias latipes* (**a**). Nanoinjection using a microneedle to administer a substance into an oil droplet in a medaka embryo (**b**)

- Feed the artemia larvae within 24 h after hatching and continue to feed twice per day. The appropriate feed quantity is when there is nearly complete feed consumption within 5 min.

6.4.2 Preparation of the Exposure Solution

- The exposure solution should be prepared immediately before use.
- Autoclave-sterilized instruments should be used.
- Glassware should be cleaned with appropriate organic solvents, followed by autoclaving and drying.
- Stock solutions of the exposure chemicals (i.e., PAHs) should be prepared in a suitable organic solvent (e.g., isooctane, depending on the chemical), and the exposure solution is diluted stepwise with triolein.
- Triolein should be sterilized by filtration through a 0.45 μm filter in advance, and approximately 1,000 mg (1,000 μl) of filtered triolein should be stored separately in a refrigerated brown vial.
- The highest concentration solution should be prepared.
  Example:
- Accurately weigh 10 mg of the target chemical in a volumetric flask using a glass Pasteur pipette.
- Dilute up to 10 ml with isooctane to produce a 1,000 μg/ml stock solution.
- Weigh 100 μl of stock solution into a brown vial.
- Using a micropipette, weigh out 100 μl of triolein and add to the vial.
- Use isooctane to wash out any triolein remaining in the micropipette and mix well.
- Ultrasonicate for 2–5 min.
- Evaporate the isooctane by blowing N_2 gas for approximately 15 min while the temperature is kept below 30 °C.
- After evaporating all isooctane, fill the vial with N_2 gas and store at room temperature or 4 °C.
- To make each concentration solution, use the highest possible concentration of test chemical in isooctane and transfer it to triolein as described above.

6.4.3 Prepare the Embedding Medium

- Dissolve 1.5 g of agarose in 100 ml of ultrapure water and boil in a microwave.
- Pour into a petri dish and allow it to harden at room temperature.
- Use the tip of a Pasteur pipette to make a hole in the hardened medium about the size of the fish egg (to hold the egg).

6.4.4 Injection Volume and Exposure Concentration

- Measure the egg diameter (mm) using a micrometer, and calculate the volume (mm^3) of the egg.
- Calculate the injection amount per egg as 0.1% of the egg volume.
  Example: For an egg diameter of 1 mm.
- The volume of the egg is $4/3\pi r^3 = 4/3\pi\ (0.5\ mm)^3 = 0.5236\ mm^3$
- The injection volume is $0.5236\ \mu l \times 0.001 = 0.52$ nl.
- Concentrations are set based on the wet weight of the egg and the EC_{50}/LC_{50} of the target chemical.
- Example: EC_{50} of the target chemical is 155 ng/g-egg and the average wet weight of the egg is 1.25 mg:
- 155 ng/g-egg × 0.00125 g-egg = 0.194 ng/egg, rounding 0.194 ng/egg to 0.2 ng/egg
- The injection quantity is 0.5 nl.
- The concentration of the test chemical is 0.2 ng/0.5 nl triolein.
- Therefore, the concentration is 0.4 ng/nl, and the low-concentration group and high-concentration group are set based on this concentration.

6.4.5 Fabrication of Microneedles for Nanoinjection

- Microneedles should be made of silica borate or aluminosilicate glass tubes.
- The microneedles should be able to administer approximately 0.5 nl, which is approximately 0.1% of the average medaka egg volume (0.52 μl).
- The glass tube is pulled with a puller (Fig. 6.6a) to obtain a tip diameter of 2–5 μm. The tip is then sharpened with a grinding machine (Fig. 6.6b) to obtain a tip angle of 30°.
- To improve durability, avoid clogging, and prolong the life, soak the tips in Sigmacote, and dry overnight at 60 °C.

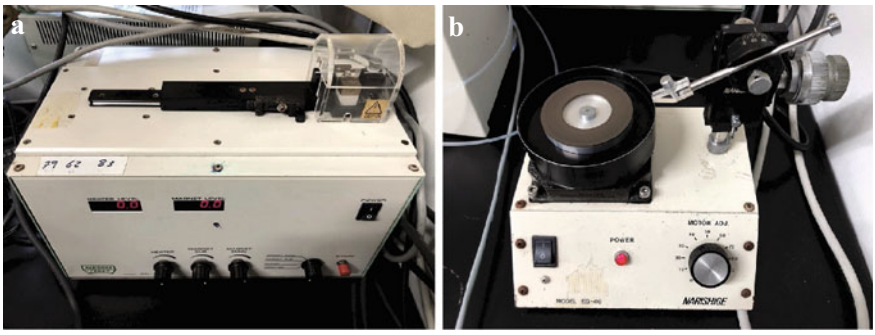

Fig. 6.6 Puller (**a**) and grinding machine (**b**)

- Next, carry out gamma sterilization or ethanol sterilization.
- Finally, wash the tips with distilled water and allow to dry.
- To calibrate the microneedles, fill them with triolein, then dispense 0.5 nl into water under the appropriate injector conditions (i.e., injection pressure = 1000 hPa, compensation pressure = 40 hPa).

6.4.6 Egg Preparation

- Expose the eggs to the test chemicals within 8 h of fertilization.
- Transfer eggs laid on that day to a petri dish and roll the eggs with ethanol-sterilized fingertips to remove the attached filaments.
- Select healthy fertilized eggs using an anatomical microscope; select only eggs at a specific developmental stage (e.g., morula, blast stage), and place them into embryo rearing medium (ERM) containing 0.9% hydrogen peroxide to prevent mold growth and soak for 10 min.
- Wash the eggs with ERM solution and store in fresh ERM solution under room temperature until injection.
- Immediately transfer the eggs to an ERM on ice to delay development. ERM solution comprises 0.1% NaCl, 0.003% KCl, 0.004% $CaCl_2$, 0.016% $MgSO_4$, and methylene blue dissolved in ultrapure water.

6.4.7 Expose Medaka Embryos to Test Chemicals Using Nanoinjection

- Fix an embryo in an egg holder with the oil droplet facing up.
- Fit the microloader tip into a pipettor that can measure 5 μl and take up the triolein solution.
- Insert the loader tip into the injection microneedle and fill it with the exposure solution.
- Attach the microneedle to the injector and attach it to the manipulator (Fig. 6.7a).
- Using an air injector (Fig. 6.7b), adjust the injection volume and inject the desired volume into the oil droplet of the medaka embryo (Fig. 6.7c).
- Form treatment groups that contain a control (un-injected), solvent control (0 ng/egg), and each concentration of test chemical.
- Transfer the treated embryos to a 6-well plate filled with approximately 10 ml of ERM solution each, with approximately 10 embryos per well and incubate at 25 ± 1 °C. For subsequent experiments, select only those that are alive after 1 day.
- Observe daily until the embryos hatch. Record the number of deaths and hatches and the state of development.
- To establish an experiment, the survival rate of the solvent control must not have significant difference compared to that of the control (i.e., un-injected).

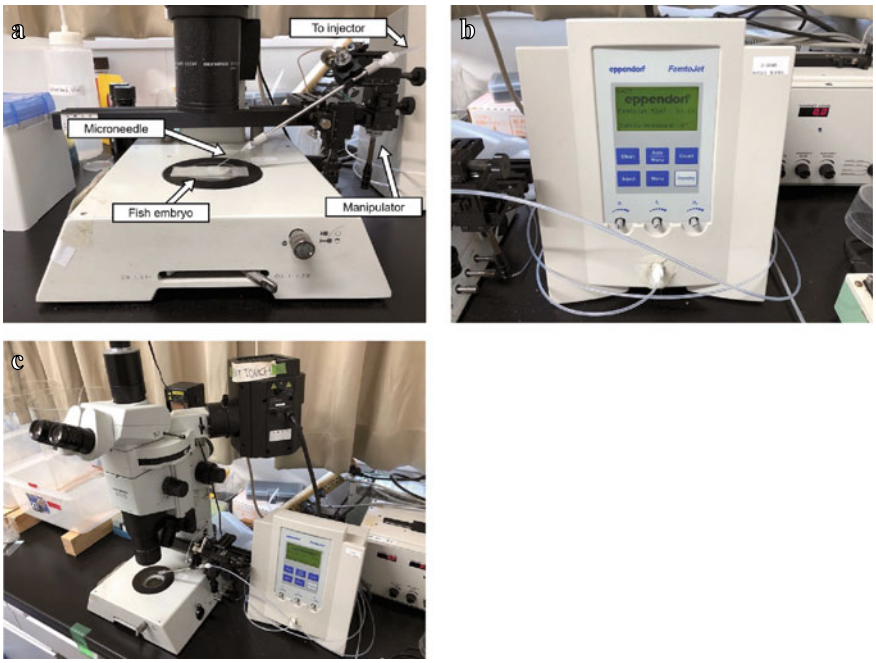

Fig. 6.7 Nanoinjection device. Attach the microneedle to the injector and then attach the injector to the manipulator (**a**). Air injector (**b**). Overview of microneedle, injector, manipulator, microscope, and air injector (**c**)

- Immediately remove dead embryos and transfer hatched larvae to a separate container.
- Analyze the effects of the exposure concentration on mortality, number of days until hatching, occurrence of abnormal development, and other related endpoints.

6.5 Assess the Effect of PAH Exposure on Fish Scales

Human bone is a connective tissue that supports the body and stores and supplies minerals essential for life. Osteoblasts are cells that secrete bone matrix, which forms hard bone, while osteoclasts are cells that dissolve the bone matrix by secreting acid and several types of enzymes. To examine the precise mechanisms of bone formation and resorption, it is necessary to evaluate the interactions between osteoblasts and osteoclasts, which can be accomplished in a co-culture system. Culturing osteoblasts is straightforward because we can use an established osteoblast strain. However, culturing osteoclasts is more challenging because of the difficulty in handling osteoclasts. Under stimulation from osteoblasts, pre-osteoclasts are transformed to an active type of multi-nucleated osteoclast (for details, see Kearns et al. 2008). Only

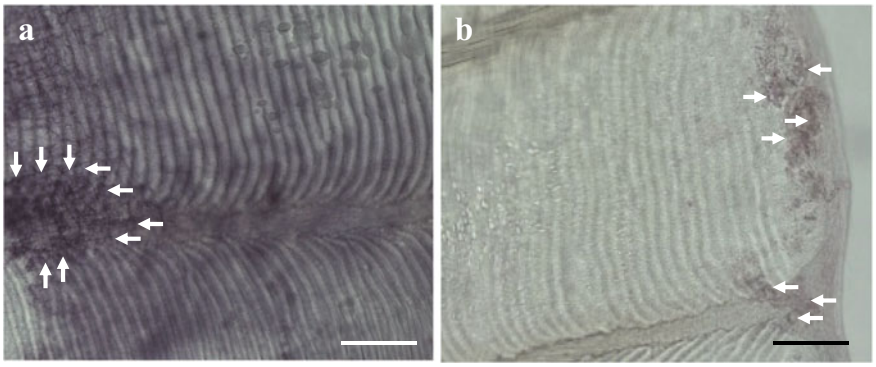

Fig. 6.8 Typical osteoblasts (**a**) and osteoclasts (**b**) in nibbler fish scales. **a** Alkaline phosphatase staining for osteoblasts (arrows), **b** tartrate-resistant acid phosphatase staining for osteoclasts (arrows). The scale bar is 100 μm

these active osteoclasts are capable of bone resorption. Thus, an in vitro bioassay that can be used to easily investigate the interaction between osteoclasts and osteoblasts has been developed. Here, we describe an in vitro bioassay system that utilizes fish scales, which contain both osteoblasts and osteoclasts (Suzuki et al. 2008).

Teleost scales are a calcified bone-like tissue that contains osteoblasts (Fig. 6.8a), osteoclasts (Fig. 6.8b), and two bone matrix layers, namely, the bony layer, which is a thin, well-calcified external layer, and the fibrillary layer, which is a thick, partially calcified layer (for details, see Bereiter-Hahn and Zylberberg 1993; Suzuki et al. 2008). The bone matrix, which includes type I collagen, osteocalcin, and hydroxyapatite, is present in scales and mammalian bone. According to experiments using ^{45}Ca-labeled calcified tissues of goldfish and killifish, scales were found to have greater potential as an internal calcium reservoir than vertebral bone, jaw bone, or otoliths (Mugiya and Watabe 1977). These findings indicated that fish scales can be used as a bone model for analyzing environmental pollutants, such as PAHs.

In our bioassay system, the activities of tartrate-resistant acid phosphatase (TRAP) and alkaline phosphatase (ALP) are respective indicators of the enzyme activity in osteoclasts and osteoblasts. These indicators sensitively responded to calcium-regulating hormones—calcitonin, parathyroid hormone, and prostaglandin E_2 (Suzuki et al. 2016a). This in vitro system has been used to analyze the influence of metals (cadmium, mercury, and gadolinium) and endocrine disrupters (bisphenol-A, tributyltin, and polychlorinated biphenyl) on osteoblasts and osteoclasts (see Honda and Suzuki 2020). Cadmium and gadolinium at concentrations as low as 10^{-13} M suppressed osteoclastic activities after 6 h of incubation (Suzuki et al. 2019). The osteoblastic inhibition by gadolinium (10^{-10} to 10^{-6} M) was approximately equal to that by tributyltin (10^{-10} to 10^{-5} M) (Suzuki et al. 2019). Thus, this bioassay system can be used to evaluate the effect of environmental pollutants on bone metabolism.

6.5.1 *In Vitro Fish Scale Bioassay*

- Add 100 μl of Leibovitz's L-15 medium (containing 1% antibiotic) to each well in a 96-well microplate.
- Using forceps, collect scales from anesthetized fish and place them into the wells.
- In goldfish, the a, b, c, e, f, and g lines are used (Fig. 6.9a). Scales on the right side are used as the control group, while scales on the left side are used as the experimental group; the activities of the scales on the two sides are approximately the same (Suzuki et al. 2009).
- In nibbler fish, scale lines a, b, and c are selected; these scales have approximately the same sizes and osteoclast/osteoblast activities (Fig. 6.9b). In each line, the removed scales are separated into two groups; the control group (white color), and the experimental group (black color) (Yachiguchi et al. 2014).
- Discard the medium from each well of the microplate. In the control group wells, replace with fresh medium without the test chemical. In the experimental group wells, replace with medium containing the test chemical.
- Incubate the microplate containing scales at 15 °C for 6 h (Fig. 6.10a).
- Remove the medium from each well.
- Wash the wells with phosphate-buffered saline.
- To analyze osteoclast activity, add 100 μl of TRAP buffer (0.1 M sodium acetate, 20 mM tartrate, pH 5.3) to each well. To analyze osteoblast activity, add 100 μl of ALP buffer (100 mM Tris-HCl, pH 9.5, 1 mM $MgCl_2$) to each well.
- Freeze the microplate at −80 °C, then store at −20 °C until use.
- Prior to analysis, bring the plate to room temperature to melt the liquid in the wells.

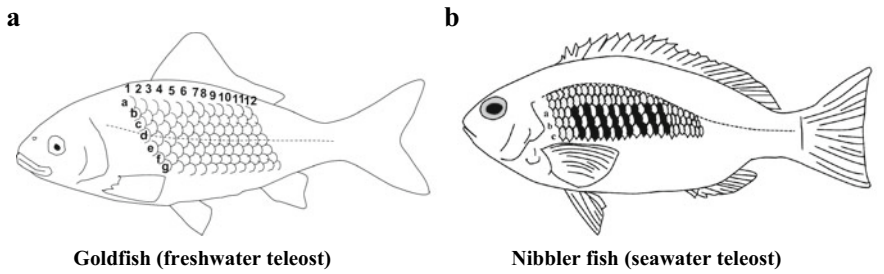

Fig. 6.9 Location of the scales used in the bioassay: goldfish scales (**a**) and nibbler fish scales (**b**). In goldfish, use the a, b, c, e, f, and g lines. The neuromasts located in the lateral line (d line) produce a calcemic hormone (the parathyroid hormone) and thus should not be used in the bioassay. The activities of the scales on the right and left sides are almost the same. Therefore, the scales on the right side are used as the control group, and the scales on the left side are used as the experimental group. In nibbler fish, use lines a, b, and c because these scales have approximately the same size and osteoblast/osteoclast activity. In each line, the removed scales are separated into two groups, a control group (white color) and an experimental group (black color)

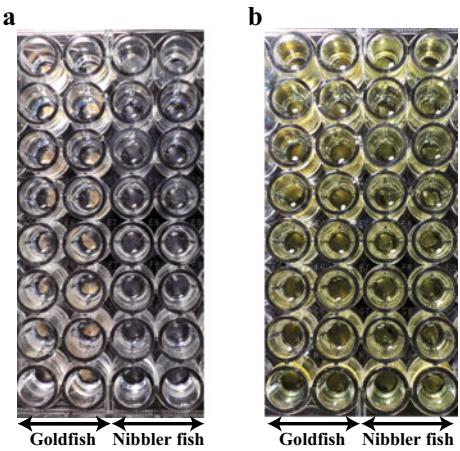

Fig. 6.10 Culturing the fish scales before enzyme reaction (**a**) and color development of alkaline phosphatase (**b**)

- To each well, add 100 μl of 20 mM para-nitrophenyl phosphate in an acid or alkaline buffer (depending on the osteoclast or osteoblast analysis).
- Incubate the plate at 23 °C for 20 min with shaking.
- Add 50 μl of 3 N NaOH to stop the reaction (Fig. 6.10b).
- Measure the absorbance at 405 nm using a microplate reader. The absorbance is converted into the amount of para-nitrophenol (pNP) produced using a standard curve for pNP.
- The surface area of scales is also measured using ImageJ.
- The ALP and TRAP activities are normalized to the surface area (mm^2) of each scale.

6.5.2 Analyze PAH-Contaminated Seawater Using the Fish Scale Bioassay

Finally, we will introduce an example investigating the influence of PAH-contaminated seawater on fish bone metabolism using fish scale bioassay (Suzuki et al. 2016b). The Suez Canal is located in Egypt and links the Mediterranean Sea to the Red Sea. Since its inauguration in November 1869, the canal has been increasingly used by ships and oil tankers. Additionally, Alexandria, a city located at the mouth of the Nile River, is an important port on the Mediterranean Sea route. It is a prominent fishing port and has rich marine resources nearby. However, crude oil and heavy oil are released through the discharge of contaminated ballast water. Thus, marine pollution of the Mediterranean Sea coast and the Suez Canal has worsened even in the absence of shipping accidents. We recently found markedly high concentrations of PAHs (approximately 1,000 ng/l) in seawater from the Suez Canal near the Red Sea side and from near the Alexandria port (500-fold higher than in the Sea of Japan) (Suzuki et al. 2016b). In both seawater samples, we detected nitro-PAHs

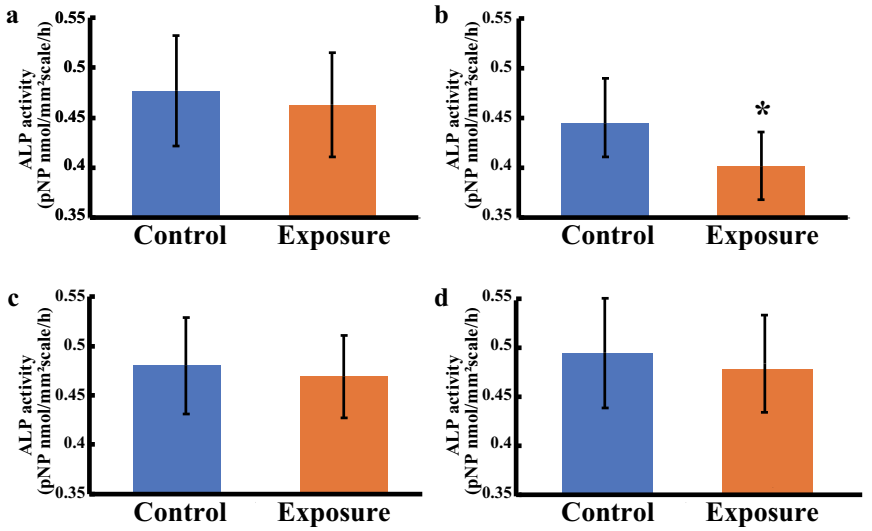

Fig. 6.11 Effect of naphthalene (6 ng/l) (**a**), acenaphthene (6 ng/l) (**b**), 2-nitrofluorene (40 pg/l) (**c**), and 3-nitrobenzanthrone (40 pg/l) (**d**) on ALP activity in cultured scales incubated for 6 h. The results are expressed as the means ± SE. The statistical significance between the control and exposed groups was assessed by paired t-test. In all cases, the significance level (*) was $P < 0.05$. $n = 9$ samples; one sample per fish. Data from Suzuki et al. (2016b)

(NPAHs), which are mutagenic and tumorigenic substances. The total NPAH level was 12.749 ng/l in seawater from the Alexandria site and 3.914 ng/l at the Suez Canal site. The samples of contaminated seawater were used in culture medium at 50x, 100x, and 500x dilution and incubated with goldfish scales for 6 h. The ALP activity was significantly inhibited by both of the seawater samples when diluted 500x, although TRAP activity remained unchanged. Additionally, the mRNA expression levels of osteoblastic markers (ALP, osteocalcin, and the receptor activator of the NF-κB ligand) were significantly decreased. To confirm the influence of PHAs and NPAHs on osteoblastic activity, we detected the levels of highly concentrated PAHs (naphthalene and acenaphthene) and NPAHs (2-nitrofluorene and 3-nitrobenzanthrone) in the two seawater samples. We analyzed the effects of these chemicals on the ALP activity in scales. After adding these chemicals, the ALP activity in the goldfish scales decreased (Fig. 6.11a, c, and d). Acenaphthene treatment significantly inhibited ALP activity in the goldfish scales (Fig. 6.11b). Therefore, contaminated seawater can suppress osteoblastic activity in goldfish scales through the additive and/or synergistic actions of these PAHs and NPAHs.

Acknowledgements We are grateful to Dr. Seiichi Uno for his valuable reviewer comments.

References

Bereiter-Hahn J, Zylberberg L (1993) Regeneration of teleost fish scale. Comp Biochem Physiol Part A 105:625–641

Chen K, Tsutsumi Y, Yoshitake S et al (2017) Alteration of development and gene expression induced by in ovo-nanoinjection of 3-hydroxybenzo [*c*] phenanthrene into Japanese medaka (*Oryzias latipes*) embryos. Aquatic Toxicol 182:194–204

Hagström BE, Lönning S (1973) The sea urchin egg as a testing object in toxicology. Acta Pharmacol Toxicol (Copenh) 1:3–49

Hano T, Oshima Y, Kim SG et al (2007) Tributyltin causes abnormal development in embryos of medaka, *Oryzias latipes*. Chemosphere 69:927–933

Hano T, Oshima Y, Kinoshita M et al (2009) In ovo nanoinjection of nonylphenol affects embryonic development of a transgenic see-through medaka (*Oryzias latipes*), olvas-GFP/STII-YI strain. Chemosphere 77:1594–1599

Honda M, Suzuki N (2020) Toxicities of polycyclic aromatic hydrocarbons for aquatic animals. Int J Environ Res Public Health 17:1363

Kasahara M, Naruse K, Sasaki S et al (2007) The medaka draft genome and insights into vertebrate genome evolution. Nature 447:714–719

Kearns AE, Khosla S, Kostenuik PJ (2008) Receptor activator of nuclear factor kappaB ligand and osteoprotegerin regulation of bone remodeling in health and disease. Endocr Rev 29:155–192

Kobayashi N (1971) Fertilized sea urchin eggs as an indicatory materials for marine pollution bioassay, preliminary experiments. Publ Seto Mar Biol Lab 18:379–406

Mugiya Y, Watabe N (1977) Studies on fish scale formation and resorption II: effect of estradiol on calcium homeostasis and skeletal tissue resorption in the goldfish, Carassius auratus, and the killifish, Fundulus heteroclitus. Comp Biochem Physiol 57A:197–202

Nassef M, Kim SG, Seki M et al (2010) In ovo nanoinjection of triclosan, diclofenac and carbamazepine affects embryonic development of medaka fish (*Oryzias latipes*). Chemosphere 79:966–973

Pillai MC, Vines CA, Wikramanayake AH et al (2003) Polycyclic aromatic hydrocarbons disrupt axial development in sea urchin embryos through a beta-catenin dependent pathway. Toxicology 186:93–108

Qiu X, Kim S, Kang IJ et al (2019) Combined toxicities of tributyltin and polychlorinated biphenyls on the development and hatching of Japanese medaka (*Oryzias latipes*) embryos via in ovo nanoinjection. Chemosphere 225:927–934

Sekiguchi T, Yachiguchi K, Kiyomoto M et al (2018) Molecular mechanism of the suppression of larval skeleton by polycyclic aromatic hydrocarbons in early development of sea urchin *Hemicentrotus pulcherrimus*. Fisheries Sci 84:1073–1079

Suedel BC, Rodgers JH Jr (1996) Toxicity of Fluoranthene to Daphnia magna, Hyalella azteca, Chironomus tentans, and Stylaria lacustris in Water-Only and Whole Sediment Exposures. Bull Environ Contam Toxicol 57:132–138

Suzuki N (1990) Structure and function of sea urchin egg jelly molecules. Zool Sci 7:355–370

Suzuki N, Somei M, Seki A et al (2008) Novel bromomelatonin derivatives as potentially effective drugs to treat bone diseases. J Pineal Res 45:229–234

Suzuki N, Kitamura K, Omori K et al (2009) Response of osteoblasts and osteoclasts in regenerating scales to gravity loading. Biol Sci Space 23:211–217

Suzuki N, Kitamura K, Hattori A (2016a) Fish scale is a suitable model for analyzing determinants of skeletal fragility in type 2 diabetes. Endocrine 54:575–577

Suzuki N, Sato M, Nassar FH et al (2016b) Seawater polluted with highly concentrated polycyclic aromatic hydrocarbons suppresses osteoblastic activity in the scales of goldfish, *Carassius auratus*. Zool Sci 33:407–441

Suzuki N, Watanabe K, Sekimoto A et al (2019) Gadolinium at low concentration suppresses both osteoclastic and osteoblastic activities in the scales of goldfish. Am J Environ Sci 15:137–144

Takai Y, Mizoguchi N, Kinoshita M et al (2020) Establishment of a Japanese medaka (*Oryzias latipes*) transgenic line expressing *Takifugu rubripes* pufferfish saxitoxin and tetrodotoxin binding protein 1, and evaluation of tributyltin toxicity via in ovo nanoinjection. Comp Biochem Physiol Part C 234:108785

Yachiguchi K, Sekiguchi T, Nakano M et al (2014) Effect of inorganic mercury and methylmercury on osteoclasts and osteoblasts in the scales of the marine teleost as a model system of bone. Zool Sci 31:330–337

Chapter 7
Submarine Ground-Water Discharge Assessment by ^{222}Rn Measurement

Tetsuya Matsunaka

7.1 Introduction

Submarine groundwater discharge (SGD) containing terrestrially derived fresh groundwater and saline recirculated seawater is an important pathway for the transfer of dissolved materials and pollutants from terrestrial to coastal areas (Burnett et al. 2001; Taniguchi et al. 2002). SGD rates, relative to total river flows, are estimated to be 0.01–10% on a global scale and 3–87% on local scales (Taniguchi et al. 2002). The discharge of groundwater into the near-shore marine environment may have significant environmental consequences as in some areas it may have been contaminated with a variety of substances including nutrients, heavy metals, radionuclides, and toxic organic compounds.

Nutrient input through SGD plays a significant role in nutrient cycling in coastal seas. In a permeable-bed coastal zone of Korea, SGD-derived nutrients contribute ~98, 12, and 76% of total inputs of dissolved inorganic nitrogen, phosphorus, and silicate, respectively, during summer (Kim et al. 2008). Provision of additional nutrient sources may be beneficial to coastal ecology (Santos et al. 2008), but SGD can also be harmful where terrestrial groundwater is contaminated with anthropogenic materials (Hu et al. 2006). The transport of nutrients to coastal waters may trigger algal blooms, some of which have negative impacts on the economy of coastal zones (LaRoche et al. 1997).

The assessment of SGD flux and its impact on the near-shore marine environment is more difficult than for riverine inputs. SGD is derived mainly from submarine springs and disseminated seepage (Burnett et al. 2006), typically with marked temporospatial variability. Various methods have been developed for the evaluation of SGD including use of a seepage meter (Taniguchi et al. 2002), piezometer (Martin

T. Matsunaka (✉)
Low Level Radioactivity Laboratory, Institute of Nature and Environmental Technology, Kanazawa University, Nomi, Japan
e-mail: matsunaka@se.kanazawa-u.ac.jp

N. Hasebe et al. (eds.), *Field Work and Laboratory Experiments in Integrated Environmental Sciences*, https://doi.org/10.1007/978-981-99-6532-8_7

et al. 2005), water-balance approaches (Taniguchi et al. 2005), and natural tracers such as CH_4, radium (^{223}Ra, ^{224}Ra, ^{226}Ra, and ^{228}Ra), and radon (^{222}Rn) (Cable et al. 1997; Moore 1996; Burnett et al. 2003). The seepage-meter and piezometer methods exclusively involve direct measurement of SGD flux or exchange between seawater and groundwater in relatively small area studies, whereas water-balance and natural-tracer methods are optimum in large area studies, with ^{222}Rn having much higher concentrations in SGD than in river water or seawater (Burnett and Dulaiova 2003).

This chapter introduces the general application of the ^{222}Rn tracer method in evaluating SGD in coastal areas, including sampling and physical observations. Drivers of SGD and a ^{222}Rn mass-balance model are also discussed.

7.2 Drivers of SGD

SGD has been defined as including all direct discharge of subsurface fluids across the land–ocean interface (Fig. 7.1; Taniguchi et al. 2002), including terrestrially driven fresh groundwater (fresh SGD) and marine-forced recirculated seawater (recirculated saline groundwater discharge). SGD driving forces include the hydraulic head, wave set-up, tidal pumping, and density/thermal convection. Additional forces include the terrestrial hydraulic gradient (gravity) resulting in downhill water flow; water-level differences across permeable barriers; tidal-, wave-, storm-, and current-induced pressure gradients in the near-shore zone; convection (salt-fingering) induced by salt water overlying fresh groundwater; seasonal inflow and outflow of seawater into the aquifer owing to movement of the freshwater/seawater interface in response to annual recharge cycles; and geothermal heating (Burnett et al. 2006).

7.3 Physical Structure of Coastal Seas

On-site cross-sectional observation of physical structures in coastal areas is essential for the identification of river-water plumes and SGD springs with relatively low water temperature and salinity, and also for the ^{222}Rn mass-balance model (Sect. 7.7). Seawater temperature and salinity are useful parameters for water mass mixing including fresh-water input. Here, water temperature and salinity were measured along a cross-section from river mouth to open ocean using a real-time conductivity–temperature–depth (CTD) profiler (RINKO-Profiler ASTD102, JFE Advantec Co., Ltd., Japan). The instrument uses a cluster of sensors to measure electrical conductivity, temperature, and pressure (depth), with salinity being calculated as a function of these factors. The profiler included measurement of other physicochemical or biological parameters such as turbidity, dissolved oxygen, pH, and chlorophyll fluorescence (Fig. 7.2a). The chlorophyll fluorescence (based on uranine concentration) is an indicator of phytoplankton concentration. Before on-site measurements, the pH sensor was calibrated, and the coating of the dissolved-oxygen sensor was checked.

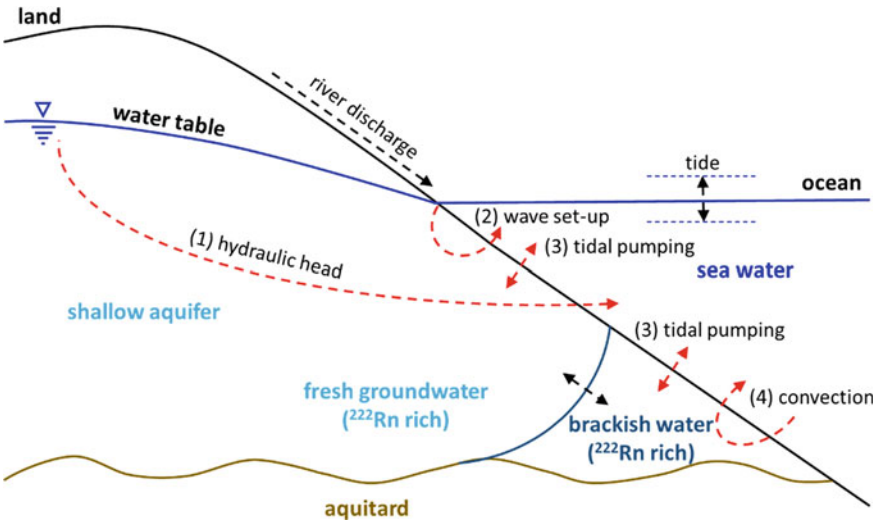

Fig. 7.1 Schematic diagram of submarine groundwater discharge, modified from Taniguchi et al. (2002) and Burnett et al. (2006). The main driving forces are indicated by red arrows

The CTD profiler was adjusted to surface conditions with the water-depth offset set to zero (Fig. 7.2b) before the sensor was lowered to the seafloor at ~0.5 m s^{-1} on a 50 m length of subaqueous cable. Oceanographic parameters were monitored vertically in real time (Fig. 7.2c).

Vertical datasets from the CTD sensor for several sites in the coastal area were integrated and converted to cross-section profiles from river mouth to open ocean using Ocean Data View (ODV; Schlitzer 2003) software. ODV is a proprietary, freely available software package for analysis and visualization of oceanographic datasets. Vertical profiles of water temperature and salinity on July 1, 2019 in Tsukumo Bay are shown in Fig. 7.3, together with the observation line from the river mouth as drawn by the ODV software. Tsukumo Bay is a relatively small drowned valley on NE Noto Peninsula, Japan. The bay entrance is ~200 m wide, the overall length is ~1,200 m, and the maximum depth is ~25 m. Two small rivers flow into the NW of the bay.

Water temperature ranged from 19.3 to 26.1 °C at the observation sites, decreasing with increasing depth; and salinity from 28.0 to 34.5, increasing with depth on July 1, 2019. Higher water temperature and lower salinity were observed in the surface layer. Most temperature and salinity data for Tsukumo Bay are within the ranges of >10 °C for temperature (Hase et al. 1999) and 32.3–34.7 for salinity (Inoue et al. 2021), as observed upstream of the Coastal Branch of the Tsushima Warm Current, which flows along the coastline of Honshu including Noto Peninsula. The lower salinity observed at the surface in Tsukumo Bay is due to the terrestrial fresh-water plume flowing transiently into the bay from the rivers. If the SGD were derived from

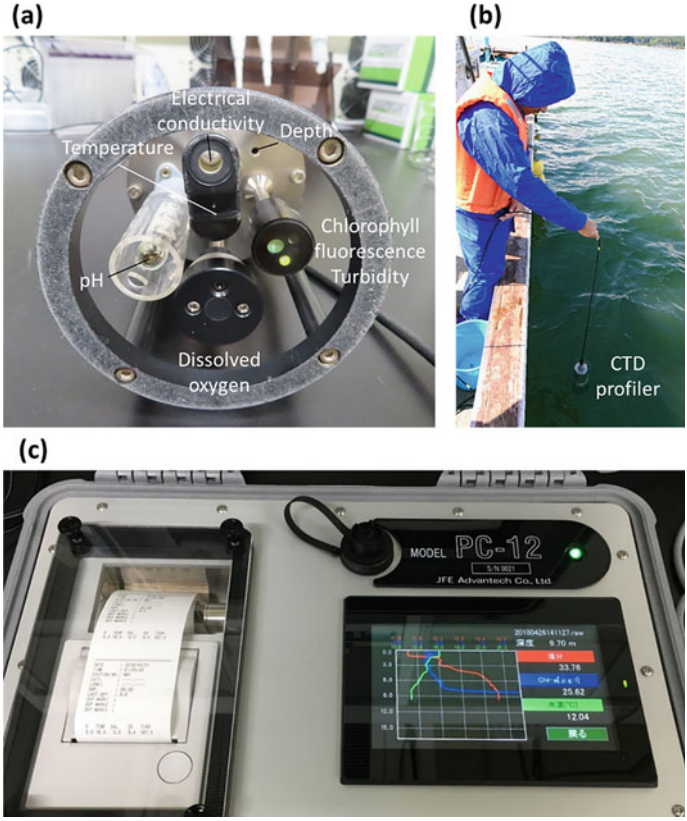

Fig. 7.2 Photographs of CTD profiler (**a**), water depth offset (**b**), and real-time monitor (**c**)

springs in the bay, water masses of relatively low water temperature and salinity would be observed at the bottom of the profiles.

7.4 ^{222}Rn as an SGD Tracer

^{238}U ($T_{1/2} = 4.47 \times 10^9$ years) is a naturally occurring radioactive element present in all rocks and soils. It decays through a series of radionuclides to ^{206}Pb (Fig. 7.4), including ^{226}Ra ($T_{1/2} = 1{,}600$ years), which decays by α particle emission to ^{222}Rn ($T_{1/2} = 3.83$ days)—a noble gas found at highly enriched levels in groundwater. The enrichment of ^{222}Rn in groundwater relative to surface water (typically 1000-fold or greater), its solubility in water, unreactive nature, and short half-life make it a potential tracer of areas of significant SGD, with elevated concentrations in seawater indicating groundwater discharge areas.

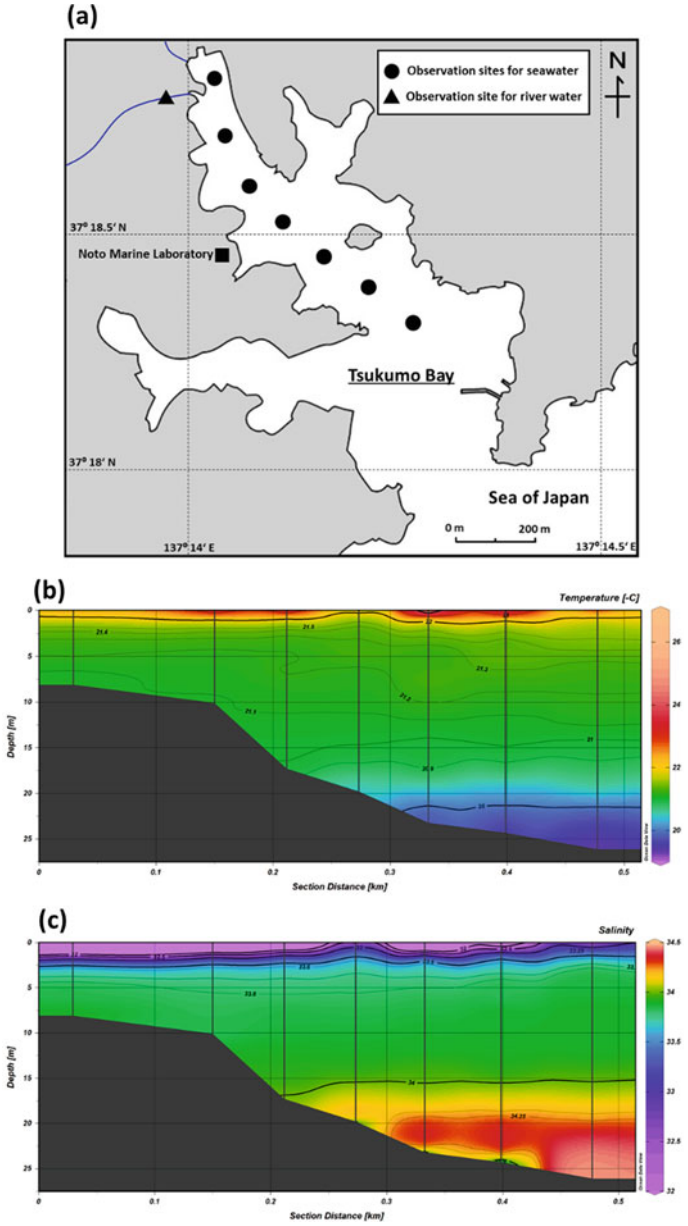

Fig. 7.3 Observation sites in Tsukumo Bay, NE Noto Peninsula, Japan (**a**). Vertical profiles of water temperature (**b**) and salinity (**c**)

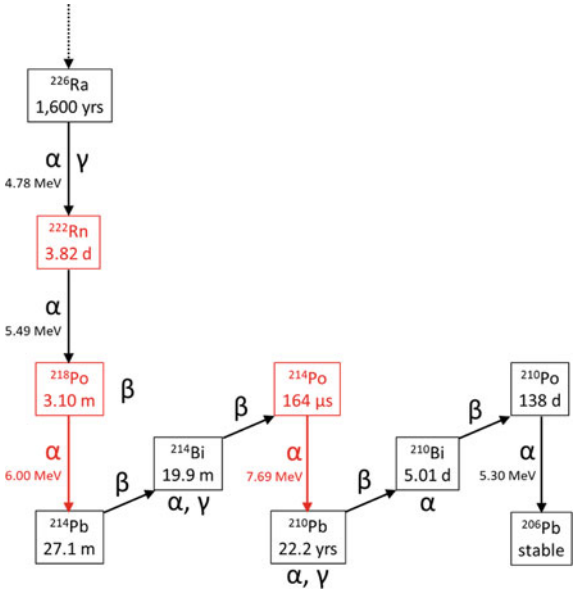

Fig. 7.4 ^{238}U decay series from ^{226}Ra, showing half-lives and principle emissions

Radioactive transformations are accompanied by the emission of one or more of α, β, or ϒ radiation, with an α particle being an He nucleus comprising two protons and two neutrons, reducing the parent atomic number by two and atomic weight by four. A β particle is an electron, with emission increasing the atomic number by one. A ϒ ray is electromagnetic radiation, with its emission not affecting the atomic number or weight. A ^{238}U nucleus decays through 14 transformations to stable ^{206}Pb (Sect. 10.6.1). ^{222}Rn itself decays through a series of short-lived nuclides ^{218}Po, ^{214}Pb, ^{214}Bi, ^{214}Po, and ^{210}Pb to ^{210}Pb, as shown in Fig. 7.4. The initial ^{222}Rn decay releases an α particle with 5.49 meV energy, forming ^{218}Po ($T_{1/2} = 3.10$ min.). ^{218}Po emits an α particle, forming ^{214}Pb with a half-life of 27.1 min, a β emitter. When ^{214}Pb decays, it becomes ^{214}Bi, which is also a β emitter. ^{214}Bi has a half-life of 19.9 min and transforms to ^{214}Po on decay. It has a half-life of only 164 μs and emits a 7.69 meV α particle. When ^{214}Po decays, it becomes ^{210}Pb, which has a relatively long half-life of 22.2 years.

Here, a RAD7 Rn analysis system (DURIDGE) was used to measure ^{222}Rn concentrations in water, based on detection of α particles emitted by the decay-product nuclides ^{218}Po and ^{214}Po.

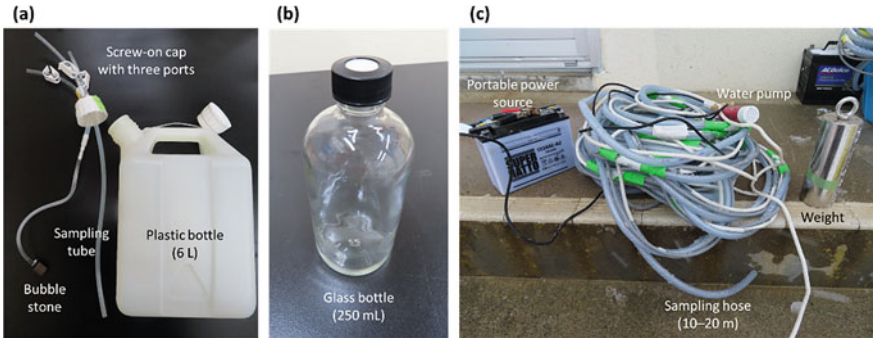

Fig. 7.5 Photographs of closed 6-L plastic bottle (**a**), 250-mL glass bottle (**b**), and sampling hose (**c**)

7.5 Water Sampling for ^{222}Rn Analysis

The determination of ^{222}Rn concentrations in coastal seawater, related watershed river water, and groundwater is essential for the estimation of SGD in the general ^{222}Rn mass-balance model (Sect. 7.7). Seawater and river-water samples were collected in pre-dried 6 L plastic bottles. Sampling times and dates were recorded for decay-correction purposes. The bottle screw-caps (Fig. 7.5a) had three ports for sampling, connection to the radon-analysis system, and connection to a gas bubbler "stone." The three tubes had plastic cocks and quick connectors to facilitate sample handling. A sampling hose (10–20 m) with a submersible water pump (Fig. 7.5c) was lowered from a ship for seawater sampling or bridge for river-water sampling, after rinsing of the hose to avoid gas bubbles. Water was pumped into the 6 L bottle, taking care to avoid agitation and bubbling, at a flow rate of ~1 L min^{-1}. Groundwater samples were collected in pre-dried 250 mL glass bottles with screw caps. Water was carefully siphoned from a bucket to the sample bottle, allowing it to overflow before capping with avoidance of trapped air. The plastic and glass bottles did not need rinsing before sampling because of the short ^{222}Rn half-life. Agitation and bubbling were minimized after sampling.

7.6 ^{222}Rn Analysis

The RAD7 Rn-in-air system provides a portable technique for measuring moderately high levels of ^{222}Rn in natural waters. The system comprises an internal air pump and an α-particle semiconductor detector with energy discrimination levels set for the detection of emissions from decay products of ^{222}Rn. The sample bottles are connected to the RAD7 in a closed loop (Fig. 7.6). Air is bubbled through the sample to release Rn, achieving equilibration between the two phases, and the Rn concentration in the air loop was determined. The sample bottle is connected to the

RAD7 in a closed air loop, with a desiccant column installed before the air inlet of the detector. ^{222}Rn from the water sample circulates continuously through the desiccant column, the detector, and back to the water sample, attaining equilibrium between water and air. The original water Rn concentration is calculated using a radon-partitioning factor between water and air for the relevant water temperature. The radioactivity of ^{222}Rn is determined from count rates of its α-emitting decay products (Fig. 7.6). Details are provided below. The technique is particularly convenient for the determination of ^{222}Rn in natural waters at field sites (Lee and Kim 2006) and is widely used in groundwater studies (Burnett et al. 2001).

Different acrylic desiccant columns were used for the different sample bottles: 6 cm diameter by 17 cm length for the 6 L bottles, and 2 cm by 15 cm for the 250 mL bottles. The columns were packed with $CaSO_4$ granules to remove moisture, which can adversely affect the Rn detection efficiency by neutralizing Po ions. An in-line air filter prevented dust particles containing Rn progeny from entering the 0.7 L detector chamber. The RAD7 system measured only the radon gas concentration in the chamber.

The internal RAD7 air pump re-circulates air at ~1 L min^{-1}, purging Rn from the water to achieve water/air equilibrium (requiring ~40 min for 4 L of water; Lee and Kim 2006), after which the radon concentration is measured using a bypass loop or grab mode (Fig. 7.6), with the Rn activity being constant at equilibrium.

The RAD7 detection chamber is a 0.7 L hemisphere, coated internally with an electrical conductor. A planar silicon solid-state ion-implanted semiconductor α detector is mounted at the center of the hemisphere. A high-voltage circuit charges the internal surface to a potential of 2.0–2.5 keV relative to the detector, creating an electric field throughout the chamber. This field propels $^{218}Po^{+}$ ($T_{1/2}$ = 3.10 min; α energy = 6.00 meV) to the detector (at ground potential), where it decays on the detector surface, producing a signal proportional in strength to the energy of α particle (β particles are not detected). The subsequent decay chain produces $^{214}Po^{+}$ ($T_{1/2}$ = 164 μsecs; α energy = 7.67 meV), with signals from the two Po isotopes contributing to an energy spectrum (Fig. 7.7), allowing the selection of either or both isotopes for ^{222}Rn determination. Use of ^{218}Po alone involves counting within 15 min (~5 half-lives) in a "sniff" mode for a rapid response to changes in Rn concentration, and rapid recovery from high concentrations, provided water/air equilibrium has been achieved. A holding time of ~3 h is required for secular equilibration within the ^{214}Pb ($T_{1/2}$ = 26.8 min)—^{214}Bi ($T_{1/2}$ = 19.9 min)—^{214}Po decay chain to allow detection of both isotopes for higher precision (the normal mode).

The Rn water/air partition ratio at equilibrium is governed by water temperature (Weigel 1978), as follows:

$$k = 0.105 + 0.405e^{-0.0502T} \tag{7.1}$$

where k is the Rn water/air concentration ratio and T is water temperature (°C). The activity of ^{222}Rn in a water sample is the sum of activities in the air loop and water in the sample bottle. Where ^{222}Rn is partitioned, the activity of ^{222}Rn in the water sample, C_{water} (Bq m^{-3}), can be represented as (Lee and Kim 2006):

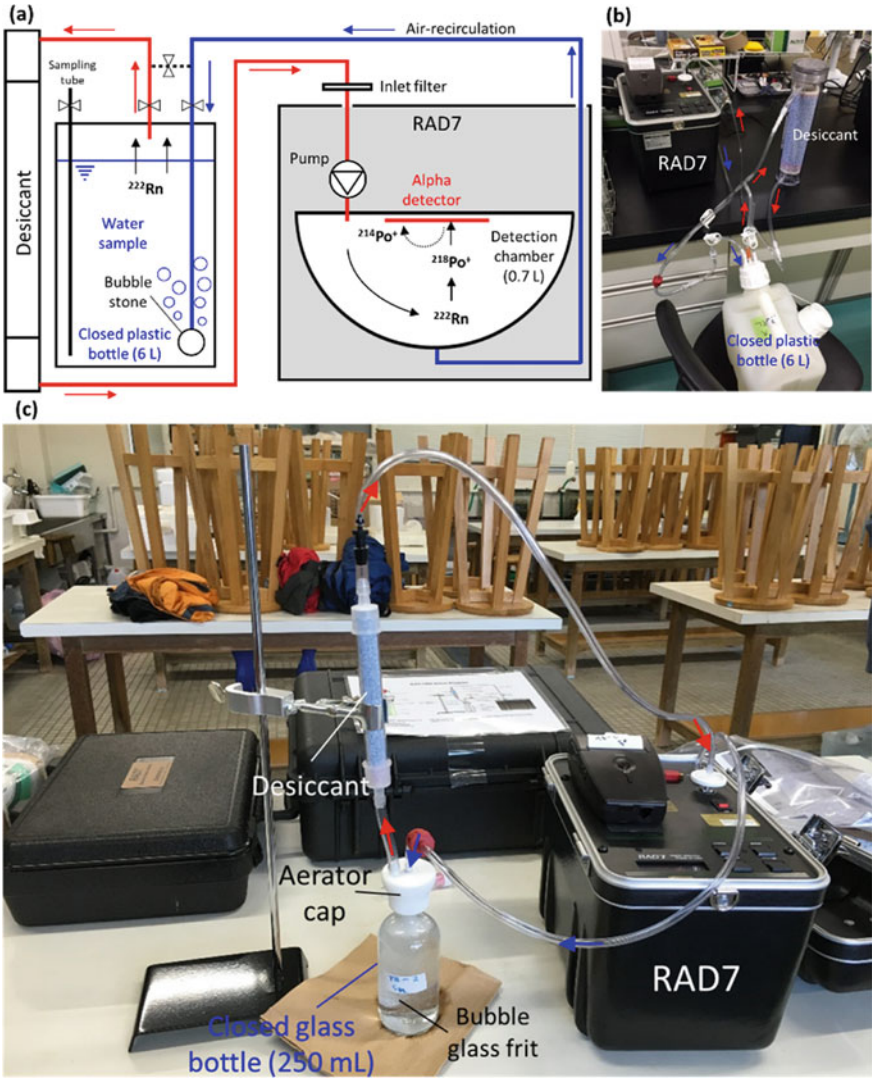

Fig. 7.6 **a** Schematic diagram of the RAD7 radon-in-air monitor, modified from Lee and Kim (2006). **b** The 6 L bottle system. **c** the 250 mL bottle system

$$C_{\text{water}} = \frac{C_{\text{air}} V_{\text{air}} + k C_{\text{air}} V_{\text{water}}}{V_{\text{water}}} \tag{7.2}$$

where C_{air} (Bq m^{-3}) is the activity of ^{222}Rn in the air loop (at water/air equilibrium), and V_{water} and V_{air} are the water volume and loop air volume (sample bottle, detection chamber, desiccant, and tubes), respectively.

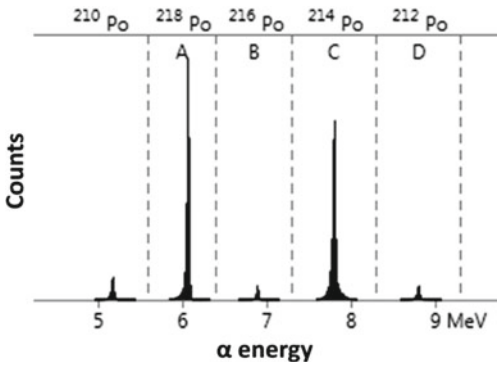

Fig. 7.7 Alpha-particle energy spectra of ^{222}Rn decay products

Measured ^{222}Ra concentrations are expressed as Bq m^{-3} water. The Bq (becquerel) is the SI unit of radioactivity. One Bq is defined as the activity of a quantity of radioactive material in which one nucleus decays per second (count per second: cps). Radon decay was corrected according to its decay constant, $\lambda_{Rn-222} = 0.181 d^{-1}$).

$$\lambda_{Rn-222} = \frac{ln2}{T_{1/2}} = \frac{0.693}{3.83} = 0.181\, d^{-1} \tag{7.3}$$

$$\text{Decay} - \text{corrected}^{222} Rn = C_{\text{water}} e^{(0.181t)} \tag{7.4}$$

Measured ^{222}Rn activities in coastal seawater, river water, and groundwater in and around the semi-enclosed Nanao Bay and Tsukumo Bay are summarized in Table 7.1. Sample bottles were aerated for 45 min for the 6 L and 5 min for the 250 mL bottles at room temperature (25 °C), and equilibrated air in the closed air loop was analyzed with 12 runs of 20 min (total 4 h) for coastal seawater and river water and 4 runs of 5 min (total 20 min) for groundwater; the results were decay-corrected and averaged. Uncertainties based on counting errors (2σ) were generally <25% for ^{222}Rn concentration.

The ^{222}Rn activities in groundwater around the Nanao Bay were in the range of 12,900–13,800 Bq m^{-3}, 2–3 orders of magnitude higher than in coastal bottom seawater in Nanao Bay and Tsukumo Bay (30.8–110 Bq m^{-3}). In contrast, the ^{222}Rn concentrations in surface river water were 608–1,060 Bq m^{-3}. Similar trends were recorded in and around Obama Bay facing Wakasa Bay (Sea of Japan), where ^{222}Rn activities were 3,600–18,600 Bq m^{-3} in groundwater, 170–3,350 Bq m^{-3} in river water, and 20.3–54.3 Bq m^{-3} in bay seawater (Sugimoto et al. 2016).

Table 7.1 Water ^{222}Rn activities in and around Nanao Bay and Tsukumo Bay

Samples	Location	Salinity (PSU)	V_{water} (L)	V_{air} (L)	Gas-liquid eqiblium time (min)	Measurement time	^{22}Rn activity (Bq m^{-3})
Seawater (bottom)	Nanao Bay	33.5	6.0	3.0	45	4 h	110 ± 23
	Tsukumo Bay	34.3	6.0	3.0	45	4 h	30.8 ± 19
River water (surface)	Nanao Bay	0	6.2	2.8	45	4 h	1,060 ± 100
	Tsukumo Bay	0	6.1	2.9	45	4 h	608 ± 57
Ground water	Nanao Bay	0	0.25	0.87	5	20 min	13,800 ± 1800
	Tsukumo Bay	0	0.25	0.87	5	20 min	12,900 ± 1800

7.7 ^{222}Rn and Salinity Mass-Balance Model

SGD in the bay and estuary was estimated using a mass-balance model for ^{222}Rn based on salinity (Sugimoto et al. 2016), dissolved Si (Hwang et al. 2016), and Ra isotopes (Hwang et al. 2005; Santos et al. 2010). The ^{222}Rn and salinity mass-balance model is introduced here. In establishing the mass-balance model for ^{222}Rn, all source and sink terms were considered, with a simple schematic diagram of the model shown in Fig. 7.8. The ^{222}Rn inputs in the coastal sea include discharge of river water, SGD, inflow from the open ocean, ^{222}Rn supported by ^{226}Ra in bay water, and diffusion from bottom sediments. Outputs (losses) include radioactive decay, outflow of bay water, and exchange with the atmosphere. In a steady state, the mass-balance model of water volume (Q), salt (S), and ^{222}Rn can be expressed as follows:

$$Q_{\mathrm{riv}} + Q_{\mathrm{SGD}} + Q_{\mathrm{in}} = Q_{\mathrm{out}} \tag{7.5}$$

where Q_{riv} is the inflow of river water (m^3 d^{-1}), Q_{SGD} is the inflow of SGD (m^3 d^{-1}), Q_{in} is the inflow of open ocean water (m^3 d^{-1}), and Q_{out} is the outflow of bay water (m^3 d^{-1}); and

$$Q_{\mathrm{riv}}S_{\mathrm{riv}} + Q_{\mathrm{SGD}}S_{\mathrm{SGD}} + Q_{\mathrm{in}}S_{\mathrm{in}} = Q_{\mathrm{bay}}S_{\mathrm{bay}} \tag{7.6}$$

where S_{riv} is salinity of river water, S_{SGD} is the salinity of SGD, S_{in} is the salinity of open-ocean water, and S_{bay} is the mean salinity of the bay. Furthermore,

$$\begin{aligned} &Q_{\mathrm{riv}}\mathrm{Rn}_{\mathrm{riv}} + Q_{\mathrm{SGD}}\mathrm{Rn}_{\mathrm{SGD}} + Q_{\mathrm{in}}\mathrm{Rn}_{\mathrm{in}} + \mathrm{Ra}_{\mathrm{bay}}\lambda_{\mathrm{Rn\text{-}222}}V + F_{\mathrm{sed}}A \\ &= \mathrm{Rn}_{\mathrm{bay}}\lambda_{\mathrm{Rn\text{-}222}}V + Q_{\mathrm{out}}\mathrm{Rn}_{\mathrm{bay}} + F_{\mathrm{atm}}A \end{aligned} \tag{7.7}$$

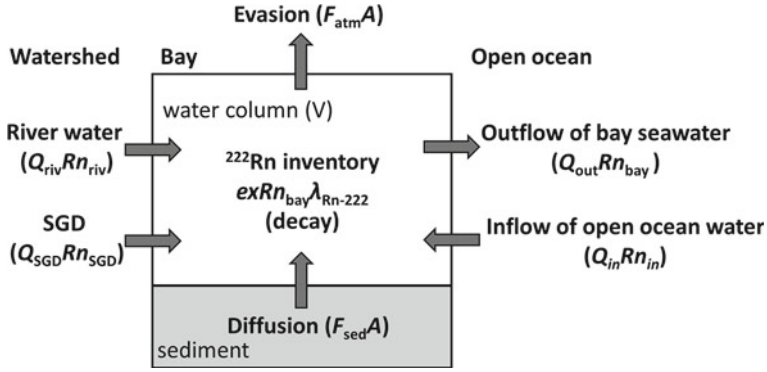

Fig. 7.8 Conceptual ^{222}Rn mass-balance model (modified from Hwang et al. 2005; Sugimoto et al. 2016). Excess Rn_{bay} (exRn_{bay}) is unsupported Rn_{bay} by Ra_{bay} or parent radionuclide of Rn_{bay}, and expressed from (Rn_{bay}–Ra_{bay})

where the following definitions apply. $Q_{riv}Rn_{riv}$ is the input ^{222}Rn flux from river water (Bq d^{-1}), based on the daily discharge of river water (Q_{riv}, m^3 d^{-1}) during the sampling period and the average activity of ^{222}Rn in river-water samples (Rn_{riv}, Bq m^{-3}). $Q_{SGD}Rn_{SGD}$ is the input ^{222}Rn flux from SGD (Bq d^{-1}), based on the unknown seepage rate (Q_{SGD}, m d^{-1}) and the average activity of ^{222}Rn in coastal groundwater samples (Rn_{SGD}, Bq m^{-3}). $Q_{in}Rn_{in}$ is the input ^{222}Rn flux from open-ocean water (Bq d^{-1}), based on the daily inflow of this water (Q_{in}, m^3 d^{-1}) and the average activity ^{222}Rn in the water (Rn_{in}, Bq m^{-3}). $Ra_{bay}\lambda_{Rn\text{-}222}\,V$ is the input ^{222}Rn flux supported by ^{226}Ra decay (Bq d^{-1}), based on the average activity of ^{226}Ra in bay water (Ra_{bay}, Bq m^{-3}). $\lambda_{Rn\text{-}222}$ is the decay constant of ^{222}Rn (0.181 d^{-1}). V is the water volume of the bay (m^3). $F_{sed}A$ is the diffusive ^{222}Rn flux from bottom sediment (Bq d^{-1}), based on the regeneration rates for ^{222}Rn (F_{sed}, Bq m^{-2} d^{-1}) and the area of bay (A, m^2). $Rn_{bay}\lambda_{Rn\text{-}222}\,V$ is the output ^{222}Rn flux due to ^{222}Rn decay (Bq d^{-1}), based on Rn_{bay} (Bq m^{-3}), $\lambda_{Rn\text{-}222}$, and V. $Q_{out}Rn_{bay}$ is the output ^{222}Rn flux from bay water (Bq d^{-1}), based on daily outflow of bay water (Q_{out}, m^3 d^{-1}) and the average activity of ^{222}Rn in bay water samples (Rn_{bay}, Bq m^{-3}). $F_{atm}A$ represents the exchange of ^{222}Rn with the atmosphere across the air–sea interface (Bq d^{-1}; Fig. 7.8). Equations (7.5), (7.6), and (7.7) for Q_{SGD} were solved by either direct measurements or reference-derived estimates of all mass-balance terms. Assuming that S_{riv} and S_{SGD} are 0, Q_{SGD} is as follows:

$$Q_{SGD}=\frac{(S_{in}-S_{bay})\{Rn_{bay}(\lambda_{Rn\text{-}222}V+Q_{riv})+F_{atm}A-Q_{riv}Rn_{riv}-Ra_{bay}\lambda_{Rn\text{-}222}V-F_{sed}A\}+S_{bay}Q_{riv}(Rn_{bay}-Rn_{in})}{Rn_{SGD}(S_{in}-S_{bay})+Rn_{in}S_{bay}-Rn_{bay}S_{in}} \tag{7.8}$$

The exchange loss of ^{222}Rn with the atmosphere ($F_{atm}A$) was calculated as follows (Macintyre et al. 1995):

$$F_{atm}A=k(C_{surface}-\alpha C_{atm})\times A \tag{7.9}$$

where $C_{surface}$ is the average ^{222}Rn activity in surface bay water (Bq m^{-3}); C_{atm} is the ^{222}Rn activity in the atmosphere (Bq m^{-3}); α is Ostwald's solubility coefficient (dimensionless); and k is the gas transfer velocity (also referred to as the piston velocity), which is dependent on wind speed (Jahne et al. 1987; Corbett et al. 1997) and was calculated as follows (Macintyre et al. 1995):

$$k = 0.45 \times u_{10}^{(1.6)} \times \left(\frac{Sc}{600}\right)^{(-a)} \tag{7.10}$$

where u_{10} is wind velocity 10 m above the water surface, Sc is the Schmidt number for Rn at a given water temperature (T, °C) ($= 3412.8 - 224.3T + 6.7954T^2 - 0.083T^3$; Wannikhof 1992), and a is a variable power function dependent on wind speed ($a =$ 0.667 for $u_{10} \leqq 3.6$ m s^{-1} and 0.5 when $u_{10} > 3.6$ m s^{-1}; Turner et al. 1996).

The diffusive ^{222}Rn flux from bottom sediment ($F_{sed}A$) was described as follows (Martens et al. 1980):

$$F_{sed}A = (\lambda_{Rn\text{-}222} nDm)^{0.5} \times \left(C_{pore} - C_{bottom}\right) \times A \tag{7.11}$$

where n is the porosity of sediments, Dm is molecular diffusion coefficient and expressed from ν(kinetic viscosity)/Sc, and C_{pore} and C_{bottom} are the average ^{222}Rn activity in pore water and bottom seawater, respectively (Bq m^{-3}).

Sugimoto et al. (2016) investigated seasonal SGD and associated nutrient fluxes in a semi-enclosed bay (Obama Bay, Japan) using a ^{222}Rn and salinity mass-balance model. SGD rates displayed large intra-annual variability of (0.05–0.77) $\times$ 10^6 m^3 d^{-1}, controlled by seasonal changes in the interaction of multiple driving forces including water-table height and seawater level. The highest SGD rate in early spring was induced by heavy snow and low sea level, with the seasonal increase in sea level gradually suppressing fresh SGD. SGD nutrient fluxes were approximately 42%, 65%, and 33% of all terrestrial fluxes of dissolved inorganic nitrogen, phosphorous, and silicate, respectively. Higher nutrient concentrations in groundwater compensated for its lower volumetric flux. Primary production was restricted mainly by phosphorous throughout the year, with phosphorous-enriched nutrient transport via SGD playing an important role in biological production.

References

Burnett WC, Taniguchi M, Oberdorfer JA (2001) Assessment of submarine groundwater discharge into the coastal zone. J Sea Res 46:109–116

Burnett WC, Dulaiova H (2003) Estimating the dynamics of groundwater input into the coastal zone via continuous radon-222 measurements. J Environ Radioact 9:21–35

Burnett WC, Bokuniewicz H, Huettel M, Moore WS, Taniguchi M (2003) Groundwater and porewater inputs to the coastal zone. Biogeochemistry 66:3–33

Burnett WC, Aggarwal PK, Aureli A, Bokuniewicz H, Cable JE, Charette MA, Kontar E, Krupa S, Kulkarni KM, Loveless A, Moore WS, Oberdorfer JA, Oliveira J, Ozyurt N, Povinec P,

Privitera AMG, Rajar R, Ramessur RT, Scholten J, Stieglitz T, Taniguchi M, Turner JV (2006) Quantifying submarine groundwater discharge in the coastal zone via multiple methods. Sc Tot Environ 367:498–543

Cable JE, Burnett WC, Chanton JP (1997) Magnitude and variations of groundwater seepage along a Florida marine shoreline. Biogeochemistry 38:189–205

Corbett DR, Burnett WC, Cable PH, Clark SB (1997) Radon tracing of groundwater input into par pond, Savanah River site. J Hydrol 203:209–227

Hase H, Yoon JH, Koterayama W (1999) The current structure of the Tsushima warm current along the Japanese coast. J Oceanogr 55:217–235

Hu C, Muller-Karger FE, Swarzenski PW (2006) Hurricanes, submarine groundwater discharge, and Florida's red tides. Geophys Res Lett 33:L11601

Hwang DW, Lee YW, Kim G (2005) Large submarine groundwater discharge and benthic eutrophication in Bangdu Bay on volcanic Jeju Island, Korea. Limnol Oceanog 50:1393–1403

Hwang DW, Lee IS, Choi M, Kim TH (2016) Estimating the input of submarine groundwater discharge (SGD) and SGD-derived nutrients in Geoje Bay, Korea using ^{222}Rn–Si mass balance model. Mar Poll Bull 110:119–126

Inoue M, Shirotani Y, Morokado T, Hanaki S, Ito M, Kameyama H, Kofuji H, Okino A, Shikata T, Yoshida M, Nagao S (2021) Kuroshio fractions in the southwestern sea of Japan; implications from radium isotopes. Cont Shelf Res 214:104328

Jahne B, Munnich KO, Bosinger R, Dutzi A, Huber W, Libner P (1987) On the parameters influencing air–water gas exchange. J Geophys Res 92:1937–1950

Kim G, Ryu JW, Hwang DW (2008) Radium tracing of submarine groundwater discharge (SGD) and associated nutrient fluxes in a highly-permeable bed coastal zone, Korea. Mar Chem 109:307–317

LaRoche J, Nuzzi R, Waters R, Wyman K, Falkowski PG, Wallace DWR (1997) Brown tide blooms in Long Island's coastal waters linked to interannual variability in groundwater flow. Glob Change Biol 3:397–410

Lee JM, Kim G (2006) A simple and rapid method for analyzing radon in coastal and ground waters using a radon-in-air monitor. J Environ Radioact 89:219–228

Macintyre S, Wanninkhof R, Chanton JP (1995) Trace gas exchange across the air–water interface in freshwater and coastal marine environments. In: Matson PA, Harris RC (eds) Biogenic trace gases: measuring emissions from soil and water, Blackwell, pp 52–97

Martens CS, Kipphut GW, Klump JV (1980) Sediment–water chemical exchange in the coastal zone traced by in situ radon-222 flux measurements. Science 208:285–288

Martin JB, Cable JE, Swarzenski PW, Lindenberg MK (2005) Enhanced submarine ground water discharge from mixing of pore water and estuarine water. Ground Water 42:1000–1010

Moore WS (1996) Large groundwater inputs to coastal waters revealer by ^{226}Ra enrichments. Nature 380:612–614

Santos IR, Niencheski F, Burnett WC, Peterson R, Chanton JP, Andrade CFF, Milani IB, Schmidt A, Knoeller K (2008) Tracing anthropogenically driven groundwater discharge into a coastal lagoon from southern Brazil. J Hydrol 353:275–293

Santos IR, Peterson RN, Eyre BD, Burnett WC (2010) Significant lateral inputs of fresh groundwater into a stratified tropical estuary: evidence from radon and radium isotopes. Mar Chem 121:37–48

Schlitzer R (2003) Ocean data view. https://odv.awi.de/en/

Sugimoto R, Honda H, Kobayashi S, Takao Y, Tahara D, Tominaga O, Taniguchi M (2016) Seasonal changes in submarine groundwater discharge and associated nutrient transport into a tideless semi-enclosed embayment (Obama Bay, Japan). Estuaries Coasts 39:13–26

Taniguchi M, Burnett WC, Cable JE, Turner JV (2002) Investigation of submarine groundwater discharge. Hydrol Process 16:2115–2129

Taniguchi M, Ishitobi T, Saeki K (2005) Evaluation of time-space distributions of submarine groundwater discharge. Ground Water 43:336–342

Turner SM, Malin G, Nightingale PD, Liss PS (1996) Seasonal variation of dimethyl sulphide in the North Sea and an assessment of fluxes to the atmosphere. Mar Chemy 54:552–556

Wannikhof R (1992) Relationship between wind speed and gas exchange over the ocean. J Geophys Res Oceans 97:7373–7382
Weigel VF (1978) Radon. Chemiker Zeitung 102:278

Chapter 8
Measuring Water Chemistry of Terrestrial Water

Keisuke Fukushi

8.1 Introduction

Terrestrial water, including river water, lake water, and groundwater is an important transport medium for hazardous substances in terrestrial environments (Drever 1997; Appelo and Postma 2005). Compared to seawater, terrestrial water exhibits wide varieties of chemical characteristics depending on the geologic, climatic, and hydrologic settings of specific sites (Sposito 1984; Drever, 1997; Appelo and Postma 2005). The transport behavior of dissolved hazardous substances, especially for toxic trace elements, invariably depends on the chemical characteristics of the water (Sposito 1984; Stumm 1987; Dzombak and Morel 1990). For example, arsenic and molybdenum mobility are strongly related to the pH and redox condition of the natural water (Fukushi et al. 2003; Smedley and Kinniburgh 2017; Tsetsgee et al. 2021). The mobility of uranium is affected strongly by dissolved inorganic carbon (DIC) as well as by pH and redox conditions (Kobayashi et al. 2020). To understand and predict the environmental behaviors of hazardous substances, it is crucially important to monitor not only the concentrations of hazardous substances but also the water chemistry prevailing at a specific site. Basic determinants of water chemistry are pH, redox potential, concentration of dissolved oxygen, and the concentrations of its major components. This chapter introduces a methodology to obtain the basic water chemistry from fieldwork and laboratory measurements.

For the discussion presented in this chapter, aqueous components are denoted as Na, Mg, Ca, K, Cl, SO_4, and DIC for sodium, magnesium, calcium, potassium, chloride, sulfate, and dissolved inorganic carbon. To express the individual ionic or molecular species, terms are used such as H^+, Na^+, and HCO_3^- for free ions, $MgCl^+$

K. Fukushi (✉)
Institute of Nature and Environmental Technology, Division of Terrestrial Environmental Studies, Kanazawa University, Kanazawa 920-1192, Ishikawa, Japan
e-mail: fukushi@staff.kanazawa-u.ac.jp

N. Hasebe et al. (eds.), *Field Work and Laboratory Experiments in Integrated Environmental Sciences*, https://doi.org/10.1007/978-981-99-6532-8_8

and $NaSO_4^-$ for aqueous complexes, and $H_2CO_3^0$ and H_2O for aqueous molecular species.

8.2 On-Site Measurements

Some parameters, including temperature, pH, redox potential (oxidation reduction potential (ORP)), concentration of dissolved oxygen (DO), and alkalinity, must be measured on-site because these parameters can change with time after separation from water bodies. The best way of measuring temperature, pH, ORP, and DO on-site is to use commercial portable meters with electrodes. In addition to these parameters, it is also useful to measure electric conductivity on-site.

pH represents a logarithmic form of activity of hydrogen ion (a_{H^+}) in water.

$$\mathrm{pH} = -\log a_{H^+} = -\log[H^+]\gamma \tag{8.1}$$

Therein, a_{H^+} is related to the mole basis concentration of hydrogen ion ($[H^+]$) and the activity coefficient (γ). A sensor for pH measurement equipped with a pH meter is the glass electrode. The solution pH is converted from electromotive forces caused by the adsorption of hydrogen ion on the glass electrode surface.

The oxidation and reduction potential (ORP) is expressed in volts (V). An ORP meter measures the potential with a combined electrode with platinum and reference electrodes. The measured ORP differs from Eh, which is a common variable in electrochemistry. To obtain Eh value from the measured ORP, it is necessary to correct the potential difference between a standard hydrogen electrode and a reference electrode. Theoretically, the Eh value is related to the ratio of concentrations of redox species, e.g., $[Fe^{2+}]/[Fe^{3+}]$. However, Eh values estimated using an ORP meter can rarely be related to specific redox pair (Appelo and Postma 2005). Therefore, the measured ORP values are usually used for qualitative purposes to detect oxidizing, reducing, and intermediate conditions.

DO represents the concentration of molecular oxygen (O_2) in water, usually in milligrams per liter.

Electric conductivity (EC) can provide preliminary information about the amounts of total dissolved ions in water. EC is quantitatively meaningful value. In fact, it can be estimated theoretically from the composition of major species (Appelo and Postma 2005). The measured EC is useful for assessing the validity of the sampling and water measurements by comparing the theoretically calculated EC (Sect. 8.4.3).

Alkalinity represents the total amount of the acid-consumable species as a unit volume (or mass) of a solution. Possible major ionic species in most of the natural water are Na^+, K^+, Ca^{2+}, Mg^{2+}, Cl^-, SO_4^{2-}, and HCO_3^-. Those species, except for HCO_3^-, do not take part in the proton consumption (or protonation) reaction in conditions of most natural waters. However, a proton added to a solution can be consumed with HCO_3^- to produce $H_2CO_3^0$. If an acid is added to a solution that does not include HCO_3^-, then the solution pH simply decreases according to the

amount of added acid. The pH of the solution is buffered in the presence of HCO_3^-, depending on its amount. Therefore, the concentration of HCO_3^- can be estimated from the acid buffer behavior of the solution revealed from acid titration experiments (Sect. 8.2.3).

8.2.1 Preparation for Electrodes

To measure the pH of natural water accurately, the pH electrode used with pH meter must be calibrated with standard pH solutions. For most natural water, the pH is 4–10. Three-point calibrations with pH 4, 7, and 9 should be done before using a pH meter. The pH electrode is immersed into pH buffer solutions for calibration, which should be done at least once a day, usually before fieldwork in the laboratory. However, if the pH exhibits an unexpected value during fieldwork, the pH electrode must be calibrated again in the field. Therefore, pH standard solutions should be brought to the field. The DO electrode must also be calibrated against an air oxygen concentration. It is noteworthy that the DO values measured by the electrode depend on the air pressure (altitude) and salinity. If fieldwork is conducted in highland or saline conditions, then the DO should be calibrated with effects of air pressure and salinity. Also, ORP and EC are measured using electrodes. However, calibration of the electrodes for these parameters is not necessary.

8.2.2 On-Site Measurement of Temperature, pH, ORP, EC, and DO

Several tools are available to collect water samples depending on the purposes. When river water is sampled from a hump of a river shore, a ladle is better for sampling. Sampling tools with a plastic substance are recommended for water sampling because metal substances can release metals to the sample water or can adsorb trace elements from the sample water. All sampling tools contacting with water must be washed several times with the sampling water in the sample. Sometimes, the collected water sample in a ladle can be transferred to other vessels. Vessels used for the water measurements must also be washed with the sample water. In addition, before measuring on-site parameters, the electrodes must be washed using the sample water.

After the washing of vessels and electrodes with sample water, the electrodes can be immersed directly into the vessels filled with sample water. It always takes several minutes to reach stable values. During stabilization, the water should be shaken occasionally or stirred gently with the electrodes. Some terrestrial natural water, such as groundwater with surrounding conditions differing from ambient conditions tend to change with time. In such cases, the parameters should be monitored quickly with special care and caution. Recent pH/ORP/DO/EC electrodes and meters can

also measure temperature because some parameters require correction according to temperature.

8.2.3 Measurement of Alkalinity

Alkalinity is measured by in-situ acid titration. Alkalinity of natural water represents the HCO_3^- concentration in most cases, which can interact with atmospheric CO_2. The amount of the interaction depends on the solution pH and CO_2 partial pressure. Change of pH or CO_2 partial pressure after separation from the water body can engender changes in alkalinity. Therefore, measurements of alkalinity should be done on site. When it is difficult to take measurements on site for some reason, the measurements should be done on the sampling day. The acids used for titrants are always solutions of strong acids: HCl or H_2SO_4. Sample water used for alkalinity titration must be filtered before titration because the colloidal matter in the solution can affect the acid–base behavior. Sample water is usually filtered with a 0.45 μm membrane. Pressurized filtration using a syringe and a syringe filter is convenient for alkalinity measurements (Fig. 8.1a). The inner wall of the syringe needs to be washed with the sample water at least twice. Syringe filters are sometimes contaminated with ionic species even when they are new. At least 5 mL of sample water must have passed through a filter before use. To calculate alkalinity, the volume of sample solution, the volume of added acid (titrant), and the concentration of the added acid must be specified. A graduated cylinder is sometimes used for relatively precise measurement of a sample water volume. It is noteworthy that the inside of the graduated cylinder must be washed with filtered sample water before each use. A micropipette that can change a dispensed volume from 0.01 to 0.1 mL is useful to add a precise volume of titrant to the sample water (Fig. 8.1b). The alkalinity of most freshwater is on the order of several meq/L. An acidic or diluted natural water is at most ten times lower, whereas an alkaline water is at most ten times higher. To cover the possible range of alkalinity, acid solutions with different concentrations should be brought to the site for fieldwork. For example, if a volume of the filtered sample water is 30 mL, adequate concentrations of acid solutions are 1 N, 0.1 N, and 0.01 N, of which solution bottles should be brought for possible use in fieldwork.

The routine used for alkalinity titration can be summarized as follows. A fixed volume (e.g., 30 mL) of filtered sample water is poured from a graduated cylinder into a pre-washed plastic bottle (Sect. 8.3.1). After a pH electrode is immersed into the bottle, the bottle is shaken gently by the pH electrode. After the pH becomes stable, the pH and the temperature are recorded as initial values. Then a certain amount of acid is added to the bottle using a micropipette. The concentration of the acid for the initial addition should be the lowest one (e.g., 0.01 N) when no information about the alkalinity is available. In addition, the volume of the initial addition should be as low (e.g., 20 μL) as possible. The solution pH is monitored using a pH meter. After the pH becomes stable, the pH value as well as the temperature is memorized. The pH addition procedure is repeated until the pH reaches 4.8 ± 0.1, which is the

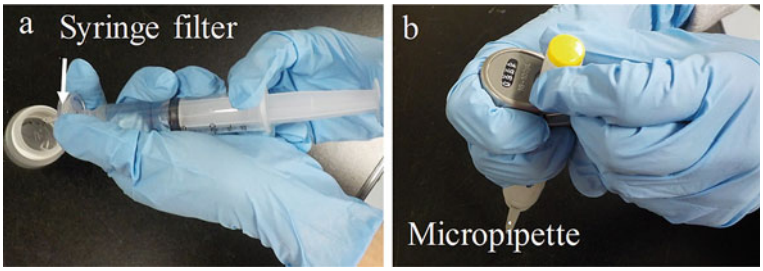

Fig. 8.1 Operation of a syringe filter (**a**) and a micropipette (**b**)

endpoint of alkalinity titration (Fig. 8.2). After the endpoint, the titration is finished with one or two more additions of acid. The amount of acid (H^+) necessary to produce pH 4.8 corresponds to the sample water alkalinity. Alkalinity is calculable using the following equation.

$$\text{Alk.(eq/L)} = \frac{\text{Added volume until endpoint (mL)} \times \text{Normality of acid (N)}}{\text{Total volume (mL)}} \tag{8.2}$$

It is noteworthy that pH buffer caused by HCO_3^- becomes weak at around pH < 5.5. A small addition of acid at the pH condition can result in a drastic decrease of pH (Fig. 8.2). Therefore, it is very difficult to reach an exact pH value at pH 4.8. The amount of added acid at an endpoint is obtainable from interpolation with two data above and below pH 4.8. Alkalinity can be estimated from simple equation presented above. However, one can also obtain alkalinity and contributions of other acid consumable species (i.e., CO_3^{2-}) from sophisticated solution theories using

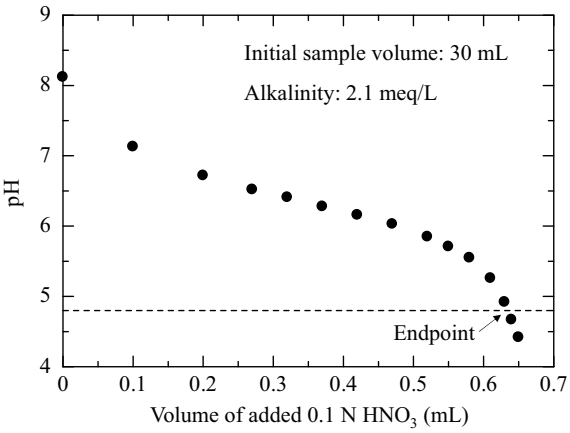

Fig. 8.2 Example of alkalinity measurement

a computer program (USGS 2012). When using the computer program, the large number of datapoints in alkalinity titration can produce accurate calculation results.

8.3 Collection of Water Samples

Major components (Na, K, Mg, Ca, Cl, and SO_4), except for DIC, as well as most trace heavy metals are preserved in sampled solutions even after separation from water bodies. Therefore, measurements of these components are usually conducted in the laboratory after sampling. To minimize artificial contamination of sample solutions, special care must be taken during sample corrections. This section introduces an adequate sampling method.

8.3.1 Preparation of Sampling Bottles

Plastic bottles are used to collect and store water samples. Glass bottles are not usually adequate for analyses of inorganic components because the dissolution of glassware results in the release of some elements to the sample solution. The best material for the storage of the water samples might be Teflon ware such as PFA bottles. However, Teflon bottles are expensive. Polypropylene (PP) bottles are usually used for water sampling. Because PP bottles are not expensive, the bottles are used on a disposable basis. Bottles used for the sampling must be washed even for the first use. The cleaning procedure of the bottles consists of soaking in dilute acid solution, rinsing with (ultra-)pure water, and drying in clean places. The soaking in acid (usually nitric acid) solution is intended to elute inorganic metals from the bottles. The pH of the dilute acid solution should be around <1, which can be prepared by 50–100 times dilution of concentrated nitric acid. Solubility of metals at pH < 1 is always high (Drever 1997). The re-adsorption of metals onto the wall of the bottles can be negligible in the acid water. Therefore, the acid solution used for the purpose need not be especially pure. The prepared acid solution can be used repeatedly for the washing of bottles if the acid water is apparently transparent and has no dirt.

Bottles should be soaked in the acid solution for at least one night. After soaking in the acid solution, the bottles and caps are rinsed with (ultra-)pure water to remove the remaining acid water that has adhered to the bottles. The rinsed water should be pure to the greatest degree possible. It is important that the bottle should be rinsed at least five times to remove the acid solution completely. After rinsing, the bottle should be placed on a clean place for drying. For use in the field, bottles should be capped and packed into clean plastic bags after drying.

8.3.2 Sampling of Water

Sampling procedures of natural water depend on measurement items. Procedures for measuring major inorganic components including Na, K, Mg, Ca, Cl, SO_4, and SiO_2 are introduced next. Several different methods can be used to measure these components. Among them, inductively coupled plasma optical emission spectroscopy (ICP-OES) is among the best options for measurement of Na, K, Mg, Ca, and Si of natural water. Actually, ICP-OES can measure many elements simultaneously. The detection limits for measurements with ICP-OES are usually sufficiently low to quantify these elements from most of the terrestrial water. In addition to these major elements, the sample water for ICP-OES measurement is useful for the measurement of some trace elements of which concentrations are higher than several tens of parts per billion. Moreover, the sample water can be used for the measurement of trace elements using an ICP-mass spectrometer. In contrast to metals, Cl and SO_4 are anionic species. Ion chromatography is the best method for measuring Cl and SO_4.

Samples for ICP-OES and ion chromatography are collected separately in different bottles. The sample water for ICP-OES is acidified, whereas that for ion chromatography is not acidified. For both samples, the sample water must be filtered using a 0.20 or 0.45 μm membrane to remove fine suspended matter. Pressurized filtration using syringe and syringe filter is convenient (Fig. 8.1b). The inner wall of the syringe needs to be washed with the sample water. At least 5 mL of sample water must have passed through a filter before use (Sect. 8.2.3). In addition, the inner wall of the sample bottles as well as the bottle caps must be rinsed three times with the filtered water. After comprehensive washing, the filtered water is collected in bottles. The water should be filled almost completely in the bottles, i.e., air in the bottle should be removed to the greatest extent possible. Before filling the bottle for ICP-OES with sample water, mix a small amount of acid into the water. The type and the concentration of the acid depend on the matrix conditions used for ICP-OES measurement. For example, if a matrix solution for a ICP-OES is 0.6 wt% HNO_3, then concentrated HNO_3 (60 wt%) is added to the sample solution to make 1 vol.%.

Leakage of sample water from the bottle can occur especially during transport by airplane. The best way to avoid leakage is to seal the joint between the bottle and the cap using Teflon seal tape (Fig. 8.3).

8.4 Measurements in the Laboratory

Solution conditions of acidified samples for ICP-OES hardly change with time, whereas those of unacidified samples for ion chromatography can change because precipitation or adsorption might occur in an unacidified solution. Samples for ion chromatography should be measured immediately after a sample is transported to the laboratory. The principles of measurements for ICP-OES and ion chromatography are described in instrument manuals and textbooks (e.g., Fritz and Gjerde 2009; Nölte

Fig. 8.3 Seal tape to seal the bottle–cap interface

2021). This section includes description of some tips to obtain the concentrations of measured components from the experimentally obtained data.

8.4.1 ICP-OES

The measured intensity of a specific wavelength derived from each element obtained under homogeneous liquid property (i.e., same matrix condition) from ICP-OES is proportional to its concentration of elements dissolved in solutions. Actually, ICP-OES can simultaneously measure the intensities derived from multiple elements if a specific wavelength from an element is not overlapped with those from other elements. To estimate the concentration of each component (element) from intensity data, the absolute calibration method is commonly applied for ICP-OES measurements. In this calibration method, intensities of standard solutions of which the concentrations are already known are measured before (or after) the measurement of sample solutions. Each standard solution for the absolute calibration method can be prepared by diluting a commercial standardized solution with a matrix solution (e.g., 0.6 wt% ultrapure HNO_3 solution) to maintain homogeneous liquid properties. The concentrations of each element are obtainable by comparing the intensity of sample solutions with those of standard solutions from calibration curves of target elements. Although ICP-OES can measure multiple elements simultaneously, certain elements cannot coexist stably with other elements in a solution. For example, Si can be precipitated from the solution when it coexists with metals, even in low-pH solutions. Therefore, when the measured elements are Na, K, Ca, Mg, and Si, two series of standard solutions are prepared separately, i.e., mixed standard solution containing Na, K, Ca, and Mg and single element (Si) standard solution. Actually, ICP-OES can measure the intensities derived from each element rapidly: within a few tens of seconds. This feature enables for multiple measurements (e.g., three times) for a single solution, which can provide the average and standard deviation (S.D.) of the intensities. Table 8.1 presents an example of relations between intensities and concentrations of K and Na from a blank matrix solution and standard solutions. The

measurements were conducted using ICP-OES (ES-710; Varian Inc., Palo Alto, CA, USA). The measured wavelengths for Na and K were, respectively, 589.592 nm and 766.491 nm. Measurements of a blank matrix solution can provide detection limits. The intensity of a detection limit of an element can be estimated from an average and an S.D. of the blank solution.

$$\text{Intensity of detection limit} = \text{Avg. intensity} + 3 \times \text{S.D} \tag{8.3}$$

For example, the average intensity and the S.D. of K are 749 and 418 respectively from Table 8.1. The intensity of the lower limit of detection can be approximately 2000. According to the relation between known concentrations and intensities, the detection limit concentration of K is between 20–50 ppb. Therefore, the detection limit of K in this case is regarded as approximately 40 ppb. The K concentrations with intensity of less than 2000 are less than 40 ppb in this case.

Actually, ICP-OES is well known to exhibit a wide dynamic range: a good linear relation exists between concentration and intensity under a very wide range of concentrations. Figure 8.4a shows a good linear relation from 10 ppb to 10,000 ppb for Na. However, it is noteworthy that the relational expression obtained from the lower concentration range is more or less different from that obtained from the higher concentration range. For example, the linear regression equation from all the standard data of the Na from Fig. 8.4a is $y = 386x - 1811$. The linear regression equation from the three data from highest concentrations (2000, 5000, and 10,000 ppb) is $y = 391x - 4755$ (Fig. 8.4b), which is close to the overall regression. However, from the three data from the lowest concentration (10, 20, and 50 ppb) is $y = 293x + 686$ (Fig. 8.4c). In this regard, the calculation of the concentration of unknown samples

Table 8.1 Intensities of standard solutions of Na and K measured using ICP-OES (ES-710; Varian Inc.)

Conc (ppb)	Intensity of Na		Intensity of K	
	Average	S.D	Average	S.D
0 (blank)	467	196	749	418
10	3424	112	1350	405
20	6789	223	1440	507
50	15,254	252	2718	524
100	32,070	391	6006	836
200	61,189	895	10,255	594
500	161,172	255	27,901	318
1000	316,297	2769	57,421	911
2000	736,540	1159	124,166	1030
5000	1,902,450	16,129	294,472	2608
10,000	3,861,920	1035	591,211	1297

using the regression equation should be done using that obtained from the similar concentration range. For example, when the sample solution intensity is 5000, the equation obtained from the standard solutions with the three lowest concentrations should be used.

The intensity–concentration relation (regression equation) is only valid for the concentration ranges of the standard solutions. If the intensity from the sample solutions exceeds the intensity of the highest concentration, then the sample solution must be diluted adequately with matrix solution to match the intensity ranges of the standard solutions.

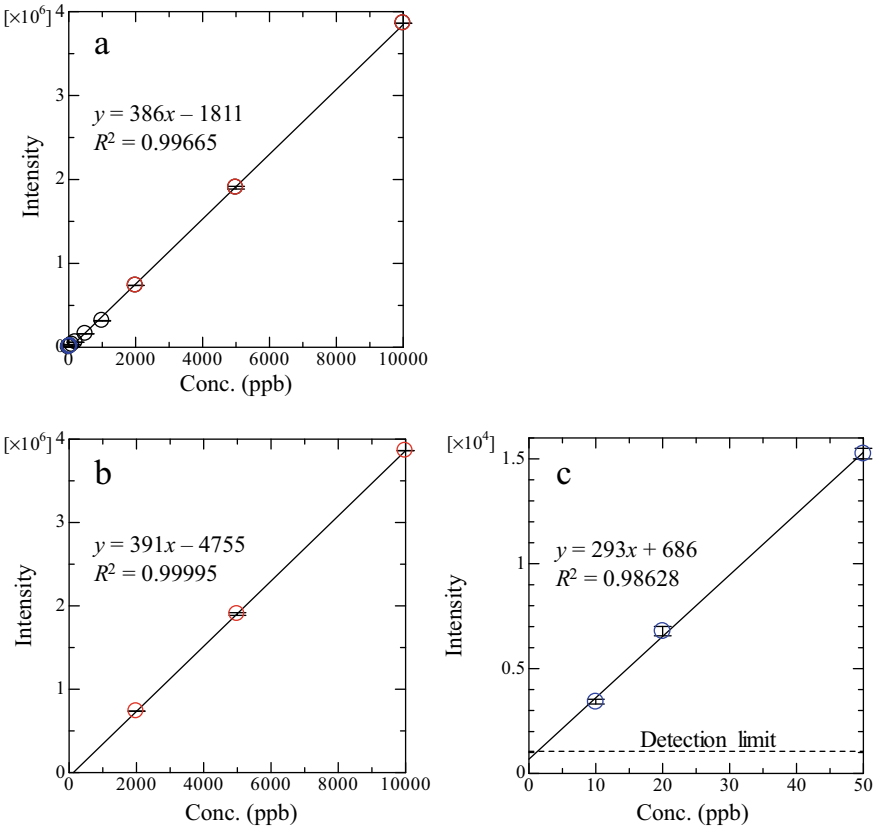

Fig. 8.4 Relation between concentrations and intensities of Na measured by ICP-OES. The relationship from all measured data is given in Table 8.1 (**a**), data of the three highest concentrations (**b**) and data of three lowest concentrations (**c**)

8.4.2 Ion Chromatography

Each ion species has its own charge (valence) and size. Ions that have flowed into an exchange column with eluent of mobile phase in ion chromatography are retained for a certain period of time depending on its charge and size. Ion chromatography monitors electric conductivity or fluorescence intensity as a function of time (Fig. 8.5). A peak area of conductivity (or intensity) at a retention time that is specific to each anion in an ion chromatogram is proportional to its concentration of an anion dissolved in a solution. It is noteworthy that the retention time of each anion can change depending on the conditions of the column and the eluent of the mobile phase. Both the retention time of each anion and the relation between the peak areas and concentrations are determined from measurements of standard solutions containing target anions before the sample solutions.

Measurements of anions concentrations in sample solutions can also be conducted using the absolute calibration method. Each standard solution for the calibration method can be prepared by diluting a commercial standardized solution with (ultra)pure water. The concentrations of each anion are obtainable by comparing the peak areas of sample solutions with those of standard solutions from calibration curves of target anions, of which the procedure is the same as ICP-OES (Fig. 8.4). Ion chromatography can also measure multiple anions simultaneously because it uses differences of the retention times of the respective anions in the exchange column

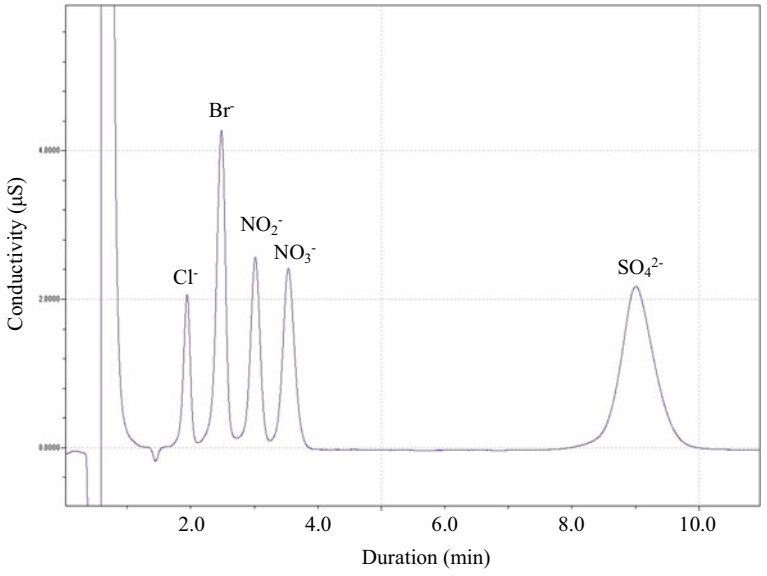

Fig. 8.5 Electric conductivity as a function of time of a standard solution (Cl^-, 2 ppm; Br^-, 10 ppm; $NO_2{}^-$, 10 ppm; $NO_3{}^-$, 10 ppm; $SO_4{}^{2-}$, 20 ppm) using ion chromatography (IC2010; Tosoh Corp., Tokyo Japan)

(Fig. 8.5). Tips for calculation of concentrations with ion chromatography using the absolute calibration method are almost identical to those for ICP-OES. The measurement times of ion chromatography are usually longer than those for ICP-OES. Therefore, the longer period of time is required to conduct multiple measurements of a single sample. In addition, the concentration range which can be measured with ion chromatography is usually smaller than that of ICP-OES. Therefore, adequate dilution of sample solutions with pure water is often necessary for measurements taken using ion chromatography.

8.4.3 Accuracy of Measurements

The accuracy of measurements of major components can be estimated from the electrical balance (*EB*) of a solution (Appelo and Postma 2005) as

$$EB\% = \frac{\text{Sum of Cations} - \text{Sum of Anions}}{\text{Sum of Cations} + \text{Sum of Anions}} \times 100 \tag{8.4}$$

where cations and anions are expressed as meq/L. Therefore, the following are obtained.

$$\text{Sum of Cations} = [\text{Na}^+] + [\text{K}^+] + 2[\text{Ca}^{2+}] + 2[\text{Mg}^{2+}] \tag{8.5}$$

$$\text{Sum of Anions} = [\text{Cl}^-] + [\text{SO}_4^{2-}] + \text{Alk} \tag{8.6}$$

Because the solution must be charge-balanced, it is possible to assess the accuracy of measurements from *EB%* quantitatively, assuming component concentrations equal to species concentrations (e.g., $[\text{Ca}] = [\text{Ca}^{2+}]$). It can be considered that analyses with absolute $EB\% < 2\%$ are reasonably accurate, whereas those with absolute $EB\% > 5\%$ are not accurate. Those with absolute $EB\% > 10\%$ are not acceptable. A negative *EB%* suggests an excess of anions or a deficiency of cations in solution, whereas a positive *EB%* suggests an excess of cations or a deficiency of anions. The information of *EB* helps to figure out problems related to the measurements. In addition, when some important species are missing in the measurements, the *EB%* becomes large. In such cases, H^+, Al^{3+}, Fe^{2+}, NH_4^+, NO_2^-, and NO_3^-, which sometimes become major species in acidic (H^+ and Al^{3+}), reducing (Fe^{2+} and NH_4^+), and contaminated water (NH_4^+, NO_2^- and NO_3^-), should be measured and considered in calculations. Under highly saline or alkaline conditions, formation of ion-pair species becomes important. For instance, the contribution of Mg^{2+} to Mg total (component) concentration in seawater is around 70%. Other 30% are comprised with $MgCl^+$ and $MgSO_4^0$ ion-pair species (Bethke 2007). To estimate the *EB%* accurately, one must

conduct speciation calculations based on thermodynamic analyses of the solution (Sect. 8.5).

The value of EC represents amounts of electrolytes in the solutions. Different ions have different molar conductivity (Appelo and Postma 2005). Therefore, EC can be calculated theoretically from the molar conductivity and concentrations of ionic species in solution. The major species of terrestrial fresh water are often Ca^{2+} and $HCO_3{}^-$. According to molar conductivities of these species at 25 °C, the EC divided by 100 can provide a good estimate of the sum of cation or anion. More sophisticated equations for theoretical EC have been proposed (McCleskey et al. 2012) and implemented in some geochemical codes, such as the Geochemist's Workbench (Bethke et al. 2021).

8.5 Speciation Analysis of Water Chemistry

The concentrations measured using ICP-OES and ion chromatography are component concentrations or total concentration of relevant species. We obtained the concentrations of Na and Cl if we measure a concentrated NaCl solution. However, species actually existed in this solution are not only Na^+ and Cl^- but also $NaCl^0$, which is an ion-pair of Na^+ and Cl^-. It is usually difficult to measure the concentrations of actual species directly. Retention times of anions in an ion chromatogram depend on the species valence and size. This finding suggests that ion chromatography measures species concentrations. However, anion species take homogeneous chemical forms in mobile phase, which are usually buffer solutions. Therefore, the concentration obtained from ion chromatography is also the component concentration.

The common and easy method of estimating the contributions of actual species is a speciation analysis of the solution. One must consider how one can estimate the concentration of $NaCl^0$ from information of the component concentrations of Na and Cl. The formation reaction of $NaCl^0$ from Na^+ and Cl^- can be expressed as:

$$Na^+ + Cl^- = NaCl^0 \tag{8.7}$$

The corresponding mass action expression is given as

$$K = \frac{a_{NaCl^0}}{a_{Na^+} a_{Cl^-}} \tag{8.8}$$

where a_i stands for the activity of the ith species. Assuming here that the activities are equal to mole basis concentrations as

$$K = \frac{[NaCl^0]}{[Na^+][Cl^-]} \tag{8.9}$$

where [i] denotes the molar concentration of the ith species. K is the equilibrium constant under a given temperature and pressure. The K of the reaction is $10^{-1.60}$ under 25 °C and 1 atm. In addition to the mass action expression, one can write mass balance relations for Na and Cl components as presented below.

$$[\mathrm{Na}] = [\mathrm{Na}^+] + [\mathrm{NaCl}^0] \tag{8.10}$$

$$[\mathrm{Cl}] = [\mathrm{Cl}^-] + [\mathrm{NaCl}^0] \tag{8.11}$$

Therein, [Na] and [Cl] come from the analytical concentrations. Here, three equations with three unknown parameters ([Na^+], [Cl^-], and [NaCl^0]) can be obtained. Therefore, we can solve the equations and estimate the concentrations of all species in the solution. The example presented above only considers the two components: Na and Cl. By contrast, natural water is always a multicomponent system. There are nine components in natural water when considering the major components with $\mathrm{H_2O}$ and H^+. Under such a multicomponent system, the number of species considered in the calculation increases drastically. Additionally, we must incorporate consideration of the activity–concentration relation in calculations based on appropriate acidity model, which is ignored in the example given above. Manual calculations of speciation analyses of natural water are almost impossible. Therefore, the speciation analyses of natural water are usually conducted using a computer program called geochemical codes. Several commercial and free geochemical codes are available. Most of the geochemical codes also include a thermodynamics database of equilibrium constants for aqueous reactions. For example, Visual-MINTEQ is free software that includes a comprehensive thermodynamics database (Gustafsson 2018). This program can be used to conduct speciation analyses easily under ambient conditions. SpecE8 in the Geochemist's Workbench is commercial software (Bethke et al. 2021). This program can expand the condition to higher temperatures and pressures.

References

Appelo CAJ, Postma D (2005) Geochemistry, Groundwater and Pollution, 2nd edn. CRC Press, Rotterdam

Bethke CM (2007) Geochemical and Biogeochemical Reaction Modeling, 2nd edn. Cambridge University Press, Cambridge

Bethke CM, Farrell B, Sharifi M (2021) The Geochemist's Workbench Release 15, GWB Reaction Modeling Guide., Champaign, Illinois

Drever JI (1997) The Geochemistry of Natural Waters: Surface and Groundwater Environments, 3rd edn. Prentice Hall, New York

Dzombak DA, Morel FM (1990) Surface Complexation Modeling: Hydrous Ferric Oxide. Wiley

Fritz JS, Gjerde DT (2009) Ion Chromatography, Fourth, Completely Revised and Enlarged Edition, Wiley

Fukushi K, Sasaki M, Sato T, Yanase N, Amano H, Ikeda H (2003) A natural attenuation of arsenic in drainage from an abandoned arsenic mine dump. Appl. Geochemistry 18:1267–1278

Gustafsson JP (2018) Visual MINTEQ ver. 3.1. Available at: https://vminteq.lwr.kth.se/
Kobayashi Y, Fukushi K, Kosugi S (2020) A Robust Model for Prediction of U(VI) Adsorption onto Ferrihydrite Consistent with Spectroscopic Observations. Environ Sci Technol 54:2304–2313
McCleskey RB, Nordstrom DK, Ryan JN, Ball JW (2012) A new method of calculating electrical conductivity with applications to natural waters. Geochim Cosmochim Acta 77:369–382
Nölte J (2021) ICP Emission Spectrometry: A Practical Guide. Second ed., Wiley-VCH
Smedley PL, Kinniburgh DG (2017) Molybdenum in natural waters: A review of occurrence, distributions and controls. Appl. Geochemistry 84:387–432
Sposito G (1984) The surface chemistry of soils. Oxford University Press, New York
Stumm W (1987) Aquatic Surface Chemistry: Chemical Processes at the Particle-Water Interface. Wiley
Tsetsgee S, Okuyama A, Ochir A, Yunden A, Odgerel E, Batbold T, Munkhsukd E-U, Takahashi Y, Munemoto T, Honda M, Fukushi K (2021) Mo Contamination in Rivers near the Erdenet Mining Area, Mongolia: Field Evidence of High Mobility of Mo at pH >8. ACS ES&T Water 1:1686–1694
USGS (2012) Alkalinity Calculator ver. 2.22. USGS. Available at: https://or.water.usgs.gov/alk/

Chapter 9
Low-Background γ-Spectrometry in Ogoya Underground Laboratory, Ishikawa, Japan

Mutsuo Inoue and Shinya Ochiai

9.1 Introduction

Large amounts of artificial radionuclides (e.g., ^{134}Cs and ^{137}Cs) were globally released by atmospheric nuclear test explosions from the middle of the 1950s and the early 1960s, and power plant accidents, such as the Chernobyl reactor accident in 1986 and the Fukushima Dai-ichi Nuclear Power Plant (FDNPP) accident in 2011. Environmental radioactive contamination has been a serious social problem. In particular, the activities of ^{137}Cs (30.2 y half-life) have often been examined in various environments for radioactive monitoring (Ikeuchi 2003). However, 50 years after the test explosions, measurement of long-lived ^{137}Cs in environmental samples using conventional γ-spectrometry has become difficult due to a decrease in the activities by radioactive decay, dispersion, and dilution during migration. Furthermore, within ten years after the FDNPP accident, the activities of radiocesium (particularly ^{134}Cs with a half-life of 2.06 y) in marine products, bottom sediments, and seawater have fallen below the detection limit in conventional γ-spectrometry. The activities of natural radionuclides (e.g., ^{226}Ra, ^{228}Ra, ^{228}Th, ^{234}Th, ^{210}Pb, and ^{7}Be) with a wide range of half-life and various geochemical behavior, and artificial radionuclides, particularly radiocesium in environmental samples (e.g., seawater, sediments, depositions, aerosols, and marine and agricultural products) have also been used as strong tracers to study environmental radioactivity, geo and cosmochemistry, and radioactive dating.

These artificial and natural radionuclides are γ-ray-emitting nuclides. However, the activities of these radionuclides are generally low. Therefore, high-precision measurement is required for low-level radionuclides in environmental samples in many research fields (Verplancke 1992) for use as chemical tracers to determine

M. Inoue (✉) · S. Ochiai
Low Level Radioactivity Laboratory, Institute of Nature and Environmental Technology, Kanazawa University, Nomi, Ishikawa, Japan
e-mail: i247811@staff.kanazawa-u.ac.jp

N. Hasebe et al. (eds.), *Field Work and Laboratory Experiments in Integrated Environmental Sciences*, https://doi.org/10.1007/978-981-99-6532-8_9

material circulation. We have thus vigorously developed a low-background γ -spectrometry system. In this chapter, we present the history of the Ogoya Underground Laboratory (OUL), which specializes in low-background γ-spectrometry, using numerous photos and figures. Furthermore, we demonstrate aspects of low-background γ-spectrometry at the OUL, including the location, features for low counting, and background levels (Hamajima and Komura 2004; Komura and Hamajima 2004) and introduce noteworthy research conducted at the OUL.

9.2 Histories of Ogoya Copper Mine and OUL

The histories of Ogoya Town and the OUL are listed in Table 9.1. The OUL (1975–) is in Ogoya Town, which is located in the southeastern part of Ishikawa Prefecture, Japan (Fig. 9.1). The Low Level Radioactivity Laboratory (LLRL) of Kanazawa University manages the OUL. The town of Ogoya flourished as a result of the former Ogoya Copper Mine (Fig. 9.2a and b). Mining in Ogoya started in 1682 at the latest, and ended in 1971. The Ogoya Copper Mine was a large contributor to the Japanese economy during the peak period with one of the largest production outputs. The Ogoya train (1920–1977) transported mining employers and residents between the old Shin-Komatsu Station and Ogoya Station (Fig. 9.2c and d). The public Ogoya Mine Museum in Komatsu City presently showcases the records of the Ogoya Copper Mine by displaying various minerals, extraction methods, and reproducing mining works using a full-scale diorama in old tunnels of the Ogoya Copper Mine (Fig. 9.2e) along with the exhibition of the old Ogoya train (Fig. 9.2f).

The Ogoya–Kuratani road tunnel (Ogoya Tunnel), which was used for the movements of employers and conveyance of goods, was also closed when the Ogoya Mine closed in 1971. Improvements to the ruined Ogoya Tunnel and construction of the OUL began in 1991, subsequent to permission from the Komatsu City government to use the Ogoya Tunnel. The length of the Ogoya Tunnel, where the OUL room was built, measures 546 m, and the maximum overburden measures 135 m at 290 m from the entrance. The 135 m of rock cover at the OUL corresponds to a water equivalent depth (meter water equivalent; mwe) of 270 m, based on the measured density of the rock that comprises the Ogoya Tunnel (2.0 g/cm^3, tuff breccia) (Fig. 9.3a-d).

In 1995, two high-purity germanium (HPGe) detectors were set up, and the first measurement was conducted for low levels of cosmogenic radionuclides in the Neagari Meteorite which fell in Neagari Town (Nomi City at present, close to Komatsu City) in February 1995. As of February 2022, the OUL is equipped with 11 well-, 5 planar-, and 1 coaxial-type HPGe detectors of high efficiency, high stability, and ultra-low background specifications (Fig. 9.3e and f).

The OUL has no on-site staff, and Ge detectors are managed by LLRL members; for instance, liquid nitrogen is supplied three times in a week to maintain the Ge-detectors, and measurement samples are exchanged in 1 day to 1 week counting intervals. Some liquid nitrogen is supplied by two generators equipped on the left

Table 9.1 Histories of Ogoya copper mine and the OUL

Age	Event
1600 s–the second half of the1800s	Ogoya Mine was operated as a gold mine for over 30 years before being closed
After the second half of the 1800s	Operation was resumed as the Ogoya Copper Mine which had one of the largest outputs in Japan in this era
End of 1971	Ogoya Copper Mine was closed. The mining town, which had once been crowded with more than 2600 residents, withered away. The Ogoya Tunnel, which had been a road used for movement of employers and for conveyance of goods, was also closed
Apr. 1975	LLRL was established for studies of low-level environmental radioactivity
1991	Construction of OUL began. The ruined tunnel was improved in four years by hand
Jan. 1995	Two Ge-detectors were set up in OUL and low-level counting was started
Feb. 18, 1995	The first low level measurements were made for cosmogenic radionuclides in the "Neagari meteorite"
Mar. 2003	Installment of two liquid nitrogen generators
Mar. 2009	Tunnel maintenance was undertaken and the tunnel floor was paved with asphalt
Aug.–Nov. 2016	Reinforcement of inside of Ogoya Tunnel
Mar. 2011–	OUL played important roles to assess world-impacted FDNPP accident in March 2011
Now (Feb. 2022)	OUL has 11 well, 5 planar, and 1 coaxial Ge-detectors. All detectors have high efficiency, stability, and ultra low-background specifications

side of the entrance (80 L/day generating capacity), and other portions are transported from the LLRL by car.

It takes only approximately 30 min from the LLRL or from Komatsu Station of to the OUL and approximately 40 min from the Komatsu Airport by car. Although Ogoya Town has heavy snow in winter (ca. 1 m snowfall) (Fig. 9.3c), the road from LLRL to OUL is maintained by Komatsu City to access the neighboring Ogoya Mine Museum. Taking advantage of this accessibility, OUL is one of the most convenient underground laboratories for the maintenance and measurement of short-lived radionuclides, such as cosmogenic radionuclides in meteorites (Komura et al. 2002).

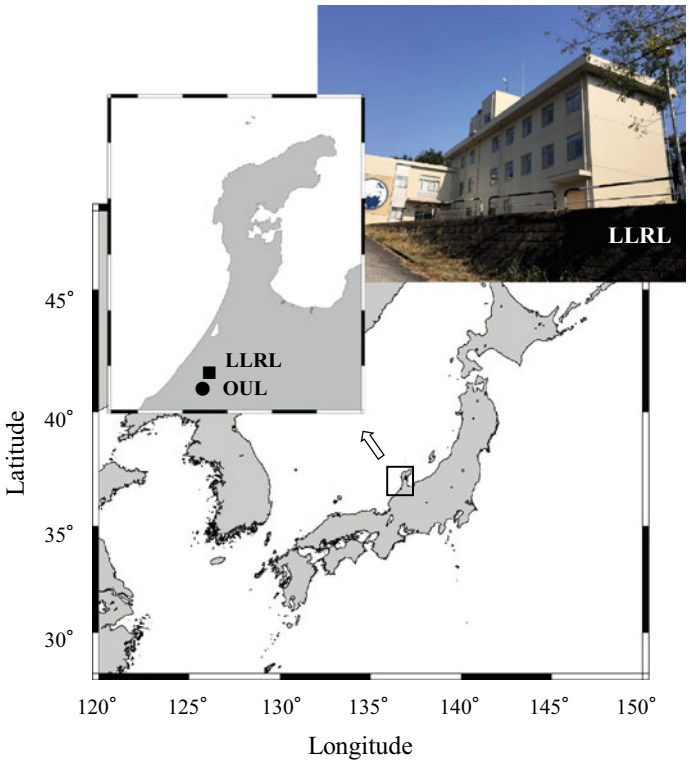

Fig. 9.1 Location of Ogoya Underground Laboratory (OUL) and the Low Level Radioactivity Laboratory (LLRL) in Ishikawa, Japan

9.3 Features of the OUL for Low-Background Counting

9.3.1 Improvements of Detection Limit

The figure of merit (*FOM*) given by $FOM = S^2/B$ is often used to evaluate the detection limit of radionuclides in low-level counting systems, where S and B are the signal intensity and background level for the γ-spectrum, respectively. The use of high-efficiency Ge detectors is effective to obtain a high S. The efficiency of well-type Ge-detectors is approximately three to four times higher than that of the planar type (El-Daoushy and Garcia-Tenorio 1995). Additionally, the use of large amounts of sample and a reduction of sample volume by drying, ashing, evaporation, compression, and chemical treatment enhances the total activities of radionuclides in the samples. However, this often enhances the B value (e.g., disturbance by ^{40}K in samples). Therefore, to obtain a high *FOM*, it is necessary to decrease B, accompanied by an increase in S.

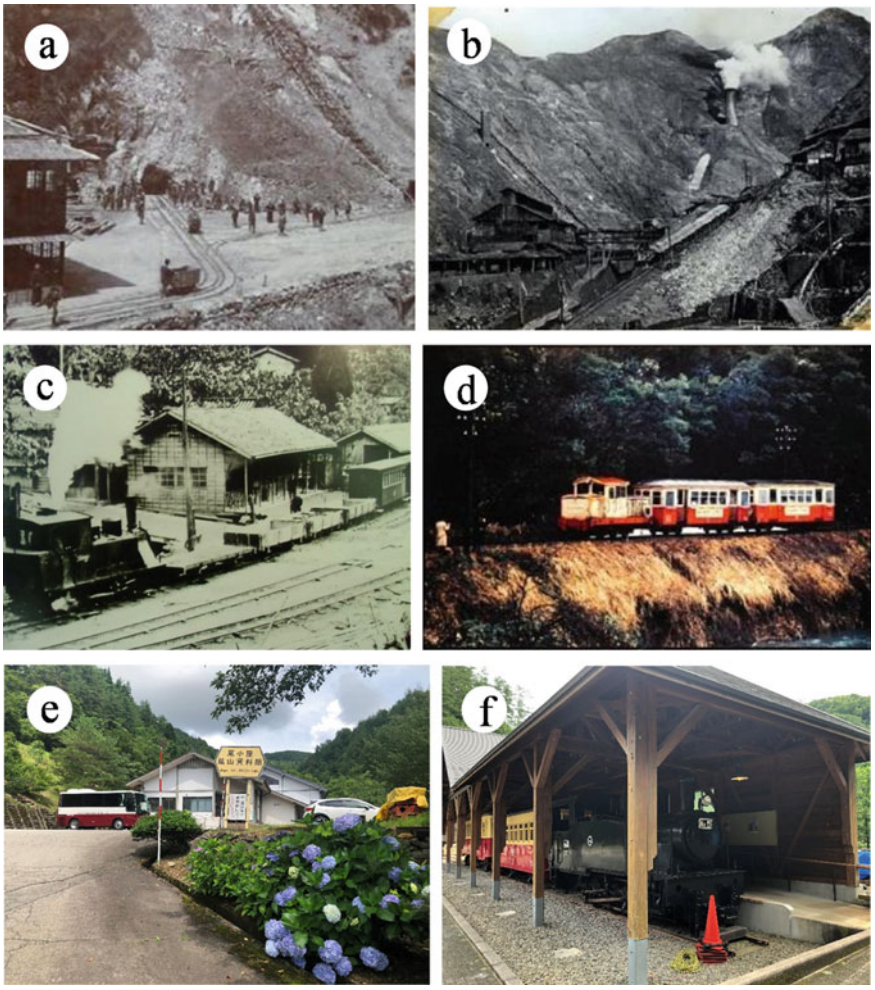

Fig. 9.2 **a**, **b** Former landscapes of ogoya copper mine, **c** old ogoya station (terminal), **d** the last run of the ogoya train (from HP of Ogoya Mine Museum), **e** Ogoya mine museum, and **f** exhibition of the ogoya train near the museum

9.3.2 Effects of Underground Laboratory

There are several underground laboratories worldwide, for example, the Super-Kamiokande in Gifu, Japan (2700 mwe) and the Gran Sasso National Laboratory in Italy (3800 mwe), which are particularly dedicated to research in astrophysics (e.g., detection of muons and neutrinos).

For low-background γ–spectrometry, it is important to reduce the background noise of detectors derived from secondary cosmic-ray components. The background

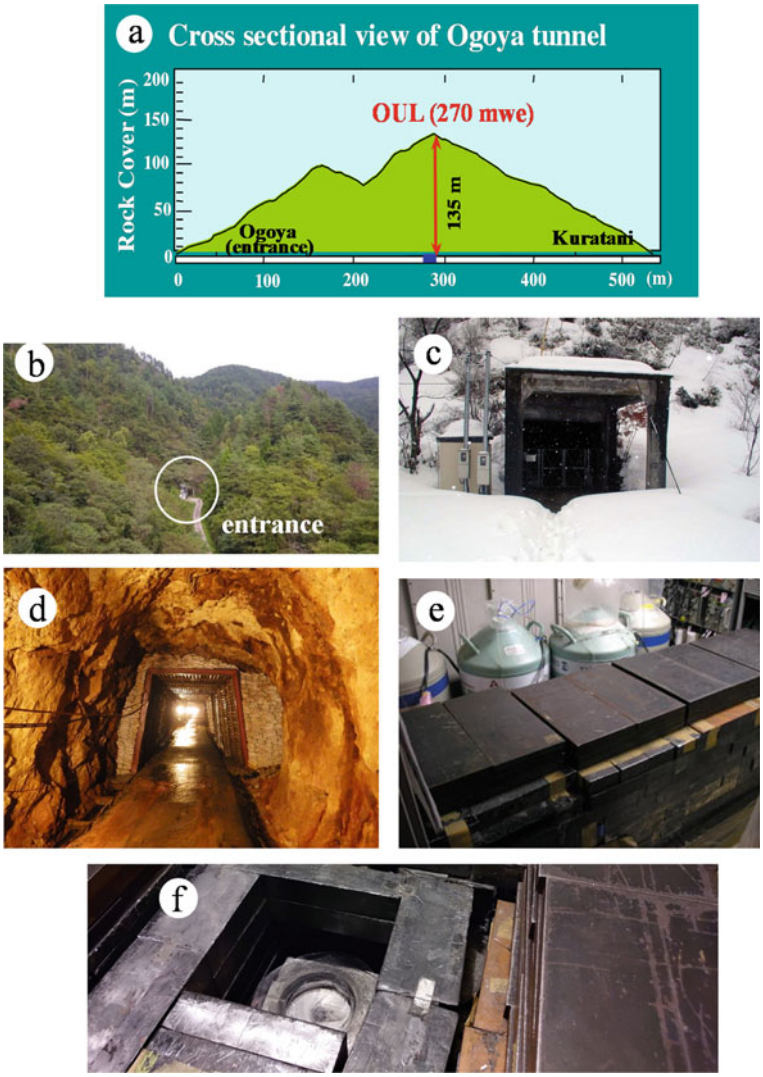

Fig. 9.3 **a** Cross sectional view of Ogoya tunnel, **b**, **c** entrance of ogoya tunnel, **d** tunnel interior, **e** Ge-detectors completely shielded, and **f** a detector in the OUL

can be reduced by utilizing a deep underground facility. The intensity of muons in the OUL (270 mwe) is approximately 1/200 relative to the ground level, although this cosmic-ray contribution is higher than that of much deeper underground facilities. However, the OUL has a much larger number of HPGe detectors (17 detectors) and all detectors focus on low-background γ-spectrometry.

9.3.3 Special Shield for the Detectors

Shielding of Ge detectors with lead iron bricks is fundamentally effective in reducing the background of detectors (Semkow et al. 2002; Trnková and Rulík, 2009). The shielding condition of a Ge detector in the OUL is schematically shown in Fig. 9.4. The lead shield is 15–20 cm thick, and its upper part is completely covered by 8 cm thick old iron plates. Old lead bricks were prepared using roof tiles from buildings of Kanazawa Castle, Ishikawa, refined approximately 200 years ago (Fig. 9.5a). The use of lead in roof tiles from Kanazawa Castle is a special instance for Japanese castles. These roof tiles have been utilized to bestow a quaint and whitish appearance due to aging. Reflecting on the half-life, 99.8% of ^{210}Pb underwent radioactive decay over 200 years (Fig. 9.5b). In laboratories in Europe, old lead from old sunken ships is used as ^{210}Pb-free shield. In the OUL, old lead bricks are placed as an inner shield (3–5 cm thick) to reduce the γ-rays emitted from the main shield. The lead bricks used for the inner shield facing the Ge-detector are hand-made using old lead to fit the space around the Ge detectors (Fig. 9.5a). Iron refined after World War II includes ^{60}Co as a tracer of the abrasion of a blast furnace. Iron plates salvaged from the battleship Mutsu built in 1920 are used as a part of shield in the OUL.

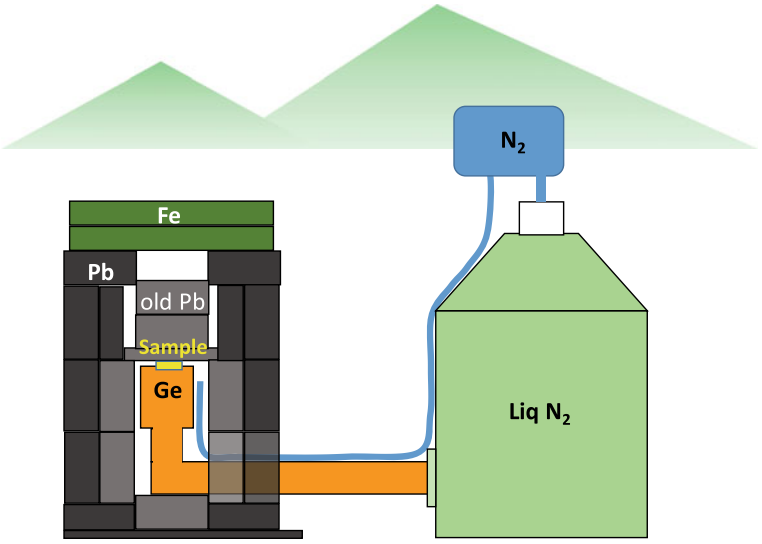

Fig. 9.4 Schematic image of a Ge-detector system in the OUL

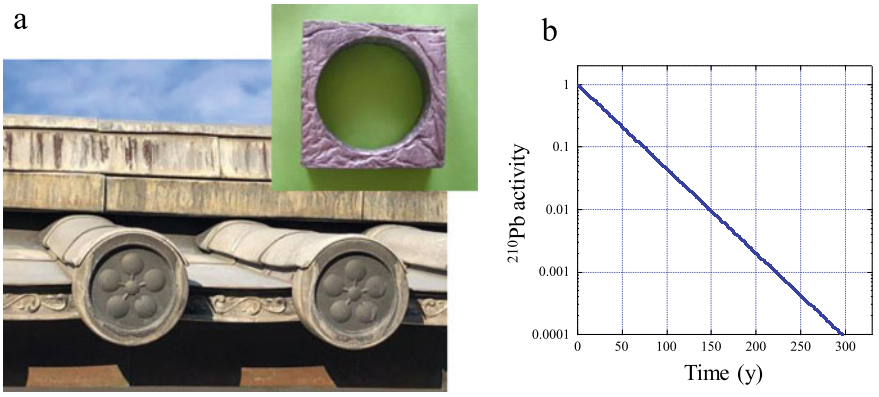

Fig. 9.5 **a** Roof tile from Kanazawa castle, Ishikawa and hand-made lead shield, and **b** radioactive decay of ^{210}Pb activity (22.3 y half-life)

9.3.4 Small Radon Effect by Tunnel Air

Radon and its daughter radionuclides (e.g., ^{222}Rn-^{214}Pb-^{214}Bi-^{210}Pb in uranium series) around the Ge-detector head interfere with low-background γ-spectrometry. Radon activity is predominantly governed by the ventilation ability in the facility and surrounding rock types in laboratories; high radon activity is a serious problem in deeper underground laboratories.

Ogoya Tunnel is mainly composed of tuff breccia, which contains 1.2–2.1 ppm uranium, 4.5–6.7 ppm thorium, and 2.0–3.7% potassium, and has lower activities than granite. The activity of radon (^{222}Rn) in the air inside Ogoya Tunnel ranges from 3 Bq/m^3 to 170 Bq/m^3, reflecting the daily variation, with an average value of 25 Bq/m^3, which is only one order of magnitude higher than the outdoor air levels in Japan (< 10 Bq/m^3; Oikawa et al. 2003). The low radon activity in the tunnel is caused by the high ventilation rate of the air inside the tunnel (e.g., high wind velocity) because both ends of the tunnel are open, as shown in Fig. 9.3a. Furthermore, nitrogen gas from the liquid nitrogen Dewar is fed into the head of the Ge detectors to expel air containing radon.

The OUL is considered to be of superior quality for low-background γ-spectrometry than deeper underground facilities worldwide, based on the rock shield by cover rock (270 mwe), complete shielding of Ge detectors with old lead, the low radon activity in the tunnel, and good accessibility.

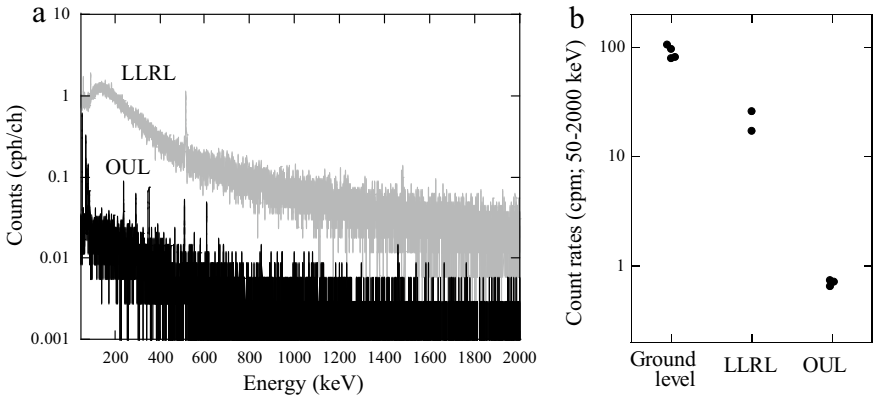

Fig. 9.6 **a** Comparison of background γ-spectra (0.25 keV/ch) and **b** integrated background count rates from 50 to 2000 keV of planar-type Ge-detectors in standard ground level laboratories, LLRL, and the OUL

9.3.5 γ-Spectra in the OUL

9.3.6 Background of γ-spectra

The background level of γ-spectrometry obtained by a planar-type Ge-detector in the OUL is compared with that partially shielded by old lead and located at ground level at the LLRL (Fig. 9.6a). Although the Ge-detector at the ground level of the LLRL is partly shielded by old lead, the background level in the OUL is one to two orders of magnitude lower.

Integrated background count rates from 50 to 2000 keV were 0.64–0.74 (mean, 0.70) counts per minute (cpm) for three planar-type Ge-detectors, 1.9 cpm for the coaxial detector, and 2.3 and 3.9 cpm for the well detectors (from data of 6 Ge-detectors acquired in Dec. 2020–Jan. 2021). In contrast, the background count rates (50–2000 keV) of the planar-type detectors in the LLRL and other ground-level laboratories are 17 and 26 (mean, 22) cpm and 79–106 (mean, 91) cpm, respectively (Fig. 9.6b). The counting rates of detectors in the OUL are ca. 1/25 and 1/100 of the ground level.

9.3.7 Application to Actual Samples

In the measurement of environmental samples with high potassium concentrations, such as marine products, we observe that a Compton continuum caused by the 1461 keV γ-ray of ^{40}K from a sample hinders the determination of low levels of

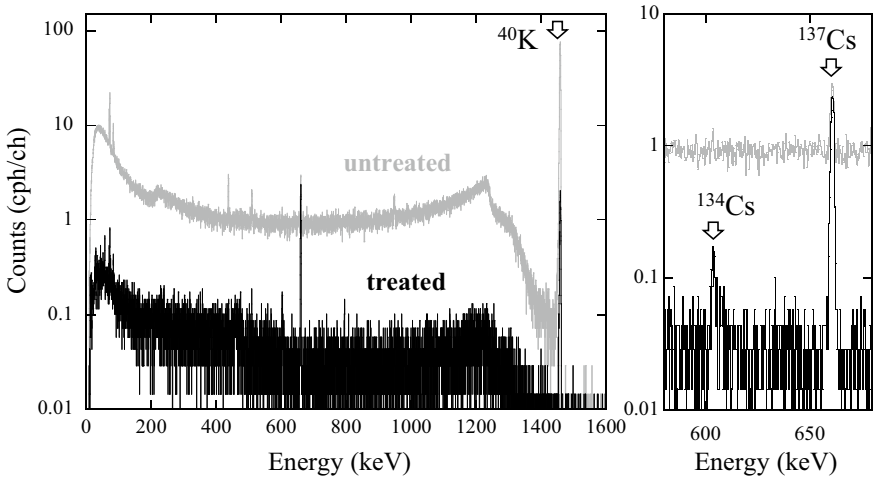

Fig. 9.7 Effect of ^{40}K-removal on γ-spectra obtained using a planar-type Ge-detector (3 counting days and 0.25 keV/ch) for an ashed fish sample at the OUL (Inoue et al. 2017)

radionuclides. Water leaching treatment on an ashed fish (Japanese flounder) sample was performed for the removal of ^{40}K (Inoue et al. 2017).

The γ-spectrum of the treated fish sample obtained in the OUL was compared with that of the untreated (ashed) sample in Fig. 9.7. The baseline of the γ-spectrum of the treated sample (0.11 cph/keV in 610–650 keV) was markedly reduced to ca. 3/100 of the untreated value (3.64 cph/keV). The faint γ-ray peak of ^{134}Cs by this treatment, which is embedded in the Compton continuum of ^{40}K in the untreated sample, was detected in the treated sample. This improved the detection limit of ^{134}Cs from ca. 20 mBq to ca. 3 mBq, which corresponds to ca. 1 Bq/kg-ash to ca. 0.15 Bq/kg-ash using 20 g of ashed sample.

9.4 Significant Research Conducted at the OUL

The history regarding research in the OUL is summarized in Table 9.2. Significant research has been conducted using Ge-detectors in the OUL during the past 25 years, such as the detection of low-level artificial radionuclides derived. from atomic power plant accidents and nuclear test explosions, such as the critical accident at JCO, Tokai-mura, Ibaraki in 1999, as well as natural and cosmogenic radionuclides using various environmental samples (see details in AR-LLRL; Komura et al. 2000).

The 2011 FDNPP accident resulted in the release of large amounts of radiocesium into marine environments over a wide region in eastern Japan. Therefore, the spatial distributions of ^{134}Cs and ^{137}Cs concentrations have emerged as strong chemical tracers in local and global water circulation since the FDNPP accident. Low levels

Table 9.2 Significant researches in the OUL

Year	Outlineof research project
1995	Measurements of cosmic ray-induced radionuclides of the "Neagari Meteorite" fallenob Feb. 18 at Neagari, Ishikawa. This is the first measurement made in the OUL
1996	Measurements of cosmic ray-induced radionuclides of the "Tsukuba Meteorite" fallen on Jan. 7 at Tsukuba, Ibaraki, and estimation of its orbit and condition during the fall
1997	Measurements of ^{137}Cs and ^{134}Cs that leaked from the bituminization facility of the power reactor and nuclear fuel development corporation by an accidental explosion on March 11
1998–2000	Identification of about 20 nuclids, such as ^{24}Na, ^{46}Sc, ^{60}Co, ^{76}As, ^{134}Cs, ^{152}Eu, ^{192}Ir, and ^{198}Au induced by environmental neutrons derived from cosmic rays
1999	Measurements of cosmic ray-induced radionuclides of the "Kobe Meteorite" fallen on Sept. 26 at Kobe, Hyogo (Identification of ^{28}Mg, ^{57}Ni, etc.)
	Assessment and investigationof environmental impact for the critically accident at JCO, Tokai-mura, Ibaraki on Sept. 30. This was marked by publication of the first special issue on the criticality accident in *J. Environ. Radioact* (2000, vol. 50)
2003	High temporal resolution measurements of airborne ^{210}Pb and ^{7}Be
2004	Simultaneous detection of short-lived cosmic ray-induced ^{18}F, ^{24}Na, ^{28}Mg (^{28}Al), ^{38}Cl (^{38}S), ^{39}Cl, ^{7}Be, and ^{22}Na in rain water
	Analysis of the residence time of Lake Biwa water by cosmic ray-induced ^{22}Na as a tracer.
2005	Identification of the highly sensitive nuclide ^{108m}Ag induced by atomic bomb neutrons at Hiroshima and Nagasaki.
	Identification of seasonal variations of the ^{228}Ra/^{226}Ra ratio in coastal seawaters and sea weeds in the Sea of Japan
2006–present	Examination of fine-resolution spatial and temporal variations of ^{228}Ra/^{226}Ra ratio to clarify water circulation around Japan Islands
2007	Analysis of depth profiles of environmental neutron flux and environmental neutron transport in seawater, fresh water, concrete, iron, and lead
	Utilization of radiometric dating by ^{228}Th/^{228}Ra ratio in bone and crustaceans
	Depth profiles of ^{137}Cs in deep seawater of the Pacific Ocean
2011–present	Studies of low-levels of ^{134}Cs and ^{137}Cs in seawaters in the Sea of Japan, East China Sea, Sea of Okhotsk, Bering Sea, and Pacific Ocean for assessments of current circulations after the FDNPP accident in March 2011
	Assessments of low-levels of ^{134}Cs and ^{137}Cs in marine products, marine sediments, settling particles, and riverine water and suspended solids in/around Japan Islands
2019–present	Analysis of lateral profile ^{226}Ra and ^{228}Ra in seawater from the Arctic to Antarctic Ocean

of radiocesium in a large number of seawater samples have been measured using Ge-detectors in the OUL, which have aided in determining the surface water circulation, convection, and mixing patterns of ocean currents as well as FDNPP-derived radiocesium around the Japanese Archipelago and northwestern North Pacific Ocean, including the Bering Sea (e.g., Inoue et al. 2019, 2020, 2021).

9.5 Social Contributions

The OUL opened as a center for joint academic contributions such as joint usage, research, and education (Ministry of Education, Culture, Sports, Science and Technology, Japan; MEXT) (2016–present), as well as for the purpose of other collaborative research with domestic and international laboratories. With regard to social contributions, the OUL also plays the following important roles: (i) provide education and training for human resources in measurement techniques of low-level counting for students and young researchers, (ii) provide know-how for low-background γ-spectrometry to other laboratories, (iii) ensure high-accuracy and highly reliability measurements of radionuclides for measurement-requested samples; and (iv) assess radioactive pollutants released by power plant accidents and radiation leakage. Furthermore, in cooperation with the Ogoya Mine Museum, Kanazawa University, and other universities and institutes, LLRL members conduct scientific tours at the OUL and hold lectures open to the public and researchers.

References

Annual Report of Low Level Radioactivity Laboratory (AR-LLRL) (2021) Institute of Nature and Environmental Technology, Kanazawa University (in Japanese). https://www.ki-net.kanazawa-u.ac.jp/EN/result/publishing/radiation/. Accessed 8 Feb 2022

El-Daoushy F, Garcia-Tenorio R (1995) Well Ge and semi-planar Ge (HP) detectors for low-level gamma spectrometry. Nucl Instr and Meth Phys Res A356:376–384

Hamajima Y, Komura K (2004) Background components of Ge detectors in Ogoya underground laboratory. Appl Radiat Isot 61:179–183

Ikeuchi Y (2003) Temporal variations of ^{90}Sr and ^{137}Cs concentrations in Japanese coastal surface seawater and sediments from 1974 to 1998. Deep-Sea Res II 50:2713–2726

Inoue M, Yamashita S, Fujimoto K, Kofuji H, Miki S, Nagao S (2017) Simple ^{40}K removal by acidified water leaching for estimating low levels of radiocesium in fishery products following Fukushima Dai-ichi Nuclear Power Plant accident. Appl Radiat Isot 120:17–21

Inoue M, Takehara R, Yamashita S, Senjyu T, Morita T, Miki S, Nagao S (2019) Convection of surface water in the northeastern Japan Sea: Implications from vertical profiles of ^{134}Cs concentrations. Mar Chem 214:103661

Inoue M, Takehara R, Hanaki S, Kameyama H, Nishioka J, Nagao S (2020) Distributions of radiocesium and radium isotopes in the western Bering Sea in 2018. Mar Chem 225:103843

Inoue M, Hanaki S, Takehara R, Kofuji H, Matsunaka T, Kuroda H, Taniuchi Y, Kasai H, Morita T, Miki S, Nagao S (2021) Lateral variations of ^{134}Cs and ^{228}Ra concentrations in surface waters

in the western North Pacific and its marginal sea (2018–2019): Implications for basin-scale and local current circulations. Prog Oceanogr 195:102587

Komura K, Hamajima Y (2004) Ogoya underground laboratory for the measurement of extremely low levels of environmental radioactivity: review of recent projects carried out at OUL. Appl Radiat Isot 61:185–189

Komura K, InoueNakamura, M (2002) Cosmogenic radionuclides in the recently fallen Kobe (CK4) meteorite. Geochem J 36:333–340

Komura K, Yamamoto M, Muroyama T et al (2000) The JCO criticality accident at Tokai-mura, Japan: an overview of the sampling campaign and preliminary results. J Environ Radioactivity 50:3–14

Ogoya Mine Museum, Komatsu City (2022) Outline of ogoya mining museum and the history (in Japanese). Accessed 8 Feb 2022

Oikawa S, Kanno N, Sanada T, Ohashi N, Uesugi M, Sato K, Abukuma J, Higuchi H (2003) A nationwide survey of outdoor radon concentration in Japan. J Environ Radioactivity 65:203–213

Semkow TM, Parekh PP, Schwenker CD, Khan AJ, Bari A, Colaresi JF, Tench OK, David G, Guryn W (2002) Low-background gamma spectrometry for environmental radioactivity. Appl Radiat Isot 57:213–223

Trnková L, Rulík P (2009) Low background shielding of HPGe detector. Appl Radiat Isot 67:723–725

Verplancke J (1992) Low level gamma spectroscopy: low, lower, lowest. Nucl Instr Meth Phys Res A312:174–182

Chapter 10
Monitoring Hydro-Geomorphological Processes in Lake-Catchment Systems Through Lacustrine Sediments

Shinya Ochiai, Noriko Hasebe, and Shinji Tsukawaki

10.1 Introduction

Terrestrial areas are habitats for human beings. The terrestrial environment varies according to, for example, its latitudinal location, topographic characteristics, and land-sea distribution, and is subject to change by global climatic change, which is driven by insolation and intrinsic forces (e.g., volcanoes). Understanding how the environmental system works in a particular area is important to predict what will happen in the future and to prepare for it.

Earth surface materials (clastic and organic materials) in the catchment area are eroded and transported by water flow, and finally flow into the downstream lakes, ponds, and artificial reservoirs (Fig. 10.1). These accumulate sequentially at the bottom of the lake; therefore, lacustrine sediment is an archive of these materials from the past to the present. In the catchment area, the transport of these materials and their physical properties (grain size and density) are strongly affected by hydrogeomorphological conditions (e.g., precipitation change, heavy rainfall events, and geomorphological changes) and anthropogenic impacts (e.g., artificial land transformation, land use change, and agricultural activities). Therefore, past hydrogeomorphological fluctuations have been reconstructed using the physical properties of lacustrine sediments (e.g., Page et al. 1994; Lamoureux 2000; Kashiwaya 2017). Additionally, materials directly input from the atmosphere and produced by in-lake activity are archived in lacustrine sediments. It can also be used as a record of past changes not only for hydrological conditions but also for chemical and biological environments (e.g., vegetation and lake water chemistry) in the lake-catchment system. These indirect parameters, which provide evidence of past environment conditions instead of direct measurements, are called the proxy data.

S. Ochiai (✉) · N. Hasebe · S. Tsukawaki
Institute of Nature and Environmental Technology, Kanazawa University, Kanazawa, Japan
e-mail: sochiai@se.kanazawa-u.ac.jp

N. Hasebe et al. (eds.), *Field Work and Laboratory Experiments in Integrated Environmental Sciences*, https://doi.org/10.1007/978-981-99-6532-8_10

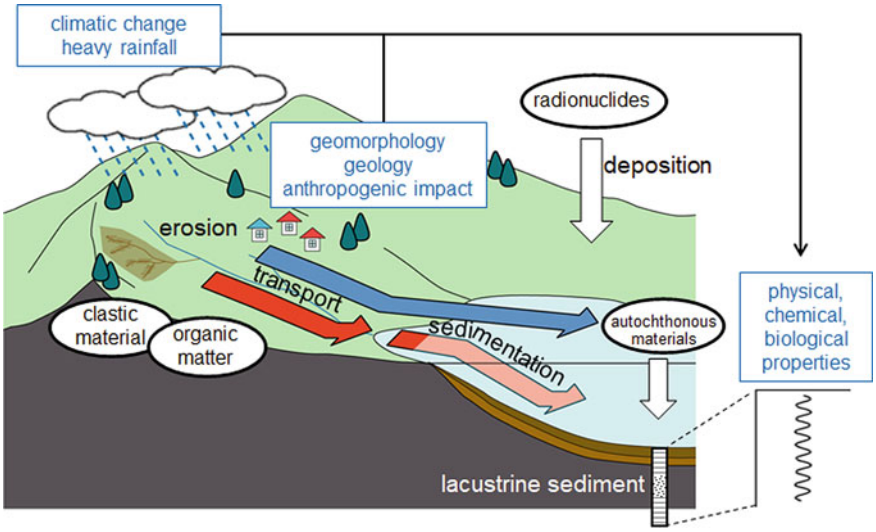

Fig. 10.1 Lake-catchment system and changes in terrestrial environments recorded in lacustrine sediment

The characteristics of lake sediments also largely depend on the geological and geographical conditions in the catchment. The geology of the catchment controls the mineral assemblages in the lake. Weathered bedrock conditions also contribute to the amount of sediment together with the amount and rate of fluid inflow. The geomorphology, which is represented as the slope angle, controls channel development. When interpreting environmental issues based on analyses of lake sediments, geological and geomorphological information in catchments should be surveyed beforehand, together with the depth profile of the lake basin. For Japanese lakes, the geology of the catchment is published by the Geological Survey of Japan, and an online geological map is available (https://gbank.gsj.jp/geonavi/). Topographic maps have been published by the Geospatial Information Authority of Japan and are also available online (https://maps.gsi.go.jp).

In this chapter, we introduce analytical methods to extract modern and past (10–1000 years) environmental information from lacustrine sediment records, particularly using physical properties.

10.2 Sampling of Lacustrine Sediments

To reconstruct past environmental changes recorded in lacustrine sediments, the sediment should be sampled whilst maintaining its structure. Usually, the bottom sediment is drilled using a cylindrical tube; this cylindrical sediment sample is called the core sample (Fig. 10.2).

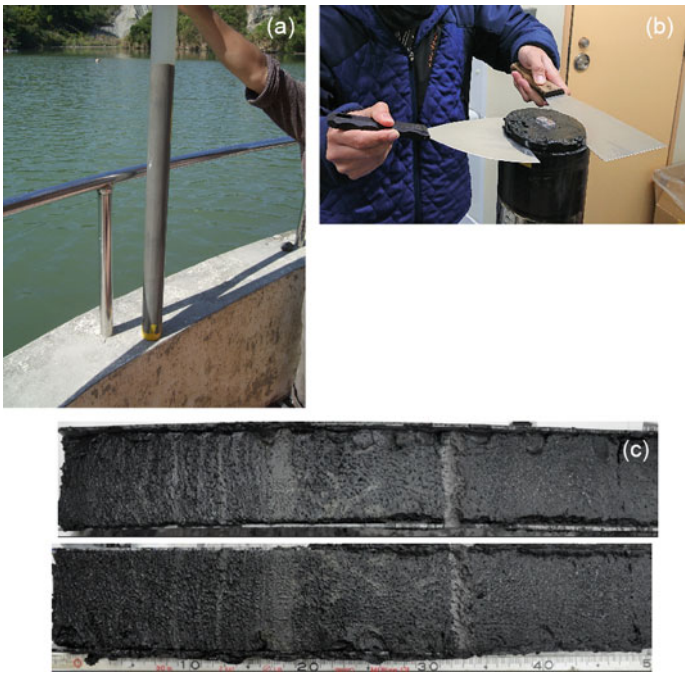

Fig. 10.2 **a** Example of surface sediment core, **b** subsampling by slicing with spatulas, and **c** sediment core divided vertically for lithological observation and subsampling

Gravity core samplers or hand-drilled samplers are commonly used to obtain short cores of relatively young (surface) lacustrine sediments. The gravity core sampler comprises a sampling tube, a weight to help the sampler penetrate to the bottom, and a check valve or sample catcher to hold the sample inside the tube (Fig. 10.3a and b). The sampler connected to the wire was dropped into the bottom of the lake, whereby the sampling tube penetrated the bottom sediment. When the sampler was pulled out from the bottom by the wire, the sediment sample was held in the sampling tube by the check valve. The hand-drilled sampler has a mechanism similar to that of a gravity core sampler. The sampler penetrates the bottom by hand instead of the gravity of the weight (Fig. 10.3c). The sampling tube was connected to the rod with the handle, and this rod could be added and elongated to the deeper part. These gravity samplers and hand-drilled samplers can collect approximately 1–2 m of core samples.

The lithological structures of the obtained core samples were first observed, and non-destructive measurements were performed. Soil color charts are useful for describing the sediment color. When fossils, such as shells or wood fragments, are found, it is worth identifying the species and keeping them sealed for radiocarbon dating. Non-destructive measurements include X-ray computed tomography

Fig. 10.3 Examples of gravity core samplers (**a** and **b**) and **c** a hand-drilled sampler used to obtain relatively short sediment cores

(CT) scanning, X-ray fluorescence (XRF) scanning, and magnetic properties. Subsequently, the core sample was sequentially separated into subsamples to analyze the physical, chemical, and biological characteristics, and age dating. For sub-sampling, the sediment core was divided vertically or horizontally. Vertical division (Fig. 10.2c) is suitable for observing the sediment structure, color properties, and some special sampling while maintaining the internal structures (e.g., remanent magnetization). However, this method is difficult to use for soft samples such as surface sediment. Horizontal division (Fig. 10.2b) can be used for high water-content surface sediments. In this case, the samples were pushed up from the lower end of the tube and sliced using a spatula.

10.3 Analytical Methods of Physical Properties of Lacustrine Sediments

10.3.1 Grain Size

Lacustrine sediments comprise clastic particles of various sizes and ranging widely from μm to cm. Grain size is strongly affected by hydrological conditions during erosion, transport, and deposition of sediments. This is an important parameter for estimating the sedimentation environment. In geology, the grain sizes of clastic materials are classified as follows.

Here, ϕ-scale is often used to explain the grain size,

$$\varphi = -\log_2 d$$

where d is the grain size (mm). Because the grain size of sediment is wide ranging, from μm to cm, the expression of grain size using the logarithm with base 2 is useful for lacustrine sediment.

Because lacustrine sediments contain particles of various sizes, their size component is generally expressed as a grain-size distribution. The size component was separated into classes, and the frequency of each class. The grain size distribution of sediments is usually measured based on sieve analysis, settling velocity, and the laser diffraction method.

Sieve analysis was performed using test sieves (Fig. 10.4). Usually, the mesh size of the test sieves corresponds to the classification of grain size, as shown in Table 10.1. Sediment samples were separated on sieves of different mesh sizes by shaking (dry sieving) or washing with water (wet sieving). After separation, the weights of the samples on each sieve were measured to calculate the grain-size distribution. This method has the advantage of being simple and can measure the grain size distribution directly. Conversely, it is difficult to use samples finer than several micrometers (fine silt).

Grain sizes finer than silt were measured based on the difference in the settling velocity of the particles. The settling velocity w_s of the particle is expressed by Stokes' law.

$$w_s = \frac{1}{18} g \frac{\rho_s - \rho_f}{\rho_f} \frac{1}{\nu} d^2$$

where ρ_s and ρ_f are the densities of the grain and water, respectively, ν is the kinematic viscosity of water, g is the acceleration owing to gravity, and d is the diameter of the grain. This indicates that the settling velocity is proportional to the grain size squared when the density of the material and viscosity of water (a function of the temperature) are constant. Therefore, grain size can be estimated from the settling velocity under controlled conditions. After dispersion in the water, the sediment concentration in the water column changes with time because of particle settling.

Fig. 10.4 Example of the test sieves with different mesh sizes

Table 10.1 Classification of sediment grain size

Clastics	mm	mm	ϕ
Boulder	256	256	–8
Cobble	64	64	–6
Pebble	4	4	–2
Granule	2	2	–1
Very-coarse sand	1	1	0
Coarse sand	0.5	1/2	1
Medium sand	0.25	1/4	2
Fine sand	0.125	1/8	3
Very-fine sand	0.063	1/16	4
Coare slit	0.031	1/32	5
Medium slit	0.016	1/64	6
Fine slit	0.008	1/128	7
Clay	0.004	1/256	8

The grain size distribution can be estimated by measuring the temporal changes in the concentration. Sediment concentration was measured by sampling with a pipette or transmittance of light or X-rays.

The laser diffraction method is based on the optical phenomena of particles in a liquid medium (Fig. 10.5). When a laser beam passes through a dispersed particle in a liquid, light is diffracted and scattered. The diffraction and scattering patterns are associated with the particle size. This method is advantageous for measuring a wide range of grain sizes (1000–0.01 μm) based on a single measurement principle. A particle size analyzer based on this method has been provided by many companies. However, a detailed calculation of the grain size from the diffraction pattern is usually

not available to users. Figure 10.6 shows an example of the grain size distribution of lacustrine sediment measured using the laser diffraction method. The grain size distribution is expressed as the frequency of each size class or cumulative percentage versus grain size. The cumulative grain size curve indicates the percentage of grains finer than a specific size. The grain size at 50% of the cumulative curve is called the median grain size, and is sometimes used to explain the average size of the sediment sample.

The grain size of lacustrine sediment reflects the hydrological conditions during transport in the river and deposition in the lake. Generally, a higher flow velocity

Fig. 10.5 Photograph of the laser diffraction particle size analyzer (SALD-2200, Shimadzu)

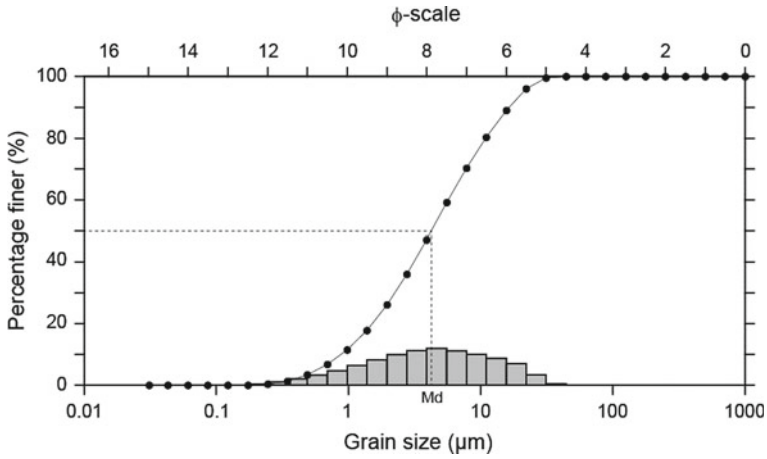

Fig. 10.6 Example of the grain size distribution of lacustrine sediment measured using the laser diffraction method. Bar graph shows the frequency of each size class. Line graph shows the cumulative grain size curve which indicates percentage finer. Md indicates the median grain size

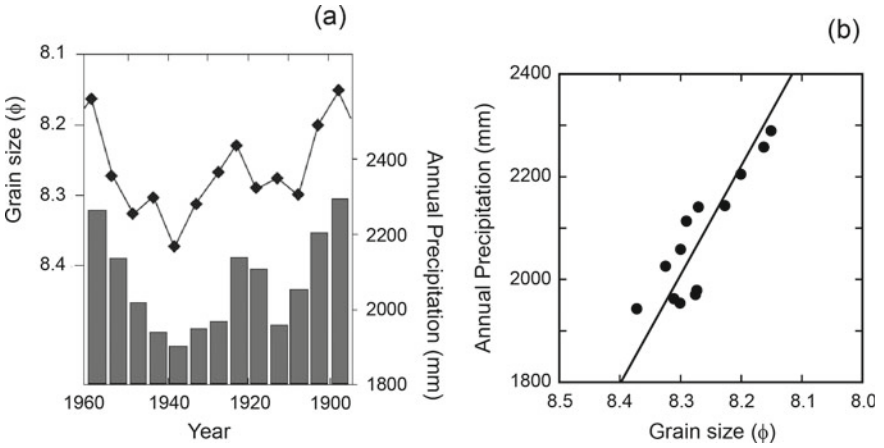

Fig. 10.7 Changes in **a** mineral grain size and annual precipitation, and **b** a relationship between mineral grain size and precipitation in Lake Yogo (modified after Shimada et al. 2002; Kashiwaya 2017)

entails the transport larger particles into river water. Therefore, the maximum size and content of larger grains in the sediment increases during high-flow conditions, such as heavy rainfall events. Based on these characteristics, the reconstruction of past precipitation in the catchment system was studied using the grain size of the lacustrine sediment core. Figure 10.7a shows the changes in grain size and annual precipitation in Lake Yogo, Japan (Shimada et al. 2002; Kashiwaya 2017). Fluctuations in grain size seemed to correspond to fluctuations in annual precipitation (Fig. 10.7b). Based on this relationship, precipitation changes were estimated for the past 1000 years in this region (Shimada et al. 2002).

10.3.2 Sediment Density

Sediment density is a parameter that indicates the mass per unit volume of lacustrine sediment. This parameter sometimes has two meanings for sediments. Absolute (true) density indicates the mass of a unit volume of sediment material. Conversely, bulk density (apparent density) indicates the mass of a unit volume of sediment with pores. In this section, absolute density is discussed.

The absolute density of the sediment was measured using an automatic pycnometer (Fig. 10.8). This instrument can measure the true volume of porous and powder materials by displacing the pores in the materials with helium gas.

Sediment is a mixture of various materials (e.g., minerals, organic matter, and biogenic particles) that have different densities. Therefore, the sediment density reflects the material composition and mixture ratio. Figures 10.9a and b indicate the vertical profiles of the sediment density and ignition loss in the sediment core

Fig. 10.8 Photograph of the automatic pycnometer (AccuPyc 1330, Micrometrics)

obtained from Sun Moon Lake (Riyuetan) in Taiwan (Ochiai et al. 2018). The vertical change in ignition loss, which indicates weight loss by heating over 500 °C, shows that the sediment in this lake is separated into two different layers. The ignition loss of the sediment generally reflects its organic matter content. Organic matter content was relatively low in the upper sediment layer and high in the lower sediment layer. This natural lake was transformed into a reservoir for a hydroelectric power plant in 1936. Before dam construction, organic-rich sediments were dominant (pre-dam sediments) in this lake. After dam construction, high-turbidity water was supplied through waterway tunnels from other catchment areas. Organic poor sediments became dominant after dam construction (post-dam sediment). Fluctuations in sediment density corresponded well with ignition loss. This indicates that the sediment density of this core was controlled by the mixture ratio of low-density organic matter and high-density mineral components in the sediment.

10.3.3 Water Content

Water content is a parameter that indicates the amount (weight) of water contained in the wet sediment sample. It is measured by the difference in masses before and after drying using an oven or freeze-dryer.

$$C_{\mathrm{w}} = \frac{m_{\mathrm{water}}}{m_{\mathrm{wet}}} = \frac{m_{\mathrm{wet}} - m_{\mathrm{dry}}}{m_{\mathrm{wet}}}$$

where m_{water} is the mass of water and m_{wet} and m_{dry} are the masses of the wet and dry sediment samples, respectively. A drying oven or freeze-dryer is usually used to dry sediment samples. An oven is suitable for simultaneously drying many samples. However, containers should be made of heat-resistant materials (e.g., glass beakers).

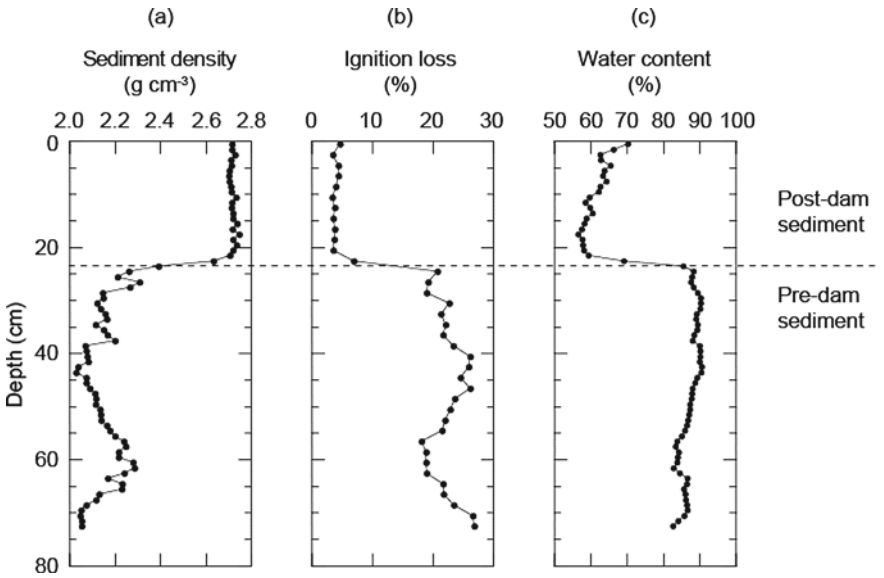

Fig. 10.9 Vertical changes in **a** sediment density and **b** ignition loss, and **c** water content of the sediment core in Sun Moon Lake, Taiwan (Ochiai et al. 2018)

A freeze-dryer can dry sediment samples without heating; therefore, it can be used to dry samples within plastic containers and bags. Freeze-drying is also suitable for parameters sensitive to heating (e.g., organic matter).

Water content reflects the porosity of the sediment. Sediments accumulated under constant and static conditions generally show a downward decrease in water content because of compaction. Water content is also closely related to other parameters such as sediment composition and grain size. Figure 10.9 shows the vertical profiles of water content, sediment density, and ignition loss in the Sun Moon Lake (Riyuetan) in Taiwan (Ochiai et al. 2018). The water content was relatively low in the surface layer (post-dam sediment) and high in the bottom layer (pre-dam sediment). These results indicate that sediment composition strongly affects the water content of lacustrine sediment.

10.4 Dating of Lacustrine Sediments

To reconstruct the environmental history based on proxy data obtained from lacustrine sediment analyses, the sedimentary age must be precisely known. Tephrochronology, which identifies the age-known widespread tephra in lake sediments, is a powerful tool when lake sediments contain such tephra layers. Radiocarbon dating was also applied when appropriate materials (e.g., plants and shells)

were included in the sediment. Here, we introduce three methodologies for analyzing bulk sediment.

10.4.1 ^{210}Pb Method

The natural radionuclide ^{210}Pb (half-life: 22.3 year) is the decay product of ^{238}U (U-series decay chain) (Fig. 10.10). ^{222}Rn, the daughter nuclide of ^{226}Ra, is released from the ground into the atmosphere. ^{222}Rn decays to its daughters and ^{210}Pb in the atmosphere and then deposits with aerosols and rain to the ground. After deposition on the ground surface, ^{210}Pb adsorbs onto clastic materials because of its high distribution coefficients (Wang and Cornett 1993; Wallbrink and Murray 1996). ^{210}Pb adsorbed by sediment is transported downstream and finally accumulates at the bottom of the lake. This characteristic has been used to trace sediment transport and estimate sedimentation age in lakes and marine sediments (e.g., Krishnaswamy et al. 1971; Appleby and Oldfield 1983; Sanchez-Cabeza and Ruiz-Fernández 2012).

^{210}Pb in lacustrine sediment samples comprises two sources: (1) ^{210}Pb, which is derived from ^{226}Ra contained in the sediment (supported ^{210}Pb), and (2) ^{210}Pb derived from atmospheric deposition (excess ^{210}Pb). The activity of the supported ^{210}Pb is substantially constant for lake sediments deposited on a historical timescale because it is supported by the concentration of ^{226}Ra (half-life: 1600 years). In contrast, the activity of excess ^{210}Pb exponentially decreases with a half-life of 22.3 year. Therefore, excess ^{210}Pb concentration is required to estimate the age of the sediment. The activities of supported ^{222}Rn, ^{214}Pb, and ^{210}Pb, which are all the decay products of ^{226}Ra (Fig. 10.10), become equal (radioactive equilibrium) after sufficient time when gaseous ^{222}Rn is maintained in the sample packed in a sealed container. Under these conditions, the activity of the excess ^{210}Pb ($^{210}Pb_{ex}$) was estimated by subtracting the activity of ^{214}Pb from the total activity of ^{210}Pb. After the radioactive equilibrium between ^{226}Ra and ^{214}Pb was established (approximately after one month), the activities of ^{210}Pb and ^{214}Pb were measured using a Ge semiconductor detector. Radioactivity measurements using Ge detectors were introduced in Chap. 9.

Several dating models have been proposed to estimate sediment age using ^{210}Pb (Sanchez-Cabeza and Ruiz-Fernández 2012). In this section, an example of age estimation based on the constant flux constant concentration (CFCS) model is introduced. If the sedimentation rate and $^{210}Pb_{ex}$ concentration in the surface layer are constant (i.e., the accumulation flux of $^{210}Pb_{ex}$ is constant), the $^{210}Pb_{ex}$ concentration exponentially decreases with depth. When the $^{210}Pb_{ex}$ concentration is expressed using the natural logarithm, the $^{210}Pb_{ex}$ concentration linearly decreases with depth.

$$lnC_i = lnC_0 - \frac{\lambda}{r} m_i$$

where C_i and C_0 are the concentrations of $^{210}Pb_{ex}$ at the *i*-th and surface layers, respectively, λ is the decay constant of ^{210}Pb, r is the sedimentation rate, and m_i

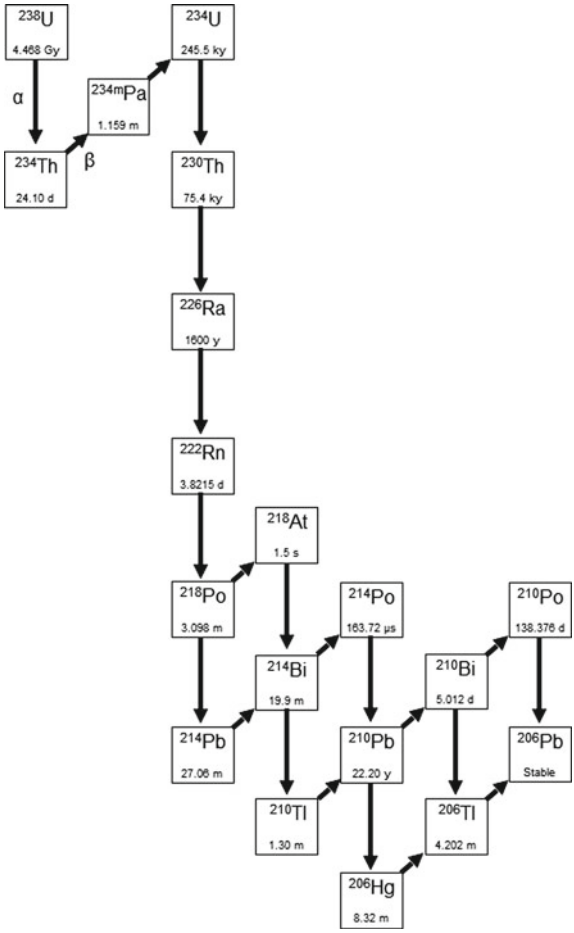

Fig. 10.10 Decay chain of the U-series. Values below the radionuclides indicate the half-lives of the radionuclides

is the mass depth of the i-th layer. The $^{210}Pb_{ex}$ concentration, sedimentation rate r, can be estimated from the slope of the regression line. The sediment age was estimated by dividing the sediment thickness by the sedimentation rate. Figure 10.11a shows the vertical profile of $^{210}Pb_{ex}$ in the sediment core obtained from the reservoir (Bishiaguro-ike) on the Noto Peninsula, Japan (Ochiai et al. 2015). The $^{210}Pb_{ex}$ concentration shown in the natural logarithm scale linearly decreased with depth, indicating that the assumption of the ^{210}Pb method is acceptable in this reservoir. In contrast, the slopes of the regression lines changed at certain depths. This suggests that the sedimentation rate changes at these depths.

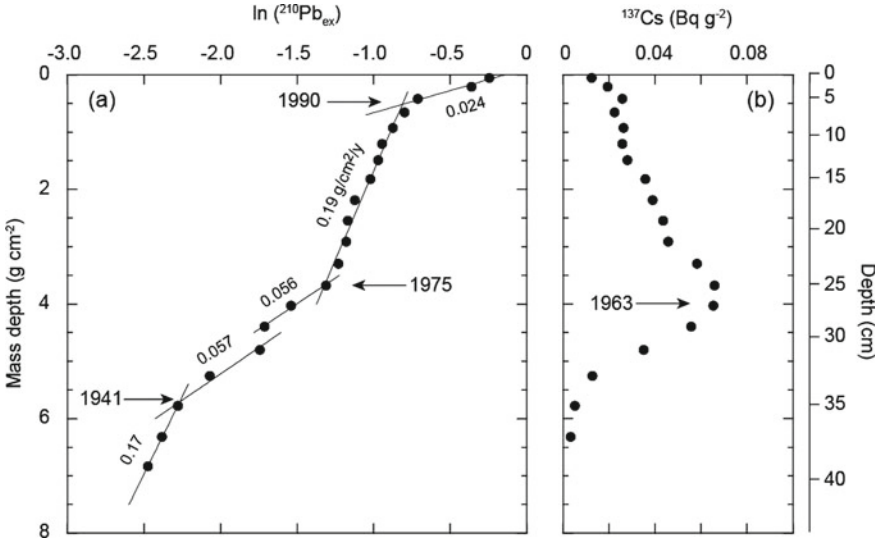

Fig. 10.11 Example of age dating based on ^{210}Pb and ^{137}Cs methods. Vertical profiles of **a** $^{210}Pb_{ex}$ and **b** ^{137}Cs concentrations of sediment core obtained from Bishaguso-ike Reservoir in Noto Peninsula, Japan (Ochiai et al. 2015). Values along the regression lines indicate sedimentation rate (g cm^{-2} y^{-1}). Values with arrows indicate the estimated age by ^{210}Pb and ^{137}Cs methods

10.4.2 ^{137}Cs Method

^{137}Cs (half-life: 30.1 year) is an artificial radionuclide whose major source in the terrestrial environment was global fallout by nuclear weapon tests in the atmosphere during the 1960s. Additionally, ^{137}Cs is also supplied by nuclear accidents (e.g., the Chernobyl Nuclear Power Plant accident in 1986 and the Fukushima Daiichi Nuclear Power Plant accident in 2011). Because of its high distribution coefficient, ^{137}Cs also has strong adsorptivity to clastic materials (Wang and Cornett 1993; Wallbrink and Murray 1996). Therefore, it has been used as a tracer of sediment in catchment areas (e.g., Walling and Quine 1992; Ritchie, 2005; Fukuyama et al. 2008). In addition to ^{210}Pb, ^{137}Cs is transported and accumulated at the bottom of the lakeby sediment transport processes. The accumulated ^{137}Cs has also been used to estimate the age of lacustrine sediments (Ritchie and McHenry 1990).

Figure 10.12 shows the temporal change in the annual ^{137}Cs deposition observed in the Kanto region in Japan (Aoyama 2018). In Japan, the fallout peak of ^{137}Cs induced by nuclear weapons tests in the atmosphere was observed in 1963. Peaks in 1986 and 2011 are related to the Chernobyl and Fukushima Daiichi nuclear power plant accidents, respectively. Therefore, the concentration peak in the depth profile of lacustrine sediment can be used as a time marker for the fallout peak in 1963. ^{137}Cs was measured using a Ge detector.

Figure 10.11b indicates the vertical profile of the ^{137}Cs concentration in the sediment core obtained from the irrigation reservoir (Bishaguso-ike) in Noto Peninsula

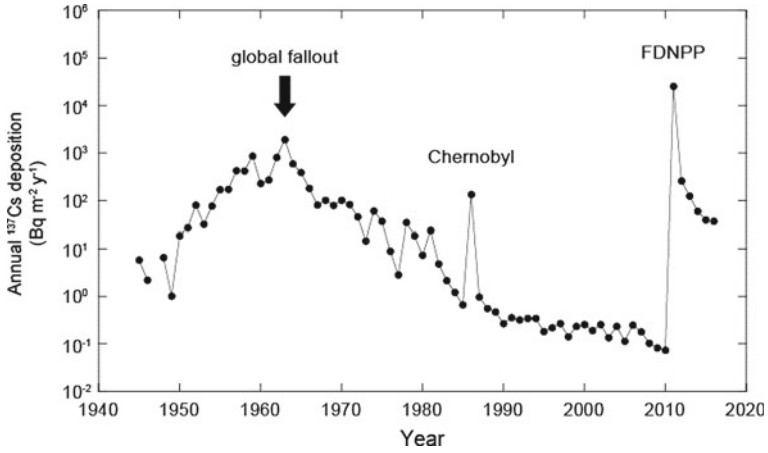

Fig. 10.12 Temporal change in annual ^{137}Cs deposition in Kanto region in Japan (Aoyama 2018). FDNPP indicates the Fukushima daiichi nuclear power plant accident in 2011

(Ochiai et al. 2015). The change in activity concentration of ^{137}Cs shows an increase with depth, and it exhibits the highest concentration at 26 cm depth. This depth of highest concentration corresponds to the fallout peak of ^{137}Cs in 1963. We can use the time marker of the ^{137}Cs peak for cross-checking of the age model established by using ^{210}Pb method.

10.4.3 Optically Stimulated Luminescence Dating

Optical luminescence dating (OSL) has been applied to quartz and feldspar (Aitoken 1998), which are common minerals usually present in lake sediments. When samples are exposed to environmental radiation, minerals store unpaired electrons, and they are emitted as a form of luminescence when they are stimulated by heat or light in the laboratory. The transportation of sediment through aeolian or fluvial processes optically erases luminescence signals stored beforehand; therefore, we can assume that the luminescence measured in the laboratory is proportional to the accumulated dose given after the deposition. We can estimate the age of deposition when we know the annual radiation dose given to the sediment, which is estimated from the concentration of radioisotopes in the surrounding environment (e.g., Ademic and Aitoken 1998, Ito et al. 2009).

The samples for luminescence dating should be collected without exposure to sunlight. After retrieving a sediment core, subsampling for OSL dating must be performed in a dark room. The outer exposed part of the sediment must be removed and used for the measurement of the annual dose. A subsample was then treated with H_2O_2 (10–30% for 24 h at room temperature) to remove organic matter and HCl (5%

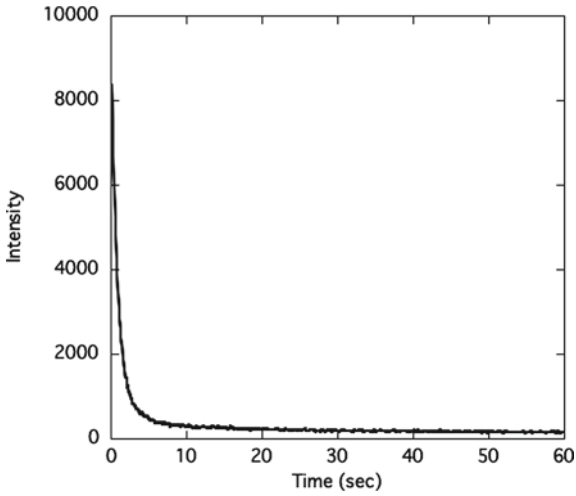

Fig. 10.13 Example of optical luminescence dating (OSL) signal

for 24 h at room temperature) to remove carbonate minerals. Magnetic minerals if any should be removed by magnetic separation, and heavy minerals are removed by heavy liquid separation with a specific density of over 2.8 g cm^{-3} (quartz and feldspar in lighter fraction). The treated subsamples consisted mainly of quartz and feldspar. To concentrate the quartz, subsample was further treated with H_2SiF_6 to dissolve feldspar (4 d at room temperature). When both quartz and feldspar were necessary, they were separated by heavy liquid separation. The resultant sediments were suspended in acetone, and liquid with suspended fine particles with a size less than ~11 μm was dropped on the small metal disk, which can be set in the luminescence reader. When the particle size is larger, the subsample is further treated with HF to remove the outer shell of the particles because of alpha damage accumulation, which is heterogeneously distributed only in the outer shell. An appropriate grain size that depends on the original grain size of the sediment should be chosen and measured using a luminescence reader. An example of OSL signal is shown in Fig. 10.13. Example of age dating applied to lacustrine sediment core is shown in Fig. 10.14.

10.4.4 Radiocarbon Dating

Radiocarbon dating, also known as ^{14}C dating, is often used to study lake sediments. Cosmogenic radiation converts the nitrogen isotope ^{14}N in the atmosphere to ^{14}C by, and ^{14}C decays back to ^{14}N, resulting in fairly constant ^{14}C isotopic ratios in the atmosphere and hydrosphere. Atmospheric or hydrospheric carbon is incorporated into, for example, plants or shells, by breathing, and they maintain a constant carbon isotopic ratio while actively exchanging their carbon with the atmosphere or hydrosphere. However, when biological activity stops, the amount of ^{14}C decreases

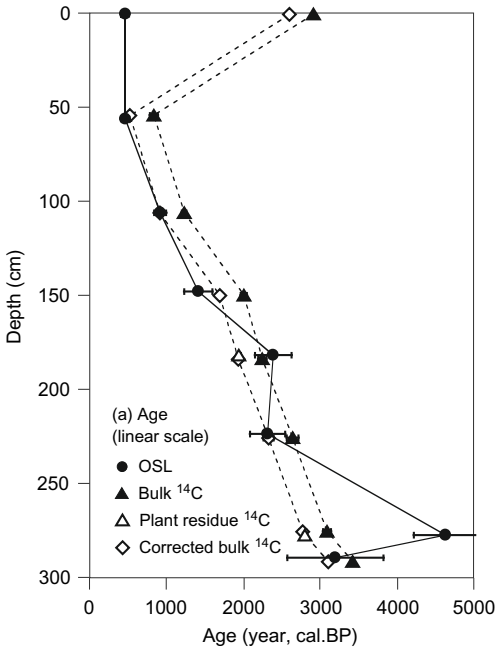

Fig. 10.14 Example of optical luminescence dating (OSL) and ^{14}C ages measured in a lacustrine sediment core from Lake Yogo, Japan (from Ito et al. 2015)

according to the time elapsed since the cessation of biological activity, and is used to date the age of the lacustrine sediment that preserves plants or shells, assuming that the biological activity of these organisms stopped there at the time of sedimentation (Watanabe et al. 2010). Bulk sediment, which is rich in organic carbon, can be analyzed when plant or shell fossils are rarely found in sediments (Xu and Zheng 2003).

Because human activities affect the atmospheric carbon isotope ratio (e.g., burning of fossil fuels, nuclear weapons testing), this method is applicable to samples deposited before 1950 CE, and the calculated age is expressed as the time back from 1950 CE, which is indicated in the unit of data (for example, ka BP, where BP stands for "before present"). The atmospheric carbon isotope ratio is subject to cosmic ray fluctuations and the amount of initial ^{14}C in a sample also fluctuates (Kitagawa and van der Plicht 1998). Therefore, radiocarbon dating can be applied to determine the age of known samples (e.g., by dendrochronology or varve counting in lake sediment) to establish a correlation curve between the apparent ^{14}C age and calendar age (Reimer et al. 2013, 2020). The data is expressed as cal BP, which indicates that correlation is considered in the data presentation.

When suitable fragments of plants or shells are found during core processing, it is preferable to prevent exposure to air to avoid contamination. The ^{14}C concentration can be measured by either beta scintillation counting or mass spectroscopy (Aravena et al. 1989, Omoto and Nakamura 2016). Many private institutions provide commercial analytical services. Figure 10.14 shows an example of OSL and ^{14}C age

determination applied to a lacustrine sediment core. Bulk ^{14}C ages commonly show a slight offset from the plant ^{14}C.

10.5 Interpretation of Analytical Data

To interpret the analytical data of lacustrine sediments and reconstruct the environmental changes based on them, it is important to clarify the relationship between analytical data of lacustrine sediments (proxy data) and observational data with instruments. For the reconstruction of the past hydrological environment, precipitation data and document records of historical disasters are comparable to the grain size and sedimentation rate measured in the sediment core. In the case of Lake Yogo (Fig. 10.7 in Sect. 10.3.1), the fluctuating grain size in the sediment core was compared with the precipitation data observed near the sampling site to clarify the relationship between grain size and annual precipitation.

The anthropogenic impacts on land use and vegetation in the catchment area were also printed in the sediment records. Land use maps, vegetation maps, and aerial photographs are useful for interpreting the fluctuations recorded in the sediment. In the case of reservoir sediments in the Noto Peninsula (Bishiaguro-ike, Fig. 10.11 in Sect. 10.4.1), the changes in sedimentation rate observed using ^{210}Pb were estimated to result from the artificial vegetation change in the catchment. This vegetation change was identified based on aerial photographs captured over different years (Fig. 10.15). The photographs indicate that the broadleaf forest covering the catchment area in 1975 was clear-cut in 1982. The influence of this clear-cut of broadleaf forest during 1975–1982 was considered as the sedimentation rate of the reservoir. Based on the vertical profile of $^{210}Pb_{ex}$ in the sediment core (Fig. 10.11a), the sedimentation rate was estimated to be 0.056–0.057 g cm^{-2} y^{-1} before 1975. In 1975, the sedimentation rate increased to 0.19 g cm^{-2} y^{-1} and remained high until 1990. This was interpreted as an increase in the erosion rate by clear-cutting the forest and exposing bare soil, and this situation continued for a further 15 years.

In this context, the characteristic of lake-catchment systems in which there is a relatively short distance between sources and sinks of the sediment is an advantage for combining observational and proxy data. Therefore, lacustrine sediment-based reconstruction of past environmental changes is also advantageous.

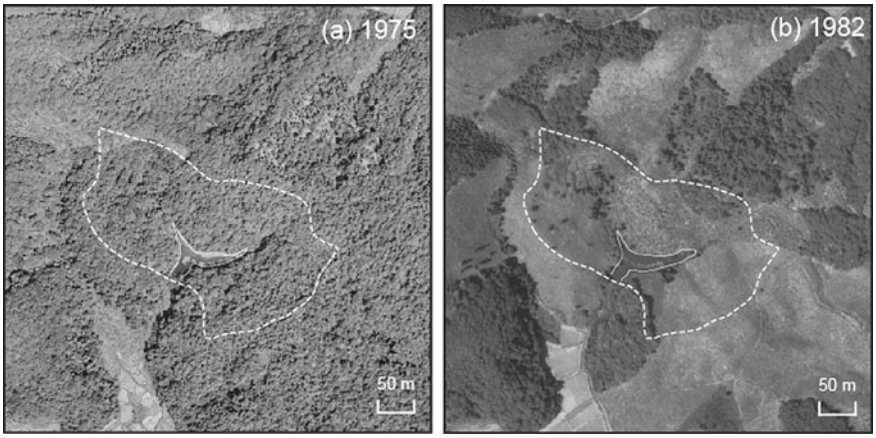

Fig. 10.15 Aerial photographs in Bishaguso-ike Reservoir in Noto Peninsula, Japan taken in **a** 1975 and **b** 1982 (Geospatial Information Authority of Japan). Dashed line indicates the watershed of the reservoir

Acknowledgements We are deeply appreciative of Ms. H. Chaki, Mr. K. Sakaguchi, Mr. T. Fujita, Mr. S. Otori, and our colleagues at the Low Level Radioactivity Laboratory at Kanazawa University for their support in editing figures and photographs.

References

Adamiec G, Aitoken MJ (1998) Dose-rate conversion factors: update. Ancient TL 16:37–50

Aitoken MJ (1998) An introduction to optical dating - The dating of Quaternary sediments by the use of photon-stimulated luminescence. Oxford University Press, p 267

Aoyama M (2018) Long-range transport of radiocaesium derived from global fallout and the Fukushima accident in the Pacific Ocean since 1953 through 2017—Part I: Source term and surface transport. J Radioanal Nucl Chem 318:1519–1542

Appleby PG, Oldfield F (1983) The assessment of ^{210}Pb data from sites with varying sediment accumulation rates. Hydrobiologia 103:29–35

Aravena R, Drimmie RR, Qureshi RM, McNeely R, Fabris S (1989) New possibilities for ^{14}C measurements by liquid scintillation counting. Radiocarbon 31:387–392

Fukuyama T, Onda Y, Takenaka C, Walling DE (2008) Investigating erosion rates within a Japanese cypress plantation using Cs-137 and Pb-210$_{ex}$ measurements. J Geophys Res 113:F02007

Ito K, Hasebe N, Sumita R, Arai S, Yamamoto M, Kashiwaya K, Ganzawa Y (2009) LA-ICP-MS analysis of pressed powder pellets to luminescence geochronology. Chem Geol 262:131–137

Ito K, Tamura T, Hasebe N, Nakamura T, Arai S, Ogata M, Itono T, Kashiwaya K (2015) Comparison of luminescence dating methods on lake sediments from a small catchment: example from Lake Yogo, Japan. In: Kashiwaya K, Shen J, Kim J (eds) Earth surface processes and environmental changes in East Asia. Springer, Japan, Tokyo, pp 221–238

Kashiwaya K (2017) Geomorphology of lake-catchment systems: A new perspective from limnogeomorphology. Springer, Singapore

Kitagawa H, van der Plicht J (1998) Atmospheric radiocarbon calibration to 45000 yr B.P.:late glacial fluctuations and cosmogenic isotope production. Science 279:1187–1190

Krishnaswamy S, Lal D, Martin JM, Meybeck M (1971) Geochronology of lake sediments. Earth Planet Sci Lett 11:407–414

Lamoureux S (2000) Five centuries of interannual sediment yield and rainfall-induced erosion in the Canadian high arctic recorded in lacustrine varves. Water Resour Res 36:309–318

Ochiai S, Nagao S, Yonebayashi K, Fukuyama T, Suzuki T, Yamamoto M, Kashiwaya K, Nakamura K (2015) Effects of deforestation on the transport of particulate organic matter inferred from the geochemical properties of reservoir sediments in the Noto Peninsula, Japan. Geochem J 49:513–522

Ochiai S, Lin JC, Jen CH, Nagao S, Kashiwaya K (2018) Changes of sedimentation environment inferred from fallout radionuclides and physical properties of sediment in Sun Moon Lake, Taiwan. J Radioanal Nucl Chem 316:1181–1187

Omoto K, Nakamura T (2016) Interpretation of disagreement of ^{14}C age between AMS and β-ray counting method—A case study in relation to ^{14}C ages of travertine terrace and Beachrock samples collected from Southeast coast of Miyako Island, SW Japan. Q J Geogr 68:183–191

Page MJ, Trustrum NA, DeRose RC (1994) A high resolution record of storm-induced erosion from lake sediments, New Zealand. J Paleolimnol 11:333–348

Reimer PJ, Bard E, Bayliss A, Beck JW, Blackwell PG, Ramsey CB, Buck CE, Cheng H, Edwards RL, Friedrich M, Grootes PM, Guilderson TP, Haflidason H, Hajdas I, Hatté C, Heaton TJ, Hoffmann DL, Hogg AG, Hughen KA, Kaiser KF, Kromer B, Manning SW, Niu M, Reimer RW, Richards DA, Scott EM, Southon JR, Staff RA, Turney CSM, Jvd P (2013) IntCal13 and Marine13 radiocarbon age calibration curves 0–50,000 years Cal BP. Radiocarbon 55:1869–1887

Reimer P, Austin W, Bard E, Bayliss A, Blackwell P, Bronk Ramsey C, Butzin M, Cheng H, Edwards RL, Friedrich M, Grootes PM, Guilderson TP, Hajdas I, Heaton TJ, Hogg AG, Hughen KA, Kromer B, Manning SW, Muscheler R, Palmer JG, Pearson CP, van der Plicht J, Reimer RW, Richards DA, Scott EM, Southon JR, Turney CSM, Wacker L, Adolphi F, Büntgen U, Capano M, Fahrni SM, Fogtmann-Schulz A, Friedrich R, Köhler P, Kudsk S, Miyake F, Olsen J, Reinig F, Sakamoto M, Sookdeo A, Talamo S (2020) The IntCal20 Northern hemisphere radiocarbon age calibration curve (0–55 cal kBP). Radiocarbon 62:725–757

Ritchie JC, McHenry JR (1990) Application of radioactive fallout cesium-137 for measuring soil-erosion and sediment accumulation rates and patterns—a review. J Environ Qual 19:215–233

Ritchie JC, Nearing MA, Nichols MH, Ritchie CA (2005) Patterns of soil erosion and redeposition on lucky hills Watershed, Walnut Gulch Experimental Watershed, Arizona. CATENA 61:122–130

Sanchez-Cabeza JA, Ruiz-Fernández AC (2012) ^{210}Pb sediment radiochronology: An integrated formulation and classification of dating models. Geochim Cosmochim Acta 82:183–200

Shimada T, Kashiwaya K, Masuzawa T, Hyodo M (2002) Hydro-environmental fluctuation in a lake - catchment system during the late Holocene inferred from Lake Yogo sediments. Trans Japan Geomorph Union 23:415–431 (in Japanese with English abstract and captions)

Wallbrink PJ, Murray AS (1996) Distribution and variability of ^{7}Be in soils under different surface cover conditions and its potential for describing soil redistribution processes. Water Resour Res 32:467–476

Walling DE, Quine TA (1992) The use of caesium-137 measurements in soil erosion surveys, Erosion and Sediment Transport Monitoring Programmes in River Basins, IAHS Publ. 210

Wang K, Cornett RJ (1993) Distribution coefficients of ^{210}Pb and ^{210}Po in laboratory and natural aquatic systems. J Paleolimnol 9:179–188

Watanabe T, Matsunaka T, Nakamura T, Nishimura M, Izutsu Y, Minami M, Nara F, Kakegawa T, Junbo W, Liping Z (2010) Last glacial-Holocene geochronology of sediment cores from a high altitude Tibetan lake based on AMS ^{14}C dating of plant fossils; implications for paleoenvironmental reconstructions. Chem Geol 277:21–29

Xu S, Zheng G (2003) Variations in radiocarbon ages of various organic fractions in core sediments from Erhai Lake, SW China. Geochem J 37:135–144

Chapter 11
Assessing Stream Water Quality Using Macroinvertebrates

Nisikawa Usio

11.1 Introduction

Stream systems are characterized by spatial hierarchies, from the largest spatial scale of watershed or basin to successively smaller scales of stream segment, reach, pool-riffle habitat, and microhabitat (Frissell et al. 1986). Local species assemblages are strongly influenced by habitat quality and complexity, which in turn are influenced by environmental factors or changes that operate at various spatiotemporal scales (Hauer and Resh 2017). For example, increases in water temperature associated with climate change, changes to flow regime and habitat complexity following deforestation in the riparian zone, and organic pollution from wastewater influence stream macroinvertebrate and fish assemblage compositions. Determinations of the environmental conditions of stream systems require extensive surveys of physicochemical factors across various spatiotemporal scales.

Biomonitoring offers another approach. The composition and diversity of stream biota are closely associated with stream physicochemical parameters such as water temperature, flow velocity, dissolved oxygen concentrations, organic pollution, and habitat complexity (Johnson et al. 2006; Li et al. 2010; Hauer and Resh 2017). Periphyton, macroinvertebrates, and fish are commonly used indicators in the biomonitoring of lotic systems (Li et al. 2010). Among the three taxa, periphyton and fish are good indicators of habitat or hydro-morphological changes, while macroinvertebrates are good indicators of organic pollution (Klemm 1990; Johnson et al. 2006). In contrast to measurements of physicochemical parameters, which directly reflect current environmental conditions, determinations of bioindicator composition can provide a longer-term picture of stream ecosystem status, because stream macroinvertebrates spend either part or all of their life cycles in streams.

N. Usio (✉)
Institute of Nature and Environmental Technology, Kanazawa University, Kanazawa, Japan
e-mail: usio@se.kanazawa-u.ac.jp

N. Hasebe et al. (eds.), *Field Work and Laboratory Experiments in Integrated Environmental Sciences*, https://doi.org/10.1007/978-981-99-6532-8_11

In this chapter, three representative water quality assessment methods are introduced that were developed to assess the water quality of Japanese streams or rivers using stream macroinvertebrates. The field and analytical procedures for each method are then described.

11.2 Macroinvertebrates

Macroinvertebrates are animals inhabiting the inorganic and organic substrata in aquatic systems. They include both free-living and parasitic taxa. In streams, Annelida (oligochaetes, leeches), Arthropoda (insects, arachnids, crustaceans), Bryozoa (moss animals), Hydrozoa (hydras), Mollusca (snails, bivalves), Nematomorpha (horsehair worms), Nemertea (ribbon worms), Platyhelminthes (planarians, cestodes, trematodes), and Porifera (sponges) are typical macroinvertebrate phyla. Taxonomic studies are advanced for some insect taxa, but not for many non-insect taxa. Technically, the term "macroinvertebrate" refers to invertebrate fauna retained on a 500 μm sieve, while those that pass through a 500 μm sieve but are retained on a 40 μm sieve are called "meiofauna" (Traunspurger and Majdi 2017). Meiofauna can be classified as permanent or temporary. Permanent meiofauna are fully benthic species that remain in the meiofaunal size range during their entire life span (e.g., harpacticoides, nematodes, rotifers), while temporary meiofauna are species that start off as meiofauna but develop into macrofauna or emerge from the benthos during their life span (e.g., early instars of aquatic insects, oligochaetes, water mites) (Traunspurger and Majdi 2017). The early life stages of many macroinvertebrates pass through a 500 μm sieve. Therefore, regardless of the conventional definition, benthic-dwelling invertebrates are collectively called "macroinvertebrates" (Hauer and Resh 2017).

11.3 Stream Habitats

Stream habitats can be coarsely classified into riffles and pools, followed by several smaller habitat units in hierarchical order (Hawkins et al. 1993). A riffle-pool sequence is determined on a relative basis. In first-level classification, riffles are characterized by shallow water, coarse substrates, high flow velocity, and a steep to gentle bed slope, whereas pools are characterized by their deeper water, finer substrates, lower flow velocity, and concave stream bed (Fig. 11.1) (Inoue and Nagayama 2019). In second-order classification, riffles can be further classified into cascades, riffles, and runs. A cascade is formed in a high-gradient stream (bed slope ≥ca. 2%), and is characterized by a stair-like stream bed often associated with abundant boulders (Appendix Fig. 11.4). Within a cascade reach, a small fall and pool-like habitats are formed. Thus, the stream bed of a cascade is steep over the segment or reach scale but can be convex within a habitat-patch scale. In a cascade, the water surface

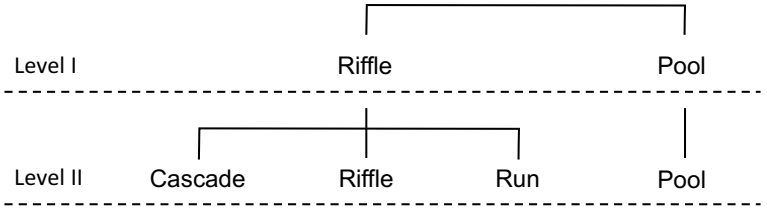

Fig. 11.1 Hierarchical classification of stream channels (based on Inoue and Nagayama 2019)

is usually rough with white bubbles, due to turbulence from fast-flowing water and small waterfalls. In low-gradient streams (bed slope < ca. 2%), riffles and runs can be identified as riffle habitats (Fig. 11.2). A riffle is a rapid-flowing reach with white bubbles on the water surface and a sloping stream bed, while a run shows a smooth flowing surface (intermediate flow velocity between riffles and pools) with uniform flow and a nearly horizontal stream bed. A riffle or run is the standard sampling unit in stream biomonitoring. However, a pool can also be surveyed if the focus of the field course involves a comparison of macroinvertebrate assemblages between different habitats (see 11.5.1).

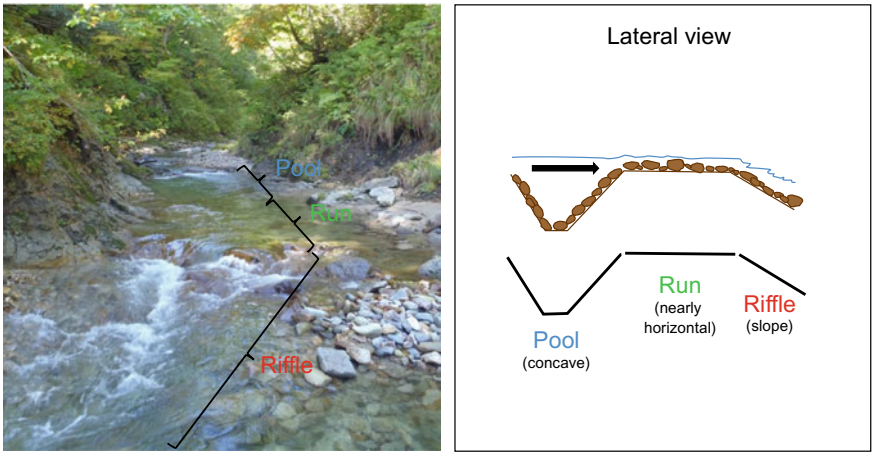

Fig. 11.2 Overhead photograph (left) and lateral (right) diagram of pool, run, and riffle habitats in a low-gradient stream. The black arrow on the lateral diagram indicates the direction of stream flow. Lateral diagram redrawn after modification from Inoue and Nagayama (2019)

11.4 Biomonitoring Methods for Stream Water Quality

To date, numerous macroinvertebrate-related metrics have been used for the bioassessment of stream systems (see review by Serrano Balderas et al. 2016). Below, I introduce measures of richness, diversity indices, and biotic indices that are particularly pertinent to the biomonitoring of stream water quality.

11.4.1 Measures of Richness

A commonly used richness measure is the number of taxa (taxonomic richness). This is simply a sum of the total number of macroinvertebrate taxa. In most cases, the taxonomic resolution is the genus or species level for major insect groups, such as Ephemeroptera, Trichoptera, and Plecoptera (EPT; Appendix Fig. 11.5), and family or higher taxonomic level for other taxa. With increasing organic matter contents or organic pollution, taxonomic richness is expected to decrease.

The main advantage of these richness measures is that they are simple and easy to understand. The main disadvantage is that the accuracy of the richness values may be low if the surveyor lacks expertise or experience in identification. Taxonomic richness may also change depending on the season due to different activity patterns of macroinvertebrates or the emergence of aquatic insects. For taxonomic richness, we cannot rule out the possibility that high species richness is driven by a high diversity of pollution-tolerant taxa, as information on the sensitivity of macroinvertebrates to water quality is not considered. In the bioassessment of stream systems, the number of EPT taxa (EPT richness) has also commonly been used, because EPT taxa are sensitive to low concentrations of dissolved oxygen and substrate changes (Barbour et al. 1999; Lydy et al. 2000; Baptista et al. 2011). Using Japan's nationwide stream census database, stronger correlations were obtained between EPT richness and various organic pollution parameters (i.e., biological oxygen demand [BOD], chemical oxygen demand [COD], dissolved oxygen, total nitrogen, ammonium nitrogen, and total phosphorus) relative to those between overall macroinvertebrate richness and organic pollution parameters (MLIT 2019). In general, polluted streams are associated with low EPT richness.

Additional insights into macroinvertebrate community compositions at different sites with differential water quality may be obtained using multivariate approaches, such as nonmetric multidimensional scaling (NMDS). Interested readers may refer to Clarke (1993) for NMDS and associated statistical tests.

11.4.2 Diversity Indices

To date, numerous diversity indices have been proposed in ecological studies (Washington 1984). These diversity indices are calculated based on the relative abundances of each taxonomic group. Shannon's diversity index (H') and Simpson's diversity index (D) are two of the most commonly used diversity indices:

$$H' = -\sum_i p_i \times 1n(p_i)$$

$$D = \sum_i p_i^2$$

where *pi* is the proportion of species *i* in the community.

Both indices consider species richness and evenness, and range between 0 and 1. For Shannon's diversity index, higher H' values indicate greater diversity, whereas for Simpson's diversity index, lower D values show greater diversity. To ensure that the value of Simpson's index increases with increasing diversity, the transformed forms of 1–D or 1/D are commonly used. In terms of richness, water with very little organic matter is generally associated with greater values of H' and 1–D (or 1/D).

The main advantage of using diversity indices is that they allow for the comparison of diversity across different sites using the same range of values. The main disadvantage is that, as for taxonomic richness, polluted streams could be represented by higher diversities of pollution-tolerant taxa.

11.4.3 Biotic Indices

In Japan, a conventional method developed by the Ministry of the Environment (MOE) and Ministry of Land, Infrastructure, Transport and Tourism (MLIT) (MOE and MLIT 2012), referred to in this chapter as the simplified method, has long been used to assess stream water quality. In the simplified method, stream water quality is a priori classified into four categories: (I) very little organic matter, (II) little organic matter, (III) moderate organic matter, and (IV) abundant organic matter. Note that in MOE and MLIT (2012), the more sensitive expressions (I) very clean, (II) slightly dirty, (III) dirty, and (IV) very dirty are used for each water quality category. However, these expressions were developed for pollution biology studies (Tsuda 1964), which are largely concerned with the changes in stream environments and macroinvertebrates in response to increasing inputs of organic pollutants from human activities. However, organic matter originates not only from human activities but also from natural processes, including organisms and environments (e.g., riparian organic matter input, carcasses, excretion, etc.). Therefore, the more sensitive expressions do not always apply where inputs of anthropogenically derived organic matter are

small and in-stream organic matter is abundant. Thus, in this chapter, water quality is categorized based on organic matter abundance (very little to abundant).

For each water quality category, 5–10 macroinvertebrate indicators are designated (see Table 11.2). On a tally sheet, investigators record the occurrence of all macroinvertebrate indicators. The most abundant two taxa (or three at maximum) are each given a score of 2 and all other indicators are given a score of 1. The water quality is determined based on the sum of indicator scores within each water quality category. When two or more categories receive an identical score, the better category is chosen. For example, when water quality categories III and IV each receive a total score of 4, the water quality would be considered Category III.

The main advantage of this method is that it is very easy to implement even for school children under the supervision of a parent or teacher. However, several disadvantages of this method have been pointed out (Tanida 2010). First, it uses too few macroinvertebrate indicators for each water level category and therefore does not provide sound assessment of stream water quality. Second, the required level of taxonomic identification is not identical across indicator taxa: some indicators require species-level identification while others only require identification to higher taxonomic levels (genus, family, order, and so forth). Third, the macroinvertebrate indicators for Categories III and IV contain lentic (e.g., *Ranatra chinensis* [Nepidae]) and brackish species (e.g., *Grandidierella japonica* [Aoridae]), which are not typical inhabitants of running water. These lentic and brackish taxa are presumably included to match the number of indicators used for Categories I and II.

In the United Kingdom, rapid bioassessment methods have been developed using selected macroinvertebrate taxa to calculate the Biological Monitoring Working Party (BMWP) metric and the associated Average Score Per Taxon (ASPT) (Armitage et al. 1983). In a range from 1 to 10, pollution-sensitive taxa are given high scores, while pollution-tolerant taxa are given low scores. To calculate BMWP, the scores of all indicator families are summed. The ASPT is calculated by dividing BMWP (total scores; TS) by the number of indicator families without considering the abundance of each taxon. The BMWP and ASPT methods have been successfully applied in various countries of the world (e.g., Gerhardt et al. 2004; Zeybek et al. 2014; Serrano Balderas et al. 2016; Kaboré et al. 2022). With reference to the UK's ASPT method, the water quality-sensitivity scores for prevalent macroinvertebrate indicators in Japanese streams were determined based on nationwide macroinvertebrate monitoring data (Yamazaki et al. 1996). The scores of some indicators were later modified slightly (Nozaki 2012) and a manual was published (MOE 2017a). The main advantage of the ASPT method is that taxonomic identification can be made at the family level without considering abundance information, yet obtained scores show a sound indication of water quality (Tanida 2010). Identification at the genus or species level is always time consuming and requires expertise in taxonomic identification. For this reason, the values of richness or diversity measures may change depending on the researcher's expertise or experience. By contrast, family-level identification can be made in a shorter time with less effort. The majority of family-level taxonomic identification may also be done in the field using reference books (Tanida and Takemon 1991; Maruyama and Takai 2016; MOE 2017b). Therefore, the ASPT

method is suitable as a rapid assessment method that retains accuracy and can be used at various levels of expertise. The main drawback is that it is nevertheless difficult to implement without an experienced instructor. Further, some macroinvertebrate families or functional groups (conventional groups) may comprise taxa that differ in their sensitivity to water quality. For example, in the Japanese ASPT method, Chironomidae are classified into two groups: those with (Chironomini) and without (others) ventral blood gills. Non-Chironomini may include various taxa with different sensitivities to water pollution.

11.5 Field Methods

In temperate and cool temperate streams, water temperature and flow regime change dramatically according to the season (spring, summer, autumn, and winter). Generally, many aquatic insects emerge between spring and early summer, with different species differing in their emergence periods or patterns. Therefore, the timing of sampling can influence the outcome of biomonitoring, especially in terms of aquatic insect diversity (e.g., EPT richness; see 11.5.2).

11.5.1 Field Sampling, Sorting, and Identification

1. Choose a riffle or run in a stream (Fig. 11.2). If the objective of the field exercise includes comparisons of macroinvertebrate assemblages between different habitats, designate a reach encompassing several different habitats (e.g., riffles, runs, pools). For a rough estimation, the length of a reach may encompass 10 times the width of the stream.
2. Two people form a team. In the stream, one person holds a D-framed net perpendicular to the stream bed while the other person kicks or rubs the substrate (hereafter, kick sampling) immediately upstream of the D-framed net for 1 min. For a D-framed net, mesh sizes of 250 μm–1 mm are typically used. To minimize net clogging by organic and inorganic matter but nevertheless efficiently collect major macroinvertebrate indicators, the use of a 1-mm mesh net is recommended in short summer field courses. Pour the contents of the D-net (a mixture of macroinvertebrates, organic materials, and inorganic materials) into a large bucket (e.g., 20 L). Change the sampling locale and perform 1-min kick sampling a total of three times. The contents of the D-net from the three sampling events may be combined to form a single sample.
3. On the stream bank, transfer the contents of the bucket into a white plastic pan. Using a small bucket (e.g., 5 L), add enough clean stream water to cover macroinvertebrates and other organic and inorganic materials. If the samples contain water, a sieve or D-framed net may be used to drain water. Using a spoon, a

portion at a time of the sample (a mixture of organic materials and macroinvertebrates) may be transferred onto the pan. The sample should be spread thinly over the entire pan so as not to completely conceal the surface of the white pan. If the sample contains too much organic materials and forms a thick layer, return a portion of the sample to the large bucket.

4. Using spring steel tweezers, collect all macroinvertebrates from the pan and transfer them into a divided plastic case or plastic cups filled with stream water, separating the organisms into easily recognized groups. Macroinvertebrates may be readily classified into phyla or order by eye using MOE (2017b).
5. Identify each taxon to the lowest taxonomic unit required using reference books. If necessary, a magnifying glass or field binocular microscope can be used for identification. A macroinvertebrate may also be placed in a small zippered plastic bag filled with stream water to observe its morphology from the ventral side. For mobile taxa, observe their swimming behavior in the container. If there are unidentifiable specimens, these can be separated by taxon into glass vials with 70% ethanol, and taken back to the laboratory for identification.
6. Alternatively, if circumstances allow, place all live specimens in wide-mouth jars or zippered plastic backs and store them on ice in a cooler until they are transported back to the laboratory for identification using a standard binocular microscope (with zoom lens). This protocol is only possible when the field site is close to the laboratory. In this case, it is advisable not to fix the samples in preservative (e.g., ethanol) so as not to change the body color of the specimens.
7. Live specimens should be returned to their original habitat after identification and enumeration.
8. Collect relevant physical data, such as water temperature, salinity, water depth, substrate characteristics, and current velocity, as these variables may also influence macroinvertebrate composition (Appendix Table 11.3). Water temperature can be measured using a thermometer. Salinity can be measured using a salinometer, which may be pertinent when survey sites include a downstream brackish area. Water depth can be measured using a folding ruler. Substrate characteristics can be visually determined based on dominant substrates (sand [diameter < 2 mm], pebble-cobble [diameter 2–256 mm], boulder [diameter > 256 mm], and bedrock [fixed rock formation]). Current velocity can be measured using a ping pong ball attached to a string (1–3 m in length) taped or glued. At the survey site, after the ping pong ball is released, record the time taken for the string to stretch the full length using a stopwatch. Current velocity can be calculated by dividing string length by the time needed for the string to stretch, as follows:

$$\text{Current velocity (m/s)} = \text{string length (m)} / \text{time needed for the string to stretch(s)}.$$

9. If applicable, note anthropogenic factors that may influence macroinvertebrate composition (e.g., agricultural or industrial effluent).

11.5.2 Data Analyses

For the purposes of a short summer field course, the Japanese ASPT method and simplified method are practical. In a comparative study involving different streams or sites, EPT richness can also be used. Below are analytical procedures for the respective methods.

11.5.2.1 Japanese ASPT Method

1. On a tally sheet, record the number of individuals for each indicator taxon, or simply check mark (✓) all indicator taxa that were identified in the field sampling (Table 11.1 and Appendix Table 11.4).
2. Calculate the total score based on Table 11.1. Average score per taxon (ASPT) can be determined using the formula ASPT = TS /NF, where TS is the sum of all scores of indicator families and NF is the total number of indicator families.
3. Because the scores of indicator families range from 1 to 10, ASPT values range from 1 to 10. Generally, higher ASPT values indicate less organic matter in the stream water. Nevertheless, ASPT values are generally less than 8 even when a stream contains little organic matter or is unpolluted, because the scores of prevalent families such as Baetidae, Hydropsychidae, and Chironomidae are relatively low (Tanida 2010).

11.5.2.2 Simplified Method

1. On a tally sheet, record the number of individuals for each indicator taxon or simply check mark (✓) all indicator taxa that were identified in the field sampling (Table 11.2 and Appendix Table 11.5).
2. Determine the most abundant two taxa (or three at maximum). These abundant indicators will be given a score of 2. All other indicator taxa will be given a score of 1.
3. Calculate the total scores of indicators separately for each water quality category (I–IV).
4. The water quality category of the surveyed site can be determined based on the highest number of scores among the four water quality categories.
5. If two or more categories receive an identical score, choose the smaller (better) category.

Table 11.1 Scores of macroinvertebrate families according to the Average Score Per Taxon (ASPT) method (adopted from Nozaki 2012 after a taxonomic update)

Taxon	Score	Taxon	Score
Ephemeroptera		Lepidoptera	
Siphlonuridae	8	Crambidae	7
Dipteromimidae	10	Coleoptera	
Ameletidae	8	Dytiscidae	5
Isonychiidae	8	Gyrinidae	8
Heptageniidae	9	Hydrophilidae	4
Baetidae	6	Psephenidae	8
Leptophlebiidae	9	Dryopidae	8
Ephemerellidae	8	Elmidae	8
Caenidae	7	Lampyridae	6
Potamanthidae	8	Diptera	
Ephemeridae	8	Tipulidae	8
Polymitarcyidae	8	Blephariceridae	10
Odonata		Psychodidae	1
Calopterygidae	6	Simuliidae	7
Epiophlebiidae	9	Chironomidae (with ventral blood gills; Chironomini)	2
Gomphidae	7	Chironomidae (without ventral blood gills; others)	6
Cordulegasteridae	3	Ceratopogonidae	7
Plecoptera		Tabanidae	6
Nemouridae	6	Athericidae	8
Perlodidae	9	Tricladida	
Perlidae	9	Dugesiidae	7
Chloroperidae	9	Gastropoda	
Hemiptera		Pleuroceridae	8
Aphelocheiridae	7	Lymnaeidae	3
Megaloptera		Physidae	1
Corydalidae	9	Planorbiidae	2
Trichoptera		Ancylidae	2
Stenopsychidae	9	Bivalvia	
Philopotamidae	9	Corbiculidae	3
Psychomyiidae	8	Oligochaeta	
Polycentropodidae	9	Oligochaeta (*Branchiura sowerbyi*)	1

(continued)

Table 11.1 (continued)

Taxon	Score	Taxon	Score
Hydropsychidae	7	Oligochaeta (others)	4
Rhyacophilidae	9	Hirudinea	2
Hydrobiosidae	9	Amphipoda	
Glossosomatidae	9	Gammaridae	8
Hydroptilidae	4	Anisogammaridae	8
Brachycentridae	10	Pontogeneiidae	8
Limnephilidae	8	Isopoda	
Apataniidae	9	Asellidae	2
Uenoidae	10	Decapoda	
Goeridae	7	Potamidae	8
Lepidostomatidae	9		
Sericostomatidae	9		
Leptoceridae	8		

11.5.2.3 EPT Richness Method

1. In the field, place the sample in a wide-mouth jar together with ethanol. The ideal concentration of ethanol preservative is 70%. Depending on the amount of organic matter content in samples, a higher ethanol concentration may be used to arrive at 70% after sample preservation and dilution. Transport the samples back to the laboratory.
2. In the laboratory, sort and identify the samples, preferably to the species or genus level, using binocular microscopes and identification keys.
3. Make a tally sheet based on the identified EPT taxa.
4. On the tally sheet, record the number of individuals for each EPT taxon or simply check mark all EPT taxa that were collected in the field sampling. Information on abundance is not considered in this method, but it would be informative to know which taxa are numerically dominant.
5. Calculate the total number of EPT taxa (EPT taxa richness).

11.5.3 Survey Equipment

Photographs of major field and laboratory equipment are shown in Fig. 11.3.

Field equipment

- Hip or chest waders
- Life jacket (recommended when waders are used)
- D-framed net (width 30 cm, mesh size 1 mm)

Table 11.2 List of indicator taxa for the simplified method (adopted from MOE and MLIT 2012)

Taxon	Order/class
Indicators for water with very little organic matter (Category I)	
Plecoptera (order)	Plecoptera
Epeorus (genus)	Ephemeroptera
Rhyacophilidae (family)	Trichoptera
Glossosomatidae (family)	Trichoptera
Blephariceridae (family)	Diptera
Amphipoda (order)	Amphipoda
Corydalidae (family)	Megaloptera
Simuliidae (family)	Diptera
Geothelphusa dehaani (species)	Decapoda
Dugesia japonica (species)	Tricladida
Indicators for water with little organic matter (Category II)	
Cheumatopsyche (genus)	Trichoptera
Sieboldius albardae (species)	Odonata
Macrostemum radiatum (species)	Trichoptera
Semisulcospira (genus)	Gastropoda
Psephenidae (family)	Coleoptera
Corbicula japonica[1] (species)	Bivalvia
Luciola cruciata (species)	Coleoptera
Clithon retropictus[1] (species)	Gastropoda
Indicators for water with moderate amounts of organic matter (Category III)	
Ranatra chinensis (species)	Hemiptera
Viviparidae (family)	Gastropoda
Asellus hilgendorfi hilgendorfi (species)	Isopoda
Erpobdella lineata (species)	Hirudinea
Gnorimosphaeroma rayi[1†] (species)	Isopoda
Grandidierella japonica[1] (species)	Amphipoda
Indicators for water with abundant organic matter (Category IV)	
Chironomidae (with ventral blood gills; Chironomini) (tribe)	Diptera
Branchiura sowerbyi (species)	Oligochaeta
Psychodidae (family)	Diptera
Physa acuta[2] (species)	Gastropoda
Procambarus clarkii[2] (species)	Decapoda

[1]Brackish species
[2]Nonnative species
[†] There are over 20 known species of *Gnorimosphaeroma* in Japan (Nunomura and Shimomura 2016). Because *G. rayi* generally inhabits the coastal marine zone, *Gnorimosphaeroma* (genus) is more appropriate as an indicator (N. Nunomura, pers. comm.)

Fig. 11.3 Photographs of survey equipment: **a** waders, **b** D-framed net, **c** buckets, **d** spring steel tweezers, **e** white plastic pan, **f** divided plastic case or plastic cups, **g** field binocular microscope or magnifying glass, **h** standard binocular microscope (for laboratory use), and **i** clip board and tally sheet or water-resistant field book

- Sieve
- Plastic buckets (5 L and 20 L)
- White plastic pan (for sorting)
- Divided plastic case or plastic cups (for sorting)
- Spring steel tweezers
- Spoon
- Plastic pipette
- Field binocular microscope or magnifying glass
- Small zippered plastic bags (for simple morphological observation)
- Clipboard and tally sheet (Appendix Tables 11.4 and 11.5) or water-resistant field book
- Pencil
- Eraser
- Reference books (mentioned in 11.6)
- Thermometer (for recording water temperature)
- Salinometer (for recording salinity) (optional)
- Folding ruler or ruler (for recording water depth)
- Ping pong ball (for recording current velocity)
- String (1–3 m) (for recording current velocity)
- Stopwatch (for recording current velocity)

- First aid kit
- Work gloves
- Long rubber gloves (for polluted sites) (optional)
- Hat.

Laboratory equipment (major items)

- Cooler (for transporting live specimens)
- Coolant or ice (for transporting live specimens)
- 100% ethanol (as a preservative)
- Wide-mouth jars or zippered plastic bags (for transporting live or fixed specimens)
- Glass vials (for transporting fixed specimens)
- Water-based pen (for labeling when ethanol is used)
- Binocular microscope (with zoom lens).

11.6 Reference Books

The photographs or illustrations found in Karita (2018) and MOE and MLIT (2012) can be used as reference books for a field course. Although these are written in Japanese, photographs or illustrations can be matched with scientific names. For Japanese readers, Maruyama and Takai (2016), Tanida and Takemon (1991), and MOE (2017b) can also be used for rapid identification in the field. Kawai and Tanida (2018) and Merritt et al. (2019) are suitable for detailed identification in the laboratory, and may be used for later confirmation. Merritt et al. (2019) provide identification keys for North American aquatic insects, but these keys are also useful for the genus- or family-level identification of many Japanese insects.

- Karita (2018)

Photographs can be used as a reference for the field identification of representative macroinvertebrates (in Japanese). Although the photographs are clear, the handbook should not be used for purposes of identification, as only representative taxa are listed.

- Kawai and Tanida (2018)

The most comprehensive and wide-ranging illustrated handbook of Japanese aquatic insects; mainly for lab use (in Japanese).

- Maruyama and Takai (2016)

Identification keys and photographs can be used as a reference for the field identification of representative macroinvertebrates (in Japanese).

- Merritt et al. (2019)

The most comprehensive and wide-ranging illustrated handbook of North American aquatic insects; mainly for lab use (in English).

- MOE (2017a)

Manual of the Japanese ASPT method (in Japanese).

- MOE (2017b)

Illustrations can be used as a reference for the Japanese ASPT method (in Japanese).

- MOE and MLIT (2012)

Illustrations can be used as a reference for the simplified method (in Japanese).

- Tanida and Takemon (1991)

Illustrations are helpful in the field identification of representative aquatic insects (in Japanese).

11.7 Database Method

When weather conditions are poor, field sampling cannot be performed. Under such circumstances, public databases can be used in lieu of field sampling. Macroinvertebrate data for selected first- and second-order rivers in Japan can be obtained from the "River Environmental Database." Hydrology and water data for selected rivers can be obtained from the "Water Information System."

Database

- River Environmental Database

  http://www.nilim.go.jp/lab/fbg/ksnkankyo/

The 1998–2019 nationwide census of fish, macroinvertebrates, zooplankton, phytoplankton, plants, birds, reptiles, amphibians, and terrestrial insects in first- and second-order rivers and reservoirs.

- Water Information System

  http://www1.river.go.jp/

Water and hydrology database (rainfall, water level, flow, and water quality) of 109 first-order Japanese rivers and 17 second-order rivers in Okinawa that are relevant to dam operations.

11.8 Questions

1. How was the water quality at the survey site(s) rated based on the ASPT and simplified methods?

2. Did you observe any differences in ASPT values or water quality categories (simplified method) along the longitudinal gradient (e.g., headwater vs. downstream) of a stream or between different streams?
3. Did you obtain high correlation between ASPT values and EPT richness?
4. How do the ASPT values or water quality categories (simplified method) change if you sample macroinvertebrates from pool (or other non-riffle habitats) instead of riffle habitats?
5. Did you observe any differences in macroinvertebrate compositions between different habitats (e.g., riffles vs. pools), between different stream reaches (e.g., headwater vs. downstream), or between different streams?
6. What environmental factors possibly affect the water quality at the study site(s)?
7. How can the ASPT and simplified methods be further improved to enhance accuracy and practicability?

11.9 Permissions and Natural Hazards

11.9.1 Permissions

- In Japan, natural streams and rivers are owned by MLIT, prefectural government, or city/village government depending on the classification of the streams/rivers. Although the majority of streams/rivers are public areas, the land adjacent to streams is often private. Permission is required from landowners to enter private land and roads.
- Some first-class streams and rivers are designated as protected areas for fisheries resources. In such streams/rivers, permission is required from the local prefectural government to collect any wildlife.
- For some fishing gear (e.g., kick nets, minnow traps), a special collecting permit from the local prefectural government is required. Even the use of D-framed nets may be subject to the acquisition of a collecting permit depending on the depth, width, or mesh size of the net. Check the website or make inquiries at the fisheries division of the local prefectural government for fishing gear regulations.
- Most macroinvertebrates are not legally protected in Japan. However, special collecting permission is required if there is the possibility of collecting (either deliberately or accidentally) some endangered species (i.e., critically endangered species [CR]) included in national or prefectural red lists. It is necessary to check the website of the Ministry of the Environment, Japan for up-to-date designated species under the Act on Conservation of Endangered Species of Wild Fauna and Flora (Act no. 75).

11.9.2 Natural Hazards

- Even during ordinary flow conditions, streams/rivers are always associated with a risk of being washed away or drowning. Use of a life jacket is recommended in a field study, especially when waders are used in swift or large streams/rivers.
- Japanese streams exhibit seasonality such that natural hazards differ depending on the season and geographical area. In central Japan, the rainy season is typically from mid-June to mid or late July, and typhoon season from mid or late August to late September. Along the Japan Sea side (including Hokuriku District) or in mountain streams, snowmelt occurs in the spring, when stream flow generally becomes high. During this period, special attention should be paid to potential high flow or flooding events.
- During or after heavy rain, streams/rivers can become very dangerous due to flooding. Always check the weather forecast before performing field sampling. Stay away from streams/rivers and ascend to high ground if a rapid increase in water level is observed.
- When surveying below a dam, be aware of dam flushing events. Such events often take place during or after heavy rain and are usually announced by the sounding of an alarm or warning messages delivered through speakers.
- When surveying in rural areas, be aware of wild animals and plants, including bears (e.g., Japanese black bear; *Ursus thibetanus japonicus*), snakes (e.g., Japanese pit viper; *Gloydius blomhoffii*, tiger keelback; *Rhabdophis tigrinus*), spiders (e.g., Japanese foliage spider; *Cheiracanthium japonicum*), wasps (Vespinae), ticks (Ixodidae), and poisonous plants (e.g., poison ivy; *Toxicodendron orientale*). As dangerous animals and plants may differ depending on the geographical area, advice from a local scientist about the necessary precautions and management methods should be sought. Japanese readers may refer to Musashino Shizen-jyuku (2017) for first aid to deal with problems due to dangerous wildlife in Japan.

Appendix

See Figs 11.4 and 11.5.

See Tables 11.3, 11.4 and 11.5.

Fig. 11.4 Photograph of a cascade in a high-gradient stream (Notto Stream, Hokkaido Prefecture, Japan)

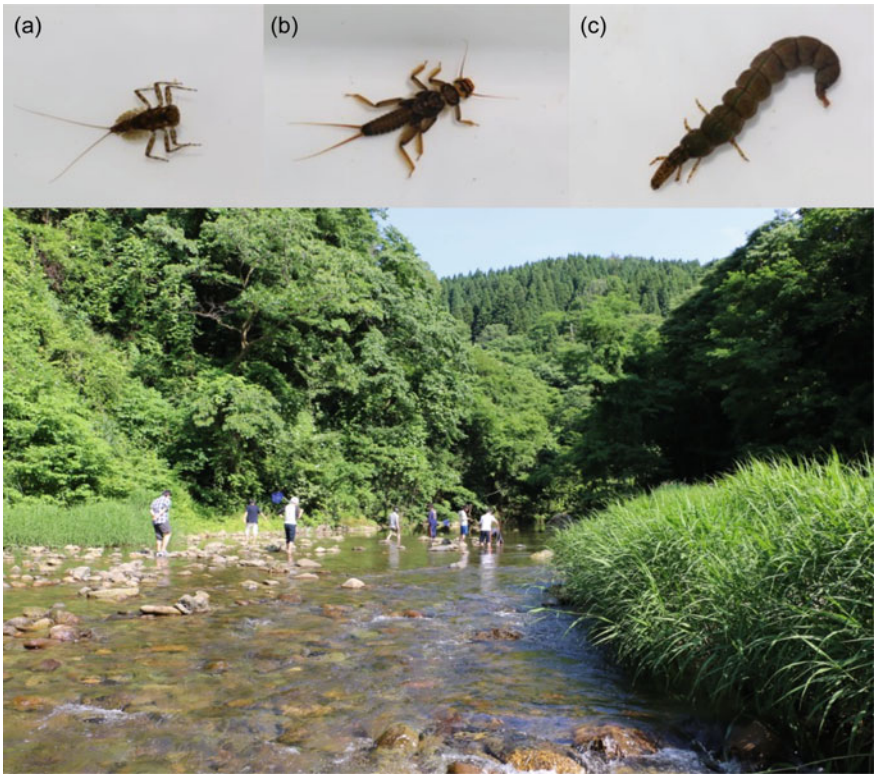

Fig. 11.5 Photograph of an upper-middle stream reach (Sai River, Ishikawa Prefecture, Japan) and representative macroinvertebrate taxa, i.e., Ephemeroptera (**a**), Plecoptera (**b**), and Trichoptera (**c**)

Table 11.3 Example of a field note

Site	
Date	
Time	
Habitat (riffle, run, pool)	
Water temperature (ºC)	
Water depth (cm)	
Substrate (sand, pebble-cobble, boulder, bedrock)	
Current velocity (m/s)	
Notes	

Table 11.4 Tally sheet for the Average Score Per Taxon (ASPT) method

Site	Date	
Taxon	Score	Numbers (or ✓)
Ephemeroptera		
Siphlonuridae	8	
Dipteromimidae	10	
Ameletidae	8	
Isonychiidae	8	
Heptageniidae	9	
Baetidae	6	
Leptophlebiidae	9	
Ephemerellidae	8	
Caenidae	7	

(continued)

Table 11.4 (continued)

Site	Date	
Taxon	Score	Numbers (or ✓)
Potamanthidae	8	
Ephemeridae	8	
Polymitarcyidae	8	
Odonata		
Calopterygidae	6	
Epiophlebiidae	9	
Gomphidae	7	
Cordulegasteridae	3	
Plecoptera		
Nemouridae	6	
Perlodidae	9	
Perlidae	9	
Chloroperidae	9	
Hemiptera		
Aphelocheiridae	7	
Megaloptera		
Corydalidae	9	
Trichoptera		
Stenopsychidae	9	
Philopotamidae	9	
Psychomyiidae	8	
Polycentropodidae	9	
Hydropsychidae	7	
Rhyacophilidae	9	
Hydrobiosidae	9	
Glossosomatidae	9	
Hydroptilidae	4	
Brachycentridae	10	
Limnephilidae	8	
Apataniidae	9	
Uenoidae	10	
Goeridae	7	
Lepidostomatidae	9	
Sericostomatidae	9	
Leptoceridae	8	
Lepidoptera		
Crambidae	7	

(continued)

Table 11.4 (continued)

Site	Date	
Taxon	Score	Numbers (or ✓)
Coleoptera		
Dytiscidae	5	
Gyrinidae	8	
Hydrophilidae	4	
Psephenidae	8	
Dryopidae	8	
Elmidae	8	
Lampyridae	6	
Diptera		
Tipulidae	8	
Blephariceridae	10	
Psychodidae	1	
Simuliidae	7	
Chironomidae (with ventral blood gills; Chironomini)	2	
Chironomidae (without ventral blood gills; others)	6	
Ceratopogonidae	7	
Tabanidae	6	
Athericidae	8	
Tricladida		
Dugesiidae	7	
Gastropoda		
Pleuroceridae	8	
Lymnaeidae	3	
Physidae	1	
Planorbiidae	2	
Ancylidae	2	
Bivalvia		
Corbiculidae	3	
Oligochaeta		
Oligochaeta (*Branchiura sowerbyi*)	1	
Oligochaeta (others)	4	
Hirudinea	2	
Amphipoda		
Gammaridae	8	
Anisogammaridae	8	
Pontogeneiidae	8	

(continued)

Table 11.4 (continued)

Site	Date	
Taxon	Score	Numbers (or ✓)
Isopoda		
Asellidae	2	
Decapoda		
Potamidae	8	
Total scores (TS)		
Number of families (NF)		
ASPT (TS/NF)		

Table 11.5 Tally sheet for the simplified method. Two (or three at maximum) numerically dominant taxa are given a score of 2. Other taxa are given a score of 1

Site		Date		
Water quality category	Taxon	Order/class	Numbers (or ✓)	Score
I	Plecoptera (order)	Plecoptera		
	Epeorus (genus)	Ephemeroptera		
	Rhyacophilidae (family)	Trichoptera		
	Glossosomatidae (family)	Trichoptera		
	Blephariceridae (family)	Diptera		
	Amphipoda (order)	Amphipoda		
	Corydalidae (family)	Megaloptera		
	Simuliidae (family)	Diptera		
	Geothelphusa dehaani (species)	Decapoda		
II	*Dugesia japonica* (species)	Tricladida		
	Cheumatopsyche (genus)	Trichoptera		
	Sieboldius albardae (species)	Odonata		
	Macrostemum radiatum (species)	Trichoptera		
	Semisulcospira (genus)	Gastropoda		
	Psephenidae (family)	Coleoptera		
	Corbicula japonica (species)	Bivalvia		
	Luciola cruciata (species)	Coleoptera		
	Clithon retropictus (species)	Gastropoda		

(continued)

Table 11.5 (continued)

Site		Date		
Water quality category	Taxon	Order/class	Numbers (or ✓)	Score
III	*Ranatra chinensis* (species)	Hemiptera		
	Viviparidae (family)	Gastropoda		
	Asellus hilgendorfi (species)	Isopoda		
	Erpobdella lineata (species)	Hirudinea		
	Gnorimosphaeroma rayi (species)	Isopoda		
	Grandidierella japonica (species)	Amphipoda		
IV	Chironomidae (with ventral blood gills; Chironomini) (tribe)	Diptera		
	Branchiura sowerbyi (species)	Oligochaeta		
	Psychodidae (family)	Diptera		
	Physa acuta (species)	Gastropoda		
	Procambarus clarkii (species)	Decapoda		
Total scores of Category I				
Total scores of Category II				
Total scores of Category III				
Total scores of Category IV				
Water quality category (I-IV)				

References

Armitage PD, Moss D, Wright JF, Furse MT (1983) The performance of a new biological water quality score system based on macroinvertebrates over a wide range of unpolluted running-water sites. Water Res 17:333–347. https://doi.org/10.1016/0043-1354(83)90188-4

Baptista DF, de Souza RSG, Vieira CA, Mugnai R, Souza AS, de Oliveira RBS (2011) Multimetric index for assessing ecological condition of running waters in the upper reaches of the Piabanha-Paquequer-Preto basin, Rio De Janeiro, Brazil. Zoologia 28:619–628. https://doi.org/10.1590/S1984-46702011000500010

Barbour MT, Faulkner C, Gerritsen J (1999) Rapid bioassessment protocols for use in streams and wadeable rivers: periphyton, benthic macroinvertebrates, and fish, Second ed. U.S. Environmental Protection Agency, Office of Water, Washington, DC. EPA 841–B–99–002

Clarke KR (1993) Non-parametric multivariate analyses of changes in community structure. Aust J Ecol 18:117–143. https://doi.org/10.1111/j.1442-9993.1993.tb00438.x

Frissell CA, Liss WJ, Warren CE, Hurley MD (1986) A hierarchical framework for stream habitat classification: Viewing streams in a watershed context. Environ Manage 10:199–214. https://doi.org/10.1007/BF01867358

Gerhardt A, Janssens De Bisthoven L, Soares AMVM (2004) Macroinvertebrate response to acid mine drainage: Community metrics and on-line behavioural toxicity bioassay. Environ Pollut 130:263–274. https://doi.org/10.1016/j.envpol.2003.11.016

Hauer FR, Resh VH (2017) Macroinvertebrates. In: Hauer FR, Lamberti GA (eds) Methods in Stream Ecology, 3rd edn. Academic Press, Burlington, MA, pp 297–319

Inoue M, Nagayama S (2019) Expressing stream habitats, In: Inoue M, Nakamura F (eds) Field and analytical methods in stream ecology. Kodansha, Tokyo, pp 95–121 (In Japanese)

Johnson RK, Hering D, Furse MT, Clarke RT (2006) Detection of ecological change using multiple organism groups: Metrics and uncertainty. Hydrobiologia 566:115–137. https://doi.org/10.1007/s10750-006-0101-8

Kaboré I, Ouéda A, Moog O, Meulenbroek P, Tampo L, Bancé V, Melcher AH (2022) A benthic invertebrates-based biotic index to assess the ecological status of West African Sahel Rivers. Burkina Faso. J Environ Manage 307:114503. https://doi.org/10.1016/j.jenvman.2022.114503

Karita T (2018) The handbook of aquatic life. Bun-ichi, Tokyo, Japan (In Japanese)

Kawai T, Tanida K (2018) Aquatic insects of Japan: manual with keys and illustrations, 2nd edn. Tokai University Press, Hiratsuka (In Japanese)

Klemm DJ (1990) Macroinvertebrate field and laboratory methods for evaluating the biological integrity of surface waters. U.S. Environmental Protection Agency, Cincinnati, OH. EPA.600/4–90/030

Li L, Zheng B, Liu L (2010) Biomonitoring and bioindicators used for river ecosystems: Definitions, approaches and trends. Procedia Environ Sci 2:1510–1524. https://doi.org/10.1016/j.proenv.2010.10.164

Lydy MJ, Crawford CG, Frey JW (2000) A comparison of selected diversity, similarity, and biotic indices for detecting changes in benthic-invertebrate community structure and stream quality. Arch Environ Contam Toxicol 39:469–479. https://doi.org/10.1007/s002440010129

Maruyama H, Takai H (2016) Genshoku kawamushi-zukan—yochu-hen [Color handbook of stream insects—juveniles]. Zennokyo, Tsukuba (In Japanese)

Merritt RW, Cummins KW, Berg MB (2019) An introduction to the aquatic insects of North America, 5th edn. Kendall Hunt, Dubuque, IA

MLIT (2019) Kongo-no kasensuishitsukanri-no shihyou-nituite (an) [A revision of a proposal for the biological indicators of river water quality management] (In Japanese). https://www.mlit.go.jp/kisha/kisha05/05/050330_.html. Accessed 22 Feb 2022

MOE (2017a) Suiseiseibutsu-niyoru suishitsu-hyouka manuaru—Nihon-ban heikinsukoa-hou [Manual of water quality assessment using aquatic organisms - the Japanese Average Score Per Taxon method] (In Japanese). https://www.env.go.jp/press/files/jp/106081.pdf. Accessed 22 Feb 2022

MOE (2017b) Kasenseibutsu-no etoki kensaku [Illustrated identification key of stream macroinvertebrates] (In Japanese). https://www.env.go.jp/press/files/jp/106083.pdf. Accessed 22 Feb 2022

MOE, MLIT (2012) Kawa-no ikimono-wo shirabeyou—suiseiseibutsu-niyoru suishitsu hantei [Investigation of stream organisms—assessment of water quality using macroinvertebrates] (In Japanese). www.mlit.go.jp/river/shishin_guideline/suisituhantei/text.pdf. Accessed 22 Feb 2022

Musashino Shizen-jyuku (2017) Kiken-seibutsu first aid handbook—Riku-hen [First aid handbook of dangerous wildlife—terrestrial version], Bunichi, Tokyo, Japan (In Japanese)

Nozaki T (2012) Biological assessment based on macroinvertebrate communities : Average score system for Japanese rivers. J Japan Soc Water Environ 35:118–121 (In Japanese)

Nunomura N, Shimomura M (2016) Isopoda from Japan (42) Suborder Sphaeromatidea: Family Sphaeromatidae (8) *Gnorimosphaeroma* (2). Aquabiology 38:738–741 (In Japanese)

Serrano Balderas EC, Grac C, Berti-Equille L, Armienta Hernandez MA (2016) Potential application of macroinvertebrates indices in bioassessment of Mexican streams. Ecol Indic 61:558–567. https://doi.org/10.1016/j.ecolind.2015.10.007

Tanida K (2010) Kasen-kankyo-no shihyou seibutsu-gaku [Indicator biology in the stream environment]. Hokuryukan Pulishing, Tokyo (In Japanese)

Tanida T, Takemon Y (1991) The illustrated handbook of Shiga's aquatic insects. Shingakusha, Kyoto (In Japanese)

Traunspurger W, Majdi N (2017) Meiofauna. In: Hauer FR, Lamberti GA (eds) Methods in Stream Ecology, 3rd edn. Academic Press, Burlington, MA, pp 273–295

Tsuda (1964) Osui seibutsu-gaku [Pollution biology]. Hokuryukan, Tokyo (In Japanese)

Washington HG (1984) Diversity, biotic and similarity indices. A review with special relevance to aquatic ecosystems. Water Res 18:653–694. https://doi.org/10.1016/0043-1354(84)90164-7

Yamazaki M, Nozaki T, Fujisawa A, Ogawa T (1996) Researches on the establishment of the standard method to evaluate lotic environments based on the biological condition of macrobenthic invertebrates in Japan. J Environ Lab Assoc 21:114–144 (In Japanese)

Zeybek M, Kalyoncu H, Karakaş B, Özgül S (2014) The use of BMWP and ASPT indices for evaluation of water quality according to macroinvertebrates in Değirmendere Stream (Isparta, Turkey). Turkish J Zool 38:603–613. https://doi.org/10.3906/zoo-1310-9

Chapter 12
Vegetation Surveys, Environmental Measurement, and Analysis: Biodiversity Conservation in *Satoyama*

Koji Ito and Nisikawa Usio

12.1 Introduction

12.1.1 What is Satoyama?

Satoyama includes various types of semi-natural grasslands, agricultural lands, forests, wetlands, and settlements where both biodiversity and agricultural and forestry productivities are maintained through moderate levels of human intervention. Satoyama supports the livelihoods of local peoples not only from the perspective of biodiversity conservation, but also by providing various ecosystem services. For this reason, Satoyama has been a major conservation target in Japan's national biodiversity strategy. Sustainable resource management and land use systems in Satoyama, or equivalent semi-natural landscapes, are recognized not only in Japan but also throughout the world. Such systems are referred to as socioecological production landscapes and seascapes (SEPLS).

The Satoyama concept has become widely known worldwide through the Satoyama Initiative, which was proposed by the Ministry of the Environment, Japan and the United Nations University Institute for the Advanced Study of Sustainability (UNU-IAS) at the 10th meeting of the Conference of the Parties to the Convention on Biological Diversity. The Satoyama Initiative is an effort to promote sustainable resource management and land use at the global scale by recognizing SEPLS throughout the world and by sharing techniques, wisdom, and lessons learned to balance biodiversity conservation and resource utilization. The initiative has further developed into an international network (IPSI; International Partnership for the

K. Ito (✉)
Center for Collaborative Study With Community, Gifu University, Gifu, Japan
e-mail: ito.koji.h3@f.gifu-u.ac.jp

N. Usio
Institute of Nature and Environmental Technology, Kanazawa University, Kanazawa, Japan

N. Hasebe et al. (eds.), *Field Work and Laboratory Experiments in Integrated Environmental Sciences*, https://doi.org/10.1007/978-981-99-6532-8_12

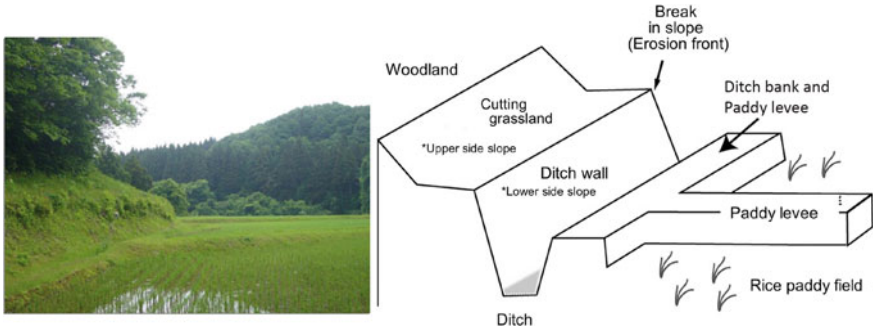

Fig. 12.1 Various field margin types in Japanese Satoyama. Modified from Ito and Katoh (2007)

Satoyama Initiative) of governments, academic institutions, and private organizations working toward sustainable conservation of secondary natural landscapes around the world.

Satoyama contains various types of semi-natural grasslands with high plant species diversity that are maintained through anthropogenic disturbance associated with agriculture and forestry management (Ito and Katoh 2007). In particular, linear or strip-shaped semi-natural grasslands such as paddy levees, stream embankments, ditch walls, and grassland along the forest edge are known as the field margin (Marshall and Moonen 2002) (Fig. 12.1). The field margin has various ecosystem functions including as a dispersal route for organisms, habitat for natural predators that consume agricultural pests as well as many other organisms, and a honey source for pollinator insects.

12.1.2 Challenges Facing Conservation of Biodiversity in Satoyama

Satoyama is currently on the brink of a major regime shift due to transformation of socioeconomic systems. In the past, grassland ecosystems such as field margins mentioned above were inhabited by a wide variety of organisms, and the dominance of competitively exclusive species was suppressed through continuous artificial management practices such as mowing, burning, and grazing associated with agricultural work. However, due to the depopulation of agricultural areas and mountain areas and the decrease in the number of farmers the management pressures on agricultural land have decreased, and vegetation succession is progressing in various manners in *Satoyama*. On abandoned farmlands, the invasion of exotic plant species distorts the succession process, creating a barrier to biodiversity conservation.

In field margin areas facing such difficulties, what research questions can you ask and what conservation guidelines can you submit based on scientific methods?

12.2 Setting a Research Hypothesis

12.2.1 Defining the Scope of Your Research Project in a Summer School

In short-term research programs such as summer schools, careful planning of study design is essential to drawing conclusions about the study hypothesis with limited resources (time and labor). Usually, preparation for hypothesis-testing research is difficult at a field site that you are visiting for the first time. In such cases, the first step is to clarify the scope of the project based on a preliminary survey of the target field, survey of related literature, and interviews with local farmers or conservationists.

The research scope used in a summer school project should be as simple as possible. The research scope provides a framework for when, where, from what perspective, and how your research will be conducted. If the scope is too wide, timely investigation will be difficult, and therefore it should be established with consideration of the amount of effort that can be invested during the research period. For students at the beginning of their exploration of environmental studies and ecology, the first hurdle to field research will be the great deal of time required to identify species and learn how to use environmental measuring devices. Therefore, in a short research program, students should focus on acquiring these research skills while engaging in several research activities.

12.2.2 Establishing the Research Questions and Hypothesis

Once the research scope is determined, the next step is to establish the research question and hypothesis. In general, research questions can be proposed for a research project. For example, "Why are the herons (e.g., *Egretta garzetta*, *Ardea intermedia*, *A. alba*, and *A. cinerea*), medium-to-large waterfowl that inhabit Japanese *Satoyama*, preferentially forage in only certain paddy fields?" In addition to the feeding environment, research questions exploring the nesting environment are other options when studying the habitats of herons.

The research hypothesis is obtained through conversion of the research question into the format "If XX is true, then XX follows." For the example given above, we could create a research hypothesis that "A higher density of the weather loach (*Misgurnus anguillicaudatus*) in paddy field is associated with more frequent visits of herons to such fields." Thus, research hypotheses are more specific questions used to draw specific conclusions based on measurable data. In general, multiple research hypotheses may be needed to answer to a single research question.

Generally, a common research topic for understanding the ecology of a species and considering conservation measures is clarification of the relationships between organisms and environmental factors. Habitat suitability and distribution models for

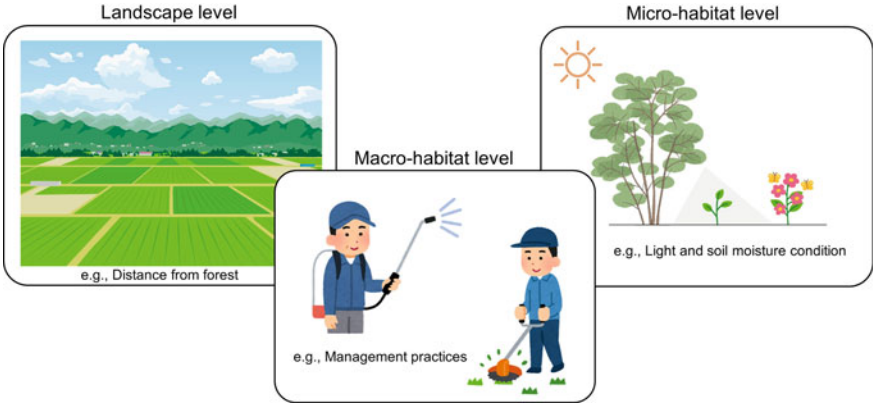

Fig. 12.2 Three hierarchical levels characterizing plant community composition at different spatial scales: landscape, macro-habitat, and micro-habitat

various species have been developed to aid understanding and prediction of species pattern and biodiversity (Guisan 2017).

To elucidate the relationships between the distribution of wildlife and various environmental factors, three hierarchical levels at different spatial and temporal scales must be analyzed, thus at the landscape, macro-habitat, and micro-habitat levels (Fig. 12.2). A plant habitat is an area wherein a plant species can obtain the resources required for growth and reproduction. The definition of a hierarchical level may vary depending on the ecology of the target species and the distribution of the local population. For example, the spatial dispersal of cherry trees, the seeds of which are spread by birds, is larger than that of violets, the seeds of which are dispersed by ants, and therefore, the spatial extent of the relevant landscape differs among target species.

The landscape level is characterized by the variety of habitats and the movements (dispersals) of a species within an area or region. The concept is used to learn and describe the ecological characteristics of an area, and how species are affected by their surroundings. The assumption is made that the environmental factors determining species distribution and diversity are represented by the spatial position of habitats within the landscape (e.g., distance from forest or an adjacent water body, habitat connectivity, elevation) and by the land-use composition surrounding the habitat (e.g., urbanization rate).

A macro-habitat is a series of contiguous, similar vegetation patches with environmental conditions favored by certain species. The relevant environmental factors include the degree of management (e.g., the intensity or frequency of mowing, the use of herbicide spray), the vegetation structures (e.g., canopy coverage, canopy height), and geomorphological and geological features (e.g., convex or concave topography, soil types).

At the micro-habitat level, various local areas with similar environmental resources or microtopographic locations, the environmental factors are light availability and soil conditions (e.g., soil moisture, soil nutrient, soil texture). These factors represent environmental conditions that can vary on the spatial scale of herbaceous plant survey quadrats, which are usually 1 × 1-m square sampling frames but may be rectangular depending on site conditions.

The appropriate hierarchical levels to assess depend on the research questions. In ecological research, statistical methods such as hierarchical linear model (also known as multilevel linear model, or mixed model), and hierarchical partitioning (e.g., Quinn and Keough 2002) can be used to evaluate the relative importance of environmental factors on species distributions across multiple hierarchical levels. However, when multiple environmental variables are incorporated into a statistical model, a larger number of quadrats is needed to estimate many parameters. Thus, focusing on a certain hierarchical level is most practical for short-term research projects.

Exercise 1

In your study field, what environmental factors are positively/negatively affecting the ecosystem and the biodiversity? List as many examples as you can think of.

Tips: Observe and interview local farmers about local issues such as habitat alterations (caused by civil engineering), changes in land use and agricultural management systems, the use of chemical pesticides and fertilizers, or the presence and prevalence of invasive species.

Exercise 2

Assume that you have set the research hypothesis "when the degree of human influence differs between paddy levees, the composition of the plant community established there also differs." What kinds of response variables (those of target organisms or communities) and explanatory variables (e.g., environmental factors related to grassland managements) should be measured? List as many as you can.

Tips: Not only the abundance/frequency of occurrence of certain species but also the numbers of species or diversity indices (e.g., Shannon-Weiner index) are useful when seeking to understand a species ecology and a plant community. Environmental variables relevant to grassland management can be obtained by interviewing farmers or by surveying indicators (e.g., the average height of vegetation reflects the mowing management strategy in play).

12.3 Study Design and Methodology

12.3.1 Study Design for Vegetation Surveys

The first challenge in an investigation is determining how to arrange the quadrats spatially, known as sampling design. Sampling is conducted for the purpose of extracting representative samples from the whole set (e.g., vegetation, the population of a certain plant species, buried seeds) of an object to clarify the overall picture with a small amount of research effort. Therefore, the extent (e.g., area or number) and strategy of sampling (random or systematic) are critical issues that must be examined. When investigating the composition of plant communities, careful selection of plots that capture vegetation heterogeneity is essential.

If you are targeting a particular plant species (e.g., endangered species or indicator species) and the number of individuals within a study site is limited and easily detectable, all individuals should be surveyed rather than sampling with quadrats.

In addition, experimental operations such as mowing may be performed using field experimental plots. See other textbooks (Quinn and Keough 2002) for sampling designs of such field experiments.

Below, we introduce sampling methods that are commonly used in vegetation surveys.

12.3.1.1 Simple Random Sampling

The term *random plots* is often misused when setting up quadrats. If sampling is to be truly random, a statistically correct randomization procedure is required, such as dividing the survey area into equal-area sections, numbering the sections with consecutive numbers, and then selecting survey locations using a random number function in a spreadsheet program (e.g., Excel). Outside of experimental settings, haphazard sampling is often adopted in lieu of random sampling for convenience.

In many cases, closer quadrats will exhibit habitat similarities, and individual plants may spread through cloning. Therefore, setting up quadrats requires consideration of the representativeness of sampling locations so that the range of vegetation variation across the entire study site is covered. To address that need, stratified random sampling, which is an improved method based on simple random sampling, was developed.

12.3.1.2 Stratified Random Sampling

For stratified random sampling in vegetation surveys, the vegetation patches that are expected to have different species compositions within the study site must be identified in advance. Random sampling is then performed for each patch type (this is known as stratification). This method was devised to capture the variation in species

composition across the entire survey area better than methods that do not consider stratification.

12.3.1.3 Systematic Sampling and the Transect Method

Systematic sampling is a method of sampling at regular intervals. For example, to evaluate the soil nutritional status of a square field, estimates are made based on sampling at the center and four corners.

The transect method is a systematic sampling method in which quadrats are set at regular intervals or continuously along a line or belt. This method is often used to investigate changes in species composition along an environmental gradient, such as distance from the water or forest edge.

12.3.1.4 Chrono-Sequence Method

The chrono-sequence method is a sampling method that aims to capture time-series changes through simultaneous investigation and comparison of sites with different histories as an alternative to direct observation methods. This method requires that conditions affecting vegetation other than vegetation history do not differ significantly among study sites. This technique is used, for example, to simultaneously investigate community patches at different vegetation succession stages to estimate the recovery process after plant community disturbance.

12.3.2 Precautions for Sampling Design

12.3.2.1 How Many Quadrats Should You Have?

When estimating the number of species, if a preliminary survey can be conducted, the required survey area is estimated using the species-area curve method. In this method, the species observed are recorded while gradually increasing the size of the square plot (quadrat), creating a species-area curve. In this manner, the area where the rate of increase in the number of species is nearly constant can be determined. If such preparations cannot be made, a rough method involves adding quadrats until new species scarcely appear in the vegetation survey. As a result, the number of quadrats may vary among vegetation study sites. In such a case, use of the rarefaction method described below allows for comparison of the number of species while considering research effort.

Even in surveys that do not aim to estimate the number of species at a site, the number of quadrats is an important decision in assessment of variation and detection of statistically significant differences of abundance. If the variation in the

target organism cannot be evaluated in advance, a study plot is typically set with approximately 10 replications per target area.

12.3.2.2 Size and Shape of the Quadrat

When determining the size of a vegetation survey quadrat, canopy height is often used as a guideline for the length of each side of the quadrat. For example, in turf herbaceous communities, the length of one side is approximately 0.5 m to 1 m, while in tall herb communities, 1 m to 2 m is often used. A quadrat does not necessarily need to be square, and in field margin areas such as paddy levees, a rectangular quadrant matching the shape of the target habitat is best.

12.3.2.3 Avoiding Pseudo-Replication

If sample replication is done improperly, the results of hypothesis testing may be inaccurate. For example, such inaccuracy occurs when multiple quadrats are set between a pair of abandoned and cultivated paddy fields to investigate the impact of abandonment of cultivation on the weed community. Although differences in plant species composition and species numbers may be observed in this study, the effects of abandonment of cultivation are not strictly compared (Fig. 12.3). Such a situation is known as pseudo-replication (Hurlbert, 1984). For proper replication, multiple pairs of abandoned paddy fields and actively cultivated paddy fields should be selected to avoid pseudo-replication.

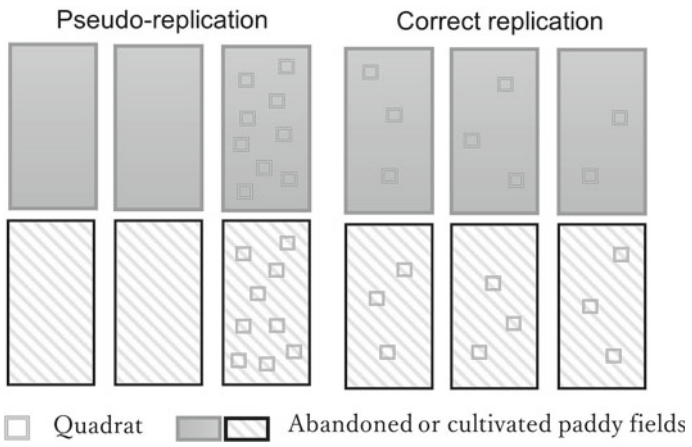

Fig. 12.3 Pseudo-replication and correct replication diagrams

Table 12.1 Braun-Blanquet scale for vegetation surveys

Braun-Blanquet scale	Vegetation cover rate (%)	Value for analysis (%)
5	75–100	87.5
4	50–75	62.5
3	25–50	37.5
2	10–25	17.5
1	1–10	5.5
+	1 or less	0.5

12.3.3 Measurement of Response Variables

12.3.3.1 Field Measurement

In surveys of herbaceous plant communities, the response variable is selected mainly from the following parameters, taking into consideration the research hypothesis and costs (time and labor).

12.3.3.2 Vegetation Cover Rate and Coverage

The percentage of the ground surface covered by plants in a quadrat is the vegetation cover rate (%) and determined visually. This is not often used as a response variable, rather as an explanatory variable, surrogate of animal habitat, or foraging intensity.

The area occupied by each plant species when the quadrat is viewed from directly above is known as coverage (%) and is usually recorded as an ordinal variable (on Braun-Blanquet scale) obtained by translating coverage (%) into a class (Table 12.1). Coverage can be easily visualized as the area of shadow (foliar cover) created when light is projected from directly above the quadrat. Therefore, when multiple plant species overlap and grow, the total vegetation cover rate may exceed 100%. Generally, the coverage is estimated visually.

A measurement that represents the degree of plant spread, such as solitary, crowded, or covering, is known as sociability. Sociability is required when conducting a phytosociology survey but is usually unnecessary if not explicitly included in the research objectives.

12.3.3.3 Biomass

To accurately evaluate the amount of biomass, plants must be harvested by species from the quadrats to measure dry weight. This method is a destructive testing process and is not suitable for tracking communities in the same location over a long period. As a non-destructive method to determine biomass, the coverage or vegetation cover

rate and maximum plant height of each species may be measured, with biomass estimated by multiplying the percent cover by the plant height. However, this estimate is not a strict measure of biomass and should be interpreted with caution.

12.3.3.4 Abundance (Number of Individuals)

Abundance or the number of individuals is rarely used in vegetation surveys targeting communities but may be used in plant surveys targeting rare species and indicator species. Individuals of clonal plants may be difficult to distinguish, as they are connected by underground stolons and rhizomes, and in such cases the number of shoots may be used rather than the number of individuals.

If abundance is too high for efficient counting, it can be evaluated through grading on a logarithmic scale. For example, for a power of 5, the possible grades are 0, 1–5, 6–25, 26–125, 126–625, 626–3125, and higher.

12.3.3.5 Presence–Absence

Presence–absence is used when you are interested only in the occurrence of a particular plant species within a quadrat. No quantitative information on focal species such as conservation target can be obtained when presence–absence is used as a measure. However, the prevalence of each plant species in the study site can be evaluated based on its frequency of occurrence across multiple quadrats.

12.3.4 Correcting Environmental Data

Environmental variables used to analyze vegetation survey data include those that can be measured in the field and those that require samples be returned to the laboratory for measurement and analysis. In exploratory research, environmental variables, which are often costly to measure and analyze, may be impractical to use. Therefore, we describe a two-step approach for identifying trends using factors that can be readily measured in the field and then more fully evaluating the appropriate environmental variables in subsequent research. Here, assuming the survey is being conducted during summer school, we introduce variables that can be measured easily and quickly in the field.

12.3.4.1 Landscape Level

Geographic Coordinate Information

Geographic coordinate information can be obtained using a commercially available global navigation satellite system (GNSS) receiver. Alternatively, a smartphone with GNSS function can be used to take photographs with geotags. The positioning accuracy of smartphones is often approximately 2–3 m. However, in research, accuracy at the sub-meter level (i.e., error of 1 m or less) is often necessary. In such cases, a dedicated receiver can be used, although such devices are expensive.

As the altitude information measured with a GNSS receiver is often ellipsoid height, it must be corrected to obtain the altitude. In Japan, the altitude data acquired by GNSS receivers represents the true altitude + 30–40 m, but some receiver models automatically correct the displayed altitude. For details, please refer to the manual of each receiver model used.

Land-Use Type in the Surrounding Area

Documenting land-use types around the study site can provide indicators of ecological processes and anthropogenic impacts at the landscape level. For example, if the forest coverage of the surrounding terrestrial area is high, a more natural environment can be maintained, and forest plant species from the surrounding area will more readily disperse into the target area. If the surrounding land use includes largely residential and commercial areas, the degree of human impact is assumed to be high. In addition, recording the cropping status of adjacent land (e.g., paddy fields, fields, abandoned land) is advisable, as the use and management practices of adjacent land affects the composition of plant species in the field margin (Biaix and Moonen 2020). If the location of the study site can be determined with high precision using GNSS, geographic information systems (GIS) and aerial photographs or satellite images may be used to assess land use around the study site.

12.3.4.2 Macro-Habitat Level

History of Agriculture and Forestry Management

To accurately determine the frequency of mowing and whether herbicides are applied at a study site, questionnaires and interviews with land managers must be conducted. When such surveys are difficult, canopy height may be used as a surrogate indicator of grassland management, as grassland height is suppressed where mowing is more frequent.

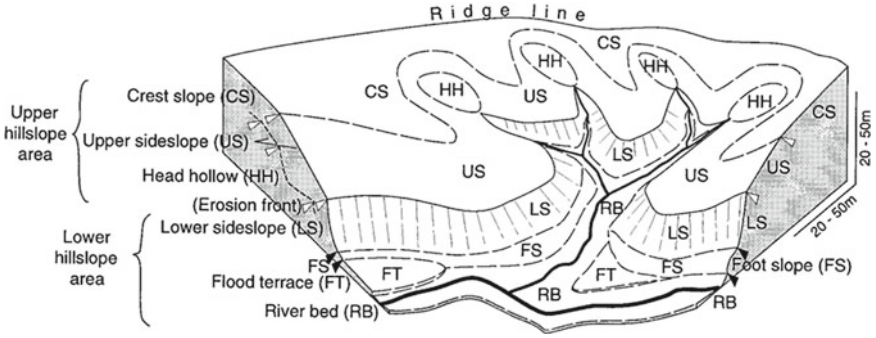

Fig. 12.4 Micro-topographical classification of hilly landscape in Japan (Nagamatsu and Miura 1997)

Fig. 12.5 Field survey tools for environmental data collection: gradometer (left) and the Yamanaka soil hardness meter (right)

Microtopographic Classification

Geomorphological classifications may be used as a comprehensive indicator of multiple environmental conditions, including moisture, light, and soil development. Microtopographic classification (Tamura 1974) is often used as a classification method representing the small-scale topographic features of a study site in Japanese hilly landscapes (Fig. 12.4).

To determine the relative height from water surface levels such as rivers and lakes, a cross-sectional graph may be created using a total station (TS) or auto-level instrument. If no such equipment is available due to cost, relative height can be obtained easily and quickly using a simple slope surveying instrument (e.g., Gradometer, Geopacks Ltd., UK) (Fig. 12.5).

Table 12.2 International classification of soil texture

Soil Texture Classification	Criterion
Sandy Soil (S)	Almost all sand, no stickiness
Sandy Loam (SL)	Feels very sandy with little stickiness
Loam (L)	Feels somewhat sandy and sticky Sand and clay in similar amounts
Silt Loam (SiL)	Little sandiness, feels smooth like flour
Clay Loam (CL)	Feels slightly sandy and quite sticky
Light Clay (LiC)	Scarce sand, adheres firmly
Heavy Clay (HC)	No sandiness, sticks very well

12.3.4.3 Micro-Habitat (Quadrat) Level

Soil Hardness

The Yamanaka-type soil hardness tester is used to measure soil hardness (Fig. 12.5). A metal pointed cone is thrust against the soil surface and the subduction depth (mm) is measured.

In soil with high hardness, water permeability is poor and plant growth may be hindered. If the activity of soil microorganisms is high, an aggregate structure may develop and soften the soil.

Soil Texture Classification

Soil texture classification is conducted based on the particle size composition of the soil. This classification reflects some soil properties that affect its role as a growth substrate for plants. For example, coarser particle size leads to better drainage, while finer particle size is associated with higher fertilizer retention capacity. As a simple method for soil texture classification, a small amount of surface soil can be collected with a finger moistened with water and evaluated based on the feel when rubbed between the thumb and index finger. Prior training using standard soil samples (Fujihira Industry Co., Ltd., Tokyo) as the judgment criteria is useful, but judgments can also be made based on Table 12.2 below.

Soil Moisture

Volumetric water content (%) and soil moisture potential (pF) are typical measured values representing soil moisture conditions. For multipoint measurement, the volumetric water content (VWC) is often measured using a time domain reflectometry

(TDR) or amplitude domain reflectometry (ADR) soil moisture meter (e.g., SM150-KIT, Environmental Measurement Japan, Co., Ltd., Fukuoka). Although these instruments are relatively expensive (≥110,000 JPY; ~840 USD as of December 2022), they have the advantage of taking measurements rapidly on-site.

As soil moisture varies over time, measurement should be completed in the shortest time possible when comparing multiple locations. In addition, due to the difficulty of detecting differences between measurements immediately after rainfall, measurement more than 2–3 days after rainfall is most suitable.

Soil Electrical Conductivity and pH

Soil pH is often affected by surface geology and base rocks. It may also be affected by anthropogenic factors such as concrete and road-surface antifreeze. No significant effect on the growth of many plants is observed around neutral pH, but plant growth may be hindered at extremely low or high pH levels. However, acidophilic plants and alkaliphilic plants exist, and soil pH is an essential factor regulating their growth. Soil electrical conductivity (EC) reflects the concentration of nutrients in the soil and provides insight into the degree of salt accumulation.

These surveys begin with on-site soil sampling. If soil is collected only at a specific point, the sample may not be representative of the overall soil environment of the study site. Therefore, to account for variability, small amounts of surface soil should be collected from multiple locations and mixed well into a single sample prior to extraction.

For this analysis, prepare the soil by diluting it with water. Place the raw (not air dried) soil sample in a plastic bottle with a lid, dilute it with distilled water (soil:water volume ratio = 1:2), and shake. To achieve this dilution, add soil up to the 150 mL line of a graduated bottle pre-filled with 100 mL water, because the soil has many voids and its exact volume cannot be measured if soil is added to the bottle first. After allowing the mixture to stand for a period, the supernatant can be measured with a handheld pH and EC meter (e.g., LAQUA twin, HORIBA Ltd., Kyoto).

Light Environment

The light environment is an indispensable environmental factor for the growth of many plants, and it greatly affects the success or failure of reproductive events such as flowering and fruiting. The method of taking hemispherical photographs using a circular fisheye lens is widely used for multipoint measurement of the light environment in the field. The light environment is evaluated by obtaining the open-air ratio (the ratio of area not covered by vegetation cover to the total celestial sphere area at a specific observation point) from the photograph.

Through analysis of these photographs in the laboratory with dedicated software such as Hemiphot.R (ter Steege 2018), the theoretical solar radiation time and estimated value of photosynthetic photon flux density (PPFD) can be calculated. Please refer to the manual of each software program for the specific methods.

Although this method is generally not suitable for multipoint measurement, the light environment can be evaluated using an illuminance meter or a quantum flux meter. Two units of the same model, one at the quadrat and the other in an open area adjacent to the quadrat, must be used simultaneously. Then the light environment of the site can be evaluated through comparison of the values measured with both instruments.

Exercise 3

A student research group set up a belt transect to record vegetation transitions across a riverside ecotone. For this study, what environmental conditions should they measure to investigate the relationship between vegetation and the environment?

Tips: In general, riparian vegetation is less disturbed by runoff during high flow or flood conditions as the distance from the river edge increases. The frequency and intensity of disturbances can affect plant community composition and structure. However, under normal flow conditions, the distance from the soil surface to the groundwater level is an important environmental factor that determines whether wet or dry plant communities can become established.

12.4 Case Study 1: Study Design to Compare the Effects of Human Management on Plant Communities in *Satoyama*

A typical field margin habitat in the *Satoyama* is paddy levee grasslands. The frequency and timing of mowing of the grasslands varies among farmers, and many areas have become poorly managed. Based on this background information, the student team set a research scope that can be assessed through a 1-day field survey. They decided to investigate how the composition of the plant community differs among three paddy levee grasslands with different mowing management practices.

12.4.1 Research Question and Scope

The research question was set as “Is the plant species diversity and composition of the paddy levee grassland affected by human management?” To answer this question, vegetation surveys using quadrats and measurements of environmental factors related to human impacts were conducted in three paddy levee grasslands with different

management levels (high, moderate, and low intensity) in the target area. The effects of environmental factors other than human management were also explored.

12.4.2 Research Hypothesis

Based on the research questions described above, the following three research hypotheses were formulated.

- If paddy levee grassland is mowed infrequently, less competitive plant species will be eliminated due to the dominance of certain more competitive plant species, and overall species diversity will decrease.
- Increasing the frequency of mowing in the paddy levee grassland enables new plant species to disperse from surrounding areas to sites where disturbance of the vegetation has occurred, increasing the diversity of plant species, and making species composition more similar across the area.
- The composition of the plant community in the paddy levee grassland is affected not only by the frequency of mowing but also by factors of the soil and light environments that fluctuate on the quadrat scale.

12.4.3 Study Design

The student team explored paddy levee grasslands in the study site and identified three plot types prior to the survey: relatively well-managed areas, mostly abandoned areas, and intermediate areas between the first two types. The team haphazardly set 10 quadrats in each of these three plots (Fig. 12.6).

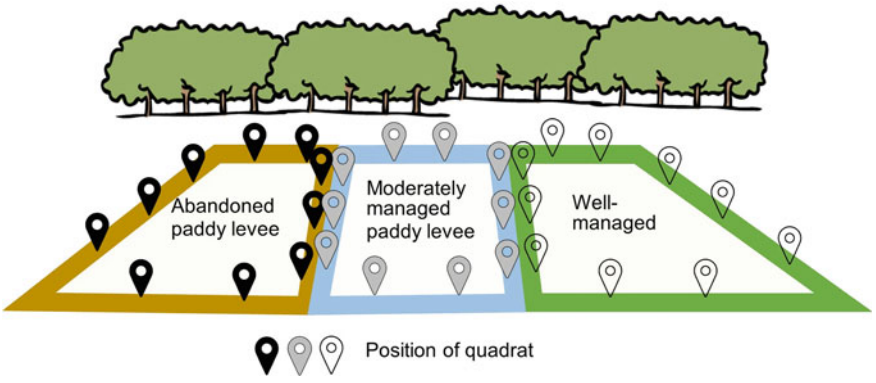

Fig. 12.6 Study design for examining comparative human influences on the plant communities of paddy levees

In the design shown in Fig. 12.6, each quadrat cannot be considered independent for assessing the impact of the mowing operation, as the mowing management operation is performed uniformly across the entire paddy levee grassland (i.e., pseudo-replication; see 12.3.2 Precautions for sampling design).

Therefore, the results obtained from this study design are simple comparisons of plant species diversity and community composition among the three selected paddy levees, and interpretation of the results must be careful and conservative. To interpret the results as representing the general response of the plant community to mowing, three or more study sites are needed for each treatment level of paddy levees with different mowing frequencies.

12.4.4 Illustrating Results and Formulating Discussion

In this section, we provide an example of how to summarize the results based on the survey design of Case 1 (see 12.4 Case Study 1) for comparison of plant species diversity among multiple habitats. We focus on the relationship between species ecology and the environment by summarizing the results using functional groups, which are species groups that respond similarly to certain environmental conditions (see 12.4.4.2 Comparing species diversity and similarity).

12.4.4.1 Data Treatment

The first step in summarizing the results is to input the survey data into a spreadsheet application such as Microsoft Excel. At that time, we strongly recommend first creating a list, as shown in Fig. 12.7, rather than directly inputting the matrix of site × plant species into the Excel sheet.

Next, the pivot table function of Excel can be used to create the matrix data required for various analyses. In addition to the site × species matrix, a separate site × environmental variable matrix should be created.

12.4.4.2 Comparing Species Diversity and Similarity

When describing the characteristics of a plant community or considering conservation strategies, the most basic and first requirement is creation of a species list for each study site. However, as the amount of information is too large to include the entire list in a paper or report, the information should be reduced using an appropriate index. Typical results are evaluated using plant species richness, diversity indices, and the composition of plant functional groups.

	A	B	C	D	E	F
1	Site	Plot	Quadrat Name	Species Name	Braun-Blanquet sacle	Converted Coverage %
2	A	1	A1_1	*Miscanthus sinensis*	5	87.5
3	A	1	A1_1	*Imperata cylindrica*	3	37.5
4	A	1	A1_1	*Platycodon grandiflorus*	+	0.5
5	A	1	A1_2	*Miscanthus sinensis*	2	17.5
6	A	1	A1_2	*Pueraria montana* var. *lobata*	2	17.5
7	A	1	A1_2	*Thalictrum minus* var. *hypoleucum*	1	5.5
8	A	1	A1_3	*Miscanthus sinensis*	4	62.5
9	A	1	A1_3	*Artemisia indica* var. *maximowiczii*	1	5.5
10	A	1	A1_3	*Picris hieracioides* subsp. *japonica*	1	5.5
11	A	2	A2_1	*Imperata cylindrica*	2	17.5
12	A	2	A2_1	*Gentiana zollingeri*	1	5.5
13	⋮	⋮	⋮	⋮	⋮	⋮

Fig. 12.7 Example of Excel datasheet input format for vegetation survey results. The coverage (Column F) is obtained by transforming Braun-Blanquet scale (column E) according to Table 12.1

Species Richness (Species Density)

Both species richness and species density are values related to the number of species; specifically, the former represents the number of species per individual number (or biomass), while the latter represents the number of species per fixed area (or volume or weight) (Gotelli and Colwell 2001).

To assess the species density of a plant community, the number of species appearing in each quadrat is commonly calculated and then the average number of species appearing per unit area is determined for each study site (or treatment category). Such local diversity in the community is known as α-diversity. On the other hand, the number of species appearing across the entire target area is designated γ-diversity. β-diversity is used as an index for evaluating the differences in species composition among sites within the target area and is obtained using one of the following two equations (Eqs. 12.1 and 12.2).

$$\beta = \gamma / \overline{\alpha} \tag{12.1}$$

$$\beta = \gamma - \overline{\alpha} \tag{12.2}$$

where $\overline{\alpha}$ is the mean value of the number of species α observed in each quadrat and γ is the number of species observed in the target area.

If circumstances allow only a limited number of habitats to be conserved, α, β, and γ diversities should be used as criteria for selecting locations for preferential

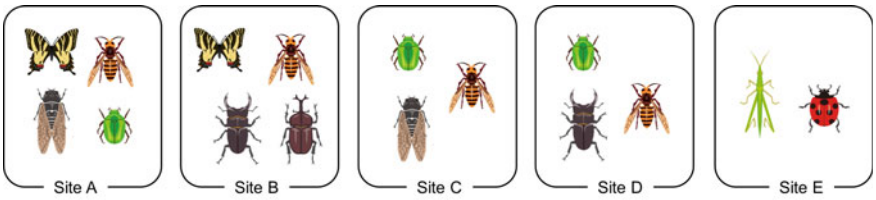

Site selection for biodiversity conservation	α diversity	β diversity	γ diversity
A+B+C+D	(4+4+3+3)/4 =3.5	6/3.5=1.71	6
A+B+D+E	(4+4+3+2)/4=3.25	8/3.25=2.46	8

Fig. 12.8 Examples of methods used to select target areas for habitat conservation based on α, β, and γ diversity

conservation. For example, rather than simply preferentially conserving areas with high α-diversity, selecting multiple habitats with high β-diversity and γ-diversity will lead to better conservation of species diversity within the region (Fig. 12.8).

Furthermore, if the amount of research effort (number of quadrats) differs greatly among study sites or treatment levels being compared, especially if insufficient research effort is used in a survey area with high β-diversity, γ-diversity may be underestimated and the measured α-diversity may not represent the situation throughout the area.

Under these conditions, a statistical method called rarefaction can be used to compare the number of species considering research effort. The freeware *Estimate S* (Colwell 2013) is widely used to calculate rarefaction. Please refer to the software manual for details of the analysis method.

Evaluation Using Diversity Indices

A diversity index evaluates diversity based on the richness and evenness of species in a community. Shannon–Wiener H' (Eq. 12.3) and Simpson index of diversity D (Eq. 12.4) are commonly used. The H' index is influenced by species occurring at low frequency, while the D index is more susceptible to effects from the dominant species.

$$H\prime = -\sum_{i=1}^{S} p_i \ln p_i \tag{12.3}$$

$$D = 1 - \sum_{i=1}^{S} p_i^2 \tag{12.4}$$

$$D = 1/\sum_{i=1}^{S} p_i^2 \tag{12.5}$$

where S is the total number of species in the community and p_i is the ratio of the abundance of species i to the total abundance of the community. When calculating Shannon–Wiener H', the base of the logarithm is e, but 2 or 10 may be used. Therefore, you must carefully check what base has in fact been used in any comparative studies. Furthermore, reciprocal Simpson's index of diversity D could be calculated (Eq. 12.5). Therefore, you must also check which index has been used.

Evaluation Based on Plant Functional Types

Plant species with similar morphological or ecological characteristics that do not necessarily align with phylogenetic relationships are called plant functional types (PFTs). Examples of PFTs include growth type, dormancy form, flowering time, seed size, disseminule form (seed dispersal type), native or nonnative species, and habitat type.

Comparing the composition of PFTs among study sites (or treatment levels) is useful for determining the characteristics of each community and the mechanism of the biological response to environmental changes. However, digitization of the database listing PFTs in Japan is incomplete. Therefore, each observed type should be validated using the literature, followed by creation of a database. For Japan, Miyawaki and Okuda (1991) and the Chiba historical Material Research Foundation (2003) are commonly used botanical pictorial resources that describe these types.

12.4.4.3 Comparison of Environmental Conditions

Comparing the mean values of various environmental variables among study sites is the first step in examining the factors that explain differences in species composition. First, a boxplot for each study site (or the treatment level) should be made representing the measured values of the environmental conditions of interest. Close observation of the raw data for outliers and differences in the mean value are essential to such comparisons. For more details on how to detect outliers and what to do with them, see Benhadi-Marín (2018).

Then, a statistical test of the difference in mean values is performed. If environmental variables with significantly different mean values are found among the study sites being compared, these variables can be evaluated to identify possible relationships with the difference in species composition. However, as this method only demonstrates a correlation, experimental work is needed to support a causal relationship.

In addition, these data can be applied to advanced statistical analysis methods, such as evaluation of the relative importance of environmental factors using statistical

models. Please refer to other textbooks for details, such as Quinn and Keough (2002) and Gotelli and Ellison (2004).

12.4.4.4 Items to Be Included in the Report

The report summarizes the research scope and hypothesis, survey design and methods, summarizing and plotting of the results, and consideration of the results (interpretation of the data and conclusions drawn from multiple results).

Exercise 4

Is a high-biodiversity community always considered to have high conservation value? In what cases can a community with low biodiversity have high conservation value? Please provide specific examples.

Exercise 5

What plant functional types are needed to assess the habitat quality of flower-visiting insects (pollinators) through vegetation surveys?

Exercise 6

What are the traits of plant species that are resilient to human disturbance? List as many functional types as you can think of.

Column 1 Tips for Plant Identification in Japan

When conducting a vegetation survey, an illustrated botanical guide and list of regional flora are useful tools for identifying species names. Some plant guides (e.g., Numata and Yoshizawa 1975) describe the correspondence between Japanese names presented in Roman letters and scientific names, which is convenient for non-Japanese speakers. Lists of flora are often published at the prefectural level in Japan. Most of these lists are limited to description in Japanese, but scientific names are provided, providing useful clues for species identification. In addition, a Red Data Book containing a list of endangered species has been published at the prefectural level, which contains some information about species distributions.

For those who have begun to learn plant species identification, the first obstacle when using a specialized pictorial guide for identification is identifying the family or genus name of the plant you want to identify. For this purpose, a comprehensive judgment must be made based on the characteristics of plant organs such as flowers, stems, and leaves, which may be frustrating if the names of these parts are unfamiliar.

In such cases, an application can be used to identify species names from images using artificial intelligence technology. As a free application for smartphones and tablets, we recommend the "iNaturalist" app, which can be used in English. In many cases, iNaturalist cannot correctly identify a species from a photograph, but instead presents candidates of higher taxonomic levels such as the genus name and family name, providing clues that can be used to identify species further using pictorial guides.

Column 2 Multivariate Analysis of Plant Communities

Statistical analysis in ecology has made remarkable progress due to the improvement of computer performance and has become an indispensable tool for students studying modern community ecology.

Multivariate statistical methods such as ordination and classification show great promise in exploratory research. Ecological knowledge about each species is undoubtedly essential to interpreting the results. However, identifying ecologically meaningful patterns from a large number of data and determining their relevance to environmental variables can be useful when constructing and verifying research hypotheses. These methods are collectively known as "data mining," and as the name suggests, finding patterns can feel like a treasure hunt. For detailed explanation of these methods, please refer to another textbook (e.g., Quinn and Keough 2002; Ŝmilauer and Lepŝ 2014; Borcard et al. 2018).

References

Benhadi-Marín J (2018) A conceptual framework to deal with outliers in ecology. Biodivers Conserv 27:3295–3300. https://doi.org/10.1007/s10531-018-1602-2

Blaix C, Moonen AC (2020) Structural field margin characteristics affect the functional traits of herbaceous vegetation. PLoS ONE 15(9):e0238916. https://doi.org/10.1371/journal.pone.0238916

Borcard D, Gillet F, Legendre P (2018) Ecology with R (Use R!) 2nd ed., Springer, Cham, https://doi.org/10.1007/978-3-319-71404-2

Chiba historical Material Research Foundation (ed) (2003) Flora of Chiba prefecture, Natural history of Chiba prefecture: supplementary volume 4, Chiba prefecture, Chiba

Colwell RK (2013) Estimates: statistical estimation of species richness and shared species from samples. Version 9. https://purl.oclc.org/sestimates

Gotelli NJ, Colwell RK (2001) Quantifying biodiversity: procedures and pitfalls in the measurement and comparison of species richness. Ecol Lett 4:379–391

Gotelli NJ, Ellison AM (2004) A primer of ecological statistics. Sinauer Associates Inc., MA

Guisan A (2017) Habitat suitability and distribution models with applications in R. Cambridge University Press, Cambridge. https://doi.org/10.1017/9781139028271

Hurlbert SH (1984) Pseudoreplication and the design of ecological field experiments. Ecol Mon 54:187–211

Ito K, Katoh K (2007) Plant Species Composition of Semi-natural Grasslands in Yatsuda Paddy Field of Tochigi. Japan. J Jpn Inst Land Arc 70(5):449–452 (in Japanese with English Abstract)

Miyawaki A, Okuda S (eds) (1991) Vegetation of Japan illustrated. Shibundo, Tokyo (in Japanese)

Marshall EJP, Moonen AC (2002) Field margins in northern Europe: their functions and interactions with agriculture. Agri Ecos Env 89(1–2):5–21

Nagamatsu D, Miura O (1997) Soil disturbance regime in relation to micro-scale landforms and its effects on vegetation structure in a hilly area in Japan. Plant Ecol 133:191–200

Numata M and Yoshizawa N (eds) (1975) Weed flora of Japan illustrated by color. Zenkoku Noson Kyoiku Kyokai, Tokyo (in Japanese).

Quinn GP, Keough MJ (2002) Experimental Design and Data Analysis for Biologists. Cambridge University Press, Cambridge. https://doi.org/10.1017/CBO9780511806384

Ŝmilauer P, Lepŝ J (2014) Multivariate Analysis of Ecological Data using CANOCO 5. Cambridge University Press, Cambridge

Tamura T (1974) Micro-landform Units Composing a Valley-head Area and their Geomorphic Significance. Ann Tohoku Geogr Assoc 26(4):189–199. https://doi.org/10.5190/tga1948.26.189

ter Steege H (2018) Hemiphot. R: free R scripts to analyse hemispherical photographs for canopy openness, leaf area index and photosynthetic active radiation under forest canopies. Naturalis Biodiversity Center, Leiden, Netherlands. https://github.com/naturalis/Hemiphot